



City Research Online

City, University of London Institutional Repository

Citation: El-Khafif, S. H. (2002). Application of Higher-Order Statistics and Subspace-Based Techniques to the Analysis and Diagnosis of Electrocardiogram Signals. (Unpublished Doctoral thesis, City, University of London)

This is the accepted version of the paper.

This version of the publication may differ from the final published version.

Permanent repository link: <https://openaccess.city.ac.uk/id/eprint/30850/>

Link to published version:

Copyright: City Research Online aims to make research outputs of City, University of London available to a wider audience. Copyright and Moral Rights remain with the author(s) and/or copyright holders. URLs from City Research Online may be freely distributed and linked to.

Reuse: Copies of full items can be used for personal research or study, educational, or not-for-profit purposes without prior permission or charge. Provided that the authors, title and full bibliographic details are credited, a hyperlink and/or URL is given for the original metadata page and the content is not changed in any way.

City Research Online:

<http://openaccess.city.ac.uk/>

publications@city.ac.uk

**APPLICATION OF HIGHER-ORDER STATISTICS
AND SUBSPACE-BASED TECHNIQUES TO THE
ANALYSIS AND DIAGNOSIS OF
ELECTROCARDIOGRAM SIGNALS**

A Thesis Submitted to the City University for
Degree of Doctor of Philosophy

By

Sahar Hafez El-Khafif

CITY UNIVERSITY

School of Engineering

2002

Table of Contents

Table of Contents.....	ii
List of Figures.....	vi
List of Tables.....	x
Acknowledgments.....	xi
Abstract.....	xii

CHAPTER 1 BACKGROUND

1.1 Introduction.....	1
1.2 The Heart.....	3
1.2.1 Intrinsic Conduction System.....	4
1.2.2 The Electrocardiogram (ECG) Signal.....	5
1.3 Definitions.....	8
1.4 Previous Work on ECG Signal Processing.....	10
1.4.1 Noise Cancellation Using Adaptive Filtering.....	11
1.4.2 Detection of ECG Signal Characteristic Points.....	11
1.4.3 ECG Signal Dynamics.....	12
1.4.4 Detection of Heart Abnormalities.....	13
1.5 The ECG Data.....	17
1.6 Aims and Objectives of This Work.....	18
1.7 Summary.....	18

CHAPTER 2 ADAPTIVE FILTERING OF THE ECG SIGNAL

2.1 Introduction.....	20
2.2 Adaptive Finite Impulse Response Filters.....	20
2.2.1 The Least Mean Square (LMS) Algorithm.....	23
2.2.2 The Least Mean Fourth (LMF) Algorithm.....	24
2.2.3 The Kalman Algorithm.....	25
2.3 Adaptive Non-Linear Filter.....	28
2.3.1 Second-order Volterra Filters (SVF).....	28
2.3.2 Adaptive Second-order Volterra Filter.....	30
2.3.3 Adaptive Third-order Volterra Filter.....	30

2.4 Model Order Selection	31
2.5 Signal-to-Noise Ratio	33
2.6 Noise Artefacts in ECG Signals	34
2.7 Results	35
2.7.1 Linear Predictors.....	37
2.7.2 Volterra Adaptive Predictor.....	43
2.7.3 Adaptive Artefact Filtering.....	45
2.8 Discussion	54

CHAPTER 3 STATISTICAL AND SPECTRAL ANALYSIS OF ECG SIGNALS

3.1 Introduction	56
3.2 Statistical Properties of the ECG Signals	56
3.2.1 Periodicity Test.....	57
3.2.2 Normality Test.....	58
3.2.3 Stationarity Test.....	60
3.3 Spectral Analysis of the ECG Signals	62
3.3.1 The Welch Periodogram.....	62
3.3.2 The Multiple Signal Classification (MUSIC) Algorithm.....	64
3.4 Detection of Ischaemic Heart Disease	71
3.4.1 Introduction.....	71
3.4.2 ECG Data Annotation.....	71
3.4.3 Analysis Technique.....	72
3.5 Results	74
3.6 Discussion	91

CHAPTER 4 HIGHER-ORDER STATISTICS/SPECTRA

4.1 Introduction	93
4.2 Higher-order Statistics/Spectra	94
4.2.1 Moments and Cumulants.....	95
4.2.2 Higher-order Spectra.....	104
4.3 Bispectral Analysis of Normal ECG Signals	109
4.3.1 Introduction.....	109
4.3.2 Results.....	110
4.4 The MUSIC Pseudo-Bispectrum	119

4.4.1 Introduction.....	119
4.4.2 Formulation of the Problem.....	120
4.4.3 Simulation Results.....	122
4.4.4 Application to ECG Signal.....	131
4.5 Discussion.....	133

CHAPTER 5 DETECTION OF HIGHER ORDER NON-LINEARITIES

5.1 Introduction.....	136
5.2 Detection of K^{th}-order Non-Linearity.....	137
5.2.1 Self-Coupling Detection Algorithm.....	138
5.2.2 The Polycoherency Indices.....	142
5.3 Results.....	143
5.3.1 Introduction.....	143
5.3.2 Bispectral Analysis of Normal/Ischaemic ECG Signals.....	144
5.3.3 Higher-order Spectral Analysis.....	148
5.4 Discussion.....	169

CHAPTER 6 NEURAL NETWORKS

6.1 Introduction.....	170
6.2 Artificial Neural Networks.....	171
6.2.1 Rational for Using Neural Networks.....	171
6.2.2 Basic Element.....	172
6.2.3 Learning Rules.....	174
6.2.4 Multi-Layer Neural Networks.....	175
6.2.5 Back-Propagation Algorithm.....	176
6.3 ANN-Based ECG Signal Classifier.....	181
6.3.1 Introduction.....	181
6.3.2 The NN Classifier Structure.....	181
6.3.3 Classifier Training and Testing.....	182
6.3.4 Implementation of the Three NN.....	184
6.4 Discussion.....	191

CHAPTER 7 SUMMARY AND FUTURE WORK

7.1 Summary.....	194
-------------------------	------------

7.2 Directions for Future Work.....	198
--	------------

APPENDICIS

APPENDIX A	CUBIC SPLINE INTERPOLATION.....	200
APPENDIX B	KAISER WINDOW.....	201
APPENDIX C	HINICH TEST.....	202
APPENDIX D	THE NEURALWORKS PREDICT PROGRAM.....	204
APPENDIX E	GLOSSARY OF TERMS.....	206
APPENDIX F	LIST OF SOFTWARE.....	210
APPENDIX G	LIST OF PUBLICATIONS.....	211

REFERENCES.....	213
------------------------	------------

List of Figures

Figure 1.1 A visual illustration of the ECG waveform.....	3
Figure 1.2 Longitudinal section of the heart.....	4
Figure 1.3 A diagrammatic representation of the conduction system of the heart.....	5
Figure 1.4 A normal 12-lead electrocardiogram.....	8
Figure 1.5 Ischaemic ECG signals from the MIT database.....	10
Figure 2.1 Block diagram of the adaptive transversal filter.....	21
Figure 2.2 Adaptive noise canceller.....	22
Figure 2.3 Flow chart for the adaptive Kalman predictor.....	27
Figure 2.4 Second-order Volterra filter.....	28
Figure 2.5 Cubic Volterra filter.....	31
Figure 2.6 Results obtained using the baseline wander filter.....	36
Figure 2.7 Filter order selection.....	39
Figure 2.8 Performance of LMS and LMF predictors.....	40
Figure 2.9 Convergence analysis of the linear adaptive predictors.....	41
Figure 2.10 Performance of the Kalman predictor.....	42
Figure 2.11 Selection of the number of samples in the input vector for Volterra predictor.....	43
Figure 2.12 Comparison between quadratic and cubic Volterra predictors.....	44
Figure 2.13 The adaptive artifact filter structure.....	45
Figure 2.14 Original signals used in the adaptive artefact filtering.....	47
Figure 2.15 Performance of LMS-based EMG filter.....	48
Figure 2.16 Performance of LMS-based MA filter.....	49
Figure 2.17 Performance of LMF artefact filters.....	50
Figure 2.18 Performance of LMS-based quadratic Volterra artefact filters.....	51
Figure 3.1 Time domain of one normal ECG cycle.....	57
Figure 3.2 Histogram of a normal ECG.....	59
Figure 3.3 Probability Distribution Function (PDF) of a normal ECG record..	59

Figure 3.4 Spectrogram of a normal ECG signal.....	61
Figure 3.5 Power spectrum of a normal ECG signal.....	64
Figure 3.6 Singular-values of the covariance matrix and the MUSIC spectrum of the whole ECG cycle.....	67
Figure 3.7 MUSIC spectra for the PR interval, QRS complex, and ST-T complex.....	68
Figure 3.8 MUSIC spectra of a normal case and two ischaemic cases.....	70
Figure 3.9 One ECG cycle from different episodes.....	75
Figure 3.10 MUSIC and MEM spectra for ten randomly selected ST-T complexes of a normal case.....	77
Figure 3.11 MUSIC and MEM spectra for ten randomly selected ST-T complexes of an ischaemic case.....	78
Figure 3.12 MUSIC spectra of ten ST-T complexes for episodes represent NLE and ICE for ST-segment depression case.....	80
Figure 3.12 continued MUSIC spectra of ten ST-T complexes for episodes represent NLE and ICE for ST-segment depression case.....	81
Figure 3.12 continued MUSIC spectra of ten ST-T complexes for episodes represent NLE and ICE for ST-segment depression case.....	82
Figure 3.13 MUSIC spectra of ten ST-T complexes for episodes represent NLE and ICE for ST-segment elevation case.....	83
Figure 3.13 continued MUSIC spectra of ten ST-T complexes for episodes represent NLE and ICE for ST-segment elevation case.....	84
Figure 3.13 continued MUSIC spectra of ten ST-T complexes for episodes represent NLE and ICE for ST-segment elevation case.....	85
Figure 3.14 MUSIC spectra of ten ST-T complexes for episodes represent NLE and ISE.....	86
Figure 3.14 continued MUSIC spectra of ten ST-T complexes for episodes represent NLE and ISE.....	87
Figure 3.14 continued MUSIC spectra of ten ST-T complexes for episodes represent NLE and ISE.....	88
Figure 3.15 MUSIC spectra of one ST-T complex.....	89

Figure 4.1 Cumulants of record No. 16539 (NSR-DB).....	101
Figure 4.2.I Cumulants of record No. 325 (ST Change-DB).....	102
Figure 4.2.II Cumulants of record No. 304 (ST Change-DB).....	103
Figure 4.3 Cumulant-based classification for normal/ischaemic cases.....	104
Figure 4.4 Bispectrum estimation using the indirect method.....	106
Figure 4.5 Bispectrum estimation using the direct method.....	107
Figure 4.6 Methodology adopted in this analysis.....	111
Figure 4.7 Bispectrum variance.....	111
Figure 4.8 Bispectrum magnitude of a normal ECG signal using the direct method.....	113
Figure 4.9 The diagonal and wall slices of the direct method bispectrum.....	114
Figure 4.10 Bicoherence-squared of a normal ECG signal.....	115
Figure 4.11 Bispectrum magnitude of a normal ECG signal using the TOR....	117
Figure 4.12 The diagonal and wall slices of the TOR bispectrum.....	118
Figure 4.13 MUSIC pseudo-bispectrum magnitude and the bicoherence- squared.....	123
Figure 4.14 MUSIC-PB, direct method and TOR bispectrum contours.....	126
Figure 4.15 MUSIC-PB, direct method and TOR bispectrum contours for short segment length.....	127
Figure 4.16 MUSIC-PB and contour plot for a sinusoid signal, $p=5$	128
Figure 4.17 MUSIC-PB and contour plot for a sinusoid signal, $p=7$	129
Figure 4.18 TOR bispectrum and contour plot for a sinusoid signal.....	130
Figure 4.19 MUSIC-PB estimation for record No. 18184 (NSR-DB).....	132
Figure 5.1 Time domain of an ECG cycle from record No. 16272 (NSR-DB) and record No. e0105 (E-DB).....	143
Figure 5.2 Bispectrum magnitude of a normal and ischaemic cases and their diagonal slices.....	146
Figure 5.3 Contour plots and diagonal slices of the bicoherence-squared indices of a normal and ischaemic cases.....	147
Figure 5.4 Bicoherence analysis of 18 normal and 21 abnormal records.....	148

Figure 5.5 The magnitude of polyspectrum slices of a normal and ischaemic cases.....	150
Figure 5.6 The total number of NSCs over all records for each order to total number of segments that has been tested for that order percent as a function of the polyspectrum order, k.....	159
Figure 5.7 The diagonal slices of the polyspectrum and polycoherency index for a sinusoid signal.....	161
Figure 5.8 Persistent characteristics of the diagonal slices of the polyspectrum and polycoherency indices for a normal and ischaemic persons.....	162
Figure 5.9 Polycoherency indices for normal and ischaemic ECGs. for k=2, k=3, and k=4.....	164
Figure 5.10 Polycoherency indices for normal and ischaemic ECGs. for k=5, k=6, and k=7.....	165
Figure 5.11 Polycoherency indices for normal and ischaemic ECGs. for k=8, k=9, and k=10.....	166
Figure 5.12 Average of the polycoherency indices measures. for polyspectrum orders k=2 to k=10.....	167
Figure 6.1 Neuron model.....	172
Figure 6.2 Activation functions of a neuron.....	174
Figure 6.3 Multi-layer feedforward neural network.....	176
Figure 6.4 Error back-propagation learning algorithm flow chart.....	179
Figure 6.5 The ECG signal NN-based classifier.....	182
Figure 6.6 Polycoherency slices used in training the NN.....	184
Figure 6.7 Training phase RMS error for NN1.....	186
Figure 6.8 Bar chart for the sum squared error at the output layer during training and test phases for NN1.....	187
Figure 6.9 Receiver operating characteristic curve of the NN2 classifier.....	189
Figure 6.10 Receiver operating characteristic curve of the NN3 classifier.....	190

List of Tables

Table 2.1 Estimated input and output SNR for the adaptive artefact filters.....	52
Table 3.1 Spectral peaks of the MUSIC spectra.....	69
Table 3.2 MUSIC results for all records.....	90
Table 4.1 Significant frequency components from the power spectrum and the bispectrum.....	114
Table 4.2 Hinich test applied to 18 normal ECG records.....	119
Table 4.3 Frequency estimates with changing the SNR.....	131
Table 5.1 Results of the self-coupling detection algorithm for $k=2$	151
Table 5.2 Results of the self-coupling detection algorithm for $k=3$	152
Table 5.3 Results of the self-coupling detection algorithm for $k=4$	153
Table 5.4 Results of the self coupling detection algorithm for $k=5$	154
Table 5.5 Results of the self-coupling detection algorithm for $k=6$	154
Table 5.6 Results of the self-coupling detection algorithm for $k=7$	155
Table 5.7 Results of the self-coupling detection algorithm for $k=8$	156
Table 5.8 Results of the self-coupling detection algorithm for $k=9$	157
Table 5.9 Results of the self-coupling detection algorithm for $k=10$	158
Table 6.1 The RMS and the classification rate obtained for NN1 classifier....	186
Table 6.2 Performance of the NN2 classifier.....	189
Table 6.3 Performance of the NN3 classifier.....	190
Table 6.4 Summary of the neural networks structures and classification rates obtained.....	191

Acknowledgments

First I would like to thank Dr. Rizk for her guidance and support. Her door was always open. I greatly appreciate her willingness to support me during my study.

I thank the staff in the department of EEIE and the MIM centre, City University and in particular Dr. Peter Weller for his cooperation in providing me with the required data from the MIT database. Also my thanks to my colleagues in the School of Engineering, especially Walid Zgallai, for their kindness and support.

My sincere thanks to my husband and my daughter for their support and patience and for my little son who provides me with some joy during the difficult times of my study.

I equally appreciate the encouragement from my mother and my lovely father who died before seeing this thesis.

Finally, I gratefully acknowledge the financial support of my country Egypt.

ABSTRACT

The first and main contribution of this research work is the higher-order statistics (HOS)-based non-linear analysis and subsequent diagnosis of abnormal electrocardiogram (ECG) signals, particularly myocardial ischaemia. In the time domain; the second-, third-, and the fourth-order cumulants have been used in the analysis. In the frequency domain; up to the tenth-order polyspectra have been exploited. This HOS-based analysis of normal and ischaemic electrocardiogram signals has led to the identification of certain key discriminant features for the two physiological states of the heart. These features are then fed to different backpropagation-based multiple layer perceptrons for classification. The second contribution is a proposed new methodology to discriminate patients with angina pectoris or with old myocardial infarction (MI) during the first 60 seconds of stress test (or in some cases using rest ECG). It is based on the pseudo-spectral MULTiple Signal Classification (MUSIC) and has the potential of being highly sensitive diagnostic signal processing tool. The third contribution is the development of a novel higher-order statistics, high-resolution estimator for quadratically coupled frequencies based on subspace spectral estimation.

Extensive studies of cumulants, bispectra and bicoherence-squared of normal and ischaemic ECG signals collected from MIT and ST-T European databases has enabled us to see key discriminant features in both the third- and fourth-order cumulant domains. In the frequency domain, the polyspectral study has been extended to the 10th-order polyspectra. By calculating one-dimensional polyspectrum slices using an algorithm developed by Zhou and Giannakis (1995) a considerable reduction in the CPU time has been achieved. Furthermore, Zhou's algorithm has been further extended to estimate the polycoherency slices which are used to characterise non-linearities in normal and ischaemic ECG signals. An important finding in this thesis is the decrease of the order of non-linearity representing the electrocardiogram signals of ischaemic patients.

This thesis also includes the results of a pilot study involving eighteen healthy subjects (MIT database) and confirmed that the ECG signal is non-Gaussian, cyclostationary and quasi-periodic. Combined spectral and bispectral analysis of the signal revealed that there are unique harmonic characteristics for the P-wave, QRS complex and T-wave and other frequencies due to harmonic interactions.

In this work three linear and one non-linear adaptive filtering/predictions techniques have been applied to noisy ECG signals and their respective performances appraised. It is shown that the Kalman filter gives the best mean-square error MSE error but its comparatively long execution time and problems arising from ill-conditioning of the state-error covariance matrix render it of limited use in ECG applications. It is also shown that the LMS-based quadratic and cubic Volterra filters are the most superior for the ECG signal prediction.

For ECG classifications; three multi-layer perceptrons employing back-propagation and modified back-propagation algorithms, and using two sets from the higher-order most discriminant features as their inputs, have yielded fairly high classification rates.

Chapter 1

BACKGROUND

1.1 Introduction

Signal processing is concerned with the representation, manipulation, and transformation of signals and the information that they carry. For example, we may wish to enhance a signal by reducing the noise or some other interference. Or process the signal to extract some information such as the words in a speech signal, the identity of a person in a photograph, or the classification of a target in a radar signal. Biomedical signal processing is concerned with the analysis of physiological signals such as the electroencephalogram (EEG), the blood pressure wave, the electrocardiogram (ECG), ...etc. The most beneficial aspect of this analysis is to extract information from these signals. This information can be used in automated interpretation and classification of the case or to facilitate, accelerate and support clinical decision-making. Examples of the tools used in signal processing techniques include linear and non-linear filtering, power spectral analysis, time frequency analysis, higher-order statistics and neural networks.

The electrocardiogram (ECG) signals examine the potential differences between the excited and non-excited parts of the heart caused by action potentials of myocardial cells. Although patterns associated with cardiac events appear clearly in the ECG signal, classification and diagnosis of the ECG signal is difficult for the following reasons (Cox, et al. 1972): 1) measurements at a distance from the heart partially obscure cardiac processes. 2) Complex variabilities are inherent in the phenomena for example wave morphology, bizarre at one location, can simultaneously appear quite normal at another. 3) Arrhythmia detection is a complex problem, often involving diverse morphologies and rhythms that vary among different subjects as well as

different time for the same subject. Inconsistency of the human observer adds another form of variability to the problem of ECG signal analysis. A study in which 125 ECG signals were analysed twice by nine experienced interpreters, the results were consistent on average in just 73 percent of the cases (Yamada 1968). Machine processing using objective measurement and classification criteria may provide more reproducible analysis.

In recent years the trend toward automated analysis of ECG signals has gained momentum. Microprocessor-based recorders have been developed, the computation power of microprocessors allows for the implementation of many digital ECG signal processing techniques. Perhaps, the most critical use of these computerised ECG systems occurs in the intensive care units (ICU) where the ECG signal processing algorithms must run in real-time. However, there are many other instruments that use such real-time algorithms. These include real-time patient monitoring in ambulatory ECG recording to detect arrhythmia or to monitor effects of cardiac drugs, operating room monitors, and ECG stress systems. Some automated systems work off-line such as, 12-lead off-line ECG signal analysis and Holter tape analysis. Holter technology produces 24 hours recording of the ECG signal of an ambulatory patient using a special tape recorder. A trained technician replays this Holter recording at high speed on a separate device called a Holter scanner, detects the various abnormalities in the ECG signal, and generates a report for the physician. Since the manual scanning of Holter tapes is a boring task and prone to errors from operator fatigue, there have been numerous attempts to automate this process. It is also suggested in recent literature dealing with the design consideration of cardiac pacemakers¹ that the latest generation of these devices employs an ECG analysis capability. These automated systems must do the following, linear and non-linear filtering of the ECG signal, identification of ECG wave components and characterisation points such as the QRS complex, J-point, the ST-segment, the P- and T-waves, see Figure 1.1, then search and detection of abnormalities, if any, and decision-making (Thakor and Zhu 1991).

¹ Pacemakers, are electronic devices that deliver regular short pulses of electricity to promote contraction of the heart muscle in people with a defect in the heart's conduction system (heart block).

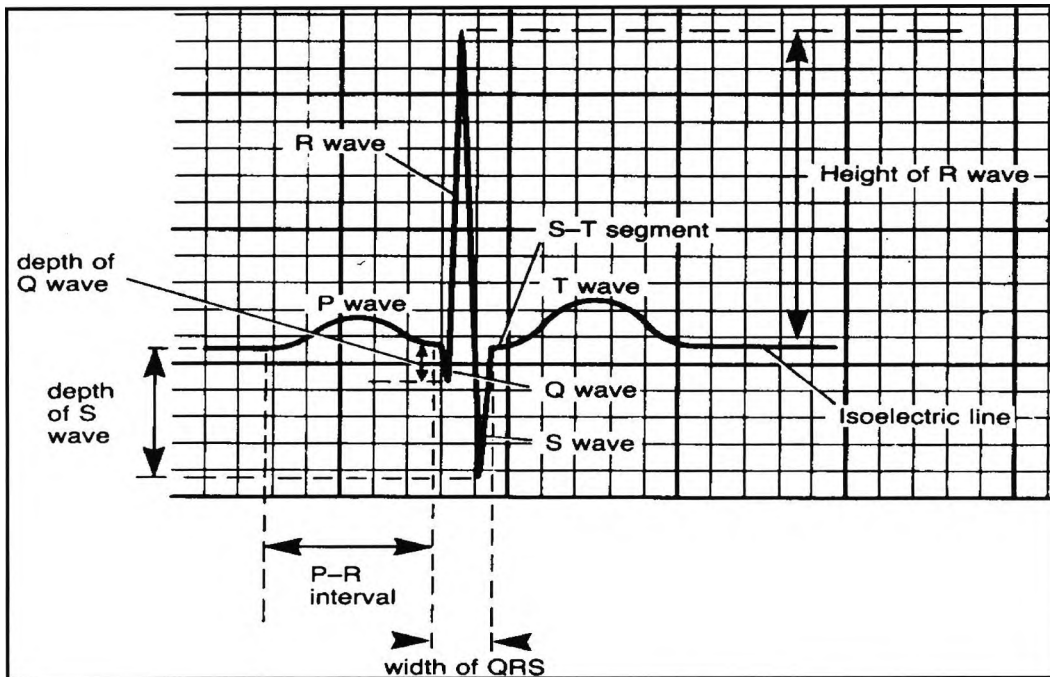


Figure 1.1 Visual illustration of the ECG waveform and its component definitions.

1.2 The Heart

The heart serves as a four-chambered pump for the circulatory system. The main pumping function is supplied by the ventricles. The atria are merely antechambers to store blood during the time the ventricles are in systole. The heart is located in the thoracic cavity, medial to the lungs. Figure 1.2 shows a longitudinal section of the heart and the major arteries and veins (Burke 1985). The upper chambers of the heart, or the atria, have thin walls and a smooth shiny inner surface. The right atrium receives venous blood from the superior and inferior vena cava and sends its blood to the right ventricle. The left atrium receives blood from four pulmonary veins and sends its blood to the left ventricle. The lower chambers of the heart are the ventricles, which have much thicker walls than the atria. The right ventricle sends its blood to the pulmonary artery and to the capillaries of the lungs to be oxygenated. The left ventricle, with walls normally about three times as thick as the walls of the right ventricle, pumps blood into the aorta and to all parts of the body.

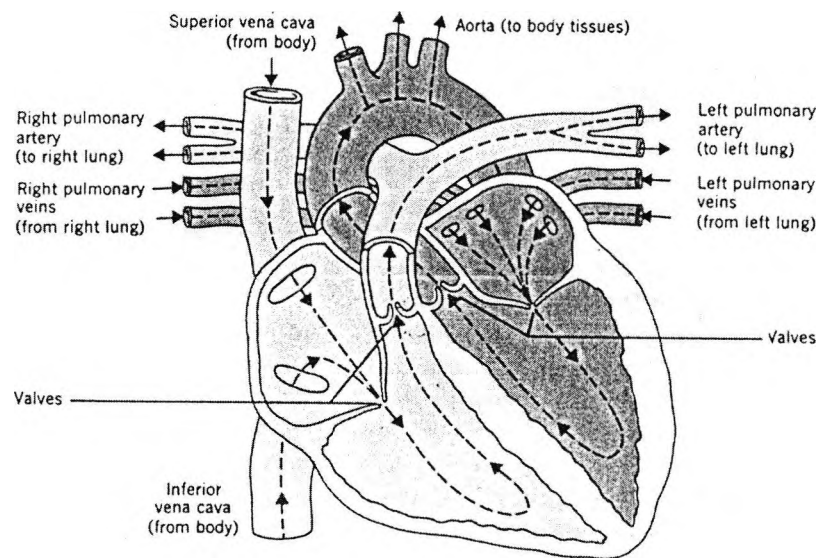


Figure 1.2 Longitudinal section of the heart showing the four chambers and the major arteries and veins as well as the blood flow through the heart (Burke 1985).

1.2.1 Intrinsic Conduction System

The heart has specialised tissue that enables it to contract rhythmically and continuously without any motor. Structures involved in this specialised conducting system are the sinoatrial (SA) node, the atrioventricular (AV) node and the bundle of His, Figure 1.3 shows the conduction system of the heart (Burke 1985). The SA node is the pacemaker that initiates the beat. It sends electrical impulses via the atrial myocardium to the AV node. The AV node sends the impulses to the bundle that branches throughout the walls of the ventricles. Contraction of heart muscle is preceded by electrical changes (depolarisation). The muscle remains depolarised for as long as the heart muscle is contracting. Repolarisation occurs when the heart muscle is relaxed. The voltage variation between contraction and relaxation (i.e., depolarisation and repolarisation) is called an "action potential". During the cardiac cycle, a series of action potentials is produced that are recorded as waves on the ECG. These waves represent different events during the heart cycle. Even though the heart has four chambers, it can be considered, from an electrical point of view, as consisting of only two chambers, since the two atria contract simultaneously and the two ventricles contract simultaneously.

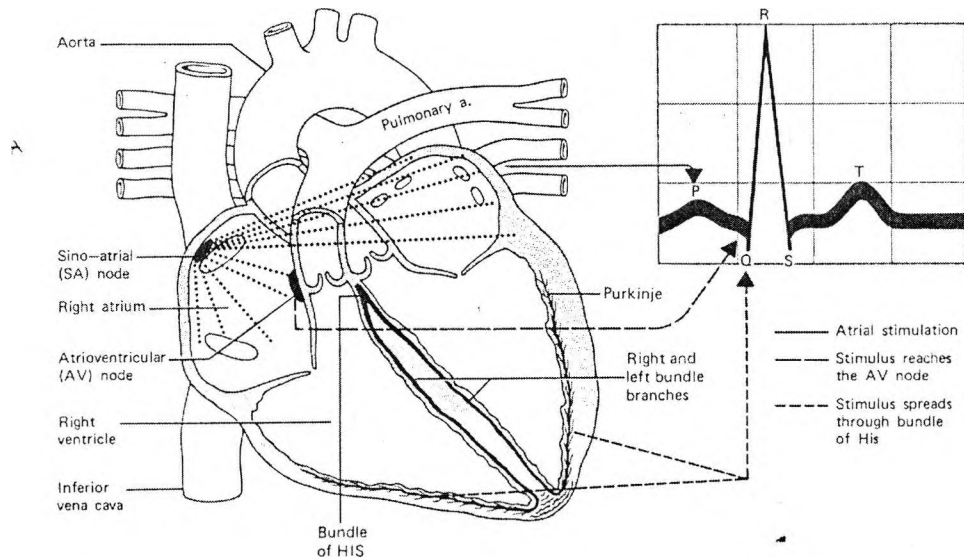


Figure 1.3 A diagrammatic representation of the conduction system of the heart showing the source of the electrical impulses and generation of the ECG signal (Burke 1985).

1.2.2 The Electrocardiogram (ECG) Signal

An electrocardiogram (ECG) is a graphic tracing of the electric current generated by the heart muscle during a heartbeat. One cardiac beat/cycle is one contraction of the heart and the relaxation period that follows, each beat of the normal heart originates in the SA node. The normal heart rate is approximately 70 beats per minute. The ECG signal provides information on the condition and performance of the heart. ECG signals are made by applying electrodes to various parts of the body to lead off the tiny heart current to the recording instrument. The four extremities and the chest wall have become standard sites for applying the electrodes; Figure 1.4 depicts a 12-lead recording of a normal ECG wave (Camm 1998). Standardising electrocardiograms makes it possible to compare them as taken from person to person and from time to time from the same person.

1.2.2.1 Interpretation of the Waveform

The normal electrocardiogram shows typical upward and downward deflections that reflect the alternate contraction of the atria and of the ventricles of the heart. Any

deviation from the normal in a particular electrocardiogram is indicative of a possible heart disorder. The normal ECG waveform in Figure 1.1 has the following components:

- The P-wave is produced by atrial depolarisation. Normal P-wave results from the spread of electrical depolarisation through the atria. Since the muscle mass in the atria is relatively small, the electrical changes accompanying their contraction are also small. Normally atrial depolarisation originates from the SA node; the pacemaker of the heart. The P-wave normally lasts less than 0.11 s and has maximum amplitude of 0.3 mV. The P-wave will be upright in the standard monitor leads. Inverted P-waves indicate that the atria have been depolarised from an unusual site, and not the sinus node.

- The P-R interval represents the time taken for the electrical impulse to reach the ventricles from the atria. The P-R interval is measured from the beginning of the P-wave to the beginning of the QRS complex. It varies from 0.12 s to 0.21 s shorter intervals being seen at faster heart rates. The segment starting from the end of the P-wave to the beginning of the Q-wave (PR-segment) is normally at zero potential and is caused mainly by conduction delay in the AV node. A shortened P-R interval precedes some atrial ectopic beats¹. The P-R interval is increased if there is atrio-ventricular block (Camm 1998; Hampton 1992).

- The QRS complex is produced primarily by the spread of electrical depolarisation through the ventricular muscle. The manifestations of atrial repolarisation are normally masked by the QRS complex. The Q-wave is the first negative deflection. The R-wave is the first positive deflection in the complex. The S-wave is a negative deflection in the complex that follows R-wave. The QRS complex duration is measured from the start of the Q-wave to the end of the S-wave and represents the time taken for ventricular depolarisation. A value of more than 0.12 s is abnormal and usually indicates an intra-ventricular conduction disorder (such as bundle branch block). The individual components of the QRS complex will vary from lead to lead such as that the R- or S-waves may be dominant, or the Q-, R- or S-waves may be missing. Exaggerated QRS complexes may indicate ventricular hypertrophy (enlargement). While small QRS

¹ Ectopic heart beat is a contraction of the heart ventricles occurring prematurely so as to disturb the regular rhythm.

complexes occur when the heart is 'insulated' from the skin by fat or inflated lungs. A pathological Q-wave has a duration of > 0.04 s and associates with a variable loss in the height of the following R-wave (Q-wave is $> 25\%$ of the R-wave height). Pathological Q-waves normally indicate a previous myocardial infarction.

- The Q-T interval represents the total time taken for depolarisation and repolarisation of the ventricles. It is measured from the beginning of the QRS complex to the end of the T-wave. It normally ranges from 0.35 s to 0.45 s and is very rate sensitive, shortening as the heart rate increases (Camm 1998). Q-T interval is prolonged in heart failure, following myocardial infarction.

- The T-wave is produced by ventricular repolarisation and might be assumed to produce a deflection in the opposite direction to the depolarisation wave (QRS) complex. However, repolarisation takes place in the opposite direction to depolarisation (i.e., from epicardium to endocardium), and the T-wave is usually in the same orientation as the preceding QRS complex. Peaked T-waves are a feature of myocardial infarction and ischaemia. T-wave inversion may be seen in numerous conditions including myocardial infarction, ventricular hypertrophy or with bundle branch block. A small positive wave called U-wave is sometimes recorded after the T-wave and it may be due to slow repolarisation of ventricular papillary muscles.

- The ST-segment is measured from the end of the S-wave to the beginning of the T-wave, see Figure 1.1. It represents the period between the end of ventricular depolarisation and the start of ventricular repolarisation. Since after the whole ventricular mass has been depolarised all fibres bear identical charges and no potential difference exists between any two points, ST-segment is normally at zero potential. Displacement of the ST-segment both up and down is common, and may accompany myocardial ischaemia or infarction (Owen, et al. 1968).

1.2.2.2 *ECG Signal Diagnostic Techniques*

The main diagnostic techniques currently used in clinical situation may include:

- ECG at rest for diagnosing chronic cardiovascular diseases,

- Exercise ECG for diagnosing coronary artery disease,
- Continuous ambulatory ECG monitoring for studying arrhythmias,
- Intracardiac ECG (invasive technique) for precise location of the regions of disorders inside the heart.

Finally, the ECG signal has been used extensively over many decades to extract information from patients, these include, for example, disorders of the heart beat (rate and rhythm); conduction defects (time delays between the SA node and the AV node); damage to the myocardium (ischaemia, infarction); atrial and ventricular hypertrophy; and effects of drug intoxication.

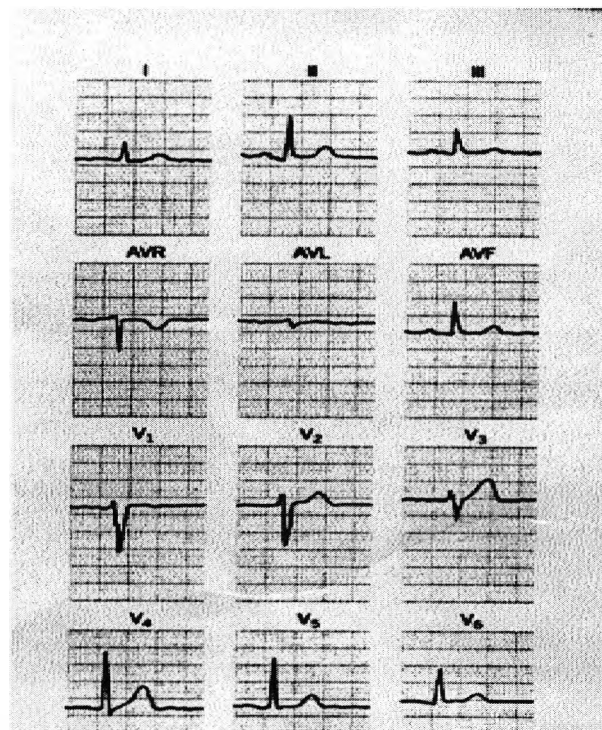


Figure 1.4 A normal 12-lead electrocardiogram (Camm 1998).

1.3 Definitions

Normal Sinus Rate and Rhythm

In normal sinus rhythm, the rhythm is regular and the rate varies between 60 and 100 beat per minute (bpm). Anything less than 60 bpm is known as sinus brachycardia.

Anything more than 100 bpm is known as sinus tachycardia. Neither is necessarily abnormal (Hampton 1992).

The Isoelectric Line (base line)

It is the level of electrical activity between contractions. It includes the ST-segment and the line between the T-wave and the next P-wave (Tompkins 1993), see Figure 1.1.

J-point

It is the first inflection point after the S-point, or may be the S-point itself in certain ECG waveforms (Tompkins 1993).

Myocardial Ischaemia

Myocardial ischaemia occurs when there is an imbalance between the supply of oxygen (and other essential myocardial nutrients) and the myocardial demand for these substances. This most commonly occurs as a result of obstructive coronary disease (Camm 1998). Ischaemia is considered to be a major complication of the cardiac function, and a prime cause for the occurrence of cardiac infarction and dangerous cardiac arrhythmias (Geddes and Cascio 1991). The main characteristic of ischaemia at the cellular level is the depolarisation of the cellular resting membrane potential. This causes a potential difference between the normal and ischaemic tissue which, in turn, causes the flow of an "injury current" (Goldschlager and Goldman 1989). This "injury current" is manifested in the ECG signal by ST-segment depression or elevation and in some cases T-wave inversion, see Figure 1.5.

Myocardial Infarction (MI)

Myocardial infarction is the death and coagulation of part of the heart muscle deprived of an adequate blood supply by coronary artery blockage in a heart attack (Youngson 1992).

Ventricular Tachycardia (VT)

Ventricular tachycardia is a disorder of the heart rhythm in which the contraction of the ventricles is initiated from uncontrolled electrical impulses arising in the ventricles instead of the SA node. Resulting in abnormally fast heart rate between 140 and 220

bpm this may persist for hours or days and may, if not treated, progress to severe heart failure and death (Youngson 1992).

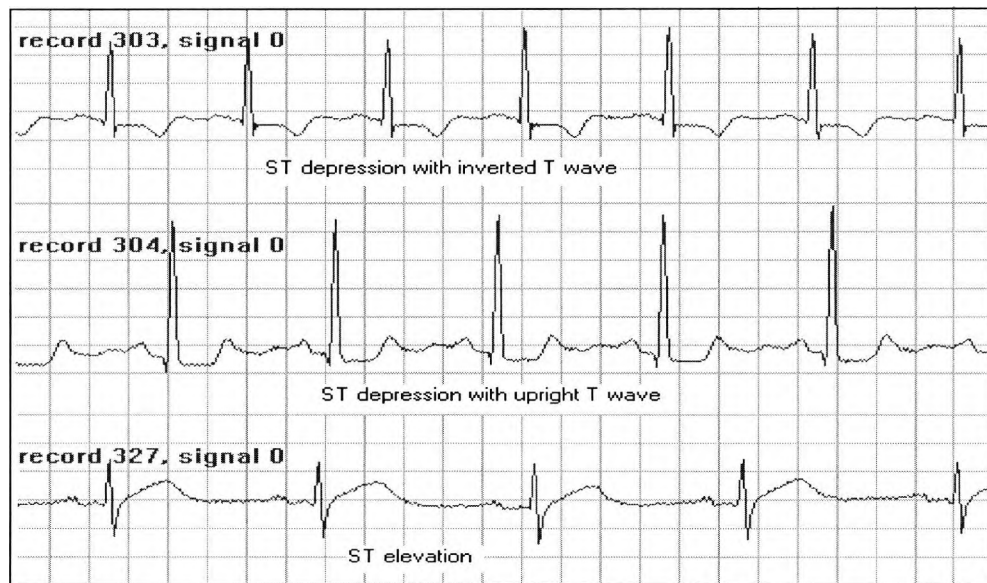


Figure 1.5 Ischaemic ECG signals from the MIT database.

Late Potentials (LPs)

Late potentials are low amplitude, 1-20 μv , high frequency, 40-250 Hz, signals in the terminal part of the QRS complex and ST-segment. LPs reflect irregular propagation of the depolarisation of the myocardium; these signals appear to arise from slowly conducting areas of the myocardium. Many observers have recorded delayed and disorganized activation directly from infarcted myocardium (Michael and Simson 1981). The presence of LPs has been established as a powerful indicator of a subgroup of patients with MI at risk of VT (Breithardt, et al. 1986; Gomis, et al. 1997; Svensson, et al. 1994; Xue and Reddy 1997).

1.4 Previous Work on ECG Signal Processing

A considerable research effort has been made on ECG signal processing and analysis techniques. A brief review will be presented in the following subsections.

1.4.1 Noise Cancellation using Adaptive Filtering

Adaptive filtering techniques have shown to be useful in many biomedical applications. The basic idea behind adaptive filtering has been summarised by Widrow, et al. (1975) and used in a variety of ECG processing applications. One simple but important application of adaptive filtering is the 60-Hz power line interference cancellation (Huhta and Webster 1973); here a reference signal representing power line interference from some part of the body (other than the ECG recording area) may be used to cancel power line interference from the ECG signal. Another application is the fetal ECG signal recording (Widrow, et al. 1975) in which the mother ECG signal is cancelled via chest leads. For a comprehensive study of non-invasive fetal heart monitoring see Zgallai (2002) and references therein. Thakor and Zhu (1991) developed specialized adaptive filter structures for noise cancellation; they also show how an adaptive recurrent filter structure detects cardiac arrhythmias. Their idea is to build an impulse response of the QRS complex and to detect as arrhythmias the signals whose impulse response deviates from normal. This recurrent filter was found to be more suited to applications such as rhythm analysis in ambulatory monitoring and less suited for diagnostic ECG signal analysis.

1.4.2 Detection of ECG Signal Characteristic Points

Detection of the QRS complex is the most important task in automatic ECG signal analysis. The QRS complex detectors are an integral part of modern computerised ECG monitoring systems. A number of QRS detectors have been designed which work in the presence of moderate noise (Hamilton and Tompkins 1986; Pan and Tompkins 1985; Thakor, et al. 1983). An algorithm based on wavelet transform (WT) has been developed for detecting ECG characteristic points (Li, et al. 1995) with multi-scale feature WT, the QRS complex can be distinguished from high P- or T-wave, noise, baseline drift, and artefact. The authors have achieved an average QRS complex detection rate above 99.8% for MIT database records' numbers 100 to 234. However, a less detection rate was achieved for noisy difficult records (105, 108, 203 and 222 which has some non QRS complex with highly unusual morphology). A higher QRS detection rate has been achieved (Xue, et al. 1992) using neural network-based adaptive

matched filtering to model the lower frequencies of the ECG which are inherently non-linear and non-stationary (e.g., the P- and T- waves, additive instrumentation noise and time varying electromyocardiogram noise) the residual which contains mostly higher frequency QRS complex energy is then passed through a linear matched filter to detect the allocation of the QRS complex using this novel approach. The detection rate for a very noisy patient record in the MIT arrhythmia database was 99.5%, which compares favourably to the 97.5% obtained using a linear adaptive whitening filter (Hamilton and Tompkins 1988) and 96.5% achieved with a band pass filtering method (Pan and Tompkins 1985). The highest QRS detection rate (99.99%) that has ever been achieved for noisy difficult records (105, 108 203, 222 which has some non QRS complex with highly unusual morphology) and for very noisy live hospital data, uses sophisticated algorithms developed by Sabry-Rizk and Zgallai (2001) and is patent binding. This method is suitable for online fully automated arrhythmia detection.

A method for ST-segment recognition was proposed by Skordalakis (1986), this method is based on approximating the ST-segment first by a straight line then by a parabola and choosing the approximation with the smaller error norm. A personal computer system for ECG signal ST-segment recognition based on neural networks was developed by Suzuki and Ono (1992). In this system the pre-processor detects the R points and divides the ECG signal into cardiac cycles, then the neural networks address the approximate locations of the J-point and the onset of the T-wave then the ST-segment is recognised as the portion of the ECG signal between these two points.

1.4.3 ECG Signal Dynamics

ECG signal dynamics is concerned with the analysis of the full ECG time series. The concept of cardiac rhythm as a periodic oscillator was challenged in the late 1980s, when research showed the heart to be associated with irregular and possibly chaotic dynamics (Babloyantz and Destexhe 1988). Several investigators have demonstrated that extremely stimulated cardiac tissue develop bifurcation patterns like period doubling or intermittence that are characteristic of non-linear dynamical systems (Chialvo, et al. 1990; Chialvo and Jalife 1987). Other authors hypothesised that the fractal structure of the His-Purkinje system may represent a structure substrate of

chaotic cardiac dynamics (Goldberger and West 1987). Evidence accumulated that strictly periodic cardiac dynamics are not accompanied by a healthy condition but on contrary turn out to be correlated with pathological states (Pool 1989). Fell, et al. (2000) applied the false nearest neighbours method and the saturation of the correlation dimension and suggested that an embedding dimension from 6 to 8 may be regarded suitable for the topological proper reconstruction of ECG signals. Supported by this non-linear nature of the ECG signal, some work has been carried out to extract material from ECG signals for diagnosis of heart disease and assessment of heart function (Mukhopadhyay and Sircar 1996; Zhang, et al. 1997).

1.4.4 Detection of Heart Abnormalities

The cardiac electrical heart activity is studied in order to detect different pathologies. Non-invasive signal processing techniques are utilised to distinguish between normal and abnormal ECG signals. The main categories of the heart disease are; 1) defects in the rhythm and rate (arrhythmia e.g., VT), 2) conduction defects (e.g., bundle-branch block), and 3) defects in the heart muscle (e.g., ischaemic heart disease). Detection of the heart abnormalities is a complex problem, so how further to extract information intensively from the ECG signals for analysis and diagnosis of the heart disease is still a topical subject. Some of the work that has been done in related areas to this research will be introduced in the next section. This will be presented from the medical and signal processing points of view.

1.4.4.1 Detection of MI (using LPs)

Time/Frequency domain-based analysis. Breithardt, et al. (1986); Breithardt, et al. (1991); Simson (1981); and Simson, et al. (1980) used the high-resolution and signal averaged electrocardiography¹ to improve the signal to noise ratio (SNR) and detect LPs. The limitations of this technique are; it removes any beat-to-beat variations from

¹ Signal-averaging is a technique to improve signal to noise ratio. High-resolution ECGs is an ECG recording with an extended bandwidth of up to 1000 Hz.

the signal, and it requires that the LPs signal be present for a considerable number of beats. A non-invasive beat-to-beat detection of LPs based on an adaptive signal enhancer was proposed by Al-Nashash (1989). That study has provided an evident that the adaptive signal enhancer can produce comparable results from a single beat and preserve beat-to-beat variations, however, only ten cases were studied. Schels, et al. (1991) developed a frequency analysis technique using the maximum entropy method (MEM) based on an autoregressive model to detect the LPs from the difference of two MEM spectra of the ST-segment. A sensitivity of 71 % was obtained using the MEM analysis. Meste, et al. (1994) characterise the LPs in time-frequency domain by means of a wavelet transform. That study has illustrated by simulated data and a few real cases that the proposed modified WT improves the analysing qualities of the WT and practically avoids interference problems of the Wigner-Ville transform.

Higher-order statistics/spectra (HOS), the detection of delayed fragmented waveforms or ventricular late potentials (LPs) continuous with the end of the QRS complex during sinus rhythm in post MI subjects has been considered by Speirs, et al. (1993). Bispectral analysis using nonparametric techniques of synthesized ECG data containing LPs was used to identify late signal components terminal in the QRS complex. Usually LPs activity cannot be obtained directly from the raw ST-segment time series, the bispectrum was shown to detect artificially introduced phase coupled features within the segment indicative of non-linearities. However, in real ECG data there is a real possibility of missing such LPs activities due to the LP signal being buried in motion artefact and lack of temporal and spectral resolution, also the LPs activity will not always extend far enough in the ST-segment to be detected (Spaargaren and English 1999). Shifting the signal start point would introduce the high energy QRS component which would saturate the bispectrum thus masking the low level signal activity. It is because of this poor sensitivity (60% (Spaargaren and English 1999)), the bispectrum is only likely to be of limited practical use (Spaargaren and English 1999). For this reason non-linear and non-stationary motion artefact suppressing using adaptive Volterra filter was being deemed necessary to suppress motion artefact (Sabry-Rizk, et al. 1998), this was followed by detection of LPs in the bispectral multiple signal classification (MUSIC) domain to improve frequency resolution over the ST-segment. Temporal resolution was taken care of by using fifteen 60 ms overlapping windows starting from

the R-wave and extending short to onset of P-wave. Sabry-Rizk, et al. (1998) achieved LPs bicoherency detection in a limited number of patients suspected of MI and other heart abnormalities at -70 dB below noise level over a range of frequencies 150-250 Hz.

Neural Networks (NNs), a combination of self-organized and supervised artificial NN models were developed to recognise LPs (Xue and Reddy 1997). The supervised NN-based model was used for classification purposes while the unsupervised one was used for pre-processing. Sensitivity and a specificity of 82 % and 86 %, respectively were obtained using this combination of NNs trained using extended delta-bar-delta learning rule. Sabry-Rizk, et al. (1999b) classified the normal and abnormal ECGs using a backpropagation NN, here slices from the third-order cumulants for limited number of patients have been used as input features. The idea is that the third-order cumulants contains information about quadratic phase coupling associated with LPs at the terminal end of the QRS complex (Sabry-Rizk, et al. 1999b).

1.4.4.2 Detection of Ischaemia

Time domain analysis, the previously mentioned techniques, i.e., the standard and signal-averaged high-resolution ECG signals, have been used by Abboud, et al. (1987) to examine the effects of transient ischaemia on the ECG signal, their methodology was based on cross-correlation analysis to compare the beat-to-beat variability in the ST-T morphology in the surface ECG and in the QRS complex in the signal averaged high-resolution ECG recordings. This technique was found not as sensitive indicator of transient ischaemia as the unipolar intra-coronary ECG, however, it did appear to be non-invasive means of detecting abnormalities (Abboud, et al. 1987). In the last few years many systems have been developed for detection and quantification of ischaemic ST-segment changes. These systems have relied on the analysis of the time domain ST changes during ambulatory ECG signal monitoring. Jager, et al. (1992) applied a two-channel algorithm for robust automated detection of transient ST changes, an ST-segment deviation detection function was calculated. Their algorithm has distinguished between ischaemic ST changes and non-ischaemic ST deviations caused by position-related changes in the electrical axis of the heart. A compartmental multivariate

analysis of exercise ECGs for accurate detection of myocardial ischaemia was developed by Sievanen, et al. (1994). This analysis was heuristically developed by determining a diagnostic criteria, which interrelate a modified ST-segment value and the maximum heart rate slop (ST/HR-slop). The diagnostic accuracy, sensitivity and specificity were 90%, 94%, and 75%, respectively. A system consists of QRS detection, parameter measurement, filtering, baseline drift correction and episode detection was developed and set up using ECG data from the European ST-T database (Taddei, et al. 1995) the authors have found that the interpretation of the ST-T changes a critical issue because many physiologic and technical factors that can alter ST-segment are unrelated to ischaemia.

HOS-based analysis, a pilot study on suspicious polyphase patterns of normal looking ECG signals for diagnoses of coronary artery disease was carried out by Sabry-Rizk, et al. (1999a). Higher-order statistics (HOS) based algorithms were employed to develop discriminant contour patterns in the multi-dimensional phase of the polyspectra (polyphase) of 'normal' looking ECGs in outpatients having weariness and general malaise or chest pain. Similar polyphase patterns have been found in a limited number of ECGs of acute myocardial infarct patients with or without diagnostic ST-segment and T-wave changes. The polyphase computation is done in milliseconds but a temporal window of 10 ECG cycles is necessary in each of the polyspectral averaging process.

NNs-based analysis, In a previous work by Maglaveras, et al. (1998) and Stamkopoulos, et al. (1998) supervised backpropagation and unsupervised Principle Component Analysis (PCA) NN-based algorithms were used for automated detection of ischaemic episodes resulting from ST-segment elevation or depression. The performance of these methods was measured using the European ST-T database. In the backpropagation-based NN the difference between an ischaemic ST-segment template and the normal template was used as input features to the NNs; a hundred and twenty input patterns have been used for training and testing the network. It was found that the average of ischaemic episode detection sensitivity is 88.62 % and that for normal episodes is 91 %. For the PCA-based NN only normal input features were used in the training phase. The results showed that by only using two non-linear components and a training set of 1000

normal samples from each file produce a total classification index of approximately 79.32 % for normal beats and higher than 75.19 % for the ischaemic beats.

1.5 The ECG Data

ECG data from the following sources have been used in this research work:

1- MIT-BIH Arrhythmia database (MIT-DB) (MIT-CD 1997). This database consists of 48 annotated records, obtained using 24-hour Holter tapes. Each record is slightly over 30 minutes in length. Each signal file contains two signals sampled at 360 Hz.

2- ST Change database (ST Change-DB) (MIT-CD 1997). This database consists of 28 records ranging in length from 13 to 67 minutes. Records 300 to 323 were obtained during exercise stress tests. These records exhibit transient ST depression in response to exercise-induced ischaemia. Records 324 to 327 show ST elevation. All signals are sampled at 360 Hz.

3- MIT-BIH Noise Stress Test Database (NST-DB) (MIT-CD 1997). This database consists of 15 thirty-minute records. Three of these records contain noise of the types typically observed in ECG records. They are obtained using a Holter recorder on an active subject, with leads placed so that the subject's ECG signal is not visible.

4- Normal sinus rhythm database (NSR-DB) (MIT-CD 1997). The NSR-DB contains 18 records, each between 20 and 24 hours, from subjects without diagnosed cardiac abnormalities. The sampling frequency is 128 Hz. Since the data files are not provided in the MIT-CD, the author collected this data on a CD-ROM from the MIT archive on the Internet (address <http://www.physionet.com/>).

5- European ST-T database (E-DB) (Taddei, et al. 1992). The E-DB consists of 90 two-channel records; each two hours in duration, taken from ambulatory ECG recordings from 79 subjects. This database is a set of long-term Holter tape recordings and digitised at 250 Hz.

1.6 Aims and Objectives of This Work

The main aim of this work is to first characterise the ECG signals in terms of their higher-order statistics/spectra then the use of this characterisation in the discrimination between normal and abnormal ECG patterns in the higher-order domain. The concerned abnormalities are myocardial ischaemia and infarction. Towards achieving this overall aim, the following specific objectives are addressed; a theoretical study on the nature of the ECG signal and its relation to the physiological conditions of the heart is undertaken. Also practical studies on the dynamics of the signal, its statistical characteristics, its frequency content and the contaminated noise and its filtering techniques are carried out. The second objective of this work is to answer an important question, that is, is it possible to detect ischaemic heart disease without exercise stress test? The third objective is to improve the resolution capability obtainable from the existing methods of bispectrum estimation by devising a novel bispectrum estimation scheme based on the subspace-based MULTIPLE Signal Classification (MUSIC) spectrum. The fourth objective is to build an automated neural network-based classifier and evaluate the use of polyspectrum and polycoherency slices as input features to this classifier.

1.7 Summary

In this chapter a brief description of the structure of the heart and its conduction system was presented. The nature of the ECG signal and its parts (P-wave, QRS complex and T-wave) were defined in terms of the source of generation, duration and amplitude. Then a brief description on the ECG signal diagnostic techniques and their use in abnormality detection was introduced. The next section highlighted some of the work that has been done in the application of different signal processing techniques to the analysis of the ECG signals. The related areas to my work are the ECG signal dynamics and abnormality detection. The different categories of databases that have been used in this work were listed. In the last section an overview of the objectives and aims of this work was presented.

The rest of the thesis will be divided as follows. In chapter 2 the theory of the linear and non-linear adaptive filtering techniques will be presented and the performance of

these filters will be evaluated through their application to filter the ECG signals. In chapter 3 the ECG signal statistical and spectral characteristics will be identified. The spectrum of normal and ischaemic ECG signals will be analysed to detect ischaemic heart disease based on this spectral analysis. The theory, mathematics and characteristics of the higher-order statistics/spectra will be introduced in chapter 4. Cumulant patterns of normal and abnormal ECG signal will be computed and appraised in chapter 4 then the normal ECG signals will be analysed using three bispectrum techniques and the existence of quadratic non-linearity will be investigated. A new bispectrum estimation technique will be introduced and applied to simulation examples and ECG signal in chapter 4. In Chapter 5 an algorithm for calculating the polyspectrum slices will be presented, also a new estimator for the polycoherency index slices, which is based on the estimated polyspectrum slices, will be presented in this chapter. Differences between normal and ischaemic ECG signals in the bispectrum domain will be assessed then the possibility of the existence of higher-order non-linearities will be investigated and evaluated for normal and ischaemic ECG signals using slices from the polyspectrum and polycoherence indices. Chapter 6 introduces an automated NN-based ECG signal classifier using input features from the polyspectrum and polycoherence indices slices. Chapter 7 is a summary of what has been achieved in the field of ECG signal analysis and classification by this thesis. This chapter also suggests the possible extensions that may be worth of further study.

Chapter 2

ADAPTIVE FILTERING OF THE ECG SIGNAL

2.1 Introduction

Many of the existing ECG signal processing techniques require relatively noise-free digitised ECG signals. Data corrupted with noise must either be filtered for moderate SNR or discarded for relatively high noise levels. ECG signal quality assurance requires not only human attention but also necessitates noise detection and elimination schemes, otherwise there would be loss of clinically significant data. These issues are important design consideration for applications in real-time electrocardiogram heart monitoring.

In this chapter several adaptive filter structures are used for noise cancellation. An adaptive filter essentially minimises a prescribed criterion, such as the mean square error (MSE), between a pre-specified desired response and the output of the filter. For noise cancellation applications the filter minimises the MSE between a primary input, which is in this case the noisy ECG signal, and a reference input, which is either noise that is correlated in some way with the noise in the primary input or a signal that is correlated only with ECG signal in the primary input. Three popular Finite Impulse Response (FIR) adaptive filtering algorithms will be described and applied to the ECG signals. A non-linear adaptive filter, namely Volterra filter, is also applied to ECG signals and its performance is appraised.

2.2 Adaptive Finite Impulse Response Filters

FIR filters are routinely used in adaptive filtering applications. Unlike the infinite impulse response filter (IIR), the FIR filter is inherently stable, because its structure

involves the use of forward path only. The presence of feedback path in the IIR filter can make it, if not properly controlled, unstable with the result that the filter oscillates. The inclusion of adaptivity, which brings a stability problem of its own, makes the use of IIR with adaptive algorithms undesirable (Hayes 1996; Haykin 1991).

The design of Wiener filters, which is a class of optimum linear discrete-time filters, requires prior information about the statistics of the data to be processed. However, adaptive filters do not require such information. In the literature the term “adaptive” is usually reserved for the sort of estimation in which the parameters of an adaptive filter are updated from one iteration to the next, the parameters become data dependent which makes it possible for the filter to perform satisfactorily in an environment where complete knowledge of the relevant signal characteristics is not available. Yet, in a stationary environment, we find that after successive iterations of the algorithm it converges to the optimum Wiener solution in some statistical sense. In a non-stationary environment, the algorithm offers a tracking capability, whereby it can track time variations in the statistics of the input data, provided that the variations are sufficiently slow. Another two important advantages of adaptive algorithms for real time applications are their fast operational speed and computational efficiency. Figure 2.1 shows a block diagram of the adaptive transversal filter with adaptive weight-control mechanism (Haykin 1991).

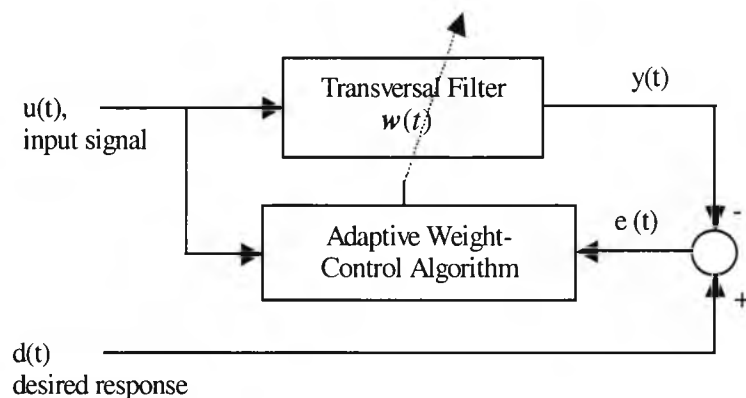


Figure 2.1 Block diagram of the adaptive transversal filter.

The operation of this adaptive filter consists of a combination of two basic processes: (a) an adaptive process, which involves the automatic adjustment of a set of tap weights,

$w(t)$, where t is the discrete time, (b) a filtering process, which involves, forming the inner product of a set of inputs, $u(t)$ and the corresponding set of weights emerging from the adaptive process to produce an estimate of a desired response, $y(t)$. Then generating an estimation error, $e(t)$, by comparing this estimate with the actual value of the desired response, $d(t)$. The estimation error is in turn used to actuate the adaptive process to minimise a specified cost function.

Consider the problem of noise cancellation in which a signal $x(t)$ is observed in the presence of an interfering signal $v(t)$, $u(t) = x(t)+v(t)$. In such applications the desired response is not available; another approach is be considered in which a delayed version of the observed signal is used as the tap input, see Figure 2.2, in this case the adaptive noise canceller takes the structure of a predictor. Suppose $x(t)$ and $v(t)$ are uncorrelated processes and $v(t)$ is random noise, the filter will be adapted to produce an estimate of the predictable part of the signal which is an estimate of the original signal, $x(t)$, (Hayes 1996; Makhoul 1975; Romare 1998).

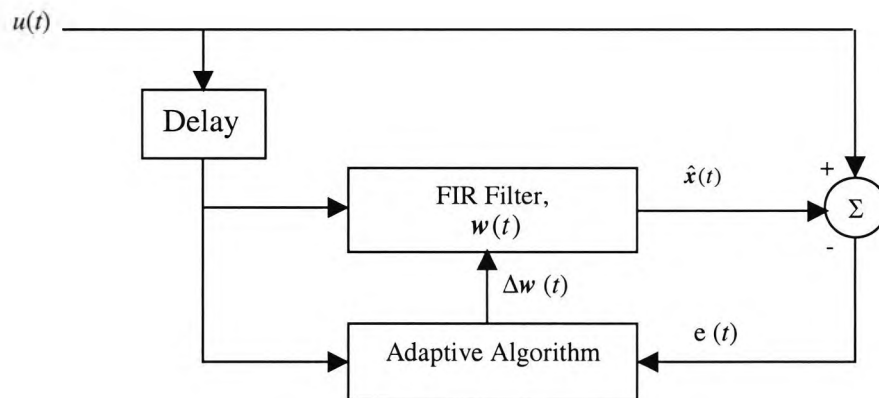


Figure 2.2 Adaptive noise canceller (predictor structure).

With a unit delay the filter uses the input vector $u(t-1)$ containing the previous m samples $[u(t-1), \dots, u(t-m)]^T$ from a tapped-delay line to produce the estimated signal, $\hat{x}(t) = u^T(t-1)\hat{w}(t)$, where $\hat{w}(t)$ is the vector containing the estimated filter coefficients $[\hat{w}_1, \dots, \hat{w}_m]^T$ and T is the transpose operator. The error term $e(t)$, which is theoretically the contaminating noise, between the current sample $u(t)$ and $\hat{x}(t)$ is fed to an adaptive algorithm which updates $\hat{w}(t)$.

2.2.1 The Least Mean Square (LMS) Algorithm

The steepest descent adaptive filter¹, which is a gradient search technique, uses a weight-vector update equation given by:

$$\hat{\mathbf{w}}(t+1) = \hat{\mathbf{w}}(t) + \Delta \mathbf{w} = \hat{\mathbf{w}}(t) + \mu \{-\nabla \xi(t)\} \quad (2.1)$$

where $\hat{\mathbf{w}}(t+1)$ is the weight vector at iteration $t+1$, $\hat{\mathbf{w}}(t)$ is the weight vector at iteration t . $\Delta \mathbf{w}$ is a change in the weights which is proportional to the negative gradient, $\nabla \xi(t)$. The proportionality constant; μ called the step-size and $\xi(t)$ is the Mean Square Error (MSE) defined by:

$$\begin{aligned} \xi(t) &= E[e^2(t)] = E[(d(t) - y(t))^2] \\ &= E[(d(t) - \mathbf{u}^T(t)\hat{\mathbf{w}}(t))^2] \end{aligned} \quad (2.2)$$

where $\mathbf{u}(t) = [u(t), u(t-1), \dots, u(t-m)]^T$

According to the steepest descent method, the weights of the filter assume time-varying form, and their values are adjusted in an iterative fashion along the error surface with the aim of moving them progressively towards the optimum solution. The MSE is a quadratic function of the filter weights, with a unique minimum found by setting the gradient to zero.

$$\frac{\partial E[e^2(t)]}{\partial \hat{\mathbf{w}}} = -2E[\mathbf{u}(t) \cdot (d(t) - \mathbf{u}^T(t)\hat{\mathbf{w}}(t))] = 0 \quad (2.3)$$

This gives the Wiener-Hopf equations (Haykin 1991):

$$\mathbf{R}_{uu} \cdot \hat{\mathbf{w}} = \mathbf{R}_{du} \quad (2.4)$$

where \mathbf{R}_{uu} is the autocorrelation matrix of the filter input vector and \mathbf{R}_{du} is the cross-correlation vector between the current sample $d(t)$ and the filter input vector.

¹ It is an iterative procedure for obtaining the parameters that minimise a function. At each iteration of the steepest descent procedure, the values of the parameters (weights) are modified in the direction in which the error function decreases most rapidly.

The LMS algorithm (Hayes 1996; Widrow, et al. 1975) is a stochastic implementation of the method of the steepest descent. When the filter operates in an unknown environment, the exact measurements of the gradient vector are not possible since this requires a prior knowledge of both \mathbf{R}_{uu} and \mathbf{R}_{du} . Consequently, the Widrow-Hoff algorithm (Widrow, et al. 1975) uses an instantaneous estimation of the gradient:

$$\hat{\nabla}E[e^2(t)] = -2\mathbf{u}(t)e(t) \quad (2.6)$$

Hence the LMS adaptation rule is:

$$\hat{\mathbf{w}}(t+1) = \hat{\mathbf{w}}(t) + 2\mu\mathbf{u}(t)e(t) \quad (2.6)$$

with the initial condition $\mathbf{w}(1) = 0$. The constant μ is an amplification factor which controls the rate of descent or convergence. The performance of the LMS is heavily dependent on the choice of the step-size μ , which sets a compromise between the rate of convergence of the weights and the excess MSE or misadjustment after convergence (Haykin 1991; Widrow, et al. 1976). With small μ the descent towards the bottom of the error surface is slow but smooth, leaving a small amount of noise in the weights and a small gradient error after convergence. With μ large the rate of descent is faster but leaves a higher gradient error. If μ is too large the algorithm may become unstable.

2.2.2 The Least Mean Fourth (LMF) Algorithm

A general class of steepest descent algorithms for adaptive filtering which allow error minimisation in the mean fourth, mean sixth, etc., sense has the following weight update rule (Walach and Widrow 1984):

$$\hat{\mathbf{w}}(t+1) = \hat{\mathbf{w}}(t) + 2\mu k e^{2k-1}(t)\mathbf{u}(t) \quad (2.7)$$

where $2k$ is the exponent of the error being minimised. Both the LMS and LMF algorithms can be viewed as special cases of the general algorithm.

For the LMF algorithm $k=2$ hence the weight update rule becomes:

$$\hat{\mathbf{w}}(t+1) = \hat{\mathbf{w}}(t) + 4\mu e^3(t)\mathbf{u}(t) \quad (2.8)$$

The behaviour of the LMF algorithm is of special interest, since under some circumstances, it will have substantially lower weight noise than the LMS algorithm.

2.2.3 The Kalman Algorithm

The Kalman filter is a member of the optimum linear discrete-time filters. The distinctive features of the Kalman filter is that its mathematical formulation is described in terms of state-space concepts and its solution is computed recursively (Kalman 1960; Kalman and Bucy 1961). The system under observation is represented by a general multi-dimensional dynamic model defined in state-space form by the process and the measurement equations:

$$\mathbf{x}(t+1) = \Phi(t+1,t)\mathbf{x}(t) + \mathbf{v}_1(t) \quad (2.9)$$

$$\mathbf{y}(t) = \mathbf{C}(t)\mathbf{x}(t) + \mathbf{v}_2(t) \quad (2.10)$$

where $\mathbf{x}(t)$ and $\mathbf{y}(t)$ are the state and measurement vectors, $\Phi(t+1,t)$ is the state-transition matrix relating the states of the system at time t to the states at time $t+1$, $\mathbf{C}(t)$ is the measurement matrix relating the states at time t to the observation at time t , and $\mathbf{v}_1(t)$ and $\mathbf{v}_2(t)$ are the process and measurement noise vectors, respectively, usually assumed to be mutually independent, zero-mean and white with covariance matrices

$$E\{\mathbf{v}_i(t)\mathbf{v}_i^T(j)\} = \begin{cases} \mathbf{Q}_i(t), & t = j \dots i = 1, 2 \\ 0, & \dots \dots \dots t \neq j \end{cases} \quad (2.11)$$

The filtering problem can be formulated using the Kalman algorithm based on the one-step prediction technique (Haykin 1991). For the ECG signal this is obtained by using a dynamic Auto-Regressive (AR) model driven by the measurement noise.

$$u(t) = \mathbf{u}^T(t-1)\hat{\mathbf{w}}(t) + v(t) \quad (2.12)$$

Equation (2.12) may be viewed as the measurement equation of the AR model. With the non-stationarity of the output attributed to the variation of the system parameters

with time according to the first order Markov process¹ (Zhang and Haykin 1983), the process equation of the AR model is.

$$\hat{w}_i(t+1) = \phi_i(t)\hat{w}_i(t) + \delta w_i(t), \quad i = 1, 2, \dots, m \quad (2.13)$$

where the ϕ_i and δw_i terms account for deterministic and random fluctuations, respectively. Putting Eq. (2.13) into matrix form gives

$$\hat{\mathbf{w}}(t+1) = \Phi(t)\hat{\mathbf{w}}(t) + \delta \mathbf{w}(t) \quad (2.14)$$

Eqs. (2.12) and (2.14) are state-space equations for the time-varying AR process. If no priory information is available on the ϕ_i terms, these are usually set to a constant $\beta \leq 1$ for all i and t , simplifying the state-transition matrix to $\beta \mathbf{I}$ (Romare 1998). The δw_i terms can also be assumed to be mutually independent, zero-mean white process with constant variance q and diagonal covariance matrix $q \mathbf{I}$ (Godard 1974). The variance of measurement noise, $v(t)$, can be estimated using the following adaptive procedure (Arnold, et al. 1998):

$$\begin{aligned} e(t+1) &= u(t+1) - \mathbf{u}^T(t)\hat{\mathbf{w}}(t) \\ \sigma_e^2(t+1) &= \sigma_e^2(t) - c \cdot (\sigma_e^2(t) - e^2(t+1))^2 \end{aligned} \quad (2.15)$$

where $e(t+1)$ is the prediction error, and the adaptation constant $0 < c < 1$ determines the speed of adaptation.

A flow chart for the prediction of the ECG signal with the Kalman filter is given in Figure 2.3. $\mathbf{K}(t, t-1)$ is the $(m \times m)$ covariance matrix of the predicted error vector in the states, i.e., $\hat{\mathbf{w}}(t) - \hat{\mathbf{w}}(t-1)$. By minimising the trace of this matrix recursively the optimum estimate of the time varying state-vector is determined. $\mathbf{G}(t)$ is the Kalman gain vector at time t .

¹ A random vector $w(t)$ is called Markov of first order, or simply Markov, if its conditional joint probability density function conditioned on all past values is the same as using the value in the immediate past.

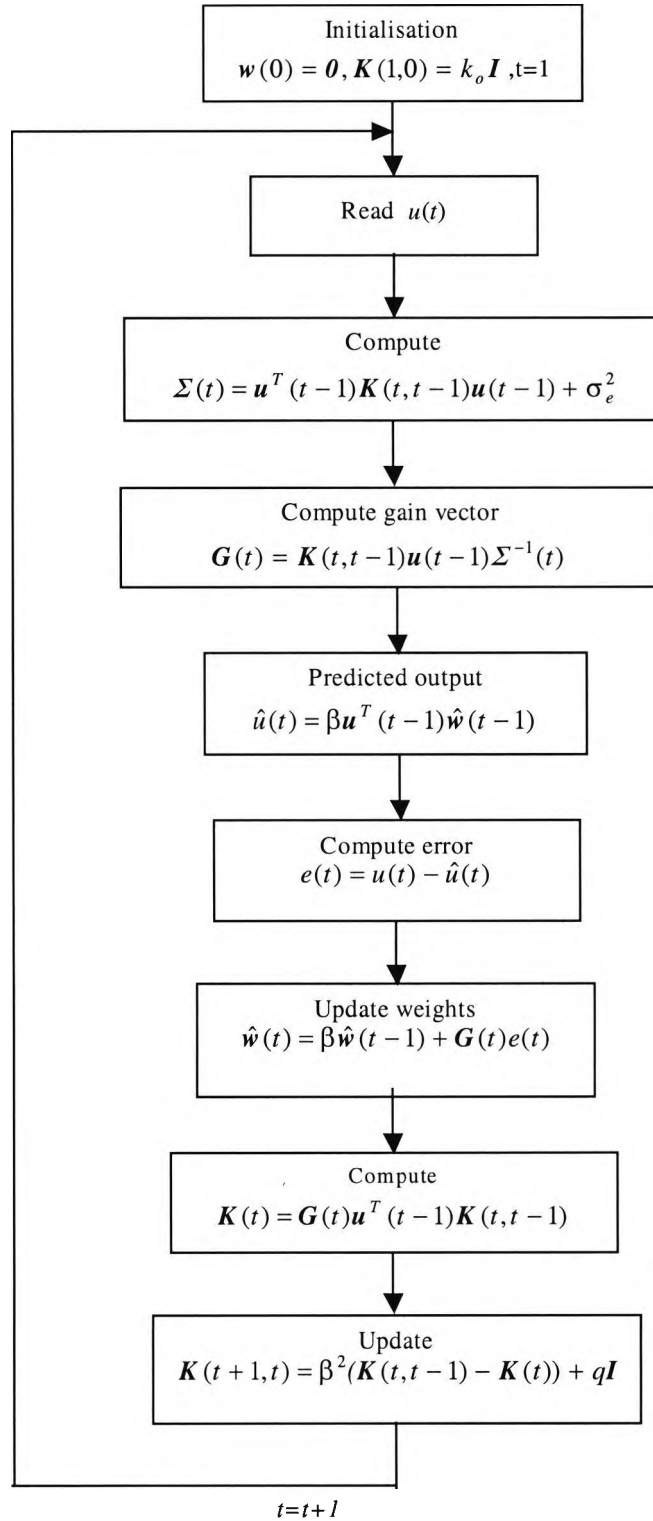


Figure 2.3 Flow chart for the adaptive Kalman predictor.

2.3 Adaptive Non-linear Filter

The concept of optimum linear filtering has had enormous impact on the recent development of various techniques to estimate and process stationary time series. The obvious advantage of a linear filter is its simplicity in design and implementation. However, in some cases, i.e., where the signal to be filtered or predicted is non-linear, the performance of a linear filter may be unacceptable because the linear predictor will only exploit the first and the second statistical moments of the signal and ignore the higher order moments. As a consequence useful information about the signal will be lost. One constructive and versatile approach to non-linear filters is to utilise the filter structure in the form of a Volterra series (Koh and Powers 1985; Schetzen 1980).

2.3.1 Second-order Volterra Filters (SVF)

The second-order Volterra filter, Figure 2.4, consists of a parallel combination of linear and quadratic filters (Davila, et al. 1987).

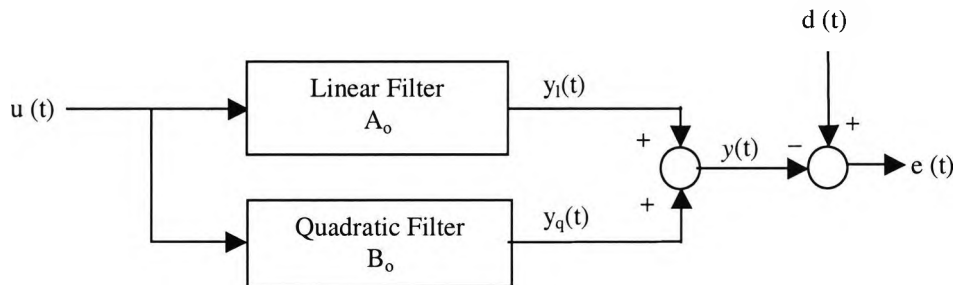


Figure 2.4 Second-order Volterra filter.

The second-order Volterra filter has the form:

$$y(t) = h_o + \sum_{i=0}^{m-1} a(i)u(t-i) + \sum_{i=0}^{m-1} \sum_{j=0}^{m-1} b(i, j)u(t-i)u(t-j), \quad (2.16)$$

$$\text{where } h_o = \sum_{i=0}^{m-1} \sum_{j=0}^{m-1} b(i, j)r_u(i-j)$$

In the matrix form this will be:

$$y(t) = \mathbf{A}^T \mathbf{u}(t) + \text{tr}[\mathbf{B}[\mathbf{u}(t) \mathbf{u}^T(t) - \mathbf{R}_{uu}]] \quad (2.17)$$

where $\mathbf{u}(t)$ is the input vector, \mathbf{A} is $(m \times 1)$ linear weight vector and \mathbf{B} is the $(m \times m)$ quadratic weight matrix, they represent the linear and the quadratic contributions of the input signal, respectively. T and tr denotes the transpose and trace operators, respectively, and $[\mathbf{R}_{uu}]_{i,j} = E[u(j-i)u(t-j+i)]$ denotes the autocorrelation matrix of $u(t)$.

$$\mathbf{A} = [a(0), a(1), \dots, a(m-1)]^T \quad (2.18)$$

$$\mathbf{B} = \begin{bmatrix} b(0,0) & \dots & b(0,m-1) \\ \dots & \dots & \dots \\ \dots & \dots & \dots \\ b(m-1,0) & \dots & b(m-1,m-1) \end{bmatrix} \quad (2.19)$$

It is assumed that the quadratic filter weights are symmetric, i.e., $b(i,j) = b(j,i)$. Given the zero-mean discrete-time, stationary, jointly Gaussian random processes $u(t)$ and $d(t)$, it can be shown that the optimum linear and quadratic filter weights which minimise the MSE are given by Davila, et al. (1987); Koh and Powers (1985):

$$\mathbf{A}_o = \mathbf{R}_{uu}^{-1} \mathbf{R}_{du} \quad (2.20)$$

$$\mathbf{B}_o = (1/2) \mathbf{R}_{uu}^{-1} \mathbf{Z}_{du} \mathbf{R}_{uu}^{-1} \quad (2.21)$$

where $\mathbf{R}_{du} = [r_{du}(0), \dots, r_{du}(m-1)]^T$

$$\mathbf{Z}_{du} = \begin{bmatrix} z_{du}(0,0) & \dots & z_{du}(0,m-1) \\ \dots & \dots & \dots \\ \dots & \dots & \dots \\ z_{du}(m-1,0) & \dots & z_{du}(m-1,m-1) \end{bmatrix} \quad \text{and}$$

$$r_{du}(j) = E[d(t)u(t-j)], \quad (2.22)$$

$$z_{du}(j,i) = E[d(t)u(t-j)u(t-i)] \quad (2.23)$$

2.3.2 Adaptive Second-order Volterra Filter

Several LMS-type adaptive algorithms have been described which attempt to recursively compute \mathbf{A}_o and \mathbf{B}_o (Coker and Simkins 1980; Koh and Powers 1985).

These algorithms have the general form:

$$e(t) = d(t) - \mathbf{u}^T(t)\mathbf{A}(t) - \mathbf{u}^T(t)\mathbf{B}(t)\mathbf{u}(t) \quad (2.24)$$

$$\mathbf{A}(t+1) = \mathbf{A}(t) + \mu_a \mathbf{u}(t)e(t) \quad (2.25)$$

$$\mathbf{B}(t+1) = \mathbf{B}(t) + \mu_b \mathbf{u}(t)\mathbf{u}^T(t)e(t) \quad (2.26)$$

where μ_a and μ_b are the step-sizes for linear and quadratic parts of the filter, respectively. With $0 < \mu_a < \lambda_{\max}^{-1}$ and $0 < \mu_b < \lambda_{\max}^{-2}$ (Koh and Powers 1985).

These parameters may also be updated using adaptive the Kalman algorithm described in section 2.2. In this case Eqs. (2.25) and (2.26) will be:

$$\mathbf{A}(t+1) = \mathbf{A}(t) + \mathbf{G}_a(t)e(t) \quad (2.27)$$

$$\mathbf{B}(t+1) = \mathbf{B}(t) + \mathbf{G}_b(t)e(t) \quad (2.28)$$

where $\mathbf{G}_a(t)$ and $\mathbf{G}_b(t)$ are the Kalman gain for the linear and the quadratic parts of Volterra filter at time t , respectively

2.3.3 Adaptive Third-order Volterra Filter

The LMS- and the Kalman-based algorithms may be extended to estimate the linear, quadratic and cubic kernels of the third-order Volterra filter. From Figure 2.5, the error signal is defined as

$$e(t) = d(t) - y(t),$$

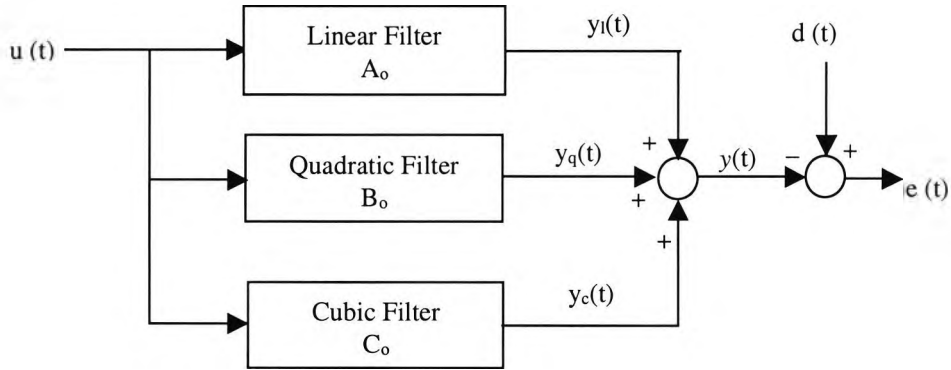


Figure 2.5 Cubic Volterra filter.

where

$$\begin{aligned}
 y(t) &= \sum_{i=0}^{m-1} a(i)u(t-i) + \sum_{i=0}^{m-1} \sum_{j=0}^{m-1} b(i,j)u(t-i)u(t-j) + \\
 &\quad \sum_{i=0}^{m-1} \sum_{j=0}^{m-1} \sum_{k=0}^{m-1} c(i,j,k)u(t-i)u(t-j)u(t-k) \\
 &= \mathbf{u}_l^T(t)\mathbf{A}(t) + \mathbf{u}_q^T(t)\mathbf{B}(t) + \mathbf{u}_c^T(t)\mathbf{C}(t)
 \end{aligned} \tag{2.29}$$

and $\mathbf{u}_q(t) = \mathbf{u}_l(t) \otimes \mathbf{u}_l(t)$, $\mathbf{u}_c(t) = \mathbf{u}_l(t) \otimes \mathbf{u}_q(t)$

The symbol \otimes indicates the Kronecker product of vectors (Sicuranza 1992). $\mathbf{B}(t)$ is m^2 vector containing the quadratic kernels and $\mathbf{C}(t)$ is m^3 vector containing the cubic kernels.

2.4 Model Order Selection

The best choice of the filter order, m , is not generally known a priori and it is usually necessary to postulate several model orders. Based on this, one then computes some error criteria that indicate which model order to choose (Marple 1987). Three well-known criteria are combined here to choose m , these will be described briefly:

Akaike Information Criteria (AIC) The AIC determines the model order by minimising an information theoretic function (Akaike 1969):

$$AIC(m) = N \ln(\hat{\rho}_m) + 2m \quad (2.30)$$

where N is the number of data samples and $\hat{\rho}_m$ is the estimated white noise variance, the linear prediction error variance will be used for this estimate, $\hat{\rho}_m = \sum_t |e_m(t)|^2$.

An extended version of the AIC criteria, that can handle the problem of the signal and noise subspaces separation, can be calculated directly from the eigen-values of the autocorrelation matrix or singular values of the data matrix of the given signal as follows (Marple 1987):

$$AIC(m) = (L - m) \ln \left[\frac{(\frac{1}{L-m}) \sum_{i=m+1}^L \lambda_i}{\prod_{i=m+1}^L \lambda_i^{-(L-m)}} \right] + m(2L - m) \quad (2.31)$$

where $L > m$: is the size of the data matrix, $\lambda_0 > \lambda_1 > \dots > \lambda_L$ are the eigen-values of the sample autocorrelation matrix.

Minimum Description Length (MDL) Criteria

MDL is defined as (Rissanen 1983):

$$MDL(m) = N \ln(\hat{\rho}_m) + m \cdot \ln(N) \quad (2.32)$$

As the probability of error in choosing the correct order in the AIC does not tend to zero as $N \rightarrow \infty$, the *MDL* criteria is said to be more statistically consistent than the AIC.

Final Prediction Error (FPE)

This criterion selects the order of the AR process so that the average error variance for a one-step prediction is minimised. It is defined as (Akaike 1969):

$$FPE(m) = \hat{\rho}_m \left(\frac{N + (m + 1)}{N - (m + 1)} \right) \quad (2.33)$$

Since these criteria may or may not work well with real data, depending on how well such data are modelled by an AR process and on whether the noise is Gaussian or not, they may be used as guide lines for initial order selection.

A particular quality measure of the filter order that is used here is the MSE defined by Mulgrew and Mclaughlin (1994). This will be useful in two ways, firstly to choose a model order from the range estimated by the above mentioned criteria. Secondly the value of the MSE will be used to compare the performance of the adaptive predictors.

$$MSE_{dB} = 10 \log_{10} \left[\frac{\sum_{t=m+1}^N e^2(t)}{\sum_{t=m+1}^N x^2(t)} \right] \quad (2.34)$$

2.5 Signal-to-Noise Ratio

In simulation studies the signal-to-noise ratio (SNR) is calculated using the following relation (Haykin 1983)

$$SNR = \frac{E[x^2]}{E[v^2]} \quad (2.35)$$

where $E[x^2]$ and $E[v^2]$ are the mean square value of the signal and the noise, respectively. In real signal applications, it is difficult to separate the signal from the noise. Stokes, et al. (1999) defined the SNR from the singular values of a rectangular data matrix, \mathbf{R}_x , constructed for a cyclic or quasi-periodic data as follows

$$\mathbf{R}_x = \begin{bmatrix} x(1) & x(2) & \dots & x(l_f) \\ x(l_f + 1) & x(l_f + 2) & \dots & x(2l_f) \\ \dots & \dots & \dots & \dots \\ \dots & \dots & \dots & \dots \\ x((L-1)l_f + 1) & x((L-1)l_f + 2) & \dots & x(Ll_f) \end{bmatrix} \quad (2.36)$$

where each row in this matrix contains one period of the signal, l_f is the fundamental period length, which is defined by Stokes, et al. (1999) as the smallest of the most frequently occurring stride-cycles, and L is the number of periods used for calculating this matrix. Applying the SVD to this matrix the SNR can be calculated as follows.

$$SNR = \frac{\sum_{i=1}^p s_i^2}{\sum_{i=p+1}^{l_f} s_i^2} \quad (2.37)$$

where $s_i, i=1,2,\dots,l_f$ are the singular values of \mathbf{R}_x and p is number of dominant singular values, which theoretically constitute the signal subspace and the sum squares of these p singular values represent the energy content of the signal. For strictly periodic process with no noise the total energy is s_f^2 (Stokes, et al. 1999).

2.6 Noise Artefacts in ECG Signals

Electrocardiogram (ECG) signals may be corrupted by various kinds of noise and artefact. Typical examples are (Friesen, et al. 1990):

1. Power line interference, the source of this interference is the ac line potential (50 Hz in the UK or 60 Hz in USA).
2. Electrode contact noise; is transient interference caused by loss of contact between the electrode and skin, which effectively disconnect the measurement system from the subject.
3. Motion artefacts (MA); are transient baseline changes caused by changes in the electrode-skin impedance as a result of patient movement.
4. Muscle contractions (EMG), cause artefactual millivolt-level potentials to be generated. These signals can be assumed to be transient bursts of zero-mean band-limited Gaussian noise.

5. Baseline wander (BW), which is mainly due to ECG signal amplitude modulation with respiration.

Frequencies in the range of 0-0.5 Hz should be removed to reduce baseline drift (Aase, et al. 2000; Ahlstrom and Tompkins 1985; Marques 1982) which is simply accomplished by using a conventional high pass filter. Power line interference can be removed either by conventional filtering (Huhta and Webster 1973) or adaptively (Sahakian and Furno 1983). The basic idea behind ECG signal adaptive filtering has been summarised by Widrow, et al. (1975) and used by Thakor and Zhu (1991), Yelderman, et al. (1983) for ECG signal enhancement, noise cancellation and arrhythmia detection. Since both the EMG and MA noises are non-stationary, and the EMG has a frequency spectrum that may overlap that of the ECG signal (Thakor, et al. 1984), Thakor and Zhu 1991 recommended the use of adaptive filtering techniques for removal of these artefacts.

2.7 Results

To quantify the performance of the aforementioned adaptive filter techniques in terms of noise cancellation in the ECG data, these algorithms have been applied to two categories of the ECG databases; the MIT-DB and the ST Change-DB (MIT-CD 1997). The data are first pre-processed to eliminate the baseline wander using a standard first-order high pass filter (HPF) with cut-off frequency 0.5 Hz (Aase, et al. 2000; Ahlstrom and Tompkins 1985; Marques 1982). Figure 2.6 shows the result obtained after applying this filter to record No. 101 (MIT-DB).

There are two problems that have to be addressed here; the first one is the non-stationarity of the ECG data when considering a time scale larger than the beat-to-beat interval (Waldo and Chitrapu 1991). The second is that, the centre frequencies of the P- and T-waves are on the lower frequency side of the ECG spectrum and that of the R-wave is in the higher frequency side of that spectrum. Therefore, if a constant-coefficient filter is used with a high cut-off frequency, only partial noise cancellation would be achieved, making it difficult to extract the P- and T-waves. Reducing the cut-off frequency will reduce the noise content but distortion of the ECG signal may occur

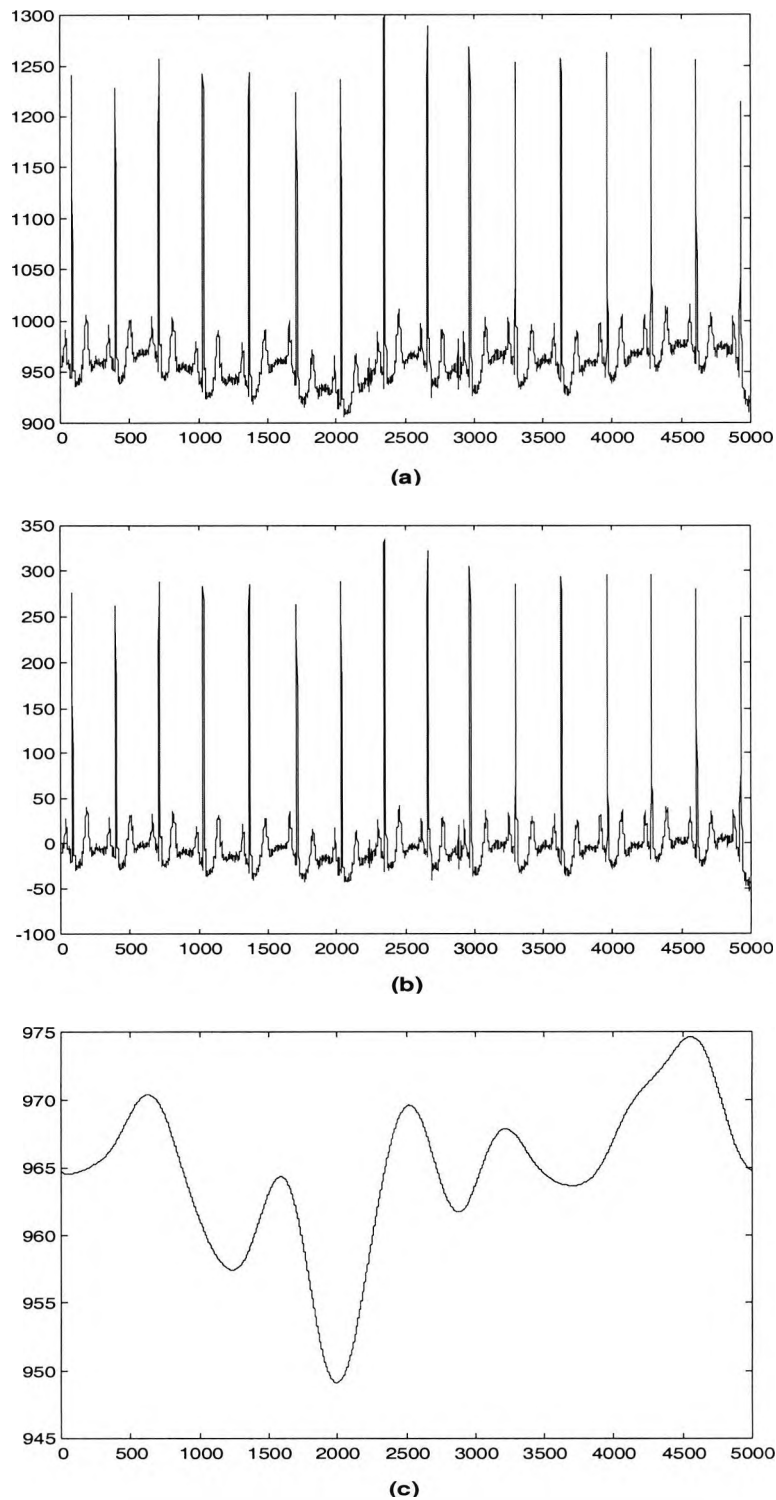


Figure 2.6 Results obtained using the baseline wander filter: (a) the original ECG signal with baseline wander from record No. 101 (MIT-DB), (b) the filtered ECG signal, and (c) the baseline noise removed from the ECG signal.

as the R-wave starts to be filtered. A well-designed adaptive filter can track all of the P-, R-, and T-waves if the degree of non-stationarity is not too high (Sabry-Rizk, et al. 2000b), i.e., if the frequency variations are sufficiently slow relative to the speed of adaptation of the filter coefficients.

2.7.1 Linear Predictors

In this section the performance of LMS, LMF and the Kalman predictors are compared using four records from the MIT-DB and ST Change-DB (MIT-CD 1997), namely No. 100, No. 101, No. 300 and No. 325. The AIC criteria represented by Eqs. (2.30) and (2.31), the MDL criterion described by Eq. (2.32) and the FPE in Eq. (2.33) are used, as the basis to select the filter order. As shown in Figure 2.7, an order between 11 and 15 can be used for minimum AIC, MDL and FPE. This result comes in agreement with the results obtained by Niranjana and Murthy (1993). As a final guide, the MSE value Eq. (2.34) and the execution time (CPU time) are calculated as a function of the model order for the LMS predictor as shown in Figure 2.7 (e), (f). The MSE is minimum at $m=14$, while the CPU time increases with the model order.

Figure 2.8 depicts the performance of LMS (LHS) and LMF (RHS) predictors ($m = 14$, $\mu = 0.3$ and 0.9 for LMS and LMF, respectively) for records No. 101 (a), (b), No. 300 (c), (d) and No. 325 (e), (f). In each of (a), (b), (c), (d), (e) and (f) the output is shown in the top panel and the squared error is shown in the bottom panel. The LMS predictor shows smaller error and faster convergence. The minimum MSE errors obtained are 0.048 (-13.17 dB) and 0.08 (-10.85 dB) for LMS and LMF predictors, respectively.

The tracking performance of an adaptive filtering algorithm is influenced not only by the rate of convergence (which is a transient characteristics) but also by the fluctuation in the steady-state performance of the algorithm due to the measurement and algorithm noise (Haykin 1991). Considering the tracking capability of the two algorithms, Figures 2.8 (a), (b) can be used as good examples to explain this issue. The input to the adaptive predictor which is the ECG signal (record No. 101), see Figure 2.6, shows a change in the amplitude at sample number 2000 onwards. This means a change in the mean value; this represents a non-stationary behaviour of the signal. In response to that

both the LMS and LMF algorithms are automatically tuned to minimise the misadjustment at the filter output, which resulted in a slight increase in the steady-state error value. Since the increase in the steady-state error is smaller for the LMS than the LMF algorithm, the former is found to have better tracking performance.

Figure 2.9 shows the MSE values with different values of the step-size for both the LMS and LMF predictors from which we recognise that the step-size stability range for the LMF is wider than that of the LMS. The Figure also shows that the percentage misadjustment, which is the difference between the minimum MSE obtained by Wiener filter and the one obtained by the LMS method, increases with the step-size, in the mean time the convergence time decreases with the step-size, so one has to carefully choose the step-size that matches the filtering requirements.

The Kalman predictor in Figure 2.10 outperforms both the LMS and LMF predictors from the points of view of the convergence time and the squared error. The best performance is achieved with the parameters q and β set to zero and one, respectively. Optimised parameters of model order $m=5$, an adaptation constant $c=0.01$ and an initial value of the covariance matrix $k_0=0.01$ are used for the predictor in Figure 2.10. The limitation of the Kalman predictor is the computation time. The mathematical complexity included in the Kalman algorithm makes its computation time longer than either of the LMS or the LMF (Kalman takes about 2.5 s/4500 samples and LMS takes 3×10^{-2} s/4500 samples for a filter order of 5 running on a UNIX machine). The minimum MSE obtained by the Kalman predictor is 0.0057 (-22.4 dB). The tracking performance for both the LMS and LMF algorithms in Figures 2.8 (a), (b) is better than that of the Kalman predictor in Figure 2.10 (a). This is because the relatively high increase in the steady-state error value at sample 2000 onwards compared to its original value for the Kalman predictor.

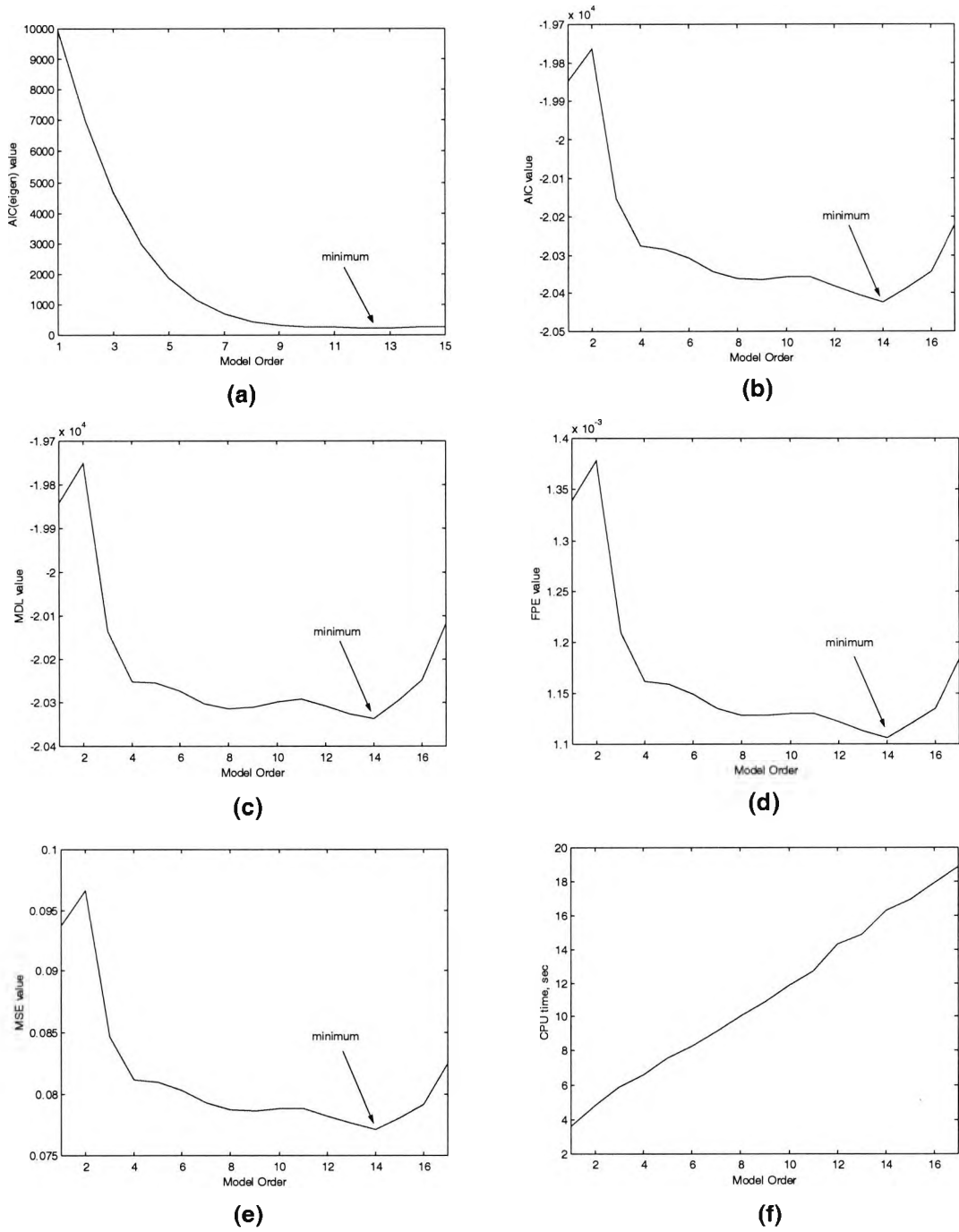


Figure 2.7 Filter order selection using the AIC criterion and its extension (b, a), respectively, MDL criterion (c) and FPE (d). (e) is the MSE, and (f) is the CPU time. Using record No. 100 (MIT-DB).

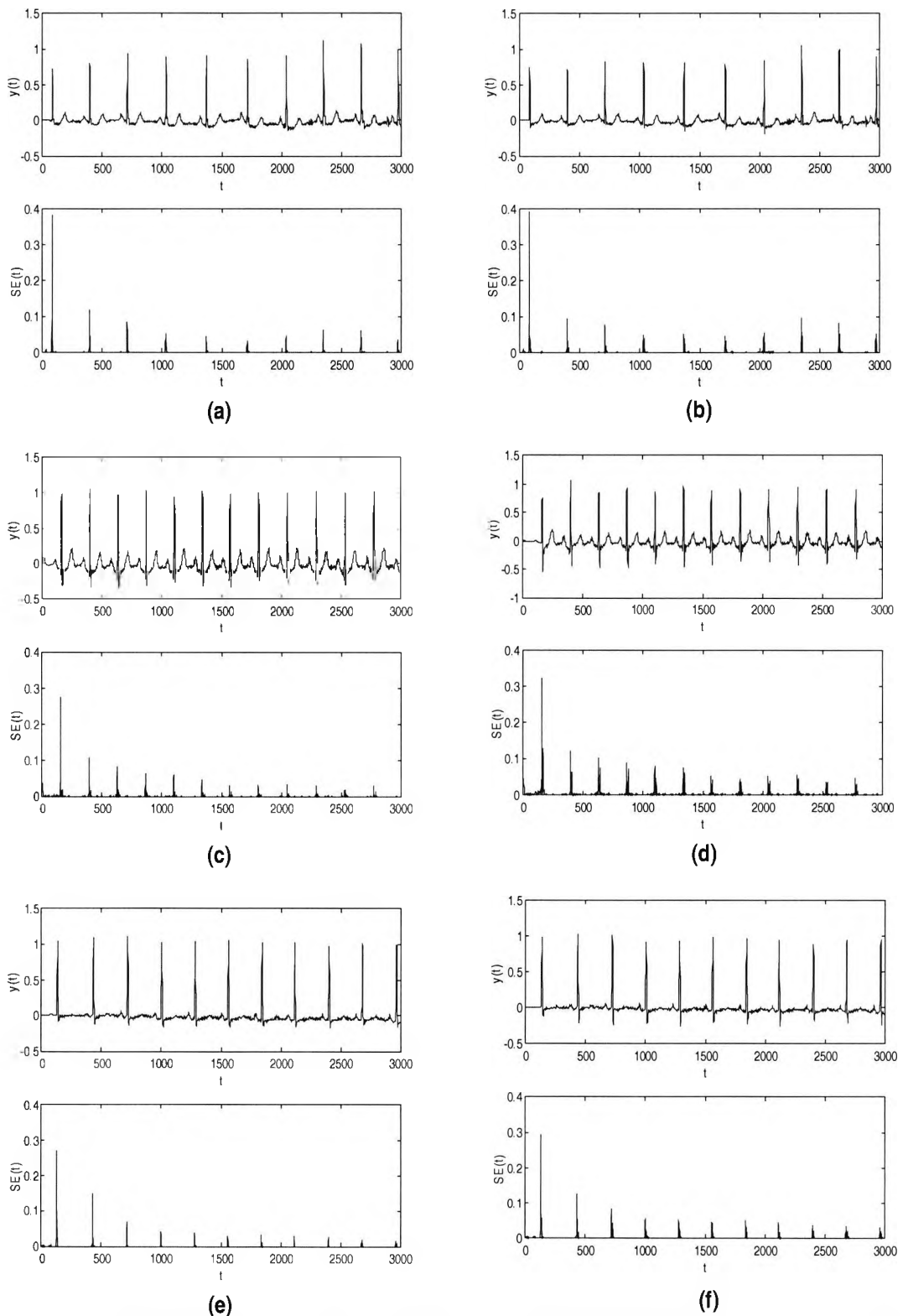


Figure 2.8 Performance of LMS (LHS) and LMF (RHS) predictors ($m = 14$, $\mu = 0.3$ and 0.9 for LMS and LMF, respectively) for records No. 101 (a), (b), No. 300 (c), (d) and No. 325 (e), (f). In each of (a), (b), (c), (d), (e) and (f) the output is shown in the top panel and the squared error is shown in the bottom panel.

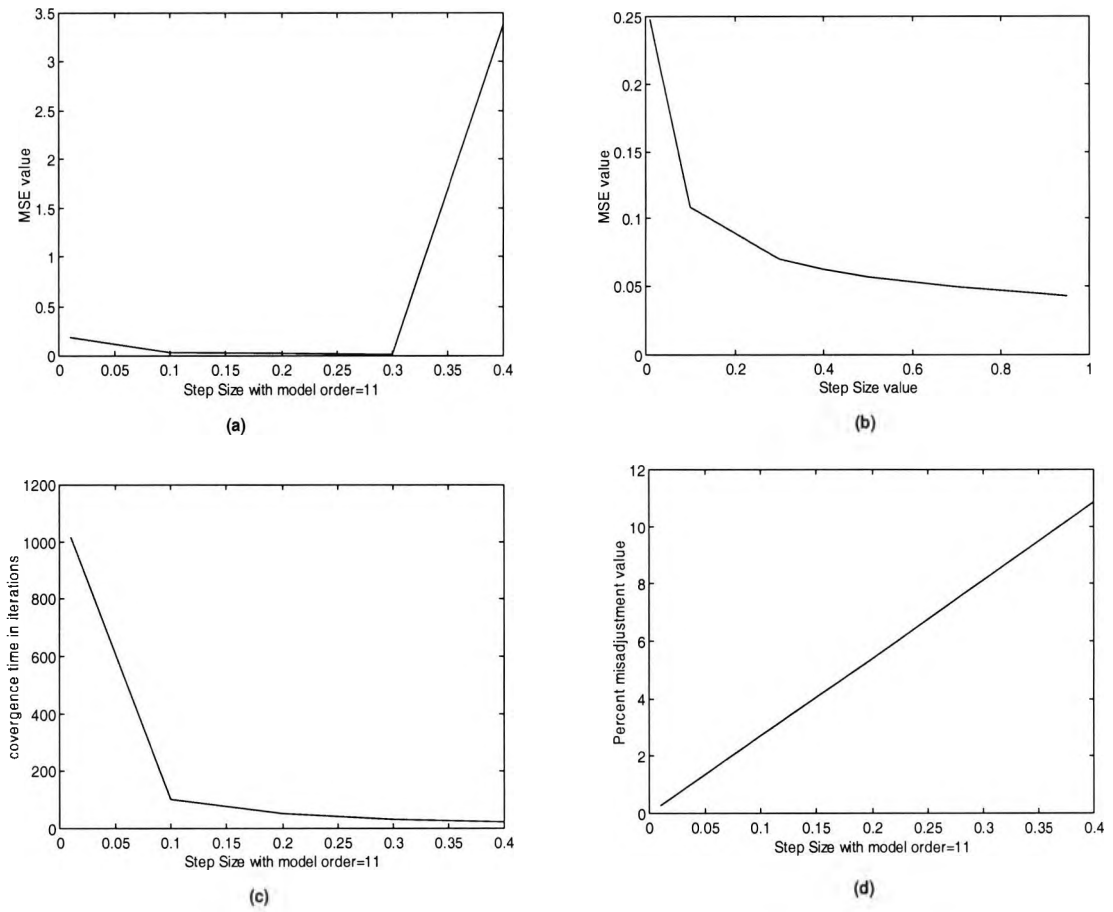


Figure 2.9 Convergence analysis of the linear adaptive predictors applied to record No. 101 (MIT-DB), with an optimised model order of, $m=11$. (a) and (b) show the MSE as a function of the step-size for both LMS and LMF, respectively. (c) and (d) show the convergence time and the percentage misadjustment as a function of the step-size.

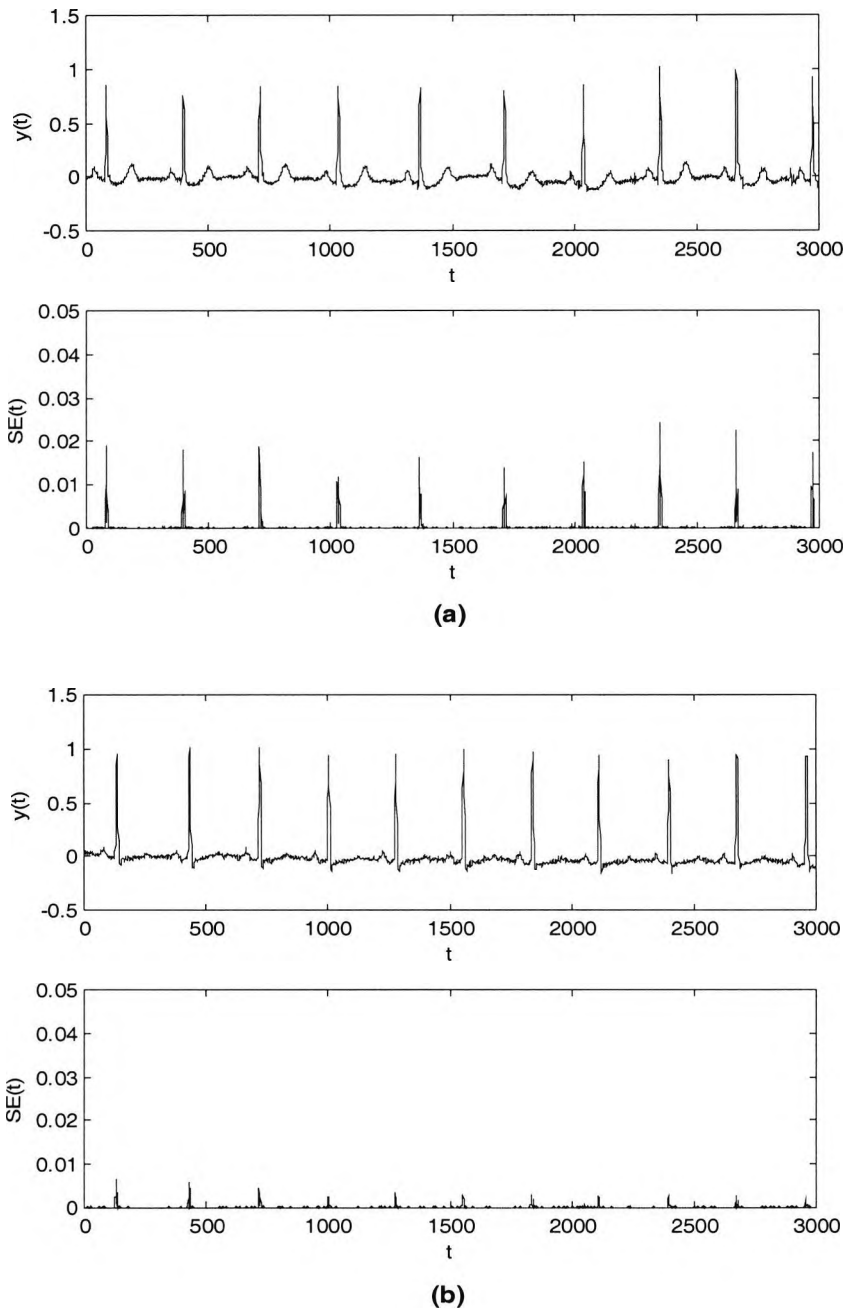


Figure 2.10 Performance of the Kalman predictor for records No. 101 (a) and No 325 (b), using $m=5$, $c=0.01$ and $k_0=0.01$. In each of (a) and (b) the output is shown in the top panel and the squared error is shown in the bottom panel.

2.7.2 Volterra Adaptive Predictor

The inherent non-linearity of the ECG signal (Xue, et al. 1992) compromises the performance of the linear filters. So it is worthwhile to investigate the performance of

Volterra filter to such a signal. As mentioned earlier, the adaptation of Volterra kernels can be obtained either by the LMS or the Kalman algorithms. The computational complexity associated with implementing the Kalman adaptive algorithm for the Volterra structures prohibits its application to the ECG data. Hence, the LMS algorithm is chosen with Volterra structure for our application. To choose the number of samples, m , in the input vector for the linear part of the Volterra predictor, the MSE value Eq. (2.34) is calculated as a function of m for fixed μ_a and μ_b as shown in Figure 2.11 (left), then for optimum μ_a and μ_b with each m as in Figure 2.11 (right). Figure 2.11 (bottom) shows the MSE as a two dimensional function of m and μ_a with μ_b equal to 0.01. From these Figures a value of m between 3 and 7 can be used for minimum MSE.

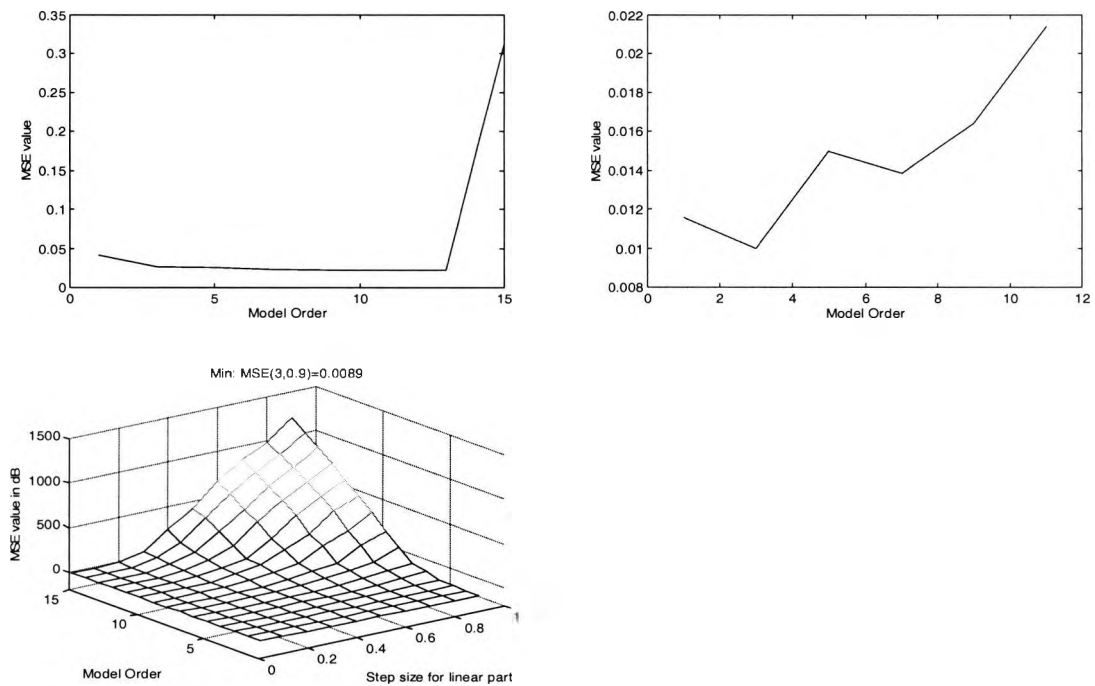
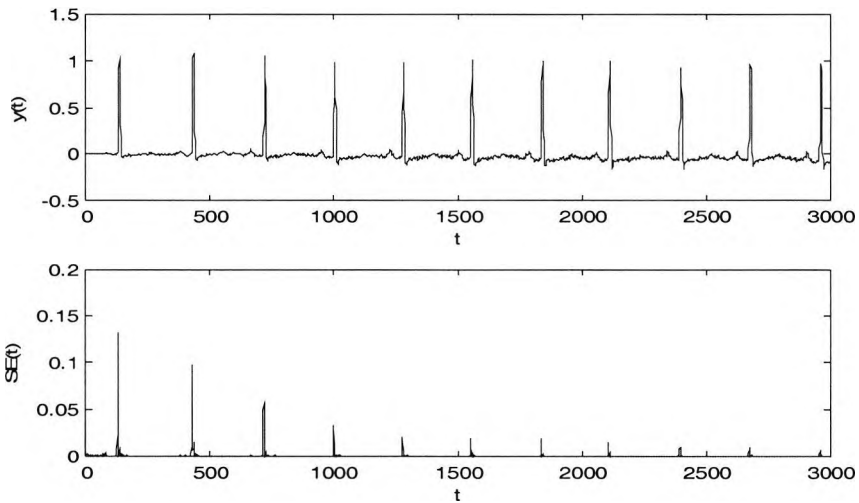


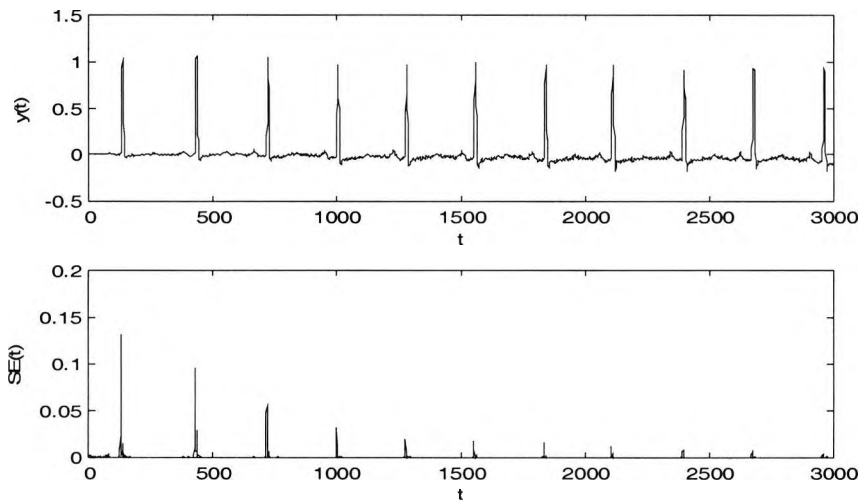
Figure 2.11 Selection of the number of samples in the input vector for Volterra predictor using record No. 101 (MIT-DB). In the left plot the selection is based on the estimated MSE for step-sizes of 0.2, 0.01, 0.0 for linear, quadratic and cubic parts, respectively, and in the right plot pre-selected optimal step-sizes are used. The bottom plot shows the value of the MSE as a function of the number of input samples and step-size of linear part with step-sizes of 0.01 and 0.0 for quadratic and cubic parts, respectively.

Figure 2.12 parts (a), (b) show the output (upper panel) and the squared error (bottom panel) for the quadratic and cubic Volterra predictors when applied to record No. 325 (ST Change-DB), respectively. In each part the top panel represents the output of the

filter and the bottom panel represents the squared error. MSE value of 0.013 (-18.86 dB) and 0.01 (-20 dB) are obtained for quadratic and cubic Volterra predictors, respectively. From these results we can conclude that the quadratic Volterra series is adequate for prediction of this ECG record.



(a)



(b)

Figure 2.12 Comparison between quadratic (a), and cubic (b) Volterra predictors applied to record No. 325 (ST Change-DB). $m=3$, step-sizes (0.9, 0.01, 0.0) for (a) and (0.9, 0.01, 0.01) for (b).

2.7.3 Adaptive Artefact Filtering

2.7.3.1 Introduction

In this section the adaptive algorithms are applied to cancel two types of the most common artefacts found in the ECG records, namely, the electromyogram (EMG) and the Motion Artefact (MA). These are obtained from NST-DB (MIT-CD 1997); each was recorded using a different lead, other than the ECG signal recording leads, to record one type of artefact. To simulate a realistic situation a weighted artefact is added to the ECG signal to form a noisy version of the signal and simultaneously used as the tap input to the filter. The weight factor is chosen to provide the desired signal-to-noise ratio (SNR) level as follows.

$$u(t) = v_n(t), \quad \text{where } v_n(t) = c v(t) \quad \text{and} \quad d(t) = x(t) + v_n(t)$$

where in this case $u(t)$ and $d(t)$ are called the reference signal (tap input) and the primary signal, respectively, see Figure 2.13, $v_n(t)$ is the normalized noise, c is the weighting constant and $x(t)$ is the ECG signal.

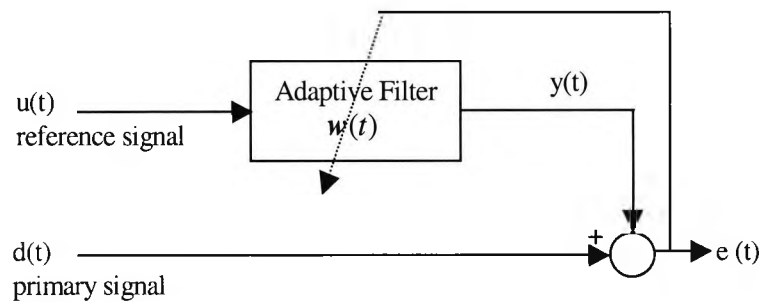


Figure 2.13 The adaptive artifact filter structure.

With zero mean signal and noise and given a target SNR defined in Eq.(2.35), the

constant c is found as $c = \sqrt{\frac{\sigma_x^2}{10^{SNR/10}}}$, where σ_x^2 is the variance of $x(t)$. The filter error,

$$e = d(t) - y(t) = x(t) + v_n(t) - y(t), \quad \text{then } e^2 = [x(t) + v_n(t)]^2 - 2y(t) [x(t) + v_n(t)] - y^2(t)$$

$$\text{or } e^2 = [v_n(t) - y(t)]^2 + x^2(t) + 2x(t) v_n(t) - 2y(t) x(t).$$

Since the signal and the noise are uncorrelated, the MSE is,

$$E[e^2] = E[(v_n(t) - y(t))^2] + E[x^2(t)]$$

Minimising the MSE results in a filter error output that is the best least-squares estimates of the signal $x(t)$ (Thakor and Zhu 1991).

2.7.3.2 Results

Record No. 100 from the MIT-DB with added noise at different SNRs is used in this simulation. Figure 2.14 shows (a) the original ECG signal, (b) the EMG noise artefact, and (c) the MA noise artefact.

Figure 2.15 depicts the performance of LMS-based EMG filter, $m = 5$ and $\mu = 0.5$ using record No. 100 (MIT-DB) and different signal-to-noise ratios; SNR = 15 dB (for parts (a) and (b)), SNR = 10 dB (for parts (c) and (d)) and SNR = 5 dB (for parts (e) and (f)). The LHS; in each of (a), (c), and (e) the primary input is shown in the top panel and the reference signal is shown in the bottom panel. The RHS; in each of (b), (d) and (f) the output is shown in the top panel and the removed artefact is shown in the bottom panel.

Figure 2.16 depicts the performance of LMS-based MA filter, $m = 5$ and $\mu = 0.5$ using record No. 100 (MIT-DB) and different signal-to-noise ratios; SNR = 15 dB (for parts (a) and (b)), SNR = 10 dB (for parts (c) and (d)) and SNR = 5 dB (for parts (e) and (f)). The LHS; in each of (a), (c) and (e) the primary input is shown in the top panel and the reference signal is shown in the bottom panel. The RHS; in each of (b), (d) and (f) the output is shown in the top panel and the removed artefact is shown in the bottom panel.

Figure 2.17 depicts the performance of LMF artefact filters, SNR = 10 dB, $m = 3$ and $\mu = 0.5$ using record No. 100 (MIT-DB) artificially contaminated with EMG noise artefact (a) and motion artefact (MA) noise (b). In each of (a) and (b); the output is shown in the top panel and the removed artefact is shown in the bottom panel.

Figure 2.18 depicts performance of LMS-based quadratic Volterra artefact filters, SNR = 10 dB, $m = 3$, $\mu_a = 0.5$ and $\mu_b = 0.1$, $\mu_c = 0.0$ using record No. 100 with artificially introduced EMG noise (a) and motion artefact (b). In each of (a) and (b) the filter output is shown in the top panel and the removed artefact is shown in the bottom panel.

The performance of the LMS-based quadratic Volterra EMG filter is approximately similar to that of the LMS filter of Figure 2.15 (d), each has $\text{SNR} = 10$ dB. This is because the input to the filter is the noise itself (not the ECG signal as in the case of predictors).

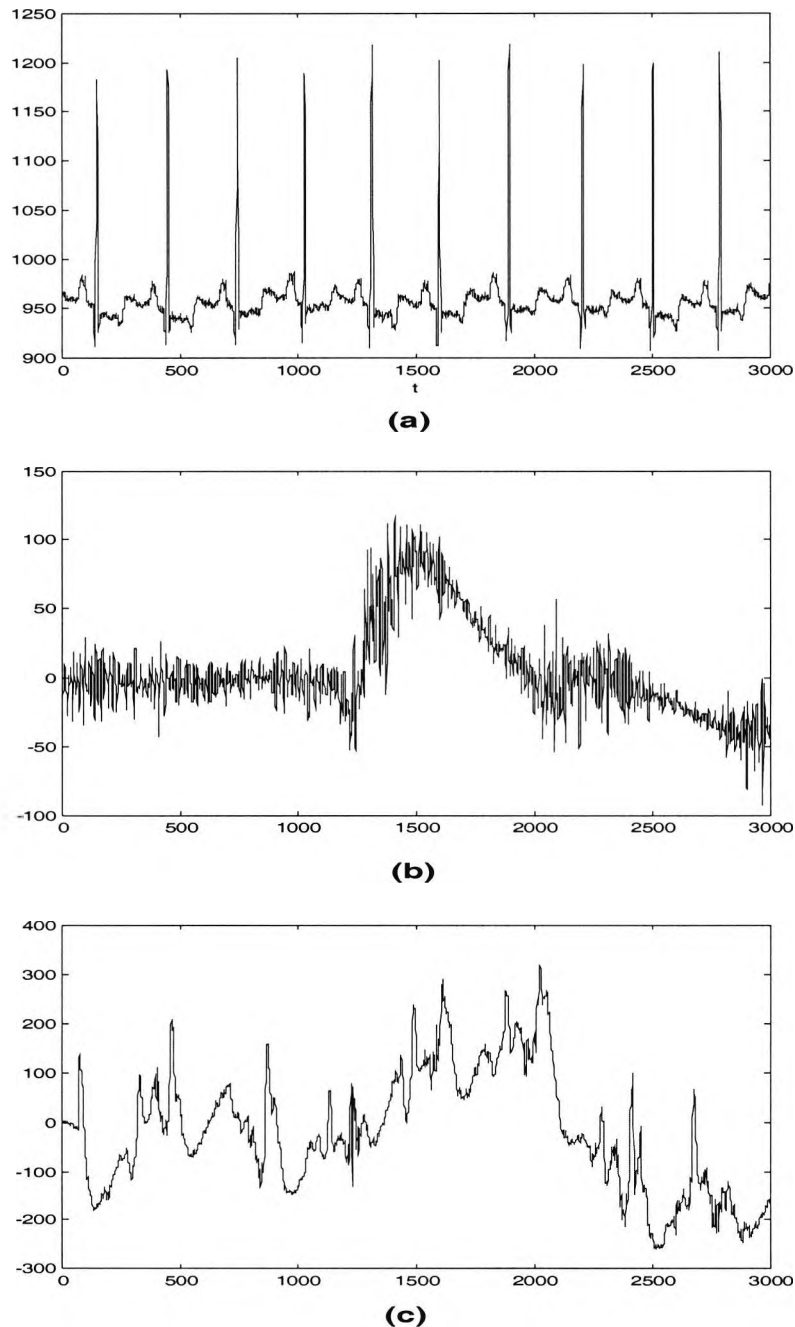


Figure 2.14 Original signals used in the adaptive artefact filtering. (a) Record No. 100 (MIT-DB), (b) the EMG noise and (c) the MA noise from NST-DB.

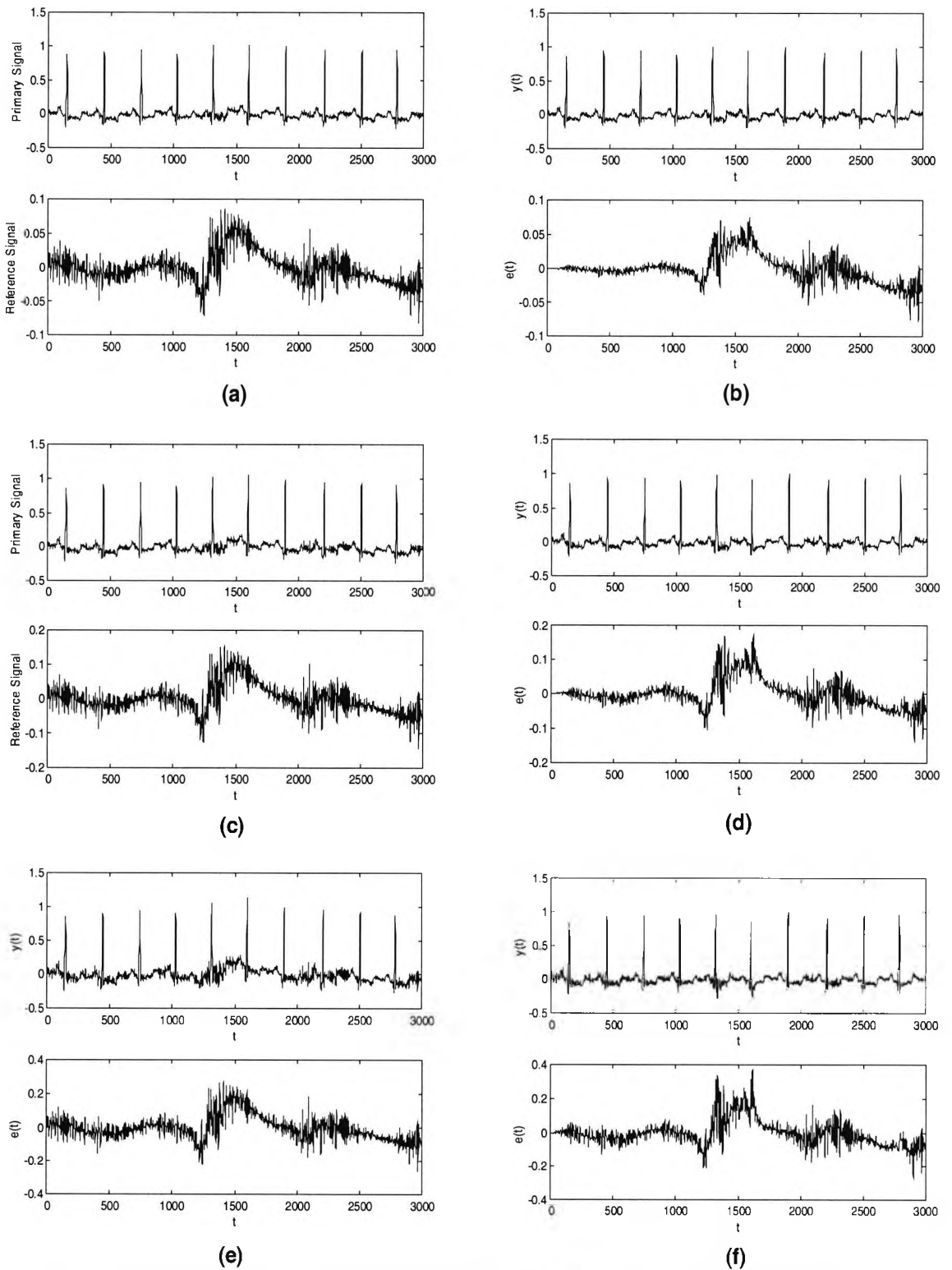


Figure 2.15 Performance of LMS-based EMG filter, $m=5$ and $\mu=0.5$ using record No. 100 (MIT-DB) and different signal-to-noise ratios; SNR=15 dB (for parts (a) and (b)), 10 dB (for parts (c) and (d)) and 5 dB (for parts (e) and (f)). The LHS shows the primary input (top panel) and the reference signal (bottom panel). The RHS shows the output (top panel) and the removed artefact (bottom panel).

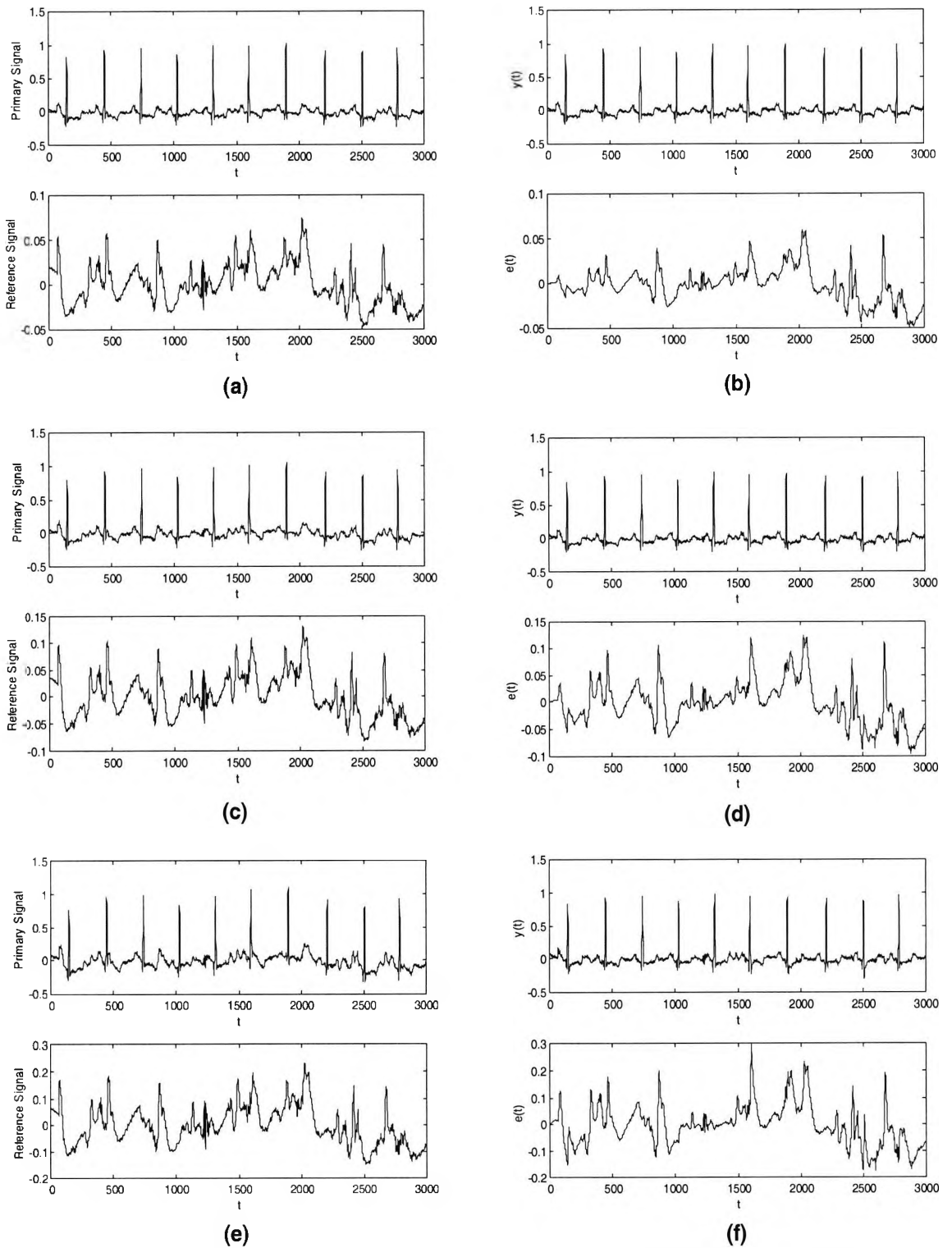


Figure 2.16 Performance of LMS-based MA filter, $m=5$ and $\mu=0.5$ using record No. 100 (MIT-DB) and different signal-to-noise ratios; SNR=15 dB (for parts (a) and (b)), 10 dB (for parts (c) and (d)) and 5 dB (for parts (e) and (f)). The LHS shows the primary input (top panel) and the reference signal (bottom panel). The RHS shows the output (top panel) and the removed artefact (bottom panel).

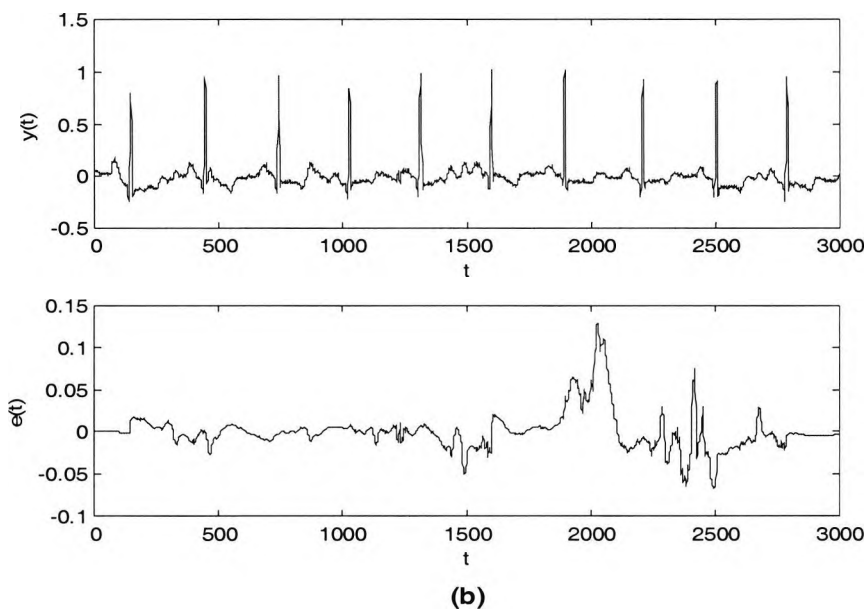
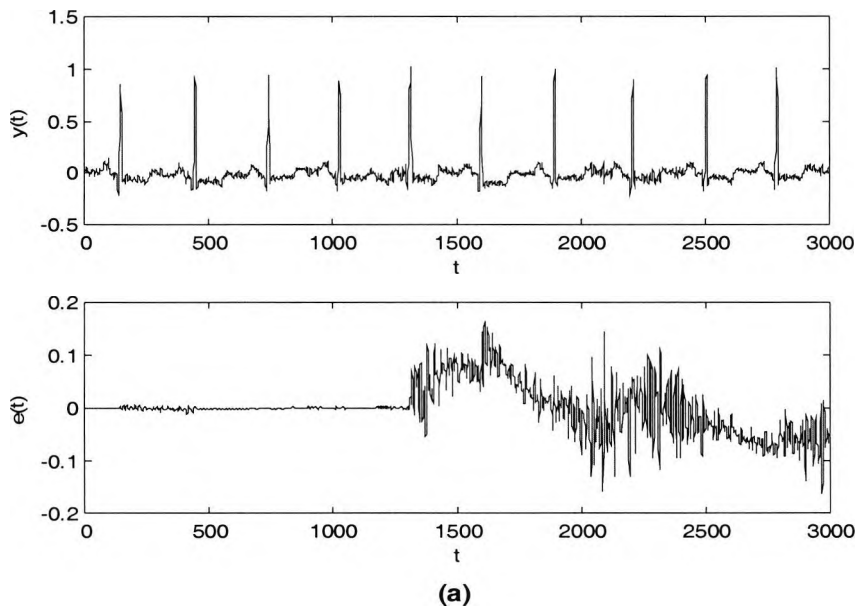


Figure 2.17 Performance of LMF artefact filters, SNR=10 dB, $m=3$ and $\mu=0.5$, using record No. 100 (MIT-DB) artificially contaminated with EMG noise artefact (a) and MA noise artefact (b). In each of (a) and (b); the output is shown in the top panel and the removed artefact is shown in the bottom panel.

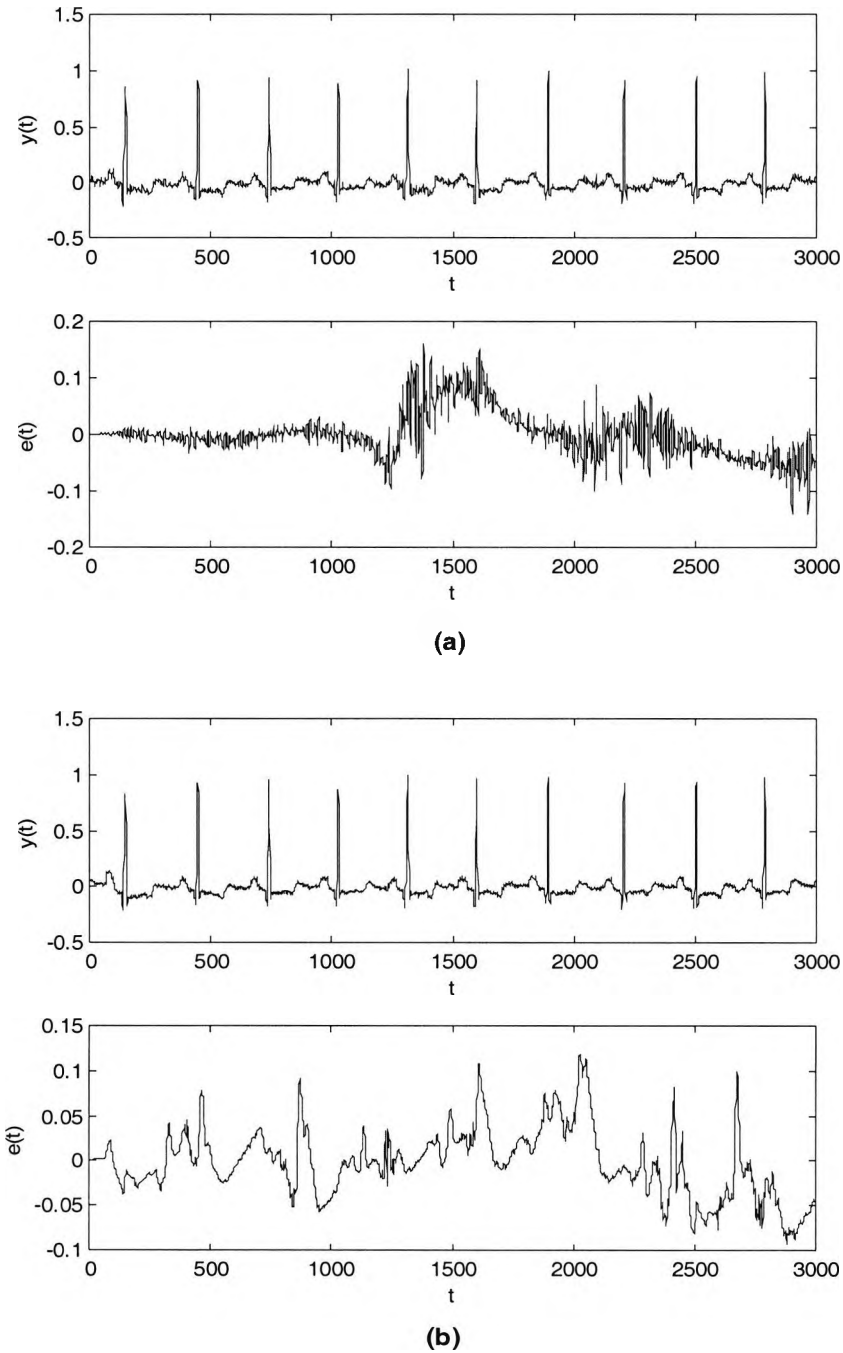


Figure 2.18 Performance of LMS-based quadratic Volterra artefact filters, $\text{SNR}=10$ dB, $m=3$, $\mu_a=0.5$, and $\mu_b=0.1$, using record No. 100 (MIT-DB) artificially contaminated with EMG noise (a) and MA noise (b). In each of (a) and (b); the output is shown in the top panel and the removed artefact is shown in the bottom panel.

2.7.3.3 SNR Evaluation

Finally the input and the output SNR are calculated for each of the previous filters using Eq. (2.37). Table 2.1 shows the results obtained using record No. 100 (MIT-DB) with artificially introduced EMG and MA noises. The singular values of the matrix in Eq. (2.36) and the number of signals in the signal subspace, p , are calculated using the SVD algorithm.

Estimated input SNR (dB)	Estimated output SNR (dB)		
	LMS	LMF	Volterra
<i>EMG noise:</i>			
15.0866	17.77	16.04	17.77
10.27	15.141	12.682	15.139
4.835	11.566	6.0	11.527
<i>MA noise:</i>			
14.6	18.63	14.838	18.629
12.165	18.099	14.858	18.093
5.713	11.516	7.855	11.49

Table 2.1 Estimated input and output SNR for the adaptive artefact filters.

The results obtained in Figures 2.15 to 2.18 and Table 2.1 indicate the following;

- The performance of the LMS-based EMG and MA filters is quite satisfactory in removing these artefacts as shown in Figures 2.15 and 2.16. The LMF-based EMG and MA filters require more than 1000 samples to converge. Also from Table 2.1, on average, the achieved improvements in the SNR are 68.13% (for EMG) and 59.3% (for MA) using the LMS filter and 17.97% (for EMG) and 20.4% (for MA) using LMF filter. It was explained by Walach and Widrow (1984) that the implementation of "higher-order error algorithms, $k>1$ " requires a certain degree of caution as in certain cases these algorithms might cause deterioration in the performance, one of these cases is when the noise is

Gaussian, in such a case the LMS will outperform the LMF. As the EMG noise is Gaussian and the MA has a distribution that is very similar to the Gaussian distribution, this makes the LMF algorithm not suitable for this application.

- In general, similar performance to that of the LMS-based EMG and MA filters is obtained using the LMS-based quadratic Volterra filters, as indicated in Table 2.1, on average, an improvement in the SNRs of about 67.9% (for EMG) and 59.2% (for MA) are achieved in the output of each of these filters. While, the LMS-based quadratic Volterra predictor outperformed the linear LMS predictor as the MSE obtained using the adaptive quadratic Volterra predictor (0.013) was approximately four times less than that obtained using the linear LMS predictor (0.048). One reason for that is, in the case of the adaptive predictors the input to the filter is ECG signal which is highly non-linear, as will be explained in chapters 4 and 5. However, for the case of the adaptive noise cancellers the input to the filter is the weighted noise.
- The improvement in the output SNR is about 68% for the EMG filter and about 59% for the MA filter, which means that the noise is partially removed. One reason for that is, the operation of these noise cancellers is based on the fact that the noise is random and uncorrelated with the signal, which may not be the real situation for the ECG signal. A second reason is that the change in the QRS complex or in the P- and T-waves morphologies from beat to beat has led to incomplete adaptation. Third, the adaptive filters may need longer operating time to reach the optimal performance.
- Motion artefact is the most difficult problem because large non-stationary MA cannot be efficiently handled with any linear filtering techniques (Sabry-Rizk, et al. 2000a; Sabry-Rizk, et al. 2000b). In this study, both the linear LMS and the quadratic LMS-based Volterra filters partially removed the MA. Also a recurrent filter, used by Thakor and Zhu (1991), in which the primary input is the ECG signal with motion artefact and the reference input is an impulse that is coincident with the beginning of the P-QRS-T complex with its adaptation takes

place for the samples spanning the signal complex leaves the MA as residual, had partially removed the MA.

2.8 Discussion

There are several advantages to the adaptive filtering approaches; the most significant feature of these filters is that they allow estimation of the underlying signal in the absence of a priori knowledge of the statistical or spectral properties of the signal and noise. These filters are easy to implement on modern microprocessors with numerical capabilities.

In this chapter the LMS, LMF, the Kalman and Volterra predictors/filters were used for linear and non-linear prediction/filtering of the ECG signals. The LMS showed faster convergence and smaller MSE than the LMF algorithm. On the other hand the LMF showed more stability. The Kalman predictor resulted in the smallest MSE value and the fastest convergence. The limitations of the LMS with respect to the Kalman algorithm are the slow rate of convergence and its sensitivity to the eigen-value spread problem (for stable LMS the step-size should be in the range $0 < \mu < 1/\lambda_{\max}$, λ_{\max} is the max eigen-value in the autocorrelation matrix of the input signal). So with the LMS algorithm a satisfactory performance can be obtained for the proper choice of μ . The computational complexity and the numerical problems arise from ill-conditioning of the state-error covariance matrix $[K(t+1, t)]$, as round-off errors accumulate and propagate from one iteration to the next, are the main limitations of the Kalman algorithm. Also the Kalman algorithm showed slower response to signal variations during tracking than during convergence. This may give the LMS a slight performance advantage in non-stationary environments. Volterra non-linear predictor resulted in a good performance with smaller MSE. This gives indication that the ECG signal contains inherent non-linearity; this particular point will be investigated in depth in chapters 4 and 5.

The adaptive artefact cancellers have yielded fairly reasonable results. Their limitation, as previously explained, is that not all the noise has been removed. This lead to the need to use higher-order (>2) non-linear Volterra filter combined with HOS for removal of these artefacts as explained by Sabry-Rizk, et al. (1998).

In the following chapters, these adaptive filters will constitute two important steps in the ECG signal pre-processing stage prior to its analysis. Since for all the ECG data available there is no channel recorded for separately measuring the noise for each record, the adaptive predictor structure will be applied. The first step is to remove the BW. If the ECG signal is contaminated with any type of artefacts, described in this chapter, then the second step is to suppress this artefact as follows, (a) non-linear and non-stationary motion artefact will be removed using adaptive Volterra LMS-based filter then transforming the signal to the bispectrum domain (Sabry-Rizk, et al. 1998), (b) since the power line interference is stationary it can be removed using a conventional band stop filter, (c) since the spectrum of the EMG noise overlaps with that of the ECG signal (Thakor, et al. 1984), adaptive filters can partially remove this artefact. As the EMG is a Gaussian signal (Friesen, et al. 1990) this makes its removal very easy by transforming the ECG signal to the higher-order domain which is the main analysis tool used in this research work (see chapters 4 and 5).

Chapter 3

STATISTICAL AND SPECTRAL ANALYSIS OF ECG SIGNALS

3.1 Introduction

In this chapter the ECG signal will be statistically characterised in terms of periodicity, Gaussianity and stationarity. In order to extract features from the frequency domain, it is important to have an accurate frequency representation of the signal and an accurate interpretation of each frequency component in its spectrum. The power spectrum of the ECG signal is estimated using the Welch method. Then a high-resolution frequency estimator namely, the Multiple Signal Classification (MUSIC) algorithm, is applied to investigate the frequency content of the whole ECG cycle, the P-wave, the QRS complex, and the T-wave of normal ECG signals. To differentiate between normal and ischaemic ECG signals in the second-order spectral domain, the high frequency regions (60 - 180 Hz) of the whole ECG spectrum and that of the combined ST-segment and the T-wave (ST-T complex) have been investigated for normal and ischaemic ECG signals using the Maximum Entropy Method (MEM) and the MUSIC algorithm.

3.2 Statistical Properties of the ECG Signals

The ECG signal's distinctive global nature of pseudo-periodicity (Niranjan and Murthy 1993), and the different features of the constituent signals (P-wave, QRS complex and T-wave) representing actions of various parts of the heart, makes it worthwhile to study these features intimately.

A brief study has been made to statistically characterise the ECG signal. A normal sinus rhythm ECG record (No. 16483) from the NSR-DB (MIT-CD 1997) will be

presented as an example from this study. An ECG cycle from this record is shown in Figure 3.1.

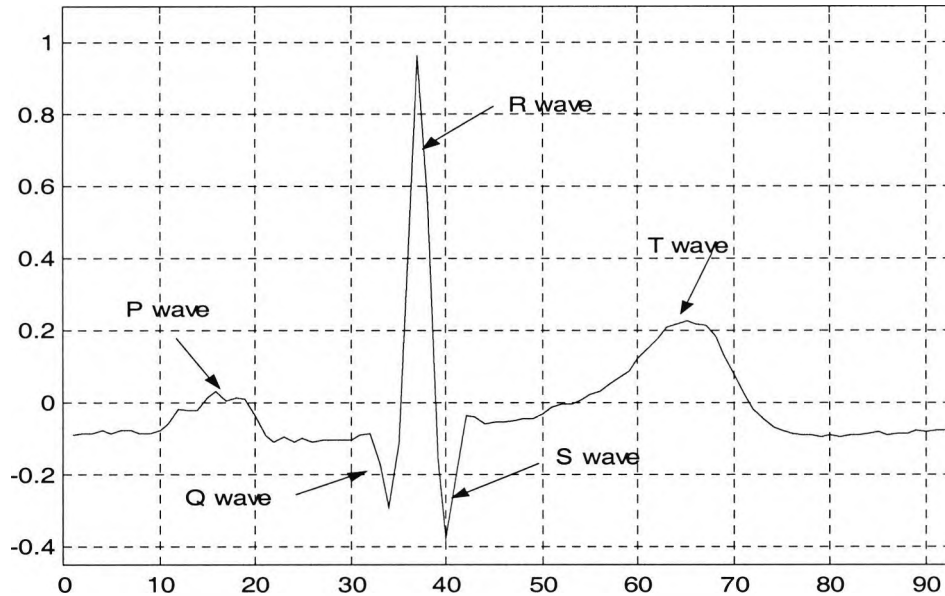


Figure 3.1 Time domain of one normal ECG cycle record No. 16483 (NSR-DB).

3.2.1 Periodicity Test

The singular values of the data matrix in Eq. (2.36), chapter two, are used by Stokes, et al. (1999) to calculate the so-called coefficient of periodicity (CP), which has been used as a measure for the degree of periodicity. The total energy in the data matrix \mathbf{R}_x is the sum of squares of its singular values, and for a noise-free periodic processes, the total energy is contained in the dominant singular value (Palit and Kanjilal 1994). This suggests the following form of CP ,

$$CP = \frac{s_1^2}{\sum_{i=1}^{l_f} s_i^2} \quad (3.1)$$

It follows immediately from this definition that $CP=1$ for strictly periodic processes. This coefficient, CP , is calculated for 18 normal ECG records using 10,000 samples from each record. The CP is found to be in the range from 0.84 to 0.98 with a mean

value of 0.89. This confirms that the ECG signal is a pseudo-/quasi-periodic signal as explained by Mukhopadhyay and Sircar (1996); Niranjana and Murthy (1993).

3.2.2 Normality Test

In this section the sample coefficients of the mean, variance, skewness and kurtosis (Press, et al. 1990) are applied to reject or accept the Normality (Gaussianity) hypothesis of the ECG signal then the histogram and the Probability Distribution Function (PDF) are plotted to show the marginal distribution of the signal's amplitude. The physical meaning of these statistics is (Mood, et al. 1974):

Mean: it is an estimate of the value around which the central clustering of a set of values occurs.

Variance: it characterises the “width” or “variability” of a distribution around its central value (e.g., mean).

Skewness: The skewness measures the degree of asymmetry of a distribution around its mean. It is a pure number, non-dimensional, that characterises only the shape of the distribution. A positive skewness indicates that the distribution is skewed to the right, whereas a negative skewness usually indicates that the distribution is skewed to the left.

Kurtosis: The kurtosis is also a non-dimensional quantity. It measures the relative peakedness or flatness of a distribution relative to a Gaussian distribution. A positive kurtosis indicates that the density is more peaked around the mean value than the density of the Normal distribution, whereas a negative kurtosis usually indicates that the density is more flat around its mean value than do the Normal distribution.

The mathematical expressions for these statistics will be introduced in chapter four. The mean, variance, skewness and kurtosis are computed from averaging of the results obtained for one hundred and three cardiac cycles. The values obtained are 0.0258, 0.284, 2.7428, and 15.1019, respectively. For Normal distribution the values of skewness and kurtosis are zero and 3, respectively, (Patel and Read 1982). A positive skewness of 2.7428 for the ECG data indicates that the sample data are skewed to the right. While a kurtosis value greater than 3 indicates that the sample distribution has

rather more values in the tail regions than would be expected for a Normal distribution, this also declare peakedness around the mean value.

The histogram in Figure 3.2 emphasises this fact as marginal distribution does not appear to be symmetric and it skews to the right. Figure 3.3 shows the PDF, which is the integration of the histogram. Both the histogram and the PDF are calculated from averaging of 103 Histograms and using 50 equally spaced bins.

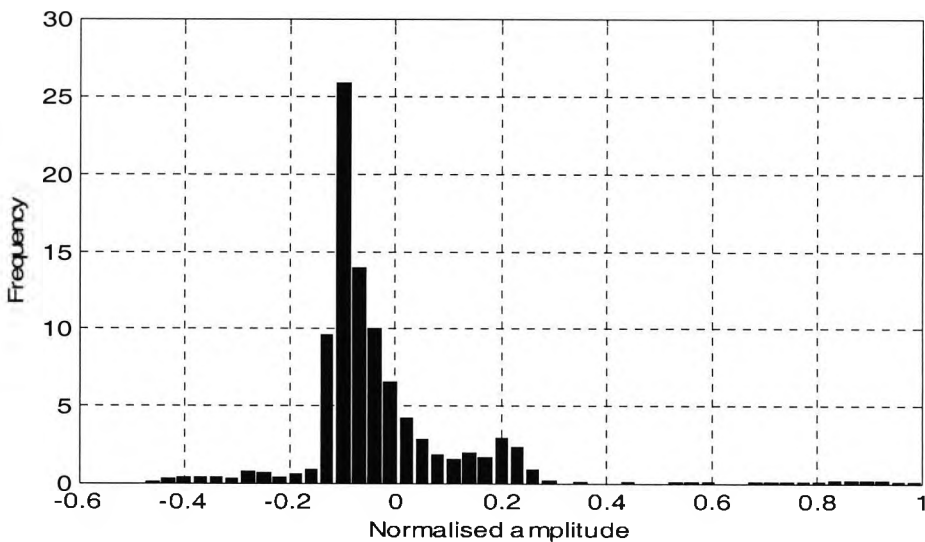


Figure 3.2 Histogram of a normal ECG record No. 16483 (NSR-DB) using 50 equally spaced bins.

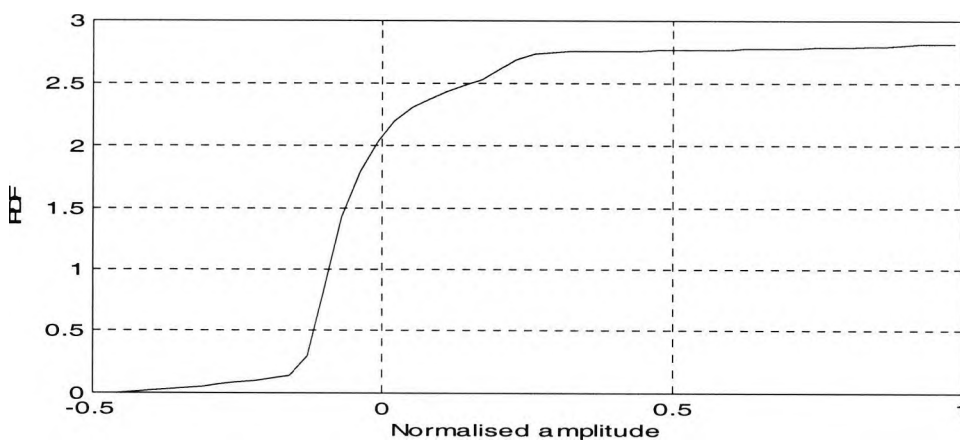


Figure 3.3 Probability Distribution Function (PDF) of a normal ECG record No. 16483 (NSR-DB) using 50 equally spaced bins.

3.2.3 Stationarity Test

We will now look at the spectrogram, which is an estimate of the short-term, time-localised frequency content of the signal. The spectrograms in Figures 3.4 (a), (b) are calculated by splitting the signal into zero overlapping segments and windowing each with Hanning window. Figure 3.4 shows that the dominant frequency tracks are between 0 and 30 Hz. Comparing Figure 3.4 (a) and 3.4 (b): Figure 3.4 (a) shows constant frequency tracks with time (especially in the dominant frequency region) which means that this segment (one cycle) can be considered stationary. Figure 3.4 (b) shows changes in the frequency tracks with time indicating that this segment (> one cycle) is not stationary. One can conclude that the ECG signal can be considered stationary within one cycle, i.e., cyclostationary. Cyclostationary processes are random processes with statistical parameters, such as mean, autocorrelation...etc. that fluctuate periodically with time (Dandawate and Giannakis 1994; Gardner and Franks 1975). These processes are characterised by the invariance of the probability distribution under shift by multiples of a certain period; this is the characterisation in the strict sense. Bennett (1958) introduced the term "cyclostationary" to denote this class of processes. Other investigators have used terms such as "periodically stationary," "periodically correlated," and "period non-stationary," to denote the same class. The cyclostationary signals are usually treated as if they are stationary simply by averaging the statistical parameters over one cycle. This is equivalent to representing the phase of the process as a random variable uniformly distributed over one cycle (Gardner and Franks 1975).

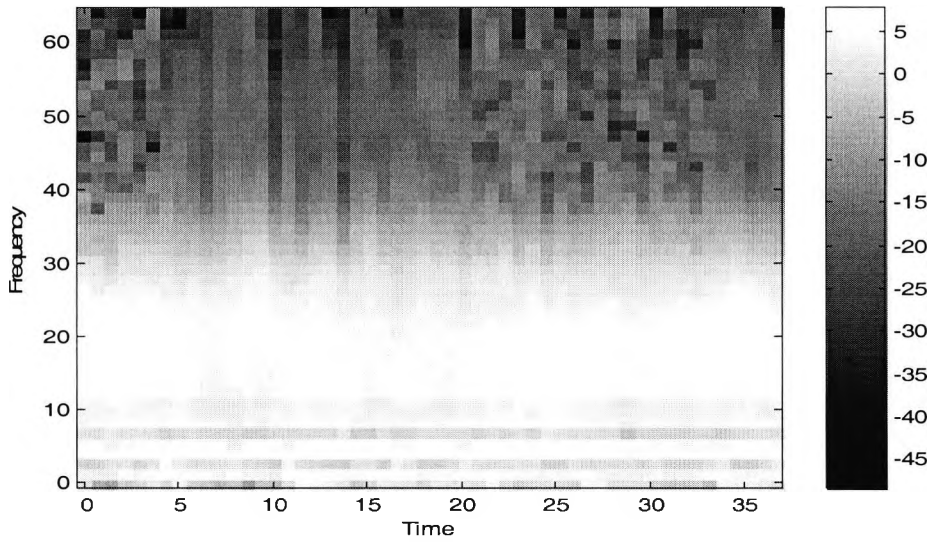
$$\tilde{x} = x(t + \varphi)$$

$$P_{\varphi}(i) = \begin{cases} \frac{1}{T} & |i| \leq \frac{T}{2} \\ 0 & |i| > \frac{T}{2} \end{cases}$$

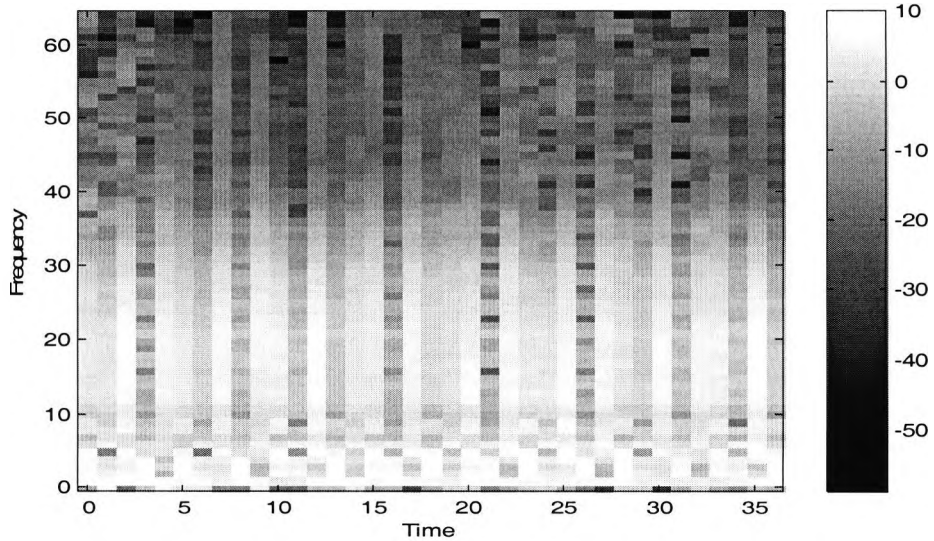
where x is the cyclostationary signal, \tilde{x} is the phase randomised signal and P_{φ} is the probability density function of φ . In this case the mean, \tilde{m}_x , and autocorrelation, $\tilde{k}_{xx}(\tau)$, of \tilde{x} can be defined mathematically as:

$$\tilde{m}_x = \frac{1}{T} \int_{-T/2}^{T/2} m_x(t) dt$$

$$\tilde{k}_{xx}(\tau) = \frac{1}{T} \int_{-T/2}^{T/2} k_{xx}(t + \tau, t) dt$$



(a)



(b)

Figure 3.4 Spectrogram of a normal ECG signal. The segment length is (a) one ECG cycle, and (b) 128 samples with overlap=0.

3.3 Spectral Analysis of the ECG Signals

The power spectrum determines the distribution of power among individual frequency components of the process (Priestley 1981). To have a concise definition of the ECG spectrum (e.g., shape and limits) the power spectrum of the whole ECG is calculated using the Welch periodogram. Then in order to understand the frequency components of this spectrum, a high-resolution frequency estimation technique namely, the Multiple Signal Classification (MUSIC) algorithm is applied to estimate the MUSIC spectra of the whole ECG cycle, the P-wave, QRS complex and T-wave.

3.3.1 The Welch Periodogram

Welch provided a computationally efficient procedure using the FFT for averaging periodograms¹ of weighted and overlapped data segments. Consider a data record $[x(0), x(1), \dots, x(N-1)]$ of N samples divided into J segments of M samples each, with l samples between adjacent segments ($l \leq M$). The weighted i^{th} segment will consist of the samples (Marple 1987).

$$x^{(i)}(t) = \text{Win}(t)x(t + il) \quad (3.2)$$

where $\text{Win}(t)$ is the window function applied to $x(t)$ for $0 \leq t \leq M - 1$. The sample spectrum of the weighted i^{th} segment is given by

$$S^{(i)}(f) = \frac{1}{UMT} X^{(i)}(f) [X^{(i)}(f)]^* = \frac{1}{UMT} |X^{(i)}(f)|^2 \quad (3.3)$$

Over the frequency range $-1/2T \leq f \leq 1/2T$, where $X^{(i)}(f)$ is the discrete FT of the i^{th} segment.

$$X^{(i)}(f) = T \sum_{t=0}^{M-1} x^{(i)}(t) \exp(-j2\pi ft) \quad (3.4)$$

¹ PSD estimates based on direct transformation of the data followed by averaging are collectively termed periodograms.

and U is the discrete-time window energy given by $U = T \sum_{t=0}^{M-1} Win^2(t)$. The average of the windowed segment periodograms yields the Welch periodogram estimate,

$$\hat{S}_w(f) = \frac{1}{J} \sum_{i=1}^J S^{(i)}(f) \quad (3.5)$$

To characterise the ECG signal in the frequency domain, the Welch method is applied to calculate the power spectrum for some records from the NSR-DB (MIT-CD 1997). Figure 3.5 shows the power spectral density of a normal ECG signal (record No. 16483). The power spectrum is smoothed with Hanning window. The number of points used for calculating FFT, (nfft) =128, $J=76$ and each segment =one ECG cycle+zero padding to 128 samples. From this Figure we can conclude that the ECG signal has a frequency spectrum that covers the frequency range 0 - 40 Hz. The frequency components with significant amplitudes are in the range 0 - 30 Hz, this comes in agreement with the previous result using the spectrogram in Figure 3.4. There are about 6 frequency components in this spectrum. These frequency components are at (1.4545, 4.3636, 8.7273, 13.0909, 16, and 20.3636 Hz). The fundamental frequency is at 1.4545 Hz, the frequencies at 4.3636, 8.7273, 13.0909, 16 and 20.3636 Hz are the third, sixth, ninth, eleventh, and fourteenth harmonics of the fundamental frequency. The relation between these frequencies and the P-wave, QRS complex and T-wave will be investigated in the next section using the MUSIC algorithm and in chapter four using the bispectrum.

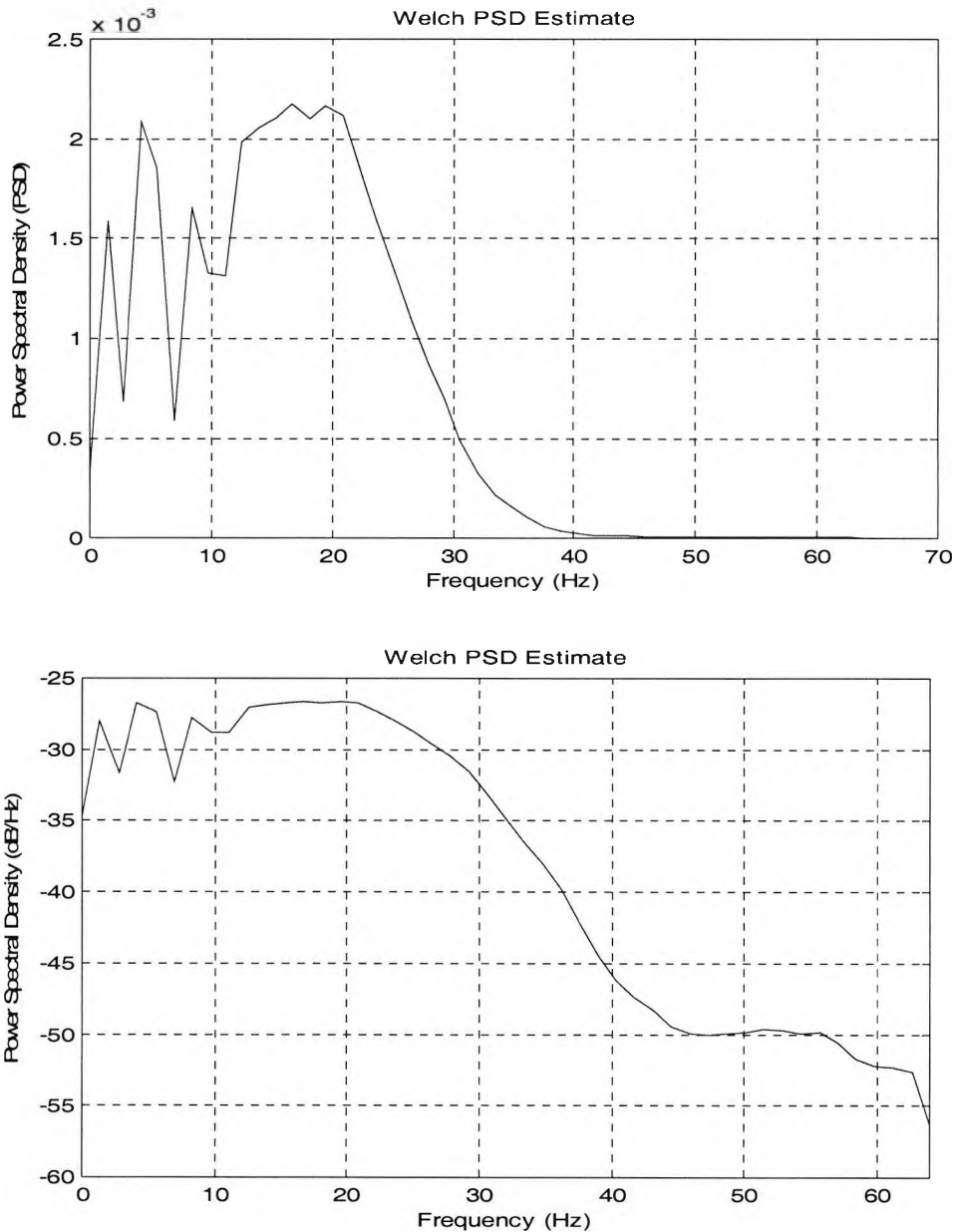


Figure 3.5 Power spectrum of a normal ECG signal (record No. 16483) in linear (up) and dB (bottom) scales.

3.3.2 The Multiple Signal Classification (MUSIC) Algorithm

The MUSIC algorithm was first presented by Schmidt (1979); Schmidt (1981). It belongs to the so-called "super/high-resolution" algorithms. It is a subspace-based algorithm, i.e., basically such an approach partitions the observation space spanned by

the eigen-vectors of the correlation matrix into two subspaces, and exploits the orthogonality of the signal and the noise subspaces to estimate the frequencies of the input signal. It is a frequency estimation technique based on eigen-decomposition or singular value decomposition (SVD) of the autocorrelation matrix or the data matrix of the input signal. Consider an input random process, $x(t)$, of the form

$$x(t) = \sum_{i=1}^p A_i e^{j\omega_i t} + W(t) \quad (3.6)$$

where $A_i = |A_i| e^{j\theta_i}$ and $\omega_i, i=1,2,\dots,p$ are the amplitudes and the frequencies of the p complex exponentials, respectively. $W(t)$ is white noise process with zero mean and variance σ_w^2 .

Let $\mathbf{R}_x \in (L+1, L+1)$ be the autocorrelation matrix of $x(t)$, with $(L+1) > p$. If the eigen-values of \mathbf{R}_x are arranged in decreasing order, $\lambda_1 \geq \lambda_2 \geq \dots \geq \lambda_L$, and if $\mathbf{v}_1, \mathbf{v}_2, \dots, \mathbf{v}_L$ are the corresponding eigen-vectors, then these eigen-vectors can be divided into two groups: the p signal eigen-vectors corresponding to the p largest eigen-values, and the $(L+1)-p$ noise eigen-vectors which, ideally, have eigen-values equal to σ_w^2 . let $\mathbf{V}_S = [\mathbf{v}_1, \dots, \mathbf{v}_p]$, and $\mathbf{V}_N = [\mathbf{v}_{p+1}, \dots, \mathbf{v}_{L+1}]$ be the signal and noise subspaces, respectively, these two subspaces are the orthogonal complement of each other (Haykin 1991)

$$\mathbf{V}_N^H \mathbf{V}_S = 0 \quad (3.7)$$

The MUSIC spectrum uses the following frequency estimation function:

$$\hat{S}_{MUSIC}(\omega) = \frac{1}{\sum_{i=p+1}^{L+1} |\mathbf{e}^H \mathbf{v}_i|^2} \quad (3.8)$$

where $\mathbf{e}^H(\omega) = [1 \quad e^{-j\omega} \quad \dots \quad e^{-j(L-p)\omega}]$ is the frequency scanning vector. This spectrum will exhibit sharp peaks at the frequencies of the complex exponentials.

3.3.2.1 *MUSIC Spectrum of the ECG*

To estimate the MUSIC spectrum, Eq. (3.8), of the ECG signal and the constituent waves (P-wave, QRS complex and T-wave), it is necessary to know the number of signals in the signal subspace. This can be accomplished by calculating the number of significant singular values of the covariance matrix of the signal, by applying the extended version of the AIC criterion in Eq. (2.31) chapter 2. Figure 3.6 (a) shows the singular values of the covariance matrix of an ECG signal from record No. 16483, NSR-DB (MIT-CD 1997). The AIC for this ECG signal is flat for orders higher than 15, which is chosen as the number of signals in the signal subspace as described by Niranjana and Murthy (1993). Figure 3.6 (b) shows the MUSIC spectrum for this record. Figure 3.7 shows the MUSIC spectra for the PR interval, QRS complex, and ST-T complex for this record. Table 3.1 shows the spectral peaks obtained from the MUSIC spectra for records No. 16483 and No. 16539 (NSR-DB). The spectrum is calculated for the whole ECG cycle, PR interval, QRS complex, and ST-T complex for both of these records. From Figures 3.6 (b) and 3.7 and Table 3.1 the MUSIC spectrum of the whole ECG cycle consists of 6 spectral peaks. The first peak at 4.0315 Hz is due to the T-wave, the second one at 15.1181 Hz is due to the QRS complex and the component at 10.0787 is due to the P-wave. This result comes in agreement with the results obtained by Sabry-Rizk, et al. (2000c); Thakor, et al. (1984). The higher frequency components at 19.1496, 23.1811, 24.1890 and 28.2205 seems to be due to interactions between the main frequency components, this observation will be investigated in the next chapter using the bispectrum. From the spectral peaks of the MUSIC spectra of the constituent waves for the two records in Table 3.1, it is observed that, the peak due to the P-wave lies in the range 6-10 Hz, and that due to QRS complex lies in the range 15-17 Hz and that for T-wave is at about 4 Hz. The peak at 2.0317 in the MUSIC spectrum for the ST-T complex of record No. 16539 may be due to the motion artefact.

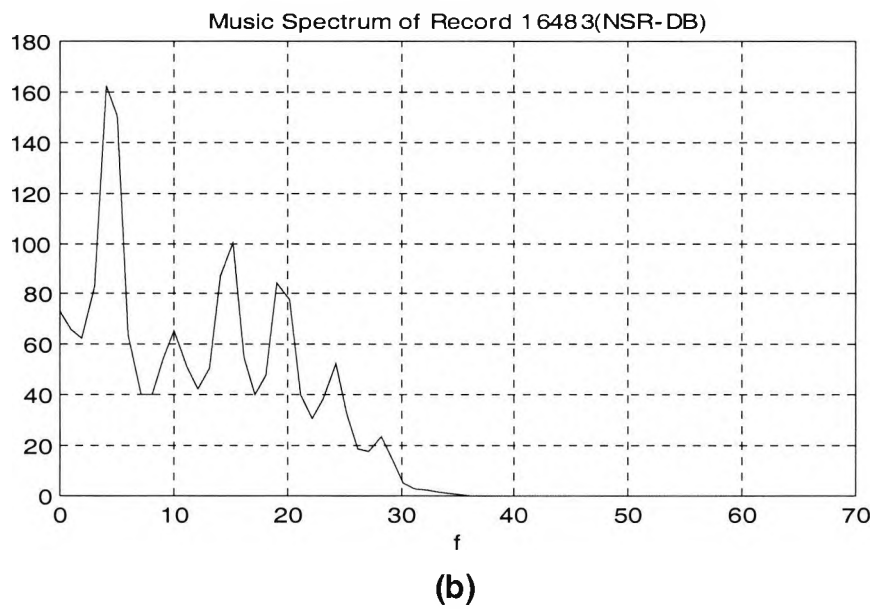
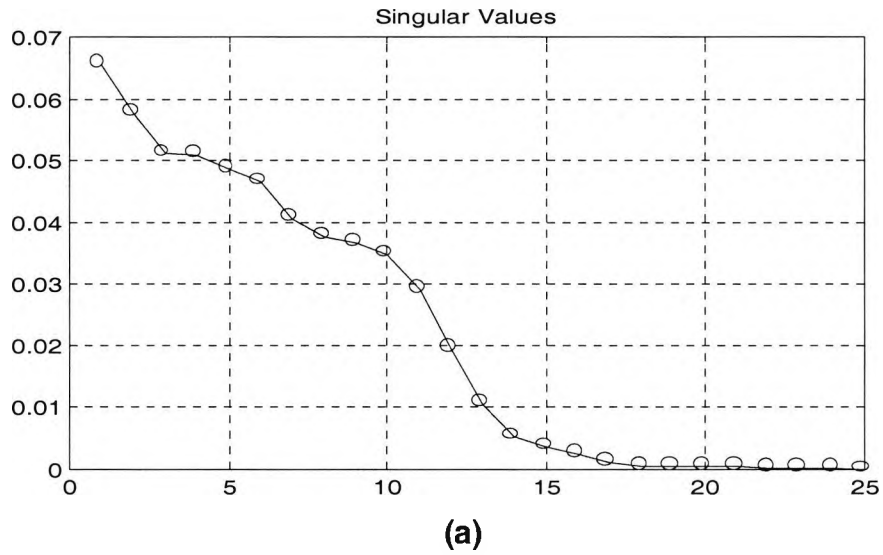
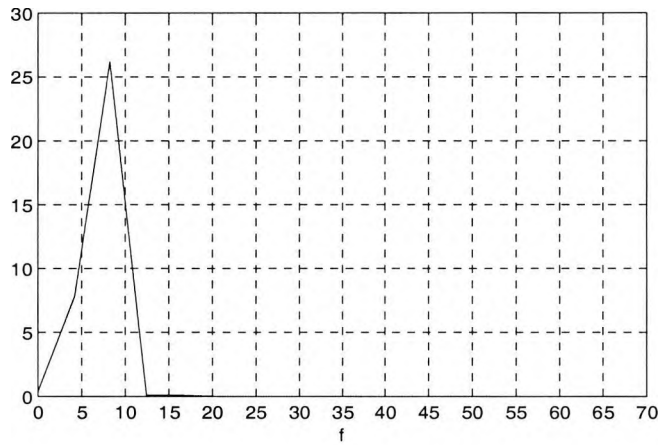
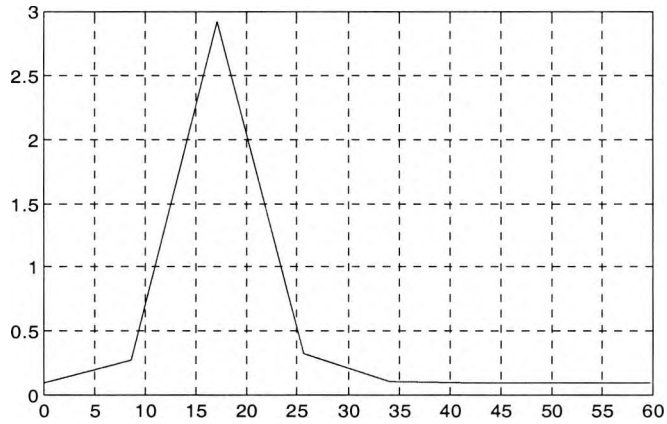


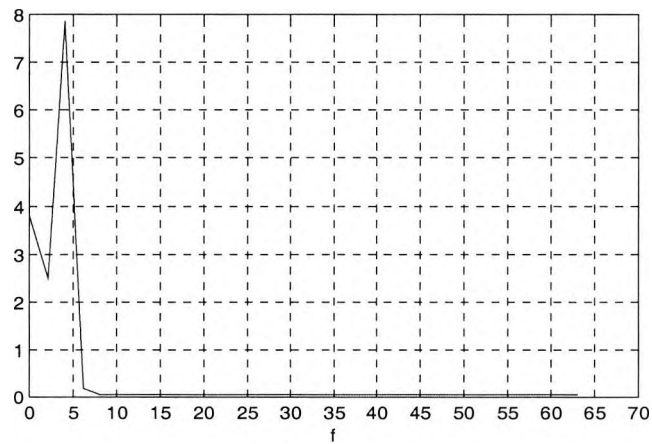
Figure 3.6 (a) Singular-values of the covariance matrix, and (b) the MUSIC spectrum of the whole ECG cycle (record No. 16483, the NSR-DB) with zero padding to 128, $p=15$ and $L=24$.



(a)



(b)



(c)

Figure 3.7 MUSIC spectra for (a) the PR interval, (b) QRS complex, and (c) ST-T complex. With zero padding to the nearest FFT length. The signal subspace parameters, $p=5$ for (a) and $=3$ for (b) and (c).

Segment	Record 16539	Record 16483
Whole ECG	4.0315, 15.1181, 10.0787, 19.1496, 23.1811 and 28.2205 Hz.	4.0315, 15.1181, 19.1496, 10.0787, 24.1890 and 28.2205 Hz.
PR interval	2.0317 and 6.0952 Hz.	8.2581 Hz.
QRS complex	17.0667 Hz.	17.0667 Hz.
ST-T complex	2.0317 Hz.	4.0635 Hz.

Table 3.1 Spectral peaks of the MUSIC spectra estimated for records No. 16539 and No. 16483 (NSR-DB).

The next step in this analysis is to compare the MUSIC spectrum of a normal ECG signal with that of an ischaemic case. The normal ECG is interpolated to threefold using cubic spline technique (see appendix A) to over sample the signal to about 360 Hz, to match the sampling rate for the ST Change-DB. Figure 3.8 shows the MUSIC spectra for these two cases. The upper panel is the spectrum for a normal subject (record No. 19830, NSR-DB). The middle and the bottom panels show the MUSIC spectra for two ischaemic cases record No. 325 (ST elevation case) and No. 301 (ST depression case), these two cases are taken from the ST Change-DB. Both of these spectra are characterised by High Frequency Components (HFC) in the higher frequency region, $f > 60$ Hz, outside the region that the normal spectrum cover, $f < 60$ Hz. These HFC are investigated in more details in the next section.

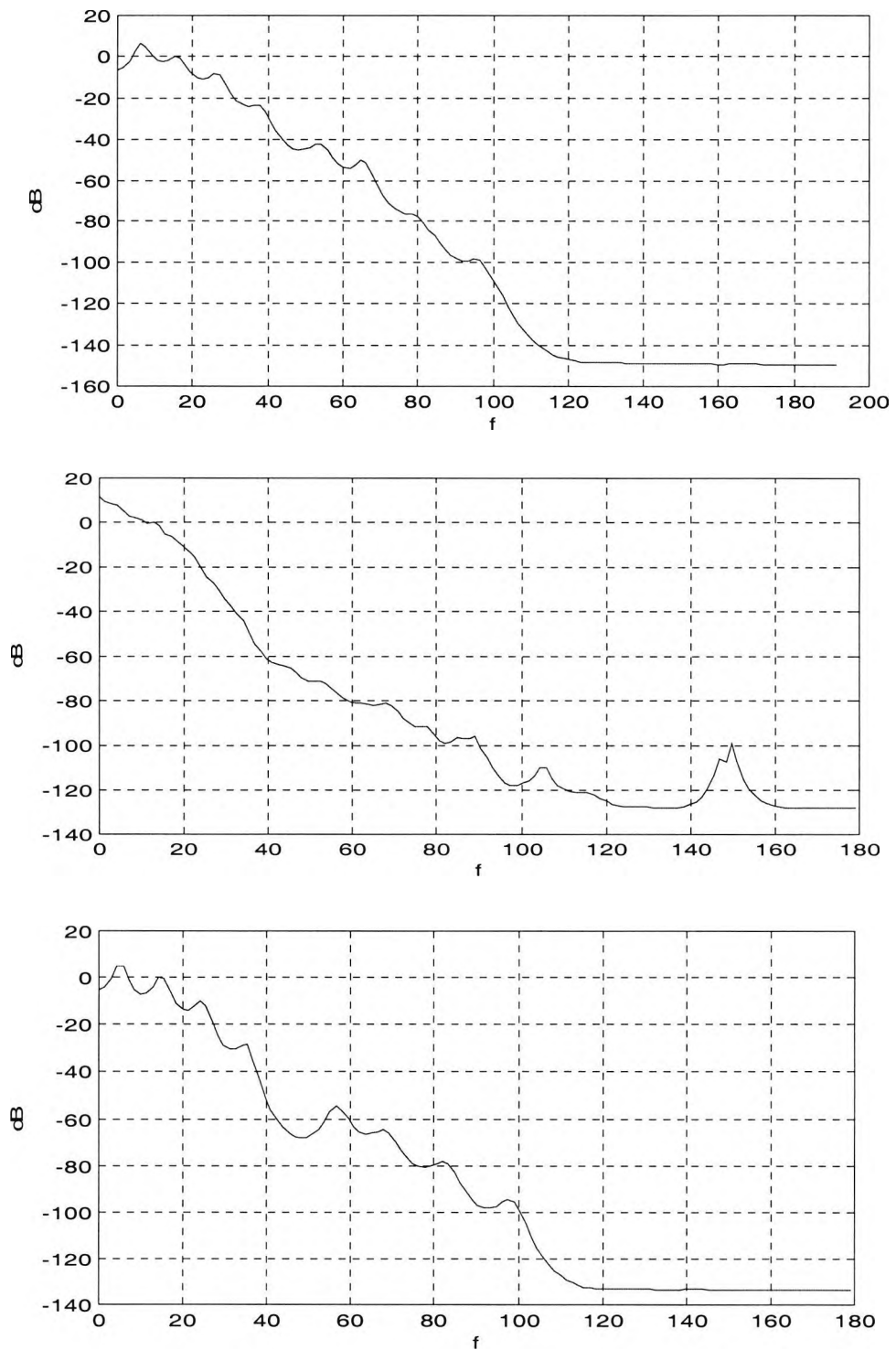


Figure 3.8 MUSIC spectra of a normal case (top, record No. 19830), and two ischaemic cases (record No. 325 in the middle and record No. 301 in the bottom). $p=16$ and $L=24$.

3.4 Detection of Ischaemic Heart Disease

3.4.1 Introduction

To maintain proper functioning, the heart must have a continuous supply of oxygen. When the oxygen supply becomes inadequate, varying degrees of ischaemia appear, angina pectoris, MI, or sudden death may occur. Any circumstance that increases myocardial oxygen demand or reduces the oxygen supply is capable of inducing angina. It is commonly noted with strenuous physical effort or emotional upsets (Camm 1998). In hospitals there are several ways of stressing the heart to assess patients with ischaemic heart disease. These include dynamic exercise¹, isometric exercise¹, pharmacological stress¹, and atrial pacing¹. Not all patients are able to do dynamic exercise, due to obesity, poor physical conditions, respiratory limitation, arthritis, diabetes, unstable angina, or risk of complication and physical incapacity in patients with recent Myocardial Infarction (MI). Cardiac stress induced by isometric exercise is often inadequate in provoking ischaemic events. Pharmacological stress by drugs such as dipyridamole or dobutamine is commonly associated with undesirable cardiac or noncardiac side effects. Although transesophageal atrial pacing has been reported to be safe it may develop sensation during the procedure also careful patient education and preparation must be made before the pacing (Armstrong 1997; Jadvar, et al. 1991; Mazeika, et al. 1992). It has been estimated that 15% to 30% of patients with suspected or known coronary artery disease are unable to perform an adequate exercise stress test (Bruce, et al. 1974; Jadvar, et al. 1991). It is therefore beneficial, using advanced signal processing techniques, to be able to detect ischaemic heart diseases even when they do not manifest themselves as ST-segment depression or elevation.

3.4.2 ECG Data Annotation

ECG data from the ST Change-DB and the NSR-DB (MIT-CD 1997) are used in this analysis. Since the ST Change-DB provides no ST-segment and/or T-wave annotation,

¹ See appendix E for definitions.

these data are annotated by two well-trained cardiologists¹. In this annotation episodes of ST depression/elevation have been carefully identified. Four groups of episodes are studied:

Group 1: this group is taken from the NSR-DB and is called Normal Confirmed Episodes (NCE).

Group 2: this group is taken from ST Change-DB at the initial resting phase of the exercise test for records No. 300 to No. 323, and from episodes that do not show elevation for records No. 324 to No. 327. In this group of episodes ischaemia could not be confirmed by the cardiologists as there is no clinically significant ST depression/elevation and the ST-T episodes look normal, i.e., Normal Looking Episodes (NLE). This group may contain episodes from either ST depression or ST elevation records.

Group 3: this group is taken from ST Change-DB at the peak effort phase of the exercise test for records No. 300 to No. 323, and from episodes that do show elevation for records No. 324 to No. 327. In this group ischaemia is manifested in the form of ST depression or elevation. Ischaemia is confirmed by the cardiologists, i.e., Ischaemic Confirmed Episodes (ICE). The ICE group may contain episodes from either ST depression or ST elevation records.

Group 4: this group is taken from ST Change-DB and includes episodes from some records in which the cardiologists could not confirm ischaemic events throughout the whole record. This group is named Ischaemic Suspected Episodes (ISE).

3.4.3 Analysis Technique

The HFC found previously in the MUSIC spectrum for ischaemic subjects using the whole ECG cycle may appear clearer and more significant in the MUSIC spectrum of the combined ST-segment and T-wave (ST-T complex) for the following reasons: 1) As explained in chapter one ischaemic heart disease mainly affects the ST-T complex. 2)

¹ Independent annotation by Dr. E.M. Elswefy, MRCP, PhD, and Dr. A. Zeida, MRCP, PhD, St. George's Hospital Medical School, London, UK and Assiut University, Egypt.

The steep slopes inside the QRS complex act as an impulse and resulted in a continuous spectrum that may cover the low amplitude high frequency components. The facts that the MUSIC algorithm is a super-resolution frequency estimation technique and it is based on single realisation of the underlying stochastic process represented by its correlation/data matrices make it useful in calculating low amplitude, high frequency components. The following strategy is adopted in this analysis

1) Pre-processing, since the baseline wander may affect the level of the ST-segment, the baseline wander is eliminated as previously described in chapter 2. All data records are visually checked beat by beat to ensure that they are free from ectopic beats, electrode disconnection and considerably high amplitude EMG and MA noises and power line interference. The NSR-DB records are interpolated to about three folds using cubic spline technique (Press, et al. 1990). Then R peaks are detected, R peak detection algorithm consists of amplitude normalisation, separation of the positive part, squaring then using certain amplitude and time thresholds to detect the position of the R peaks (Tompkins 1993). ST-T complexes are started 50 msec after the R peak (18 samples), with segment size of about 400 msec; which is equivalent to about 150 samples.

2) Investigate the MUSIC spectrum of ST-T complex from NCE and ICE groups and report the differences between these two spectra.

3) As a reference, apply the MEM method, which is a parametric high-resolution technique to calculate the previous spectra and compare the results. The MEM spectrum is calculated from:

$$S_{MEM}(f) = \frac{U_m}{\left| 1 + \left[\sum_{i=1}^m a_{m,i}^* \exp\{-j2\pi fiT\} \right] \right|^2} \quad (3.9)$$

where: $S_{MEM}(f)$: output power spectral density, U_m : the power of the white noise or prediction error, f : frequency, T : sampling interval, $-1/2T \leq f \leq 1/2T$, and $a_{m,i}$: the AR-parameters, of a prediction error filter of order m . More detailed reviews of the Burg algorithm may be found in (Burg 1967; Marple 1980).

- 4) Calculate the MUSIC spectra for ST-T complexes from ICE and NLE groups of the same patient and analyse the difference.
- 5) Estimation of the optimal order of the process is a delicate problem, unresolved in the literature of ECG analysis until now. An order range from 13-20 has been used by Schels, et al. (1991) to detect LPs using the MEM spectrum. An empirical analysis combined with model order selection criteria described in chapter 2 showed that the number of signals in the signal subspace and the AR order for the MEM should be chosen in the range 15-20 to obtain a clear picture of the HFC in the MUSIC spectrum of the ST-T complexes.
- 6) The diagnostic accuracy (the fraction of correct diagnoses), the sensitivity (the fraction of correctly diagnosed ischaemic segments) and the specificity (the fraction of correctly diagnosed normal segments) are calculated to evaluate the performance of the analysis (Sievanen, et al. 1994).

3.5 Results

Time domain plots for the different types of episodes that have been used in this analysis are shown in Figure 3.9. One ECG cycle from each type of episode is included in this Figure. The top two ECG cycles represent NCE (record No. 16483, NSR-DB (MIT-CD 1997)) and ISE (record No. 316, ST Change-DB (MIT-CD 1997)), the middle represent ICE and NLE for ST depression case (record No. 300, ST Change-DB) and the two in the bottom represent ICE and NLE for ST elevation case (record No. 324, ST Change-DB).

Figure 3.10 shows the results obtained using MUSIC (top) and MEM (bottom) for normal case (record No. 16539, NSR-DB). Figure 3.11 is the corresponding spectra for an ischaemic case (record No. 327, ST Change-DB). Ten randomly selected ST-T complexes from each episode are analysed using the MUSIC and the MEM algorithms. The spectrum of each of these ten segments is calculated and superimposed in a cascade diagram (waterfall 3-D plot).

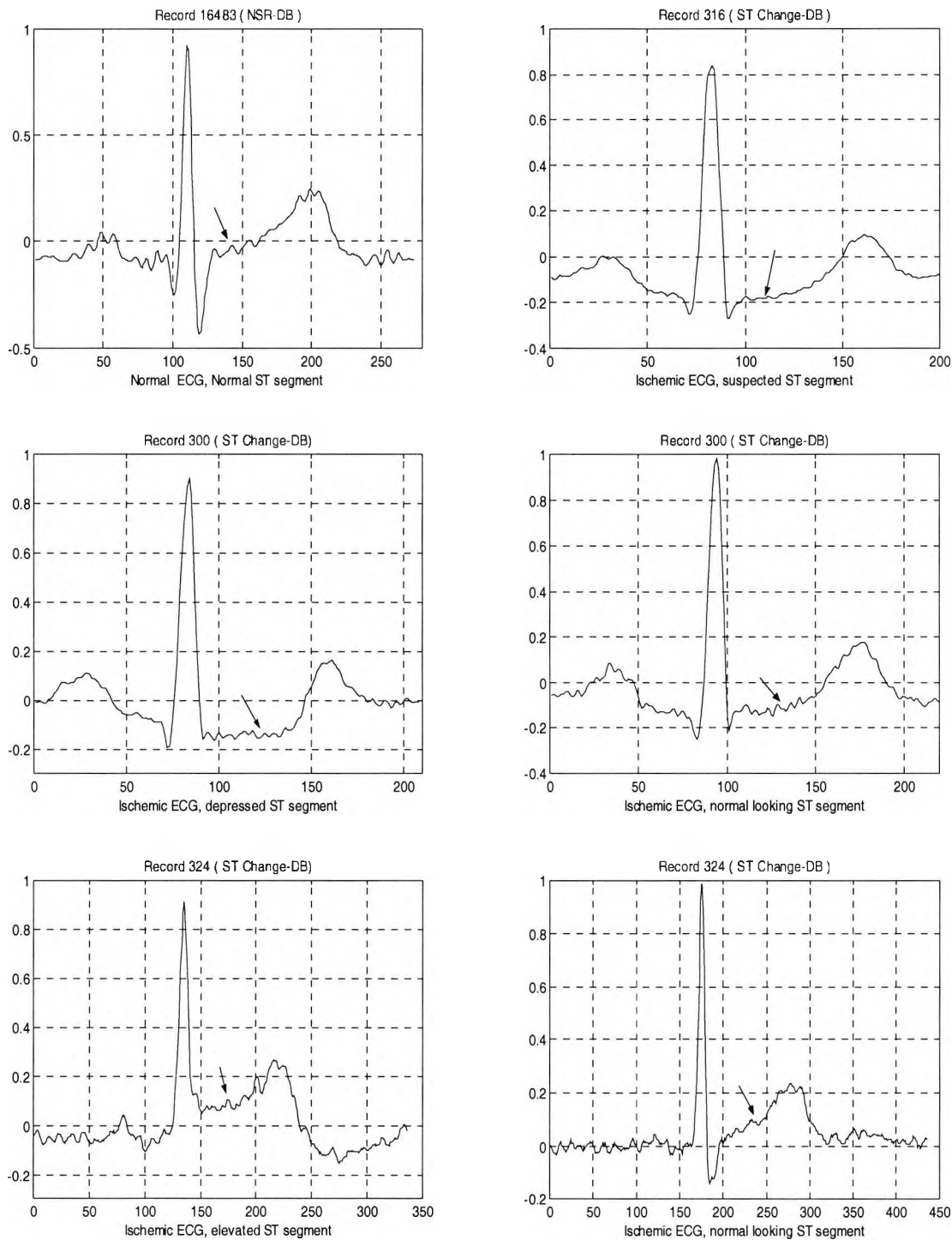


Figure 3.9 One ECG cycle from different episodes, NCE, ISE, NLE, ICE (ST-depression) and NLE, ICE (ST-elevation) from top to bottom, respectively.

Since no amplitude normalisation has been applied to the resultant spectra from the MUSIC and MEM algorithms, the two methods resulted in different amplitude ranges as depicted in Figures 3.10 and 3.11. Both methods reveal high frequency components (HFC) in the range $60 \text{ Hz} < f < 180 \text{ Hz}$ for the ischaemic case. Since this ischaemic case is a MI patient these HFC represent the so-called LPs, which are defined in chapter 1. Better resolution is obtained using the MUSIC algorithm. A previous work by Schels, et al. (1991) suggested that Burg technique (MEM spectrum) in the original form is insufficient for the analysis of the ST-segment and to enhance the visual differentiation of LPs, the authors developed a frequency analysis technique based on the difference between two MEM spectra. In the present study the MUSIC spectrum clearly reveals the LPs / HFC.

Using 50 randomly selected ST-T complexes from each type of episode for each data record, the MUSIC spectra of a total of 1800 ST-T complexes (700 from the NCE, 350 from the NLE, 550 from the ICE and 200 from the ISE) are estimated. This is equivalent to analysing about 1494 sec from the data. Figures 3.12, 3.13 and 3.14 depict 3-D waterfall plot of the MUSIC spectra for different types of episodes. Each Figure consists of three parts plotted in three pages for data taken from different parts of the data file. Each part shows the MUSIC spectra of two types of episodes in two panels. In each panel the spectra of 10 complexes from one type of episodes are shown as 3-D waterfall plot. Prominent spectral peaks in the range $60 \text{ Hz} < f \leq 100 \text{ Hz}$ characterise the MUSIC spectra of the episodes that represent ST-segment depression as shown in Figure 3.12. Prominent spectral peaks in the range $60 \text{ Hz} < f < 180 \text{ Hz}$ characterise the MUSIC spectra of the episodes that represent ST-segment elevation are shown in Figure 3.13. Figure 3.14 (a) shows the MUSIC spectra of the ST-T complexes of a normal case (No. 18184), there are no detectable spectral peaks in the high frequency range. Figure 3.14 (b) represent an ISE case (record No. 316), the existence of spectral peaks in the range $60 \text{ Hz} < f \leq 100$ confirms the database classification, i.e., ST-segment depression for this record.

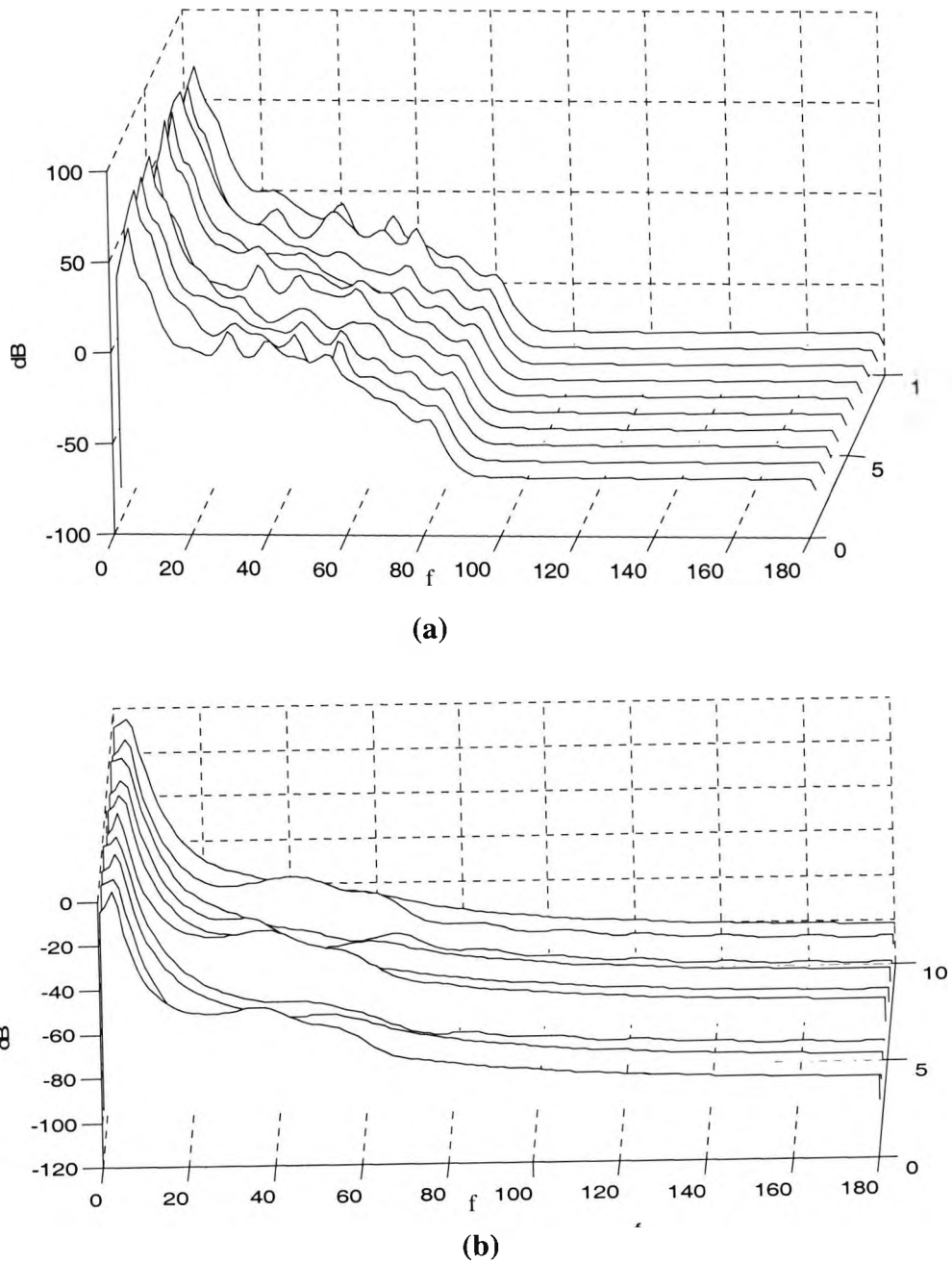


Figure 3.10 MUSIC (a) and MEM (b) spectra for ten randomly selected ST-T complexes of a normal case (record No. 16539, NSR-DB). Using a segment size of about 150 samples.

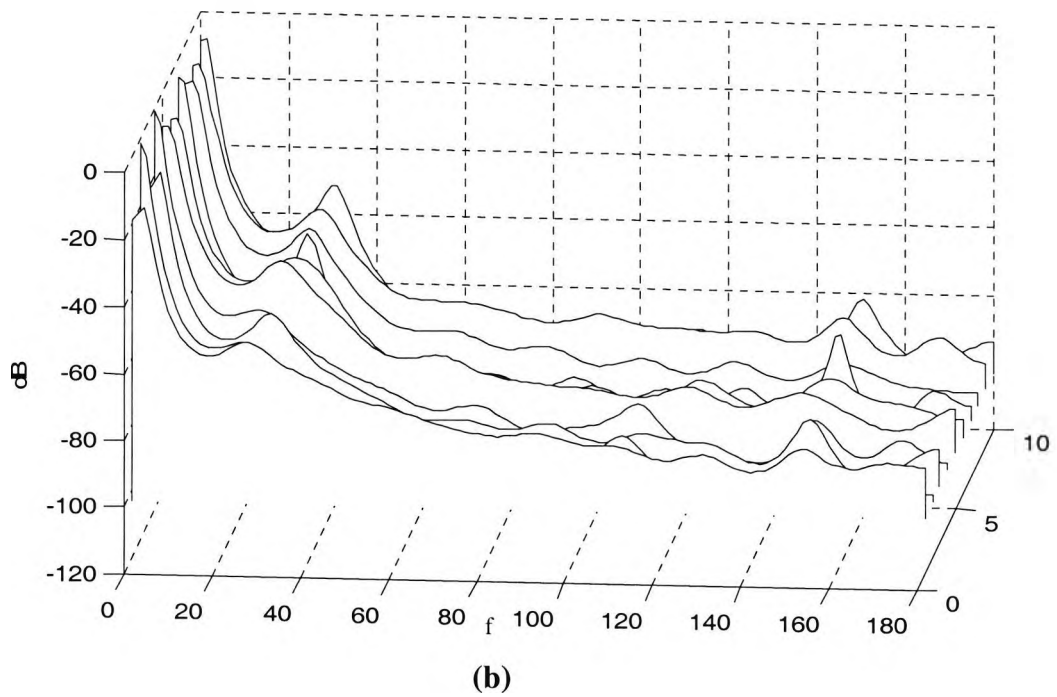
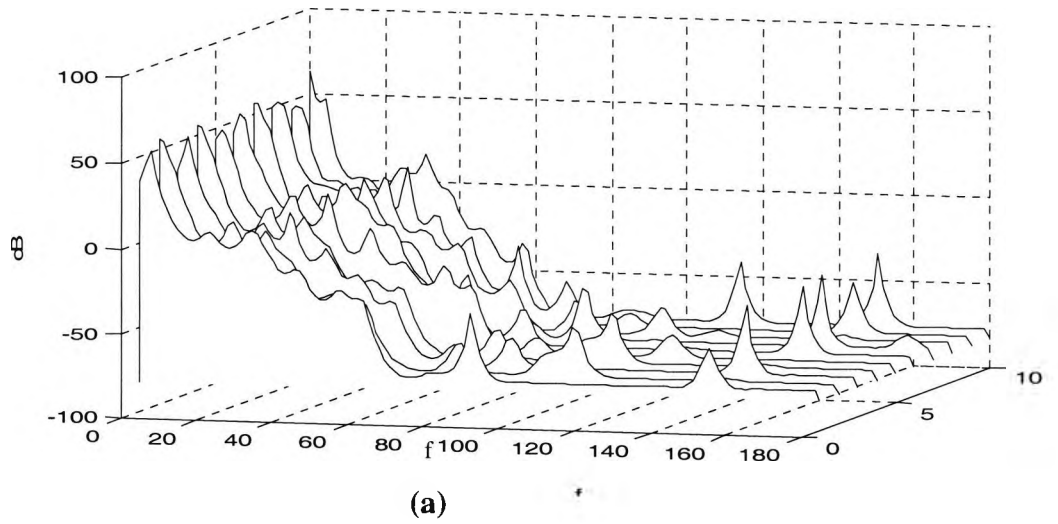


Figure 3.11 MUSIC (a) and MEM (b) spectra for ten randomly selected ST-T complexes of an ischaemic case (record No. 327, ST Change-DB). Using a segment size of about 150 samples.

Comparing Figures 3.12 (a) and 3.12 (b) which represent ICE's and NLE's for ST-segment depression case, respectively, we can conclude that the spectral peaks in the range in $60 \text{ Hz} < f \leq 100 \text{ Hz}$ are obvious in episodes that represent the initial resting phase of exercise test just like that in the peak effort phase of the exercise. Comparing Figure 3.13 (a) and 3.13 (b), which represent ICE's and NLE's for ST-segment elevation case, respectively, one can notice the spectral similarity between these episodes.

From the above two observations it may be possible to detect ischaemia by applying high-resolution spectral analysis techniques on little effort exercise test or even resting ECG signals. This result is important considering some ischaemic cases in which ischaemia cannot be detected without exercise test such as chronic stable angina. A dominant spectral peak at about 85 Hz in the cases of ST-segment depression and at about 150 Hz in ST-segment elevation cases characterises the MUSIC spectra of about 70% of the total number of segments. This spectral peak can be used as a significant feature to differentiate between normal, depressed, and elevated ST-segments. Figure 3.15 shows the MUSIC spectra for one segment from each of these three cases.

Table 3.2 summarises the results obtained for all normal and ischaemic cases. From this table the accuracy, sensitivity and specificity of the analysis are calculated as follows (Green and Swets 1966; Jager, et al. 1991):

Accuracy = $(TP+TN)/\text{Total number of segments}$,

Sensitivity = $TP/(TP+FN)$, and

Specificity = $TN/(TN+FP)$.

where TP: true positive, number of correctly diagnosed ischaemic segments, TN: true negative, number of correctly diagnosed normal segments, FN is the false negative, number of incorrectly diagnosed ischaemic segments, and FP is the false positive, number of incorrectly diagnosed normal segments.

According to these definitions, the resulted accuracy, sensitivity and specificity are 84%, 80%, and 91%, respectively.

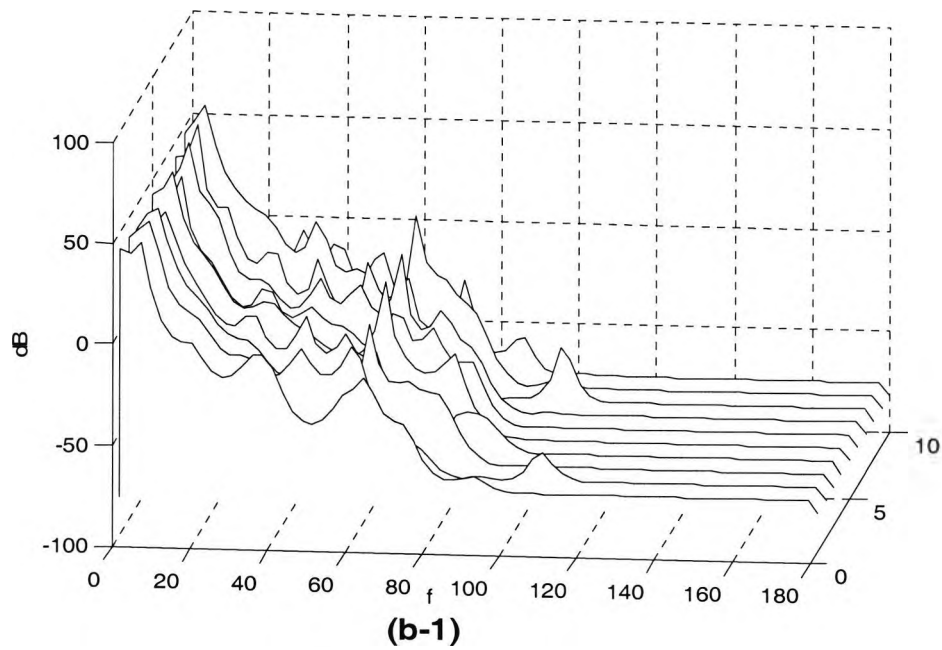
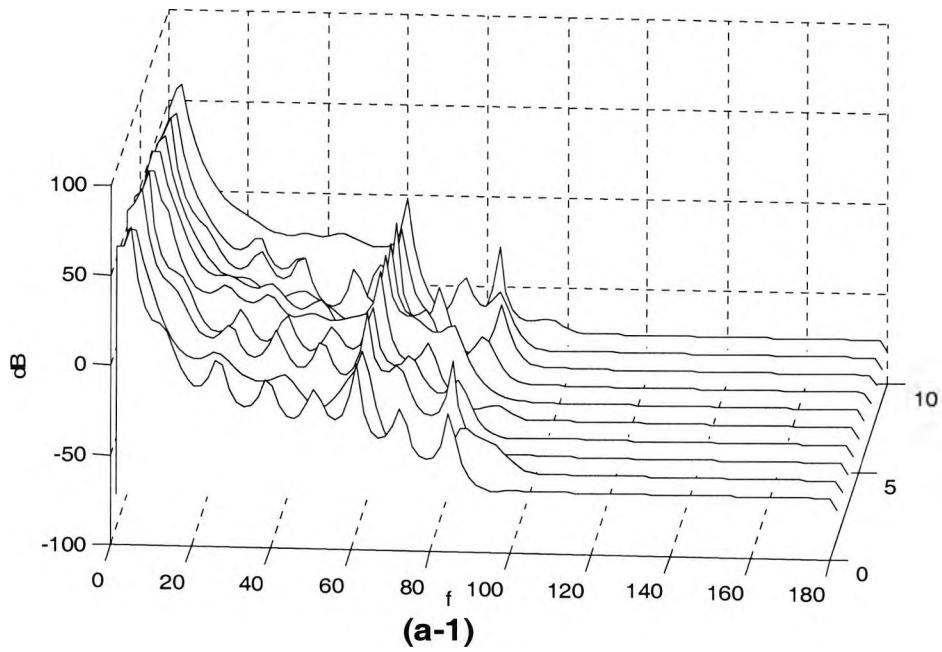
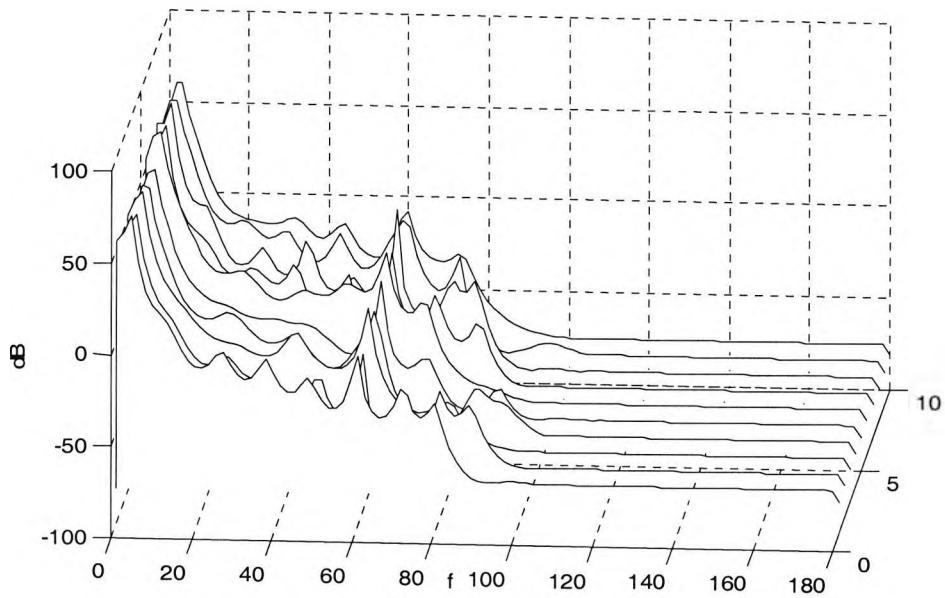
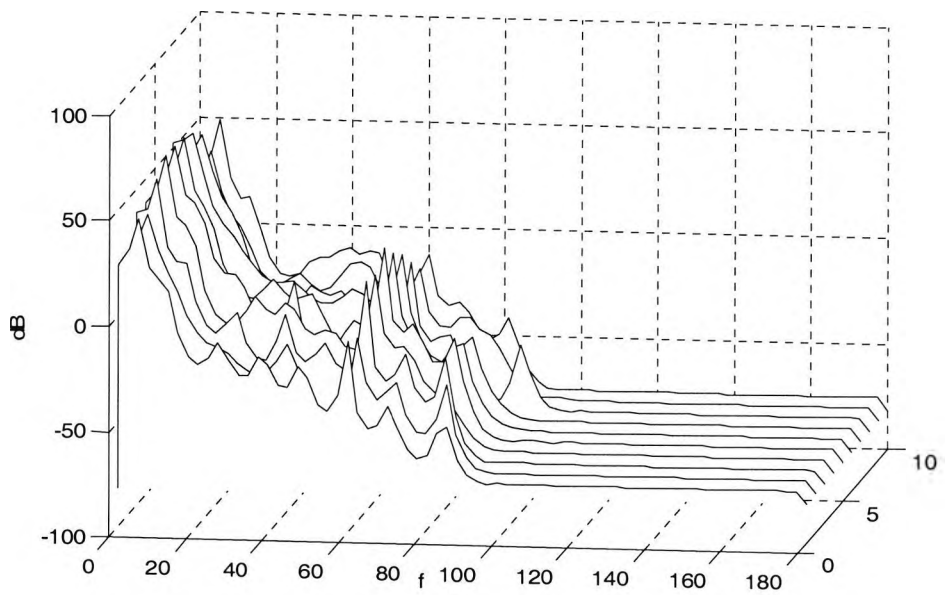


Figure 3.12 MUSIC spectra of ten ST-T complexes for episodes represent NLE (a-1), and ICE (b-1) for ST-segment depression case (record No. 301,ST Change-DB). Using a segment size of about 150 samples.



(a-2)



(b-2)

Figure 3.12-continued MUSIC spectra of ten ST-T complexes for episodes represent NLE (a-2), and ICE (b-2) for ST-segment depression case (record No. 301, ST Change-DB). Using a segment size of about 150 samples.

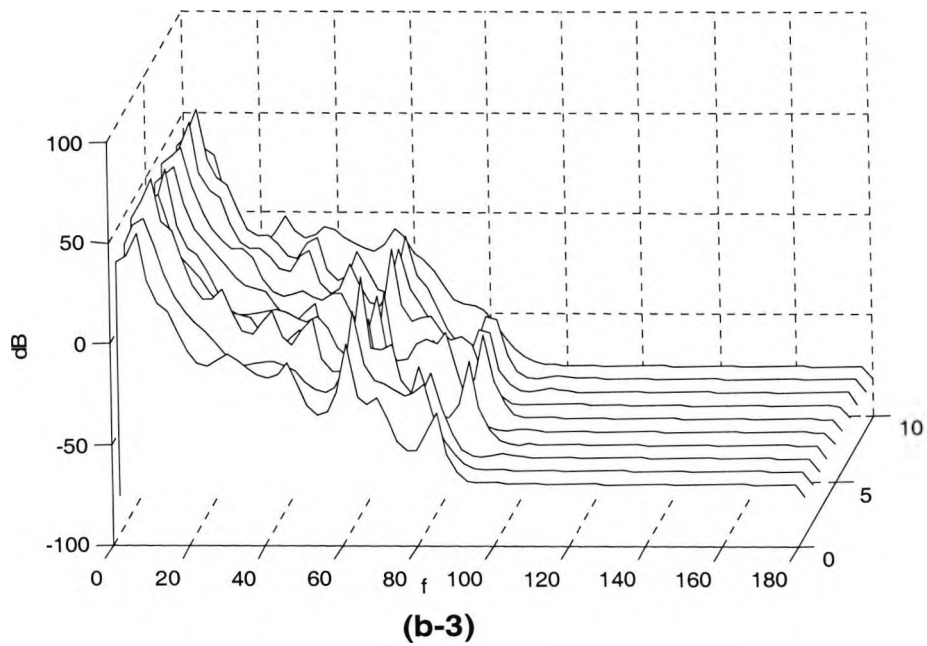
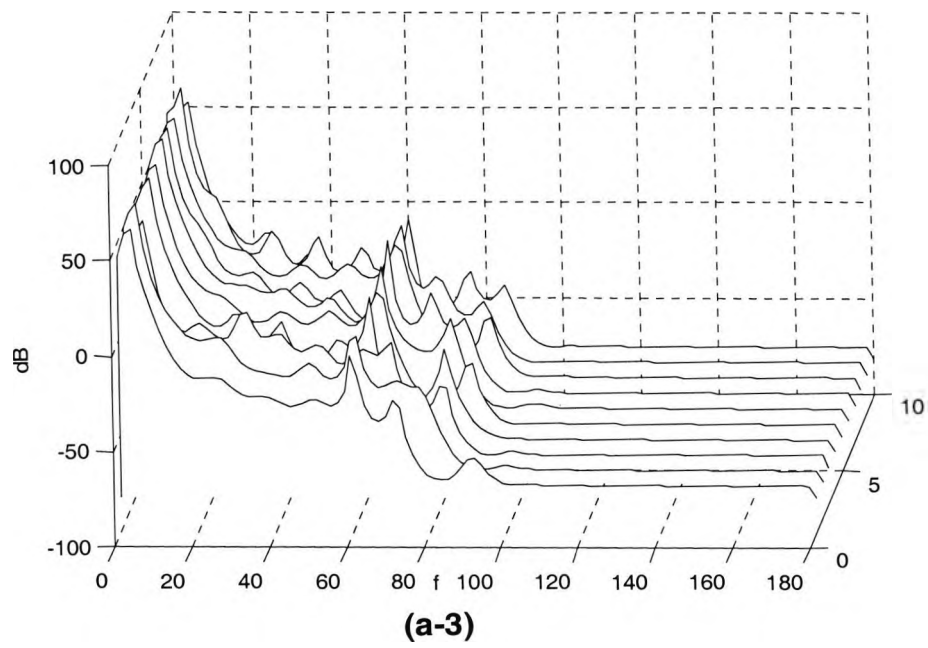


Figure 3.12-continued MUSIC spectra of ten ST-T complexes for episodes represent NLE (a-3), and ICE (b-3) for ST-segment depression case (record No. 301, ST Change-DB). Using a segment size of about 150 samples.

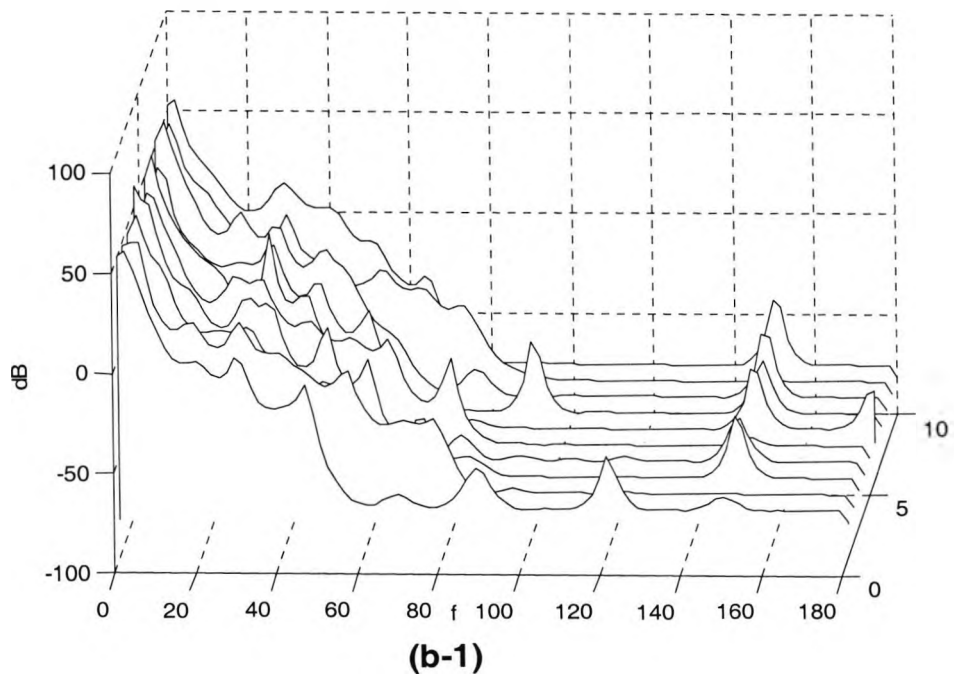
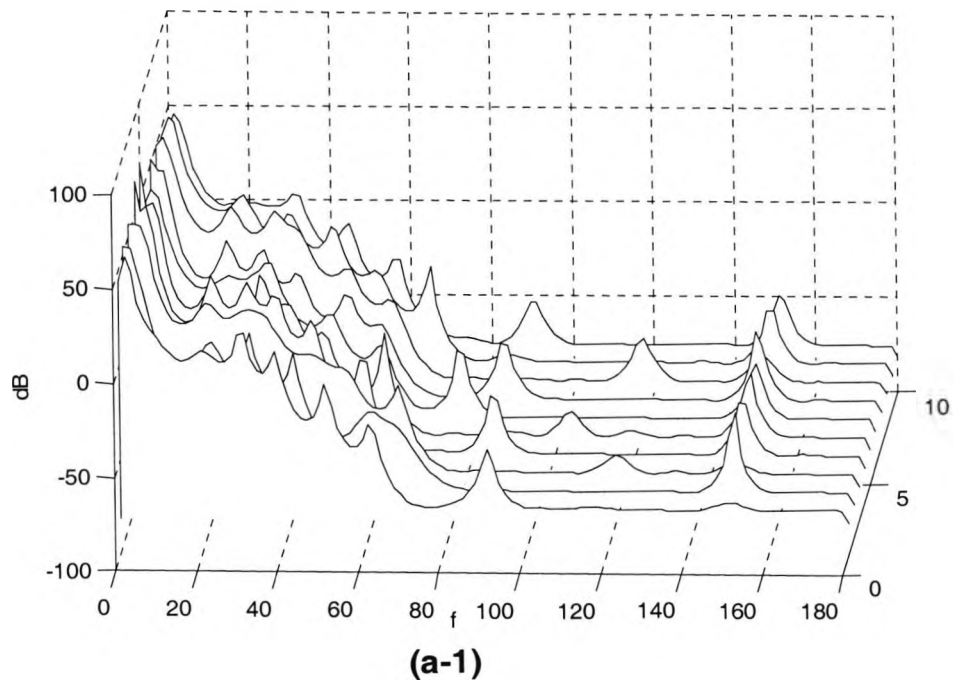
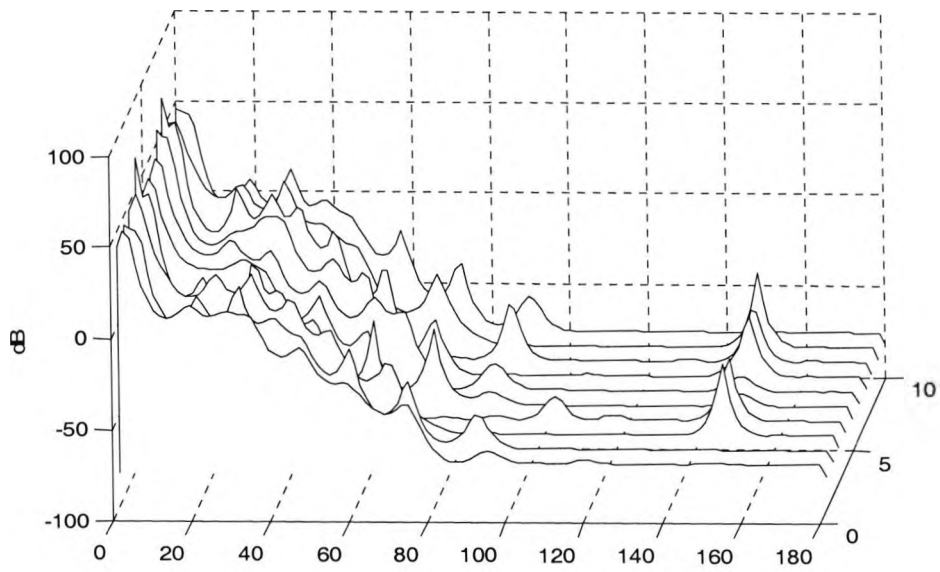
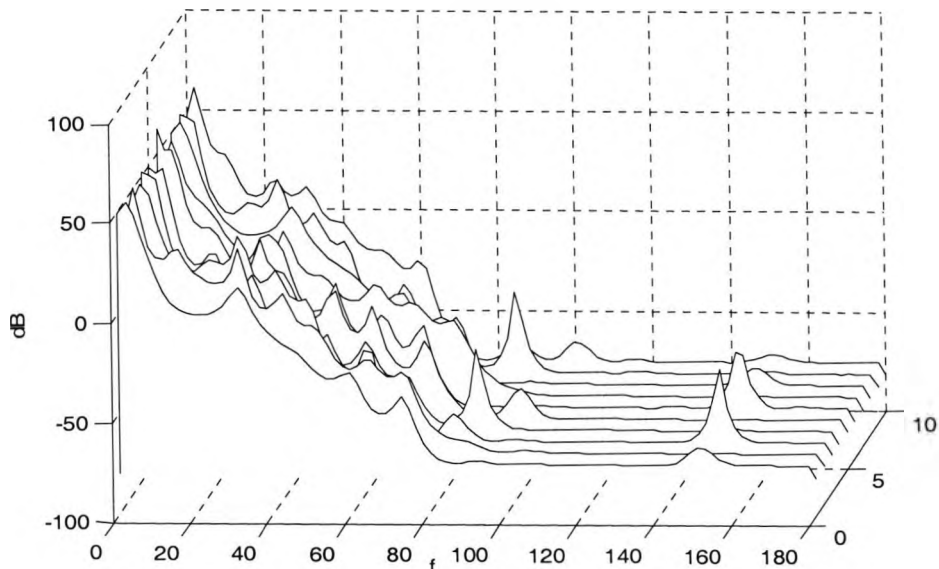


Figure 3.13 MUSIC spectra of ten ST-T complexes for episodes represent NLE (a-1), and ICE (b-1) for ST-segment elevation case (record No. 325, ST Change-DB). Using a segment size of about 150 samples.

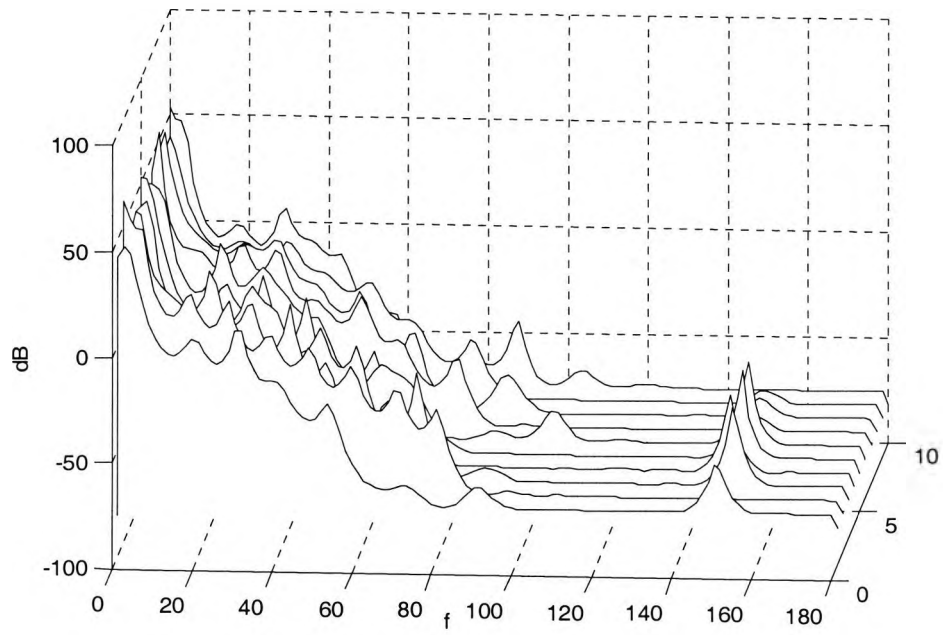


(a-2)

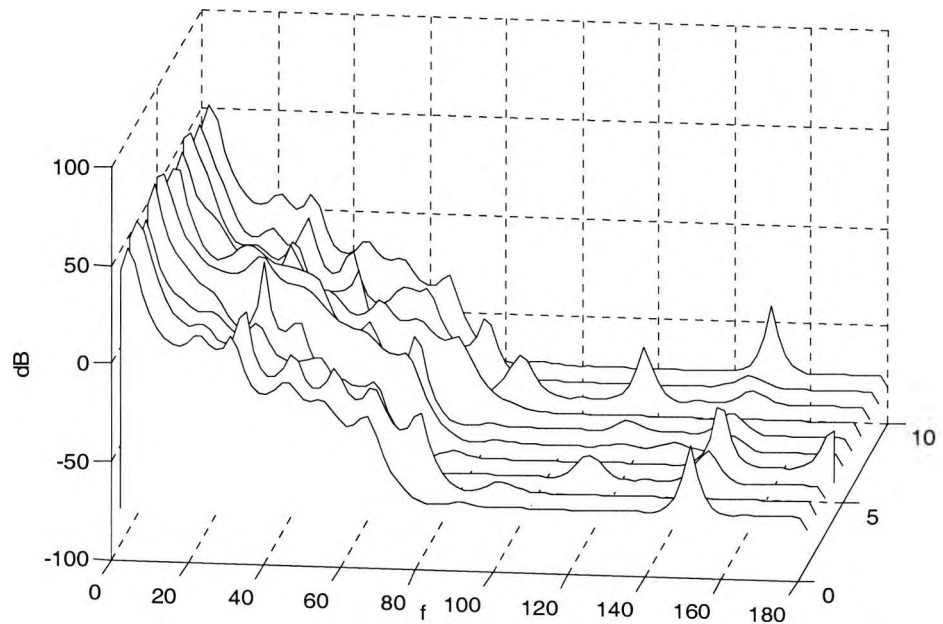


(b-2)

Figure 3.13-continued MUSIC spectra of ten ST-T complexes for episodes represent NLE (a-2), and ICE (b-2) for ST-segment elevation case (record No. 325, ST Change-DB). Using a segment size of about 150 samples.



(a-3)



(b-3)

Figure 3.13-continued MUSIC spectra of ten ST-T complexes for episodes represent NLE (a-3), and ICE (b-3) for ST-segment elevation case (record No. 325, ST Change-DB). Using a segment size of about 150 samples.

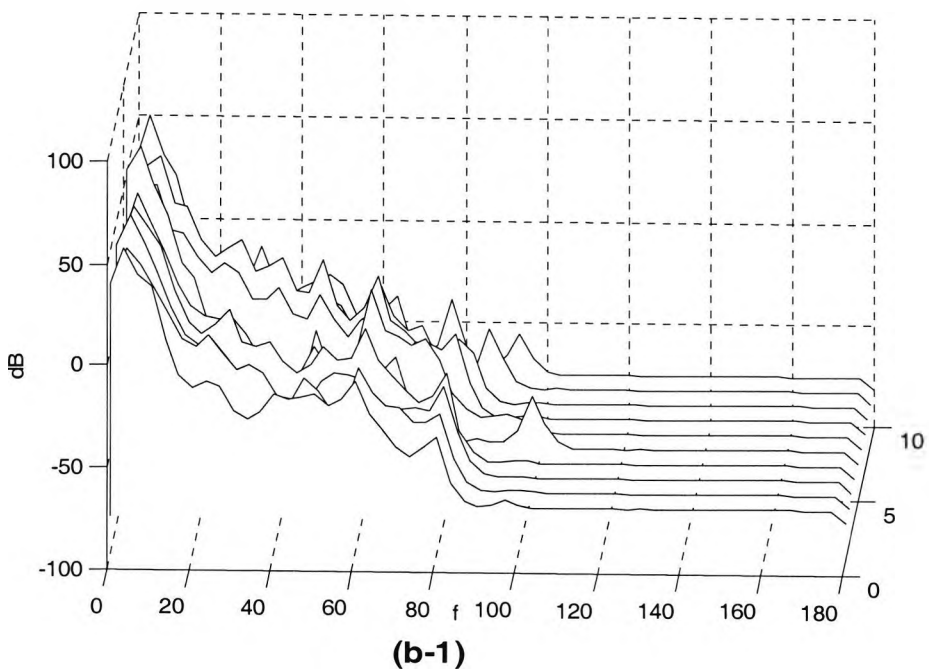
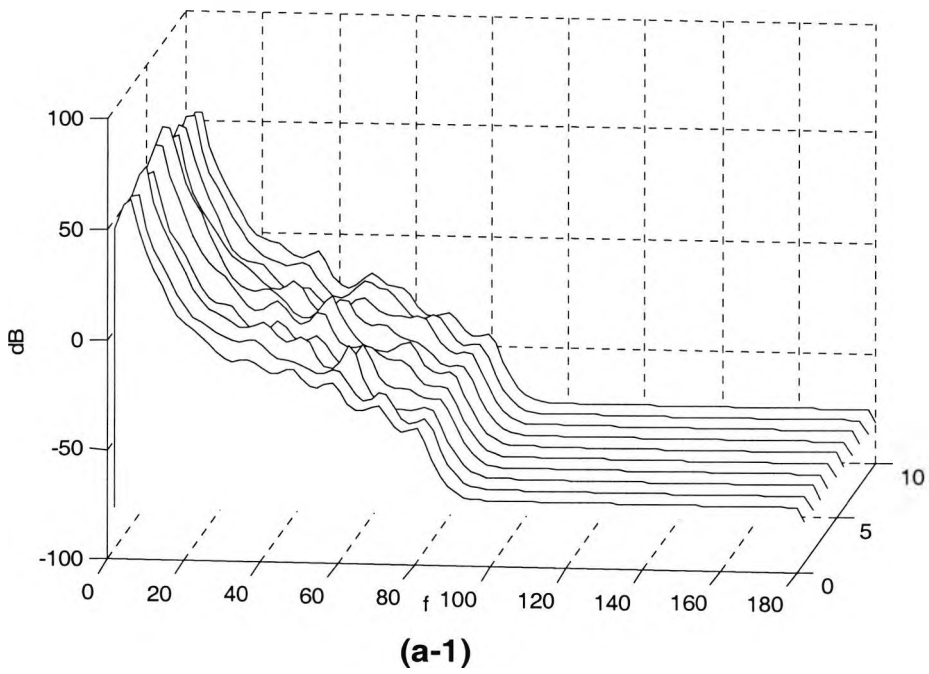


Figure 3.14 MUSIC spectra of ten ST-T complexes for episodes represent NCE (a-1), and ISE (b-1) for a normal case (record No. 18184) and an ischaemic case (record No. 316, ST Change-DB). Using a segment size of about 150 samples.

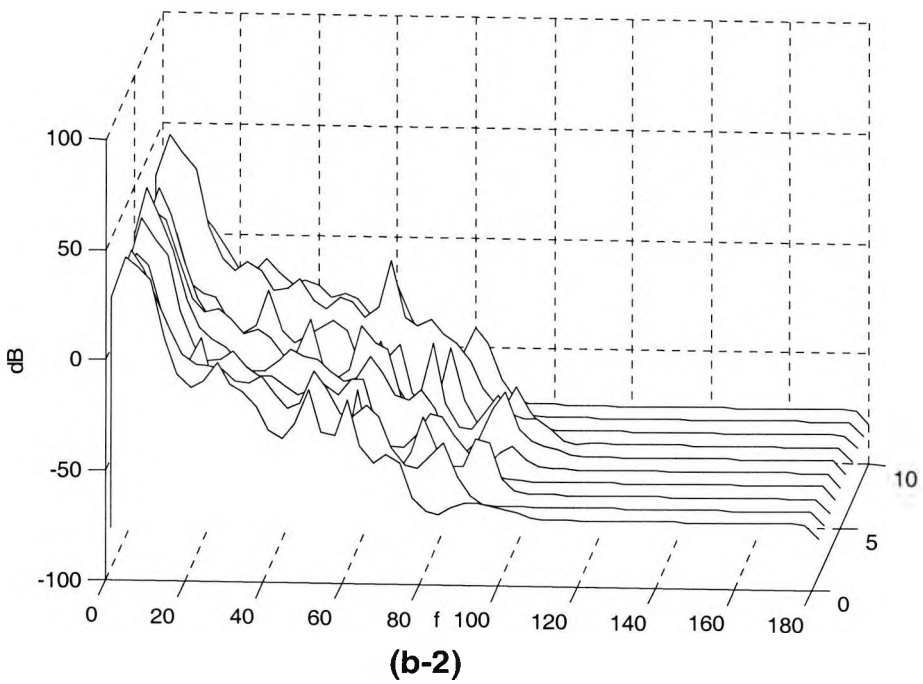
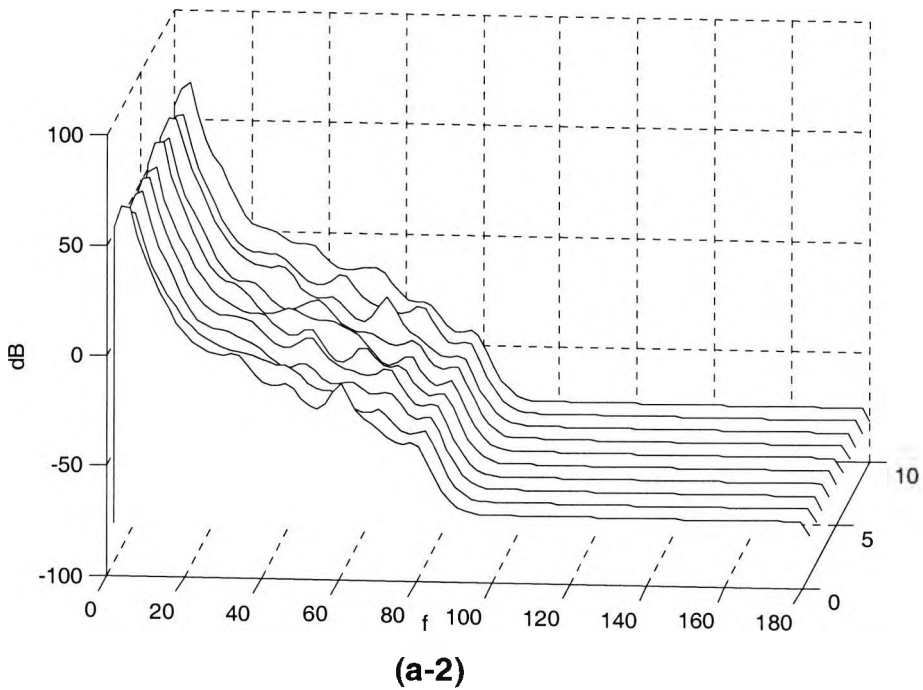


Figure 3.14-continued MUSIC spectra of ten ST-T complexes for episodes represent NCE (a-2), and ISE (b-2) for a normal case (record No 18184, NSR-DB) and an ischaemic case (record No. 316, ST Change-DB). Using a segment size of about 150 samples.

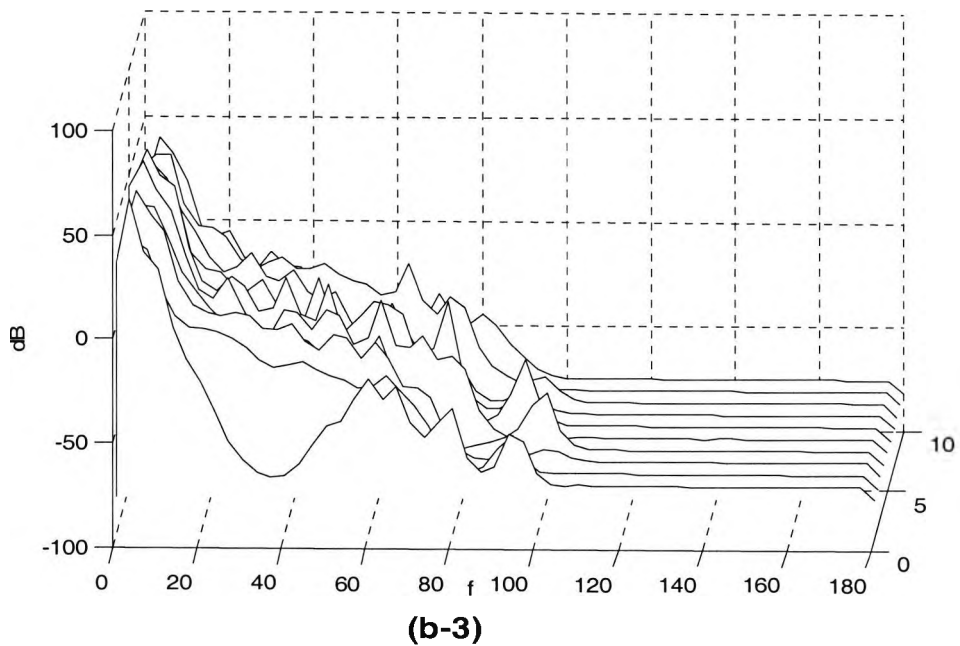
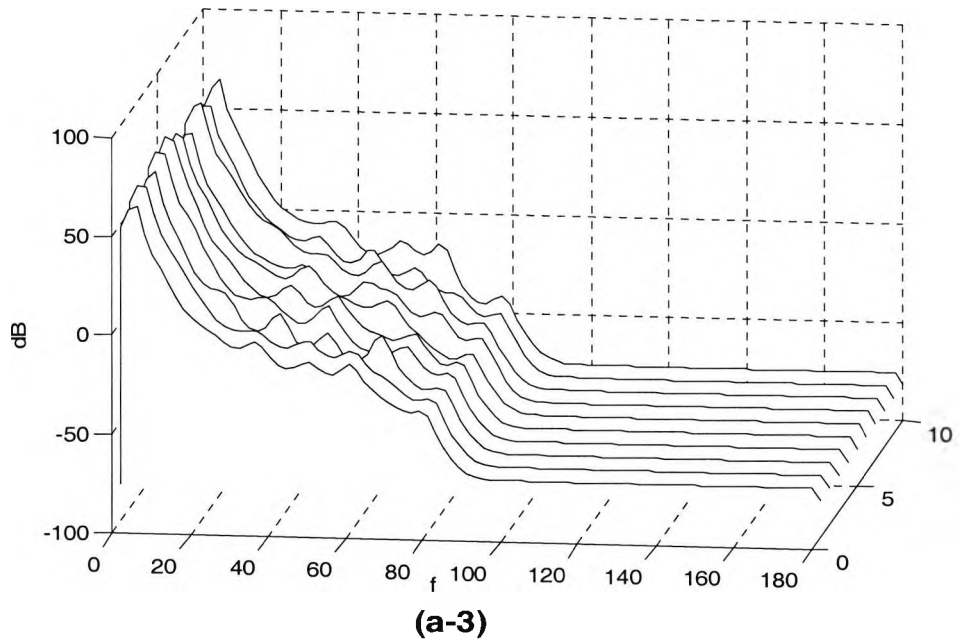


Figure 3.14-continued MUSIC spectra of ten ST-T complexes for episodes represent NCE (a-3), and ISE (b-3) for a normal case (record No. 18184, NSR-DB) and an ischaemic case (record No. 316, ST Change-DB). Using a segment size of about 150 samples.

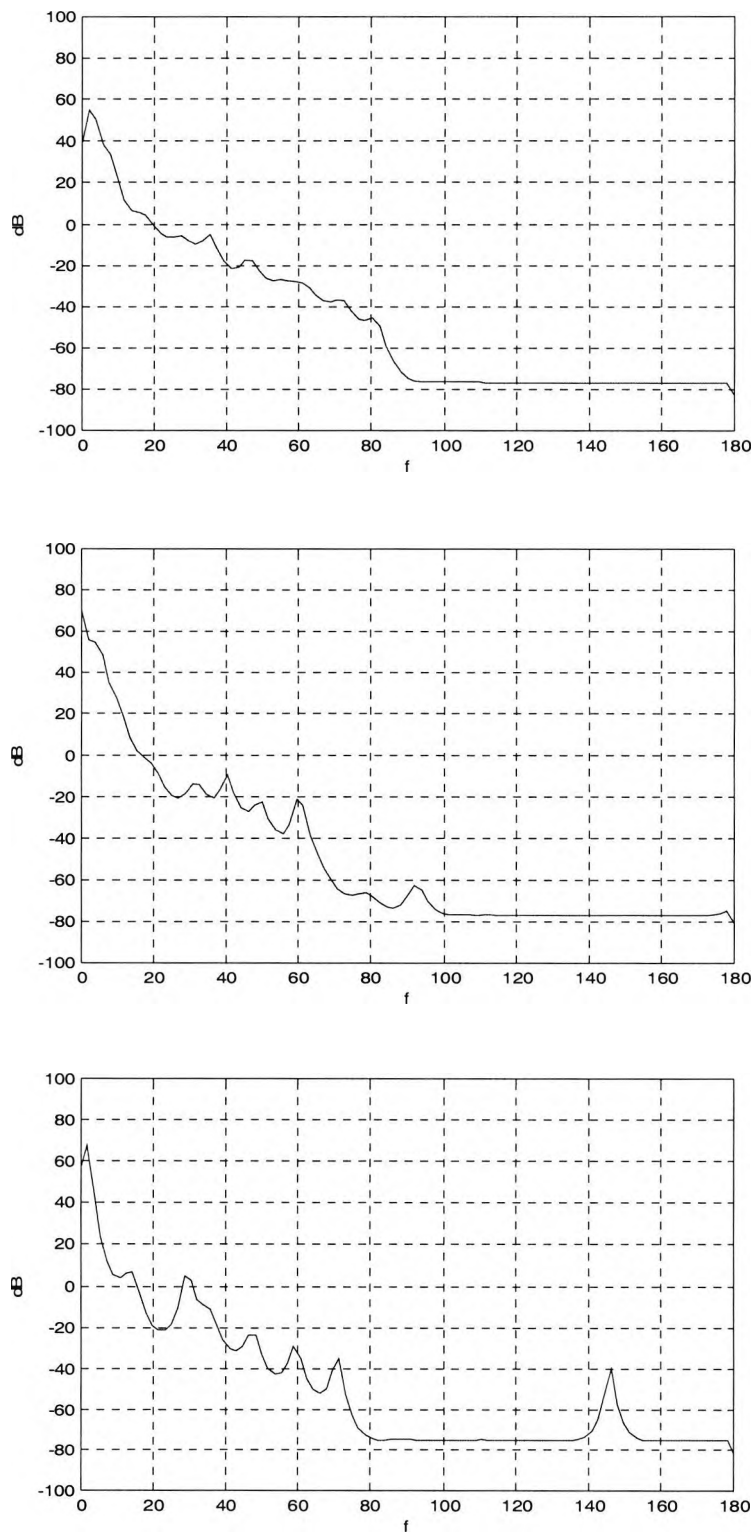


Figure 3.15 MUSIC spectra of one ST-T complex for NCE (top), ICE (middle, ST-segment depression) and ICE (bottom, ST-segment elevation). Using a segment size of about 150 samples.

Record Number	Segment description	No. of segments with high frequency components out of 50	
		$f > 60$ Hz	$100 > f < 180$ Hz
16483	NCE	2	—
16539	NCE	3	—
16795	NCE	—	—
19830	NCE	7	—
16272	NCE	13	—
16420	NCE	11	—
16265	NCE	3	—
16773	NCE	5	—
16786	NCE	2	—
18177	NCE	4	—
18184	NCE	1	—
19088	NCE	5	—
19093	NCE	1	—
17052	NCE	4	—
300	ICE	44	—
300	NLE	40	—
301	ICE	41	—
301	NLE	43	—
302	ISE	43	—
303	ICE	43	—
304	NLE	37	—
304	ICE	34	2
306	ICE	40	—
307	ISE	41	1
311	ICE	45	1
311	NLE	41	—
316	ISE	39	—
317	ISE	35	10
320	NLE	33	3
320	ICE	41	1
324	ICE	30	27
324	NLE	36	40
325	ICE	35	41
325	NLE	36	49
326	ICE	35	27
327	ICE	37	41

Table 3.2 MUSIC results for all normal and ischaemic records.

3.6 Discussion

In this chapter some statistical properties of the ECG signal have been calculated. The results come in agreement with other research work in this field. It has been shown that the ECG signal is a quasi-periodic, non-Gaussian and cyclostationary signal. Linearity properties of the ECG will be investigated in the following two chapters using higher-order statistics.

The frequency domain of the ECG signals was studied and the results showed that the signal is harmonic in nature and its spectrum extends in the frequency range from 0 to 40 Hz. Some spectral components in this band (0 - 40 Hz) are due to the constituent waves (P-wave, QRS complex, and T-wave) and others in the frequency range 0 - 3 Hz are due to the contaminated noise (motion artefact and EMG). The high frequency components tend to be due to coupling between the fundamental frequency and the harmonics. This will be investigated in the next chapter using the bispectrum.

In the literature a number of methods have been proposed for detection of ischaemic events using the analysis of ST-segments. These methods were based on digital filtering, time domain analysis of the first derivative of the signal and wavelet-based methods (Hsia 1986; Li, et al. 1995; Weisner, et al. 1982). They tend to measure specific parameters (such as degree of depression, ST-T duration etc...) in ways critically dependent upon the correct detection of the J-point on the ECG signal. Uncertainty regarding J-point position may lead to inaccurate estimation of the ECG parameters related to the ST-T complex. In the time domain, there are many problems contributing to poor detection and incorrect classification of the ST-segment, include: slow baseline drift, noise, sloped ST changes, patient-dependent abnormal ST-segment depression levels and varying ST-T patterns in the ECG of the same patient (Stamkopoulos, et al. 1998). This work differs considerably from previously used algorithms in that: 1) the current investigation examined the existence of abnormality (ischaemia) rather than the detection of ST-segment depression/elevation, 2) it used information coming from the whole ST-T pattern, and 3) This information was analysed in the frequency domain.

Recently late potentials (LPs) have been proposed to identify a subgroup of patients with MI at risk of VT, see chapter one, (Breithardt, et al. 1986; Meste, et al. 1994; Schels, et al. 1991; Simson, 1981). This work enhances the concept of LPs to include the abnormal high frequency components (HFC) found in the MUSIC spectrum of the ST-T complexes of the ECG signals to identify patients with myocardial ischaemia and/or infarction.

The frequency analysis of the normal episodes taken from normal subjects showed insignificant HFC. For ischaemic subjects, these HFC were found for the same patient not only in episodes that represent peak effort phase of exercise ECG (i.e., episodes show ST-segment depression) but also in episodes representing the initial resting phase of exercise ECG (i.e., episodes do not show ST-segment depression). The HFC are also found in some resting ECG recordings (No. 324 to No. 327, ST Change-DB), for both episodes that show and that do not show ST-segment elevation of the same patient.

In this chapter we tried to answer an important question, that is, is it possible to detect ischaemia without exercise test? In some ischaemic cases such as chronic stable angina and old MI the resting ECG show normal ST-T episodes. But from signal processing point of view the dynamics of the generator (the heart) of the signal have changed, this implies changing the dynamics of the ECG signal itself which in turn can be detected using signal processing techniques. The MUSIC analysis of two different types of episodes from the same patient (100 ST-T complexes) showed the spectral similarity between these episodes, which means similar dynamics over the whole record despite of the innocent appearance of some episodes. Hence it may be possible to detect ischaemia by applying high-resolution spectral analysis techniques on low levels of exercise stress test or even resting ECG signals. In this analysis high-resolution was obtained using the MUSIC algorithm compared to the maximum entropy method (MEM). The estimated accuracy, sensitivity and specificity of the analysis offered a promise in the direction of the detection of ischaemia without exercise test.

Having defined the Gaussianity, periodicity, stationarity and the second-order spectral characteristics of the ECG signals, the following two chapters will explore the ECG signal in the higher-order statistical domain and define its linearity characteristics.

Chapter 4

HIGHER-ORDER STATISTICS/SPECTRA

4.1 Introduction

This chapter is concerned with the characterisation of the ECG signals in the higher-order statistics (HOS) domain. Non-Gaussianity and non-linearity of the signal will be identified using HOS. In the time domain, the second-, third- and fourth-order cumulants are estimated for normal and ischaemic ECGs to investigate their different characteristics. In the frequency domain, the three-dimensional bispectral patterns are investigated for normal ECG signals. For the ischaemic case, the bispectral analysis is dealt with in chapter 5. Also, the bispectrum magnitude and bicoherence-squared index are used in this chapter to detect and quantify quadratic phase coupling which includes both frequency and phase coupling. This in turn will be used to classify ischaemic abnormality in ECG signals in chapter 5.

In this chapter some definitions for higher-order statistics are given along with relevant mathematical formulae. Descriptions of the estimation techniques of the cumulants and bispectra are also given. Basically, three methods for bispectrum estimation are considered in this chapter, namely, (i) the direct, (ii) the indirect, and (iii) the third-order recursion methods. The direct method, which involves calculating the triplet product of the FFT of the signal (Nikias 1993), is primarily used for bispectrum estimation in this analysis. The indirect method, which calculates the FFT of the third-order cumulants, and the method referred to as the Third-Order Recursion (TOR) for bispectrum estimation (Nikias 1993; Raghuvver and Nikias 1985), are also applied to the same ECG signals for comparison. Hinich tests for non-Gaussianity and non-linearity (Hinich; 1982) are then applied to individual records to further confirm, statistically, their hypothesis.

This chapter also introduces a new algorithm aimed at improving the resolution capability of the bispectrum. This new bispectrum estimator is an eigen-decomposition-based technique and it is reminiscent of the spectral Multiple Signal Classification (MUSIC) approach (Haykin 1991). In this thesis, it is called the MUSIC Pseudo-Bispectrum (MUSIC-PB). It is used to calculate the quadratic phase coupling by estimating; (i) a Toeplitz matrix from the third-order cumulant, (ii) the signal and noise subspaces, and (iii) pseudo-bispectral peaks. In order to test the algorithm, simulated sinusoidal signals are first introduced before dealing with the actual measured ECG signals. It is worth reporting here, that the MUSIC-PB estimator is different from the method adopted by (Sabry-Rizk, et al. 1997b; Sabry-Rizk, et al. 2001b; Zgallai 2002) to calculate: (i) the spectral MUSIC, (ii) the bispectrum of the spectral MUSIC in which the signal and noise subspaces have been filtered to further enhance the signal over the desired frequency band (Sabry-Rizk, et al. 2000c).

4.2 Higher-order Statistics/Spectra

The higher-order statistics (HOS); also known as cumulants, are related to the more familiar moments and may be expressed in terms of them. Higher-order spectra (polyspectra) are the multi-dimensional Fourier Transforms (FT) of the cumulants of stationary signals. Just as the FT of the autocorrelation (the power spectrum) is a useful tool, so are the FT of cumulants. A key characteristic which differentiates cumulants from correlations is that cumulants are blind to all kinds of Gaussian process, whereas correlations are not. This means that cumulants automatically improve the SNR. Another important advantage of working with cumulants and polyspectra, is that they preserve phase information about the underlying process. On a practical level, one very attractive property of cumulants is that the cumulant of the sum of two statistically independent random processes equals the sum of the cumulants of the individual processes. Therefore, it is easy to work with cumulants as operators. Higher-order moments, by contrast, do not have this property (Mendel 1991). There are several motivations behind the use of the higher-order statistics/spectra in the ECG signal analysis and diagnosis (Sabry-Rizk and Zgallai 1999; Sabry-Rizk, et al. 1998):

- 1- To eliminate Gaussian noise. This implies improving the SNR of the ECG data.
- 2- To characterise non-Gaussian components of the ECG signal and non-Gaussian noise artefacts (Hinich and Gary 1990).
- 3- To characterise certain types of non-linearity associated with normal and abnormal ECG signals.
- 4- To enable accurate detection, classification and coding of heart abnormalities using artificial neural networks (Sabry-Rizk, et al. 1999b).

4.2.1 Moments and Cumulants

4.2.1.1 Definitions

If $[x(t)]$, $t=0, \pm 1, \pm 2, \pm 3, \dots$ is a real stationary discrete-time signal and its moments exist up to order k , then (Nikias 1993)

$$\begin{aligned} Mom[x(t), x(t + \tau_1), \dots, x(t + \tau_{k-1})] &= m_n^x(\tau_1, \tau_2, \dots, \tau_{k-1}) \\ &= E[x(t), x(t + \tau_1), \dots, x(t + \tau_{k-1})] \end{aligned} \quad (4.1)$$

This represents the k^{th} -order moment function of the stationary signal, which depends only on the time difference $\tau_1, \tau_2, \dots, \tau_{k-1}$, $\tau_i=0, \pm 1, \dots$ for all i . The second-order moment function, $m_2^x(\tau_1)$ is the autocorrelation of $[x(t)]$ whereas $m_3^x(\tau_1, \tau_2)$ and $m_4^x(\tau_1, \tau_2, \tau_3)$ are the third- and fourth-order moments, respectively. $E[.]$ denotes statistical expectation.

The k^{th} -order cumulant function of a non-Gaussian stationary random signal $x(t)$ can be written as

$$c_k^x(\tau_1, \tau_2, \dots, \tau_{k-1}) = Cum[x(t), x(t + \tau_1), \dots, x(t + \tau_{k-1})] \quad (4.2)$$

For a zero-mean random process, for $k=3,4$ only, the k^{th} -order cumulant of $[x(t)]$ can be defined as (Mendel 1991):

$$c_k^x(\tau_1, \tau_2, \dots, \tau_{k-1}) = E[x(\tau_1), \dots, x(\tau_{k-1})] - E[g(\tau_1), \dots, g(\tau_{k-1})] \quad (4.3)$$

where $[g(t)]$ is a Gaussian random process with the same second-order statistics as $[x(t)]$. Cumulants, therefore, not only display the amount of higher-order correlation, but also provide a measure of the distance of the random process from Gaussianity. If $x(t)$ is Gaussian then the cumulants are all zero, for all $k > 2$. The second-, third- and fourth-order cumulants of zero-mean $x(t)$, are (Mendel 1988).

$$c_2^x(\tau) = E[x(t), x(t + \tau)] \quad (4.4a)$$

$$c_3^x(\tau_1, \tau_2) = E[x(t), x(t + \tau_1), x(t + \tau_2)] \quad (4.4b)$$

$$c_4^x(\tau_1, \tau_2, \tau_3) = E[x(t), x(t + \tau_1), x(t + \tau_2), x(t + \tau_3)] \\ - c_2^x(\tau_1)c_2^x(\tau_3 - \tau_2) - c_2^x(\tau_2)c_2^x(\tau_3 - \tau_1) - c_2^x(\tau_3)c_2^x(\tau_2 - \tau_1) \quad (4.4c)$$

4.2.1.2 Relationship Between Moments and Cumulants

The relationship between moment and cumulant sequences of $x(t)$ are:

first-order cumulants

$$c_1^x(\tau) = m_1^x = E[x(t)] \quad (\text{mean value}) \quad (4.5)$$

second-order cumulants

$$c_2^x(\tau_1) = m_2^x(\tau_1) - (m_1^x)^2 \quad (\text{covariance sequence}) \quad (4.6)$$

third-order cumulants

$$c_3^x(\tau_1, \tau_2) = m_3^x(\tau_1, \tau_2) - m_1^x[m_2^x(\tau_1) + m_2^x(\tau_2) + m_2^x(\tau_2 - \tau_1)] + 2(m_1^x)^3 \quad (4.7)$$

fourth-order cumulants

$$\begin{aligned}
c_4^x(\tau_1, \tau_2, \tau_3) &= m_4^x(\tau_1, \tau_2, \tau_3) - m_2^x(\tau_1).m_2^x(\tau_3 - \tau_2) \\
&\quad m_2^x(\tau_2).m_2^x(\tau_3 - \tau_1) - m_2^x(\tau_3).m_2^x(\tau_2 - \tau_1) \\
&\quad - m_1^x[m_3^x(\tau_2 - \tau_1, \tau_3 - \tau_1) + m_3^x(\tau_2, \tau_3) + m_3^x(\tau_2, \tau_4)] + m_3^x(\tau_1, \tau_2) \quad (4.8) \\
&\quad + (m_1^x)^2[m_2^x(\tau_1) + m_2^x(\tau_2) + m_2^x(\tau_3) + m_2^x(\tau_3 - \tau_1) + m_2^x(\tau_3 - \tau_2) + m_2^x(\tau_2 - \tau_1)] \\
&\quad - 6(m_1^x)^4
\end{aligned}$$

If the process $[x(t)]$ is zero-mean ($m_1^x = 0$), it follows from (Eq 4.6) and (Eq 4.7) that the second- and third-order cumulants are identical to the second and third-order moments, respectively. However, to generate the fourth-order, we need knowledge of the fourth-order and second-order moments, i.e.,

$$\begin{aligned}
c_4^x(\tau_1, \tau_2, \tau_3) &= m_4^x(\tau_1, \tau_2, \tau_3) - m_2^x(\tau_1).m_2^x(\tau_3 - \tau_2) \\
&\quad m_2^x(\tau_2).m_2^x(\tau_3 - \tau_1) - m_2^x(\tau_3).m_2^x(\tau_2 - \tau_1) \quad (4.9)
\end{aligned}$$

By putting $\tau_1 = \tau_2 = \tau_3 = 0$ and assuming $m_1^x = 0$ we obtain:

$$\gamma_2^x = E[x^2(t)] = c_2^x(0) \quad (\text{variance}) \quad (4.10a)$$

$$\gamma_3^x = E[x^3(t)] = c_3^x(0,0) \quad (\text{skewness}) \quad (4.10b)$$

$$\gamma_4^x = E[x^4(t)] - 3[\gamma_2^x]^2 = c_4^x(0,0,0) \quad (\text{kurtosis}) \quad (4.10c)$$

A 1-D slice of the k^{th} -order cumulant can be obtained by freezing $(k-2)$ of its indices. A diagonal slice is obtained by setting $\tau_i = \tau$, $i=1,2,\dots,k-1$. These 1-D slices are very useful in applications of cumulants in signal processing (Nikias and Mendel 1993).

4.2.1.3 Estimation of Higher-order Cumulants

Let $[x(1), x(2), \dots, x(N)]$ be the given data set, then we have the following (Nikias and Mendel 1993):

- 1- Segment the data into J segments of M samples each, i.e., $N=J.M$.
- 2- Subtract the average value of each segment.

- 3- Assuming that $[x^{(i)}(t), t=0,1,\dots,M-1]$ is the data set per segment ($i=1, 2,\dots,J$), the estimates of higher-order moments are given by:

$$m_k^{(i)}(\tau_1,\dots,\tau_{k-1}) = \frac{1}{M} \sum_{t=s_1}^{s_2} x^{(i)}(t)x^{(i)}(t+\tau_1)\dots x^{(i)}(t+\tau_{k-1}) \quad (4.11)$$

where: $k=2,3,\dots, i=1,2,\dots,J, \tau_k=0,\pm 1, \pm 2,\dots, s_1=\max(0,-\tau_1,\dots,-\tau_{k-1}), s_2=\min(M-1,M-1-\tau_1,\dots,M-1-\tau_{k-1})$ and $|\tau_k| \leq L_k$, where L_k determines the region of support of the estimated k^{th} -order moment function.

- 4- The average over all segments

$$\hat{m}_k^x(\tau_1,\dots,\tau_{k-1}) = \frac{1}{J} \sum_{i=1}^J m_k^{(i)}(\tau_1,\dots,\tau_{k-1}) \quad (4.12)$$

For stochastic signals, generate the cumulants $c_k^x(\tau_1,\dots,\tau_{k-1})$ using Eqs. (4.6, 4.7 and 4.9), with $m_1^x=0$.

4.2.1.4 Cumulant Analysis of ECG Signals

The second-, third- and fourth-order cumulants are calculated for 18 normal records from the NSR-DB (MIT-CD 1997) and 15 ischaemic records from the ST Change-DB (MIT-CD 1997). Before calculating the cumulants special care of appropriate segmentation of the ECG signals should be taken. For example, for periodic signals the segment length, M samples, should be a multiple integer of the period (Nikias 1993). Since the ECG signals are quasi-periodic and cyclostationary (chapter 3), therefore for reliable cumulant estimates, and to meet the quasi-periodicity property, the segment length should be a multiple integer of the mean period length, lp , where lp is the mean number of samples in an ECG cycle calculated over the whole data length, N . For cyclostationarity property, the segment length, M samples, should be much smaller than $2Xlp$. Based on this, the range, " $M \leq$ nearest power of 2 to the number of samples in lp ", has been used for estimating cumulants (Gardner and Franks 1975; Waldo and Chitrapa 1991). The ECG data are segmented into 50 segments ($J = 50$), each contains M

samples, with $M = 128$ for NSR-DB, and $M = 256$ for ST Change-DB. Figures 4.1 and 4.2 show the typical second-, third-, and fourth- order cumulant patterns and slices for each of normal (record No. 16539, NSR-DB) and ischaemic (record No. 325, ST Change-DB) cases, respectively. The Figures (4.1 and 4.2) show the ECG signal (a), the second-order cumulants (b), the third-order cumulants and its diagonal slice (c, d) and the diagonal and wall slices of the fourth-order cumulants and their diagonals (e, f, g, and h). The diagonal slices are used here to reduce the computational time and they do contain useful information from the higher order domain keeping the advantage of improved SNR. The ischaemic case has myocardial infarction (MI), and the subject's ECG signal show ST-elevation. Figures 4.1 and 4.2 highlight the following:

- 1- Deviations from zero in the third- and fourth-order cumulants indicates deviations from Gaussianity. The ECG signal can be regarded as non-Gaussian. A non-Gaussian signal contaminated with Gaussian observation noise would therefore have the noise component suppressed by transforming to higher-order domain.
- 2- The cumulant patterns reflect typical statistical features in the ECG signals, which reduce the variability among different beats taken from the same subject. On the other hand, differences between different subjects are enhanced.
- 3- The second-order cumulants of a normal ECG signal follows the pattern shown in Figure 4.1 (b), while the second-order cumulants of ST-elevation case (record No. 325) in Figure 4.2.I (b) shows an elevated segment starts at $\tau \cong 10$ to $\tau \cong 60$. Also, it has been observed that the second-order cumulant sequence of each of the ST-depression cases exhibits depression, see Figure 4.2.II.
- 4- The second-, third- and fourth-order cumulants of the ischaemic cases show higher degrees of correlation than that of the normal ECG signals. The characteristic peaks of the second-order cumulants and that of the diagonal slices of higher-order cumulants occupy larger regions for ischaemic cases (lags, $\tau = 3$ to 5 samples for normal cases and $\tau = 10$ to 20 samples for ischaemic cases).

This last observation presents a new feature for the differentiation between normal and ischaemic ECGs. This feature will be defined as the normalised area under the curve of

second-order cumulants and the curve of the diagonal slices of the higher-order cumulants. This can be represented mathematically as follows:

$$NAC2 = \frac{1}{\tau_{2\max}} \int_0^{\tau_{2\max}} \frac{c_2(\tau)}{c_2(0)} d\tau \quad (4.13a)$$

$$NADC3 = \frac{1}{\tau_{3\max}} \int_0^{\tau_{3\max}} \frac{c_3(\tau, \tau)}{c_3(0,0)} d\tau \quad (4.13b)$$

$$NADC4 = \frac{1}{\tau_{4\max}} \int_0^{\tau_{4\max}} \frac{c_4(\tau, \tau, \tau)}{c_4(0,0,0)} d\tau \quad (4.13c)$$

where $NAC2$ is the Normalised Area under the curve of second-order cumulants (c_2). $NADC3$ is the Normalised Area under the curve of the Diagonal slice of the third-order cumulants (c_3). $NADC4$ is the Normalised Area under the curve of the Diagonal slice of the fourth-order cumulants (c_4). $\tau_{2\max}$, $\tau_{3\max}$ and $\tau_{4\max}$ are the maximum lags used in calculating the second-, third-, and fourth-order cumulants, respectively. Figure 4.3 depicts the results obtained from this analysis.

Analysing the results presented in Figure 4.3, a number of observations can be obtained by considering all of the cumulant orders used. First, the estimated $NACs$ of the abnormal cases are typically higher than those of the normal cases. Second, the abnormal and normal cases are completely separable by a constant threshold value of 0.3, for $NADC4$ feature we find that we can achieve very high specificity in all of the 33 records. Third, using the same threshold for both $NAC2$ and $NADC3$ results in less accuracy in the classification, missing ten abnormal cases in the former and four abnormal cases in the latter. The success rate of the fourth-order cumulant compared to the lower orders is an indication of complexity of the ECG signal.

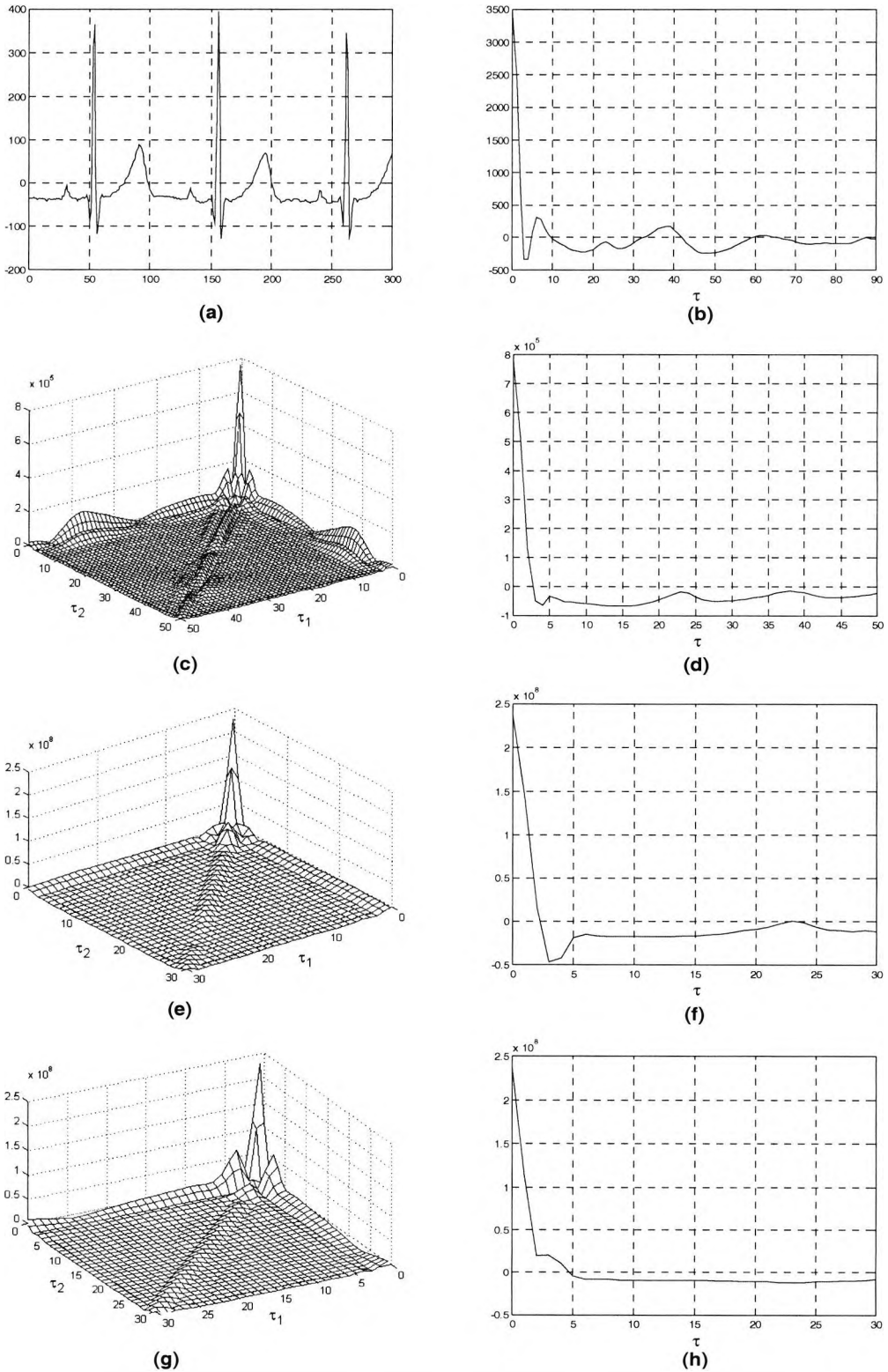


Figure 4.1 Cumulants of record No. 16539 (NSR-DB); (a) the ECG signal, (b) the second-order cumulant, (c) the third-order cumulant, and (d) its diagonal slice, (e) the diagonal tensor of the fourth-order cumulant, and (f) its diagonal slice; (g) the wall tensor of the fourth-order cumulant, and (h) its diagonal slice. Segment length = 128 samples, τ (max) = 90, 50, and 30 samples for second-, third- and fourth-order cumulants, respectively.

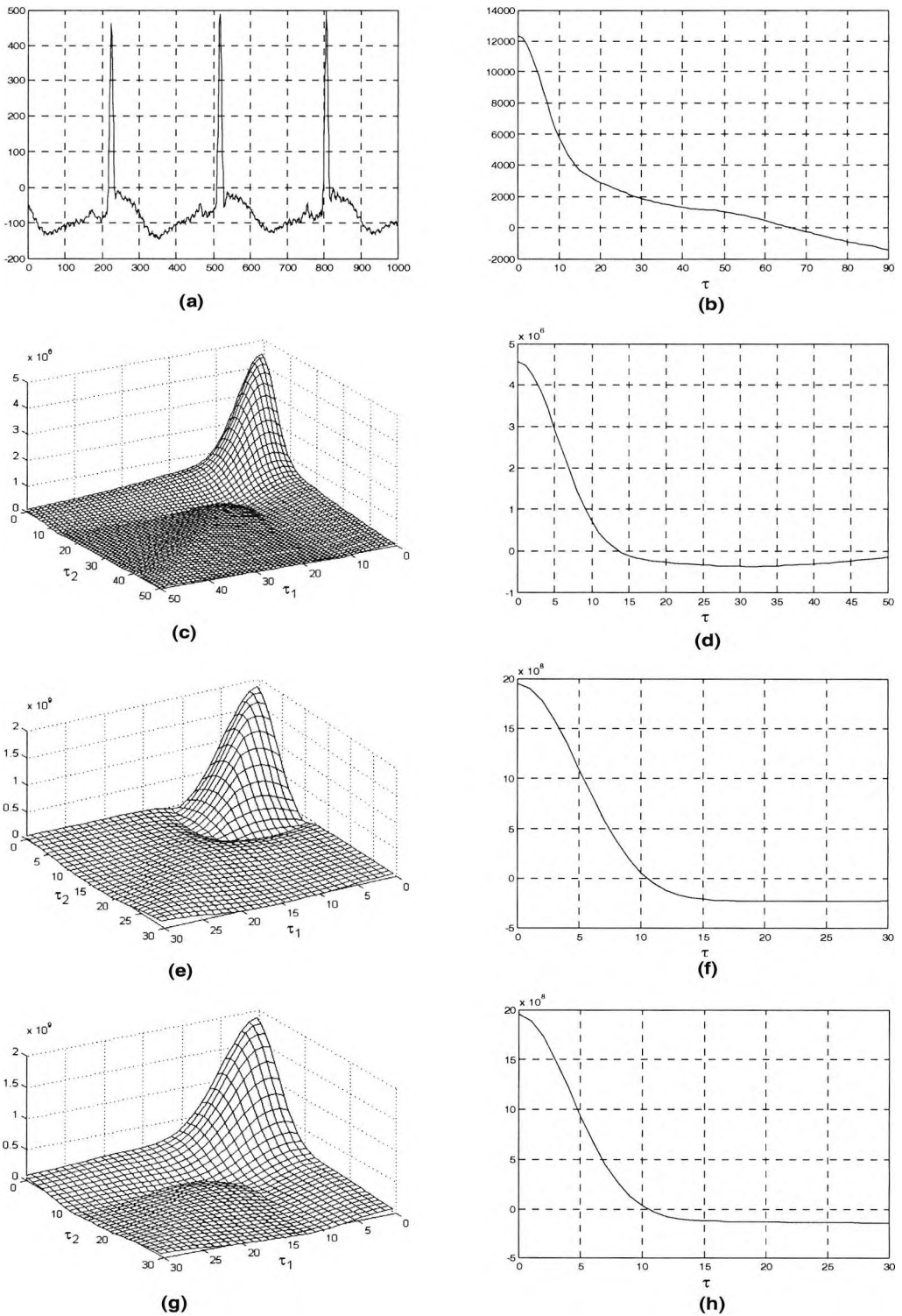


Figure 4.2.I Cumulants of record No. 325 (ST Change-DB); (a) the ECG signal, (b) the second-order cumulants. (c) The third-order cumulants, (d) its diagonal slice. (e) The diagonal tensor of the fourth-order cumulants, (f) its diagonal slice. (g) The wall tensor of the fourth-order cumulants, (h) its diagonal slice. Using segment length = 256 samples and τ (max) = 90, 50 and 30 samples for the second-, third- and fourth-order cumulants, respectively.

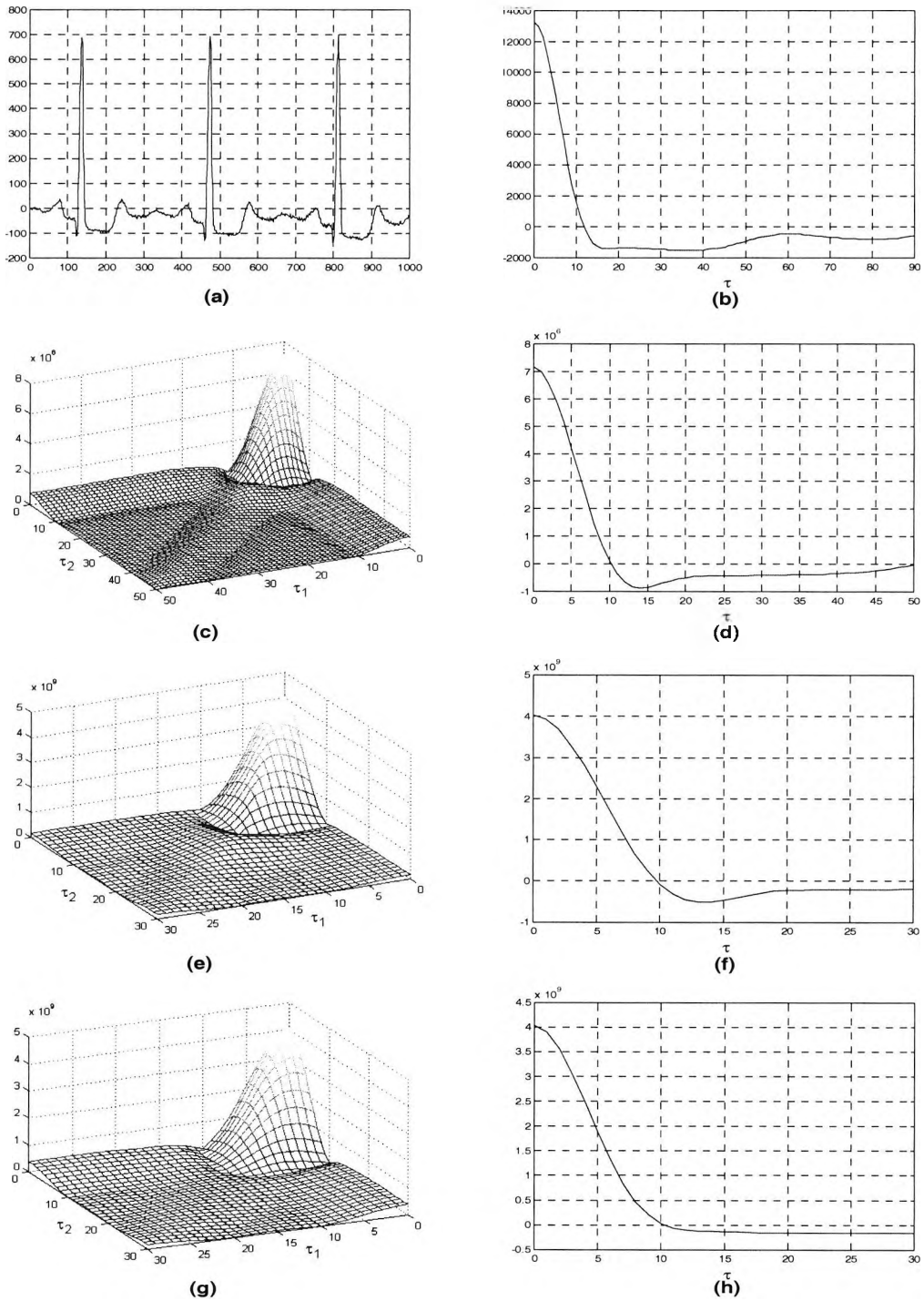


Figure 4.2.II Cumulants of record No. 304 (ST Change-DB); (a) The ECG signal, (b) the second-order cumulants. (c) The third-order cumulants, (d) its diagonal slice. (e) The diagonal tensor of the fourth-order cumulants, (f) its diagonal slice. (g) The wall tensor of the fourth-order cumulants, (h) its diagonal slice. Using segment length = 256 samples and τ (max) = 90, 50 and 30 samples for the second-, third- and fourth-order cumulants, respectively.

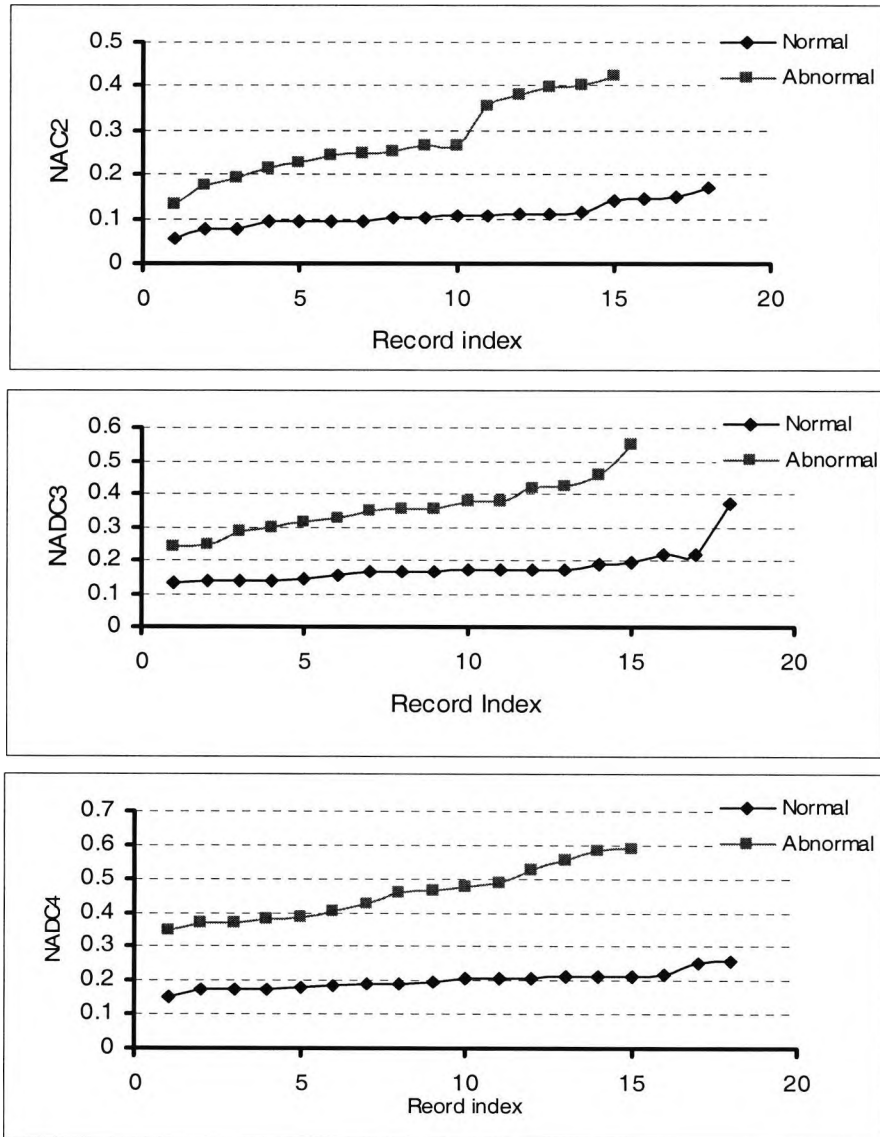


Figure 4.3 Cumulant-based classification for normal/ischaemic cases. In each part the x-axis represents the record index. The y-axis represents $NAC2$ (top), $NADC3$ (middle) and $NADC4$ (bottom). τ (max)=90, 50, and 30 samples for second-, third-, and fourth-order cumulants, respectively.

4.2.2 Higher-order Spectra

Higher-order spectra (also known as polyspectra) are defined in terms of Higher-Order Statistics (HOS). The k^{th} -order spectra $C_k^x(\omega_1, \omega_2, \dots, \omega_{k-1})$ of the process $[x(t)]$ is defined as the FT of the k^{th} -order cumulant sequence (Nikias and Raghuveer 1987):

$$C_k^x(\omega_1, \dots, \omega_{k-1}) = \sum_{\tau_1=-\infty}^{+\infty} \dots \sum_{\tau_{k-1}=-\infty}^{+\infty} c_k^x(\tau_1, \dots, \tau_{k-1}) \cdot \exp\{-j(\omega_1\tau_1 + \dots + \omega_{k-1}\tau_{k-1})\} \quad (4.14)$$

In general, $C_k^x(\omega_1, \dots, \omega_{k-1})$ is complex and a sufficient condition for its existence is that

$c_k^x(\tau_1, \dots, \tau_{k-1})$ is absolutely summable (i.e., $\sum_{\tau_1=-\infty}^{+\infty} \dots \sum_{\tau_{k-1}=-\infty}^{+\infty} c_k^x(\tau_1, \dots, \tau_{k-1}) < \infty$). The power

spectrum, bispectrum and trispectrum are special cases of the k^{th} -order spectrum Eq. (4.14) for $k=2,3,4$, respectively. The bispectrum, which is the third-order cumulant spectrum, has been previously used in many areas of practical applications such as seismic deconvolution, signal reconstruction, detection of quadratic phase coupling and deviations from normality. In the next section different methods of bispectrum estimation and application to ECG signals will be presented.

4.2.2.1 *Bispectrum Estimation*

There are two chief approaches that can be used to estimate higher-order spectra, namely, the conventional/nonparametric approach (Fourier type) (Brillinger 1965; Huber et al. 1971; Rosenblatt and Van Ness 1965) and the parametric approach (Nikias and Raghuvver 1987; Raghuvver and Nikias 1986; Rosenblatt 1980). The conventional methods are straightforward and their implementation is based on Fast Fourier Transform (FFT) algorithms. The bispectrum can be estimated using the conventional approach by two techniques (Mendel 1991; Nikias 1993): 1) the indirect class of techniques, in which the bispectrum is estimated as the 2-D FT of the third-order cumulants. 2) The direct class of techniques, in which the bispectrum is estimated directly from the average triple products of FT coefficients of the data segments. Hence, the direct class of methods for higher-order spectrum estimation is similar to the "average periodogram" or the Welch method for power spectrum estimation. The parametric techniques first estimate the parameters of the underlying data, generating a model and then use this model to compute the polyspectra. These models are in the classes of moving average (MA), auto-regressive (AR), or auto-regressive moving average (ARMA) processes.

4.2.2.2 Indirect Method of Bispectrum Estimation

The block diagram in Figure 4.4 summaries this method of estimation.

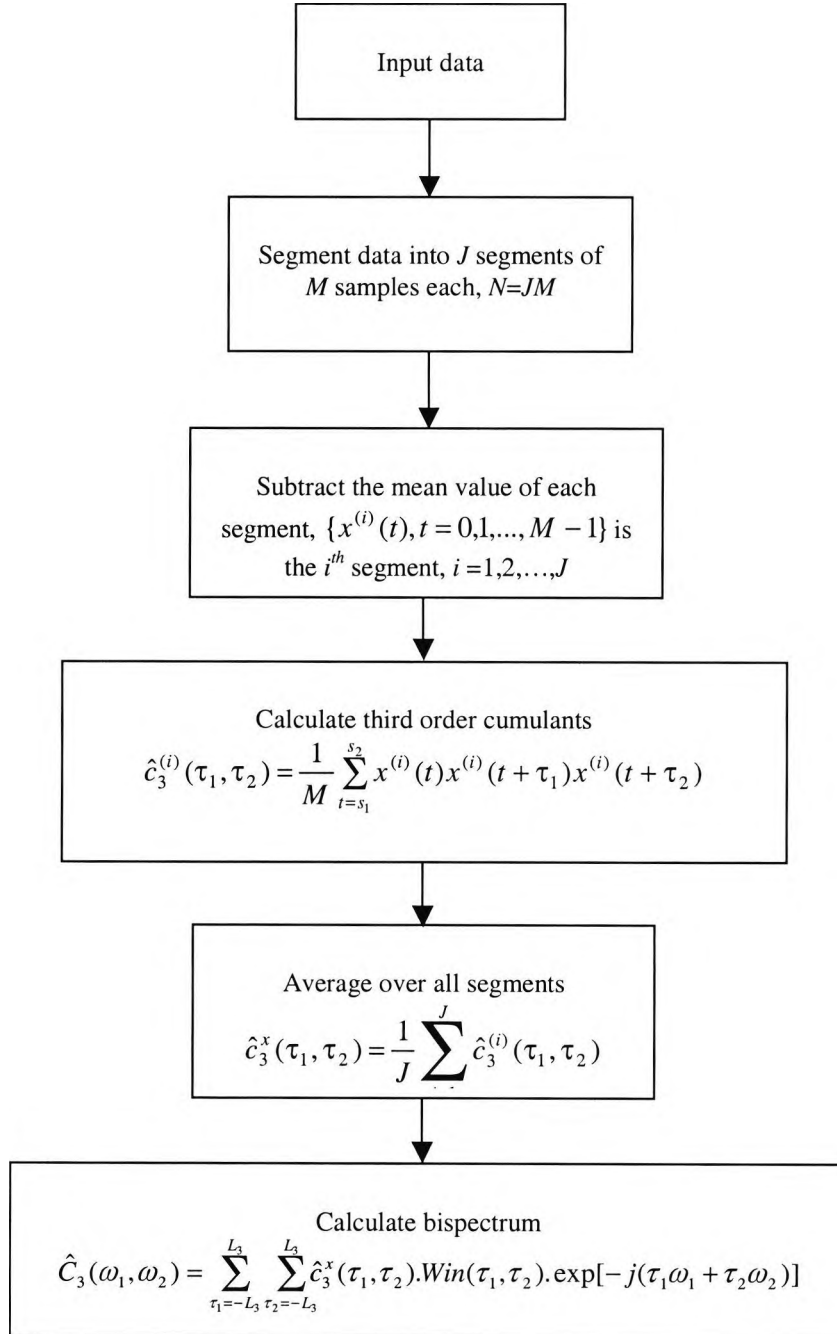


Figure 4.4 Bispectrum estimation using indirect method, where $Win(\tau_1, \tau_2)$ is a 2-D window function.

4.2.2.3 Direct Method of Bispectrum Estimation

The bispectrum of a stochastic process $x(t)$ is mathematically defined as (Kim and Powers 1978):

$$C_3^x(\omega_1, \omega_2) = E\{X(\omega_1) X(\omega_2) X^*(\omega_1 + \omega_2)\} \quad (4.15)$$

where $X(\omega)$ is the FT of the signal $x(t)$ and $X^*(\omega)$ is its complex conjugate. The block diagram Figure 4.5 shows the steps for this estimation.

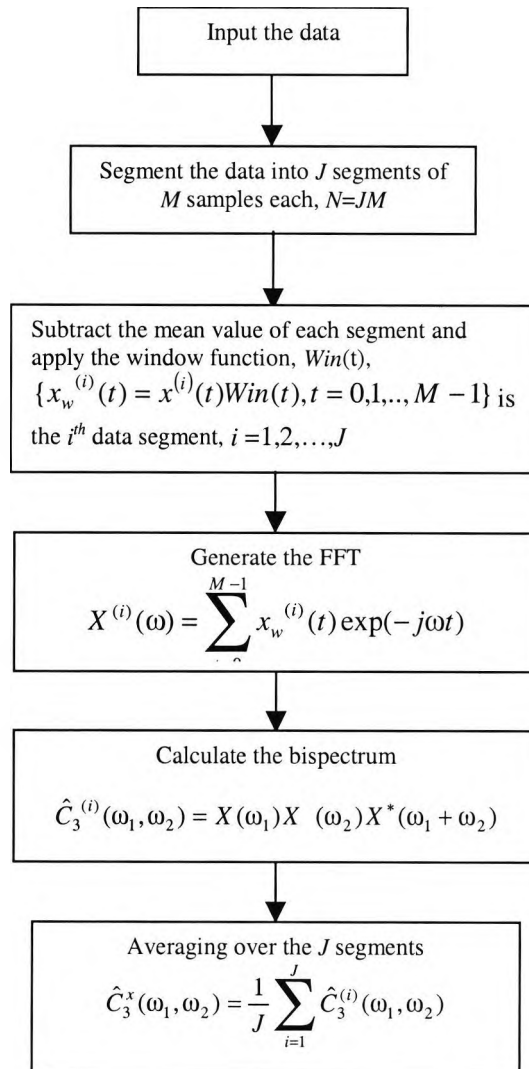


Figure 4.5 Bispectrum estimation using the direct method.

4.2.2.4 Quadratic Phase Coupling

There are situations where, because of interaction between two harmonic components of a process, there is a contribution to the power at their sum and/or difference frequencies. Three frequencies are harmonically related when one of them is the sum or the difference of the other two. Such a phenomenon could be due to second-order nonlinearities which gives rise to certain phase relations and is called quadratic phase coupling. A special case is when we have two components with one being at twice the frequency of the other this is called quadratic self-coupling (Nikias 1993). The bispectrum is a useful tool in analysing quadratic non-linear interactions among different frequency components of a signal and in checking for the presence of second-order non-linearity, via the detection of quadratically phase-coupled frequencies (Huber, et al. 1971).

4.2.2.5 The Normalised Bispectrum (Bicoherence)

The bicoherence index; $bic(\omega_1, \omega_2)$, also called the normalised bispectrum, quantifies the extent of phase coupling between two frequency components. It is defined as (Huber, et al. 1971; Nikias 1993).

$$bic(\omega_1, \omega_2) = \frac{|C_3^x(\omega_1, \omega_2)|}{\sqrt{S^x(\omega_1)S^x(\omega_2)S^x(\omega_1 + \omega_2)}} \quad (4.16)$$

Theoretically the $bic(\omega_1, \omega_2)$ can take any value between zero and one. When the component at $(\omega_1 + \omega_2)$ is produced entirely due to the phase coupling of components at ω_1 and ω_2 , then the bicoherence index at (ω_1, ω_2) is one, which implies that the frequency components at ω_1 , ω_2 , and $(\omega_1 + \omega_2)$ are non-linearly coupled modes and suggests the existence of quadratic non-linearity. When all the three components are uncorrelated the bic is zero, which implies the absence of coherence and suggests that these three components may be spontaneously excited independent modes of the system (Kim and Powers 1979). In practice, however, the bicoherence index often exceeds one. One of the reasons is that the power spectra and bispectra of each segment are smoothed by different windows. Another reason is when the power spectrum and the

bispectrum are calculated using different models in the case of parametric techniques of power spectrum and bispectrum estimation. A comprehensive study on the statistics of the bicoherence indices can be found in (Sebert and Elgar 1989).

4.2.2.6 Statistical Properties of Conventional Methods

In general, the indirect and direct estimates of bispectrum are different. They become identical if they are estimated without windowing. For sufficiently large segment size M and total length of data N , the conventional methods provide asymptotically unbiased and consistent estimates (Nikias 1993).

$$E\{\hat{C}_3^x(\omega_1, \omega_2)\} \equiv C_3^x(\omega_1, \omega_2) \quad (4.17)$$

with asymptotic variances:

$$\begin{aligned} \text{Var}\{\text{Re}[\hat{C}_3^x(\omega_1, \omega_2)]\} &\equiv \text{Var}\{\text{Im}[\hat{C}_3^x(\omega_1, \omega_2)]\} \\ &\equiv \frac{1}{2} \sigma_3^2(\omega_1, \omega_2) \end{aligned} \quad (4.18)$$

$$\sigma_3^2(\omega_1, \omega_2) = \begin{cases} \frac{UL_3^2}{MJ} S^x(\omega_1)S^x(\omega_2)S^x(\omega_1 + \omega_2) & \text{indirect} \\ \frac{N_3^2}{MJ} S^x(\omega_1)S^x(\omega_2)S^x(\omega_1 + \omega_2) & \text{direct} \end{cases} \quad (4.19)$$

where $0 < \omega_1 < \omega_2$, J is the number of records, M is the number of samples per record and U is the total energy of the bispectrum window, which is unity for rectangular window. L_3 is the region of support for bispectrum estimates. $N_3 = M/(2win_3 + 1)$, win_3 is the size of the smoothing window. $S^x(\omega)$ is the true power spectrum.

4.3 Bispectral Analysis of Normal ECG Signals

4.3.1 Introduction

Recently the bispectrum has been shown to be a very useful diagnostic tool in experimental studies of non-linear wave interactions in random media. In particular, it

has been shown that the bicoherence spectrum may be used to discriminate between non-linearly coupled waves and spontaneously excited ones. Applications have appeared in oceanography (Hasselmann, et al. 1963), plasma physics (Kim and Powers 1978; Kim and Powers 1979), biomedical signal analysis (Muthuswamy, et al. 1999; Sabry-Rizk, et al. 1999a; Sabry-Rizk, et al. 1995a; Sabry-Rizk, et al. 1998; Sabry-Rizk, et al. 1999b; Sabry-Rizk, et al. 1995b; Sabry-Rizk, et al. 1995c; Sabry-Rizk, et al. 1997b; Sabry-Rizk, et al. 2000c; Zhang, et al. 2000) and fetal and mother ECG non-invasive blind source separation (Sabry-Rizk, et al. 2000a; Sabry-Rizk, et al. 2000b; Sabry-Rizk, et al. 1997a; Sabry-Rizk, et al. 1996; Sabry-Rizk, et al. 2001a; Zgallai 2001). In this research work the possibility of such quadratic non-linear interactions between different frequency components of the ECG signal has been investigated. It is also beneficial to develop familiarity with the bispectral features of the normal ECG signal in a noise-free environment. This investigation may in turn be helpful in discovering changes in physiological states of the heart; this might help as a reference against which abnormal ECG signals can be diagnosed. A comparison between different bispectrum estimators will be also introduced through the application to normal ECG signals.

4.3.2 Results

In chapter three, the power spectrum is calculated to analyse the frequency content of normal ECG signals. In this section, some components of this spectrum will be identified based on the frequency content of the bispectrum. The bispectrum, which is an ensemble average of a product of three spectral components, is used to detect if one of these spectral components is due to quadratic interaction between the other two. This is followed by calculating the bicoherence-squared index which is then applied to measure the degree of phase coherence of the triple wave harmonics.

Eighteen records from the NSR-DB and record No. 300 from the ST Change DB with $J = 50$, $M = 256$ samples, $L_3 = 64$, and $win_3 = 5$ are used in this analysis. In the pre-processing phase of the analysis, the ECG signal is high-pass filtered ($f_c = 0.5$ Hz) to remove the baseline wander and the adaptive filters (see chapter two) are applied where necessary. The R peaks of the ECG data are detected using the same algorithm

mentioned in chapter three (see section 3.4.3). Then, the mean length of one cycle, l_p , is calculated. This l_p is then used to divide the whole data into a number of cycles. Each cycle is considered as one segment, 50 segments are used for each NSR-DB record. The estimated bispectrum is the average of the bispectra of individual segments. Figure 4.6 shows the steps adopted in this analysis. A Kaiser smoothing window with $\alpha = 0.5$ is applied throughout this analysis, see appendix B for more details.

The power spectrum was calculated in chapter three using the Welch Method. The direct method of bispectrum estimation is mainly adopted in this analysis as it results in a much lower variance (of the order of 10^{-3}) of that calculated by the indirect method as depicted in Figure 4.7. Figures 4.7a and 4.7b are the bispectrum variance for the indirect and direct methods, respectively, estimated from Eq. 4.19.

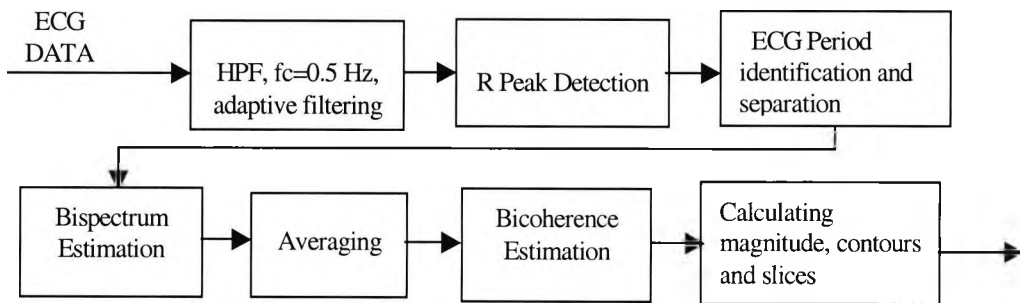


Figure 4.6 Methodology adopted in this analysis.

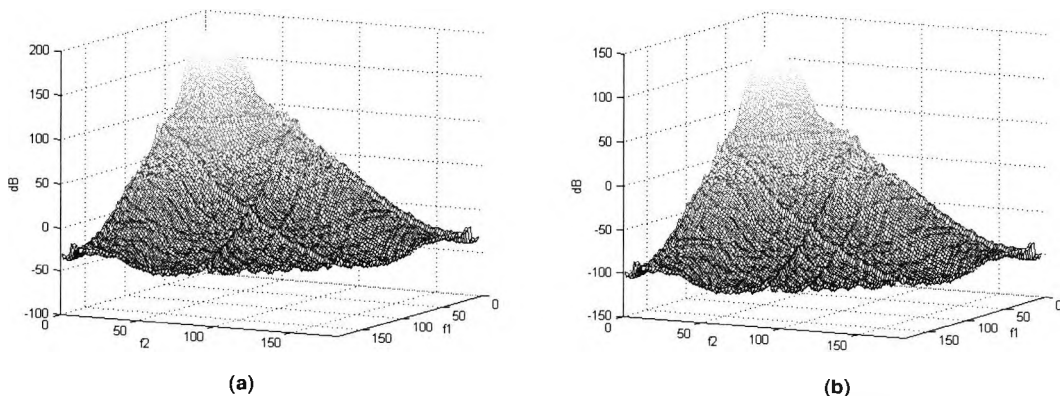


Figure 4.7 Bispectrum variance using (a) the indirect and (b) the direct method of bispectrum estimation with Kaiser window. $J=50$ records, $M=256$ and using record No. 300 (MIT-DB).

The following two subsections (sections 4.3.2 and 4.3.3) present the results of the analysis of the ECG signal using a nonparametric method (i.e., the direct method) and a parametric one (i.e., TOR method) of bispectrum estimation, respectively.

4.3.2.1 *ECG Analysis using the Direct Method Bispectrum*

Figure 4.8 depicts (a) three-dimensional (mesh plot) bispectrum magnitude of a normal ECG signal obtained from the NSR-DB record No. 16483, and (b) the bispectrum contour. Figure 4.9 shows the diagonal slice (top), and the wall slice (bottom) of the bispectrum magnitude. Figure 4.10 shows (a) the corresponding bicoherence-squared contour, (b) the diagonal, and (c) the wall slices. Table 4.1 includes the significant frequency components found in the power spectrum and bispectrum of record No. 16483 (NSR-DB).

Observations from Figures 4.8, 4.9, 4.10 and Table 4.1 indicate the following: the power spectrum exhibits a peak at the fundamental frequency (1.4545 Hz), and peaks at (4.3636, 16 and 8.7273 Hz). These are due to the T-wave, QRS complex, and P-wave, respectively, as explained using the MUSIC algorithm in chapter three. The bispectrum and bispectrum contour show many peaks in the low frequency region (0 - 20 Hz). From Table 4.1 one can conclude that the peaks at (13.0909 Hz) and that at (20.3636 Hz) are due coupling between components at (8.7273, 4.3636) and at (16, 4.3636), respectively. A cursory look at Table 4.1 reveals the existence of several harmonics, $\omega_i = i \omega_0$, where i is an integer. The bicoherence-squared contour indicates a high degree of phase coupling between frequency components in the region (0 - 20 Hz), which means that the above mentioned two triple waves are due to a phase coupling phenomenon. The diagonal slice of the bispectrum in Figure 4.9 shows a self-frequency coupling at the fundamental frequency (1.4545 Hz), third (4.3636 Hz), sixth (8.7273 Hz), and ninth (13.0905 Hz) harmonics. The bicoherence diagonal and wall slices of Figure 4.10 show that most of the peaks in the region of interest (0 - 20 Hz) are >0.9 . This strongly points at the quadratic phase-coupling phenomenon and hence the quadratic non-linearity (Kim and Powers 1979).

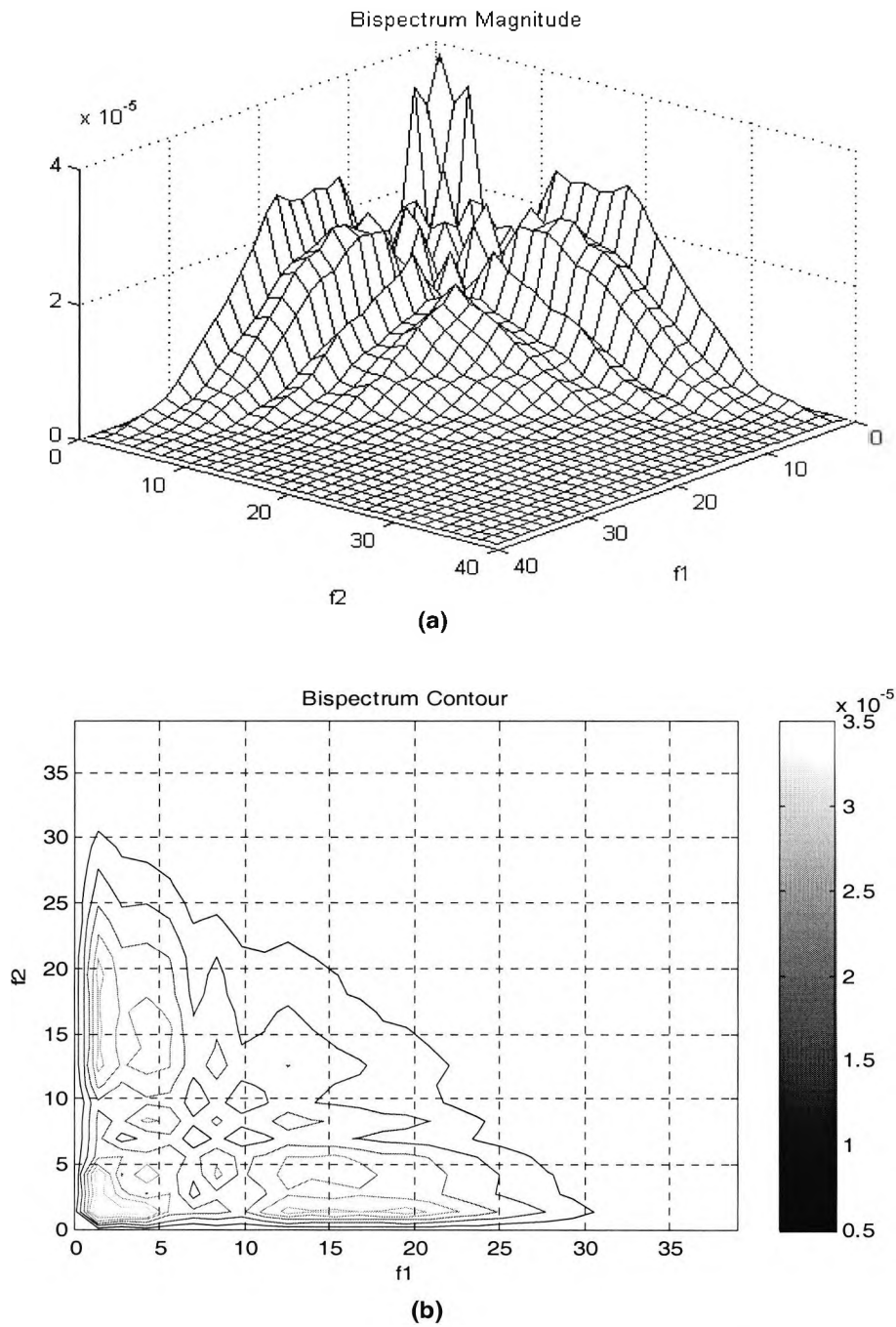


Figure 4.8 Bispectrum magnitude of a normal ECG signal (record No. 16483, NSR-DB) using the direct method of estimation. (a) mesh plot, and (b) contour plot. The segment length, M , is one ECG cycle and number of segments, $J=50$.

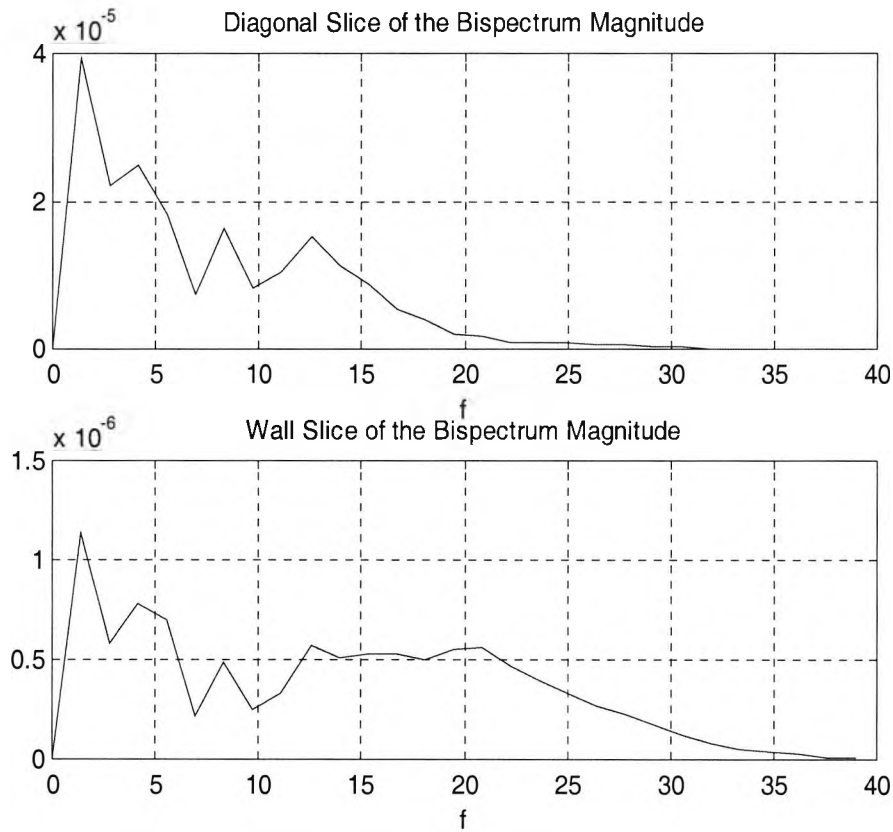


Figure 4.9 The diagonal (top) and wall (bottom) slices of the bispectrum magnitude of record No. 16483.

Spectrum peaks	Bispectrum peaks			
	f1	f2	Diagonal	Wall
1.4545	1.4545	1.4545	1.4545	1.4545
4.3636	1.4545	2.9091	4.3636	4.3636
20.3636	1.4545	4.3636	13.0909	20.3636
13.0909	4.3636	8.7273	8.7273	13.0909
16	1.4545	11.6364		16
8.7273	1.4545	13.0909		8.7273
	1.4545	14.5455		
	1.4545	16		
	1.4545	17.4545		
	1.4545	18.9091		
	1.4545	20.3636		

Table 4.1 Significant frequency components from the power spectrum and the bispectrum of record No. 16483.

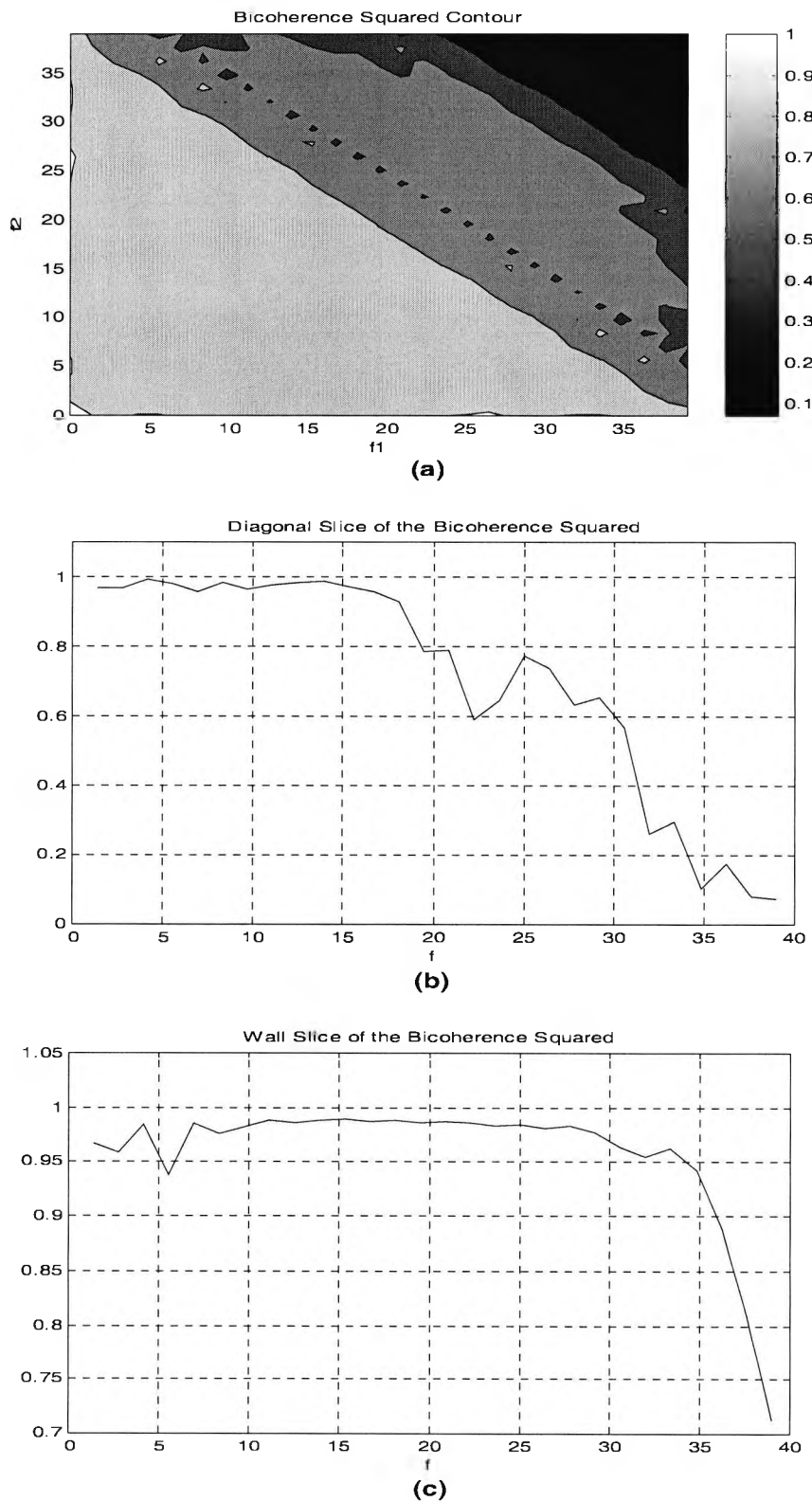


Figure 4.10 Bicoherence-squared of a normal ECG signal (record No. 16483) using the direct method of estimation. (a) The magnitude contour, and the diagonal (b) and wall (c) slices. The segment length, M , is one ECG cycle and number of segments, $J=50$.

4.3.2.2 ECG Analysis using the TOR Bispectrum

Nikias (1993); Raghuveer and Nikias (1985) suggested that, the parametric methods possess much higher resolution capability than the frequency resolution of the conventional methods and the techniques which are based on AR modelling of the third-order cumulants are shown to be high-resolution quadratic phase coupling detectors. Hence a parametric technique, namely, Third Order Recursion (TOR) method is utilised to show a more resolved picture of the bispectrum and to confirm the results obtained by the direct method. Using the TOR method, the bispectrum is defined as (Raghuveer and Nikias 1985):

$$C_3^x(\omega_1, \omega_2) = \gamma_4 H(\omega_1) H(\omega_2) H^*(\omega_1 + \omega_2) \quad (4.20)$$

The TOR method is based on the AR modelling of the third-order cumulants. γ_4 is the kurtosis of the driving noise and $H(z) = 1/A(z)$, $a = [1, a(1), \dots, a(m)]^T$ are the parameters of the AR model of order m . The TOR bispectrum of record No. 16483 (NSR-DB) is estimated after pre-processing of the ECG signal using the above mentioned steps. An AR model of order 15 is used; the model order criteria mentioned in chapter two have been used as the first guideline for this choice. Figure 4.11 confirms the existence of quadratic coupling in the same region (0 - 20 Hz). Its diagonal slice in Figure 4.12 reveals the self-phase coupling phenomenon as with the previous method (El-Khafif, et al. 2001).

Comparing the two bispectra, the TOR bispectrum shows a smoother look than the one estimated by the direct method. The frequency resolution of the TOR method is independent of the time domain segment. On the other hand, the frequency resolution of the direct method is roughly the reciprocal of the time domain interval ($1/M$). For the case of the ECG signal, this is ≤ 0.01 , depending on the length of one cycle. This resolution is fairly adequate for our application. Also as the factor of choosing the correct AR model order is not included in the direct method, this method is computationally efficient and produces more reasonable frequency estimates. In addition, the variance of parametric frequency based estimators is $O(M^{-1})$ as opposed to $O(M^{-3})$ exhibited by nonparametric frequency estimators (Brillinger 1980).

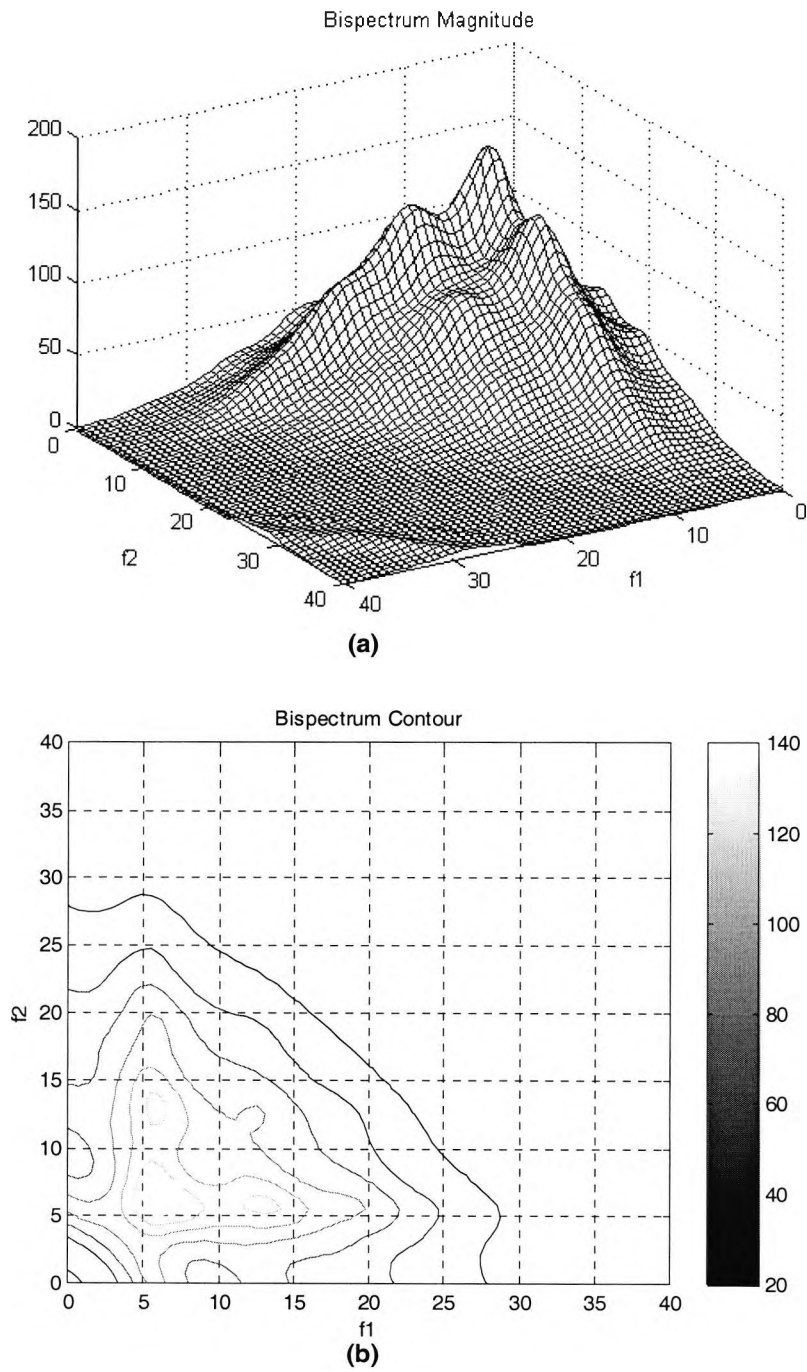


Figure 4.11 Bispectrum magnitude of a normal ECG signal (record No. 16483) using the TOR method. (a) 3-D plot, and (b) contour plot. The segment length, M , is one ECG cycle and number of segments, $J=50$.

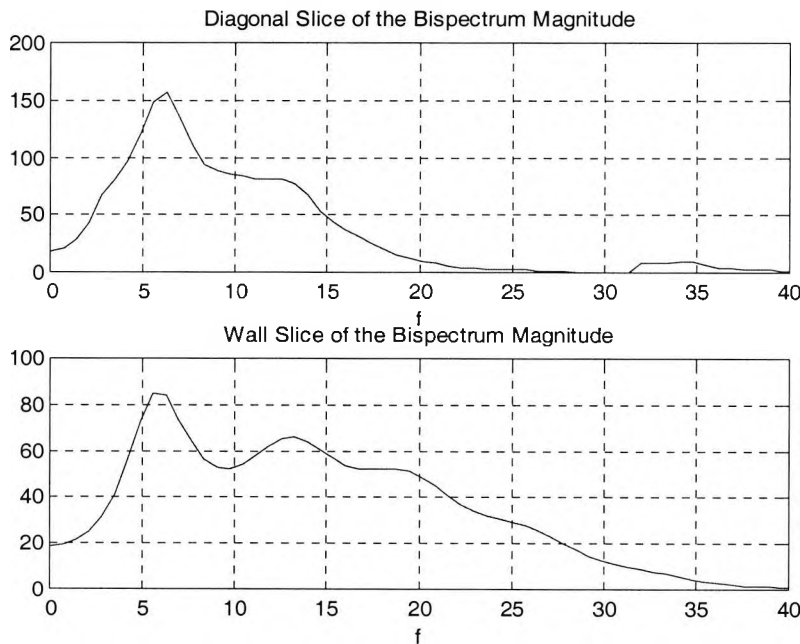


Figure 4.12 The diagonal (top) and wall (bottom) slices of the TOR bispectrum magnitude of record No. 16483.

4.3.2.3 *Hinich Test*

A statistical test developed by Hinich (1982), which makes use of the statistical properties of the bispectrum, is applied to statistically test the hypothesis that the ECG signal bispectrum is non-zero (i.e., the signal is non-Gaussian) and that the signal is linear (see appendix C for a brief description).

The test is applied to 18 normal ECG records from NSR-DB (MIT-CD 1997) using 1024 samples for the FFT and a resolution /smoothing parameter, $c=0.51$. Table 4.2 includes the estimated (R_e) and the theoretical (R_t) values. The estimated (R_e) is the sample inter-quartile range of the statistics, S-Gauss¹. It should be noted; from Table 4.2 that these values are not close to each other for all records indicating that the signal is not linear. Furthermore, large values of the test statistics for Gaussianity, S-Gauss, with Probability of False Alarm², $PFA = 0$, are obtained for all records. It is certain that

¹ S-Gauss is the test statistics for Gaussianity.

² PFA is the probability that we will be wrong in accepting the alternate hypothesis, i.e., the data are non-Gaussian.

the signal has non-zero bispectrum and hence is non-Gaussian; this statistically confirms the results obtained using the cumulant and the bispectrum analysis (El-Khafif, et al. 2001).

Record No.	S-Gauss	R_e (estimated)	R_t (theory)
16483	7409.40	149.81	24.60
16539	11708.73	261.90	31.08
16795	6108.89	137.42	22.26
19830	9262.47	67.26	27.50
17052	9298.48	222.28	27.69
16265	13766.02	203.11	33.76
16272	11341.84	227.95	30.41
16273	7784.34	122.53	25.19
16420	10876.72	182.30	30.02
16773	15148.64	119.54	35.21
16786	11408.57	126.63	30.61
18177	12021.78	182.52	31.38
18184	16886.74	201.15	37.29
19088	10317.68	225.77	29.12
19090	13026.39	194.73	32.64
19093	14043.10	139.32	33.72
19140	9848.28	165.90	28.37
17453	15120.39	215.70	35.32

Table 4.2 Hinich test applied to 18 normal ECG records.

4.4 The MUSIC Pseudo-Bispectrum

4.4.1 Introduction

Recently some attention has been focussed on developing eigen-structure algorithms based on higher-order statistics for sinusoidal frequency estimation and related problems (Forster and Nikias 1991; Leyman and Durrani 1994; Porat and Friedlander 1991; Swami and Mendel 1991). Several techniques for estimating quadratic phase coupling based on nonparametric and parametric bispectrum estimation exist in the

literature. The nonparametric techniques suffer from limited frequency resolution for short data segments and the parametric ones may result in unstable models. On the other hand the eigen-decomposition-based techniques such as the spectral MUSIC and its variants constitute effective methods for frequency estimation. The high-resolution capability of these algorithms motivates their extension to the higher-order domain. A MUSIC-like method for estimating quadratically coupled frequency pairs in a noise corrupted complex harmonic process was proposed by Parthasarathy, et al. (1994). In that algorithm the authors based their analysis on eigen-decomposition of a matrix with a complete orthogonal eigen-structure¹ derived from the third-order cumulants. They constructed a search function for frequency estimation using the signal eigen-vectors. The proposed algorithm herein involves constituting a Toeplitz matrix² from the diagonal slice of the third-order cumulant matrix. It applies SVD to this matrix to separate the signal and the noise subspaces. By exploiting the orthogonality between these subspaces a frequency estimation function is constructed using the noise singular vectors. Instead of calculating the true cumulant bispectrum, the newly developed MUSIC-based spectral function is aimed at enhancing the frequency components embedded in the third-order cumulants.

4.4.2 Formulation of the Problem

Recall the MUSIC algorithm previously described in chapter three, where the frequency estimation function was defined as:

$$\hat{S}_{MUSIC}(\omega) = \frac{1}{\sum_{i=p+1}^{L+1} |\mathbf{e}^H \mathbf{v}_i|^2} \quad (4.21)$$

where $\mathbf{e}^H(\omega) = [1 \quad e^{-j\omega} \quad \dots \quad e^{-j(L-p)\omega}]$ is the frequency scanning vector and \mathbf{v}_i , $i = p+1, p+2, \dots, L+1$ constitute the singular vectors of the noise subspace.

¹ An orthogonal eigen-structure means a matrix with orthonormal set of eigenvectors.

² An $(n \times n)$ matrix is called Toeplitz if all the elements along each of the diagonals have the same value.

Since the data matrix used in the MUSIC algorithm does not contain phase information about the process, a Toeplitz matrix derived from the diagonal slice of the third order cumulants is used in this work for bispectrum estimation. This very matrix has been used by Raghuveer and Nikiyas (1985) in estimating the bispectrum using the TOR method. The third-order cumulant of a discrete time process, $x(t)$, which is third-order stationary and has zero-mean is defined in Eq. (4.4b) as $c_3^x(\tau_1, \tau_2) \equiv E[x(t)x(t+\tau_1)x(t+\tau_2)]$. The matrix \mathbf{R} is calculated from the diagonal slice, $c_3^x(\tau, \tau)$ as follows:

$$\mathbf{R} = \begin{bmatrix} c_3^x(0,0) & c_3^x(1,1) & \dots & c_3^x(L,L) \\ c_3^x(-1,-1) & c_3^x(0,0) & \dots & c_3^x(L-1,L-1) \\ \vdots & \vdots & \dots & \vdots \\ c_3^x(-L,-L) & c_3^x(-L+1,-L+1) & \dots & c_3^x(0,0) \end{bmatrix} \quad (4.22)$$

The SVD of the matrix $\mathbf{R} \in (L+1) \times (L+1)$ is, in general, given by Golub and Van Loan (1989)

$$\mathbf{R} = \mathbf{U} \mathbf{\Sigma} \mathbf{V}^T, \quad \mathbf{U} \mathbf{U}^T = \mathbf{U}^T \mathbf{U} = \mathbf{I}_{L+1}, \quad \text{and} \quad \mathbf{V} \mathbf{V}^T = \mathbf{V}^T \mathbf{V} = \mathbf{I}_{L+1} \quad (4.23)$$

where the columns of \mathbf{U} and \mathbf{V} are the left and right singular vectors, respectively. $\mathbf{\Sigma}$ is a diagonal matrix whose diagonal entries are the singular values of \mathbf{R} . Eq. (4.21) can be re-written as follows:

$$\hat{S}_{MUSIC}(\omega) = \frac{1}{\sum_{i=p+1}^{L+1} |\mathbf{v}_i(\omega)|^2} \quad (4.24)$$

$$\text{where } \mathbf{v}(\omega) = \sum_{t=0}^{N-1} \mathbf{v}(t) e^{-jt\omega} \quad (4.25)$$

From which and based on the definition of the direct bispectrum estimation, the following bispectrum frequency estimation function is proposed:

$$\hat{B}(\omega_1, \omega_2) = \frac{1}{\sum_{i=p+1}^{L+1} \mathbf{v}_i(\omega_1) \mathbf{v}_i(\omega_2) \mathbf{v}_i^*(\omega_1 + \omega_2)} \quad (4.26)$$

Since only the phase-coupled components contribute to the third cumulants of the process (Nikias 1993), this frequency estimation function will show peaks only at the phase-coupled frequencies. Theoretically these peaks tend to infinity. The bicoherence in Eq. (4.16) can be calculated using the MUSIC spectrum and bispectrum as follows

$$bic(\omega_1, \omega_2) = \frac{\hat{B}(\omega_1, \omega_2)}{\sqrt{\hat{S}_{MUSIC}(\omega_1) \hat{S}_{MUSIC}(\omega_2) \hat{S}_{MUSIC}(\omega_1 + \omega_2)}} \quad (4.27)$$

4.4.3 Simulation Results

Example 1: Consider the process used by Raghuveer and Nikias (1985)

$$x(t) = \sum_{i=1}^3 \cos(2\pi f_i t + \varphi_i) + W(t) \quad (4.28)$$

where $f_1 = 0.109375$, $f_2 = 0.1875$, $f_3 = f_1 + f_2$ and $W(t)$ is a -30 dB WGN. Sixty-four segments of 128 samples each are formed. To insure statistical independence of the segments, φ_1 , φ_2 and φ_3 are drawn independently from a uniform distribution on $[0, 2\pi]$ and $W(t)$ is generated independently for each segment. To test the performance in the presence and absence of phase coupling, the MUSIC pseudo-bispectrum (MUSIC-PB) is calculated for: (case-1) $\varphi_3 = \varphi_1 + \varphi_2$, and (case-2) $\varphi_3 \neq \varphi_1 + \varphi_2$. Figure 4.13 (a) shows the magnitude bispectrum and Figures 4.13 (b), and (c) show the bicoherence-squared for 'case-1' and 'case-2', respectively. A signal subspace of, $p=6$ with $L=15$ are used in bispectrum estimation. The peak in the bispectrum is at the correct location, i.e., at (f_1, f_2) . The bicoherence-squared shows a peak at (f_1, f_2) for 'case-1' indicating total phase coupling and it is zero for 'case-2' viewing the absence of phase coupling.

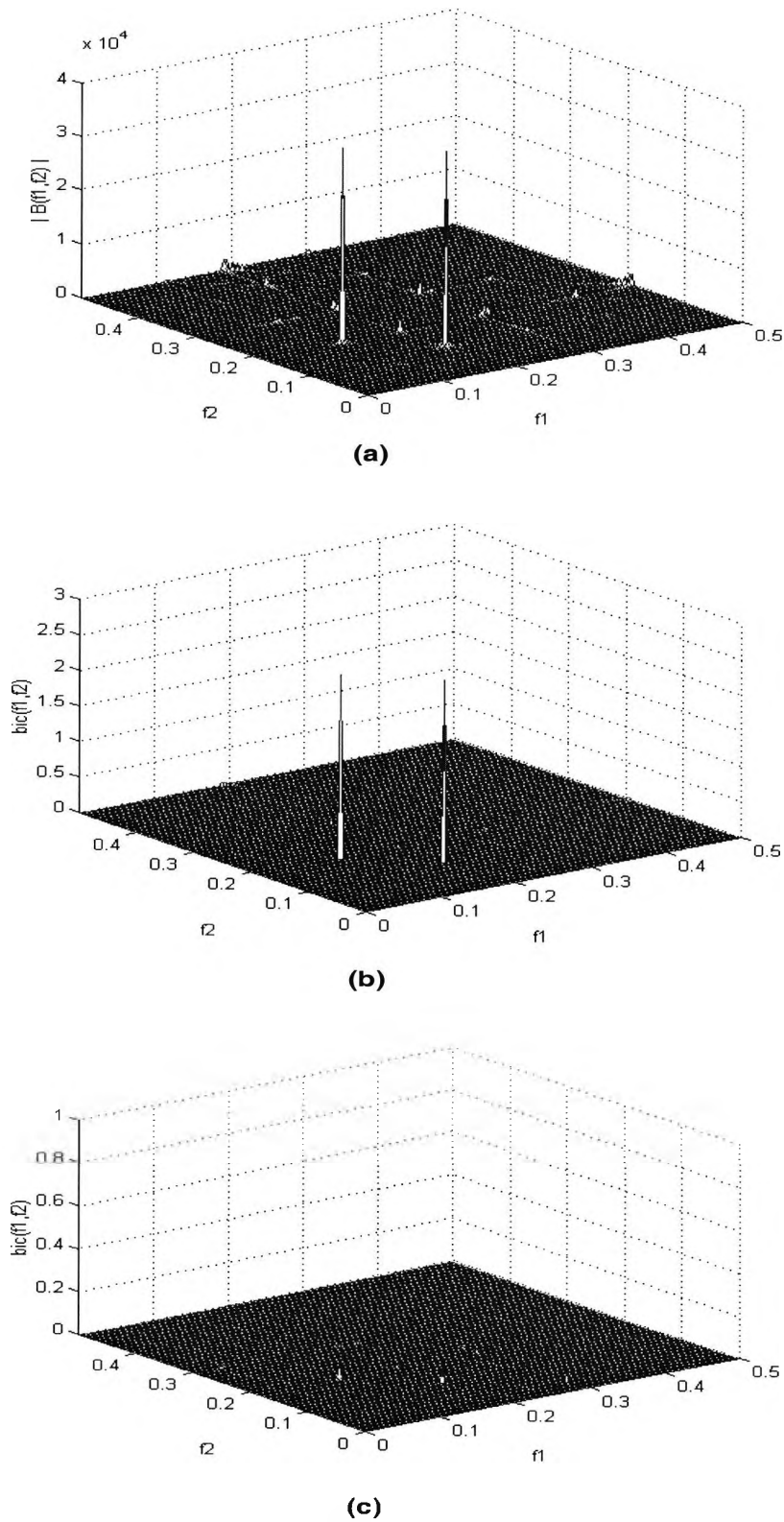


Figure 4.13 MUSIC pseudo-bispectrum magnitude (a), and the bicoherence-squared for $\varphi_3 = \varphi_1 + \varphi_2$ (b), and $\varphi_3 \neq \varphi_1 + \varphi_2$ (c). Segment length=128 and the number of segments=64.

Example 2: In this example, the performance of the proposed algorithm is compared to the performance of the direct and the TOR methods for long and short data segments to detect quadratic phase coupling of the process

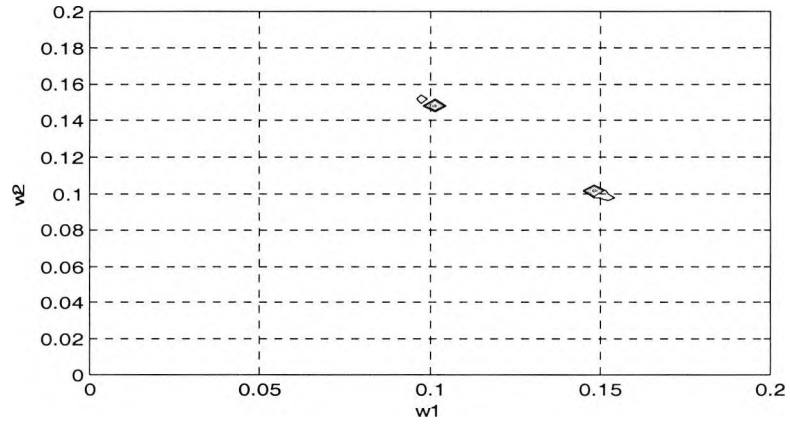
$$x(t) = \sum_{i=1}^6 \cos(2\pi f_i t + \varphi_i) + W(t) \quad (4.29)$$

where $f_1 = 0.1, f_2 = 0.15, f_3 = f_1 + f_2$ and $\varphi_3 = \varphi_1 + \varphi_2, f_4 = 0.19, f_5 = 0.17, f_6 = f_4 + f_5$ and $\varphi_6 \neq \varphi_4 + \varphi_5$. $W(k)$ and φ_i are simulated as explained in example 1. This example is implemented for two cases: (case-1) sixty-four segments of 128 samples, and (case-2) sixty-four segments of 64 samples. Figure 4.14 shows the resultant bispectrum contour plots using (a) the MUSIC-PB, (b), direct method, and (c) the TOR method for 'case-1'. For 'case-1' there is no significant difference between the results obtained using these three methods. For short segment length, 'case-2', better resolution is obtained using the MUSIC-PB as shown Figure 4.15. A signal subspace of, $p=12$ with $L=24$ for the MUSIC-PB and an AR model order of 30 for the TOR are used in the calculations.

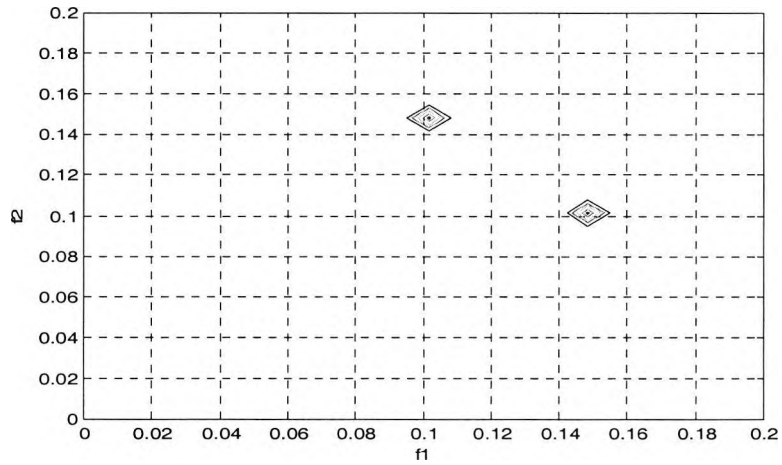
Example 3: In this example the performance of MUSIC-PB in retrieving closely spaced self-coupled harmonics is tested. The process in example 2 is used to simulate two pair of harmonics with the following values, $f_1 = 1.0, f_2 = 2.0$ Hz and $\varphi_2 = 2\varphi_1, f_3 = 1.1, f_4 = 2.2$ and $\varphi_4 = 2\varphi_3$. $W(k)$ and φ_i are simulated as explained in example 1. Sixty-four statistically independent segments of 128 samples each are used. The results obtained are shown in Figures (4.16, 4.17) and Figure 4.18 using the MUSIC-PB and the TOR methods, respectively.

Example 3 shows that the choice of the number of signals, p is very effective on the performance of the MUSIC pseudo-bispectrum. In Figure 4.16, where $p=5$, the MUSIC-PB cannot resolve the two peaks and it splits them into many peaks between 1.0 and 1.1 Hz. The main peak's amplitude is 7.9×10^4 and spurious peak's amplitude, at 2 Hz, is 1.6×10^4 . While using $p=7$ in Figure 4.17 the two peaks are clearly resolved, the main two peak's amplitudes are $1.2 \times 10^5, 0.74 \times 10^5$ and spurious peak's amplitude, at 2 Hz is 0.34×10^5 . On the other hand better resolution is obtained in Figure 4.17 over the TOR bispectrum in Figure 4.18. For the TOR bispectrum, the main two peak's

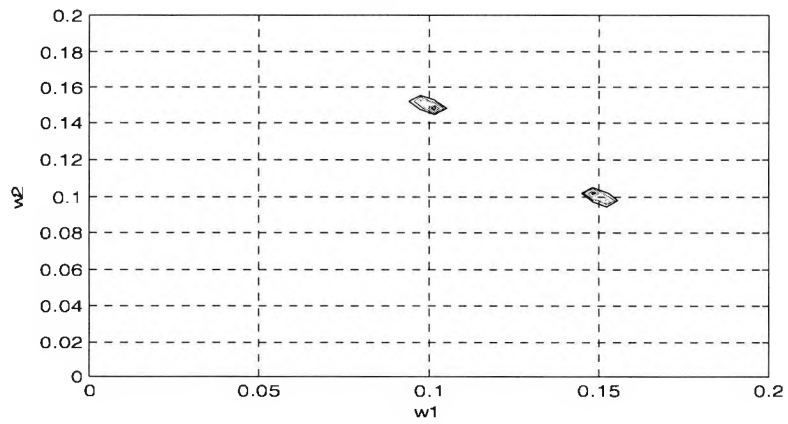
amplitudes are 1.07×10^4 , 0.854×10^4 and spurious peak, at 2 Hz, $=0.48 \times 10^4$. The three bispectra show a spurious peak, at 2 Hz. Compared to the main peaks, the spurious peak is less competent for the MUSIC-PB. The amplitude of spurious peak in Figure 4.16 is the smallest one, where $p=5$. However, choosing $p=7$ in Figure 4.17 improves the resolution but increases the amplitude of that peak.



(a)

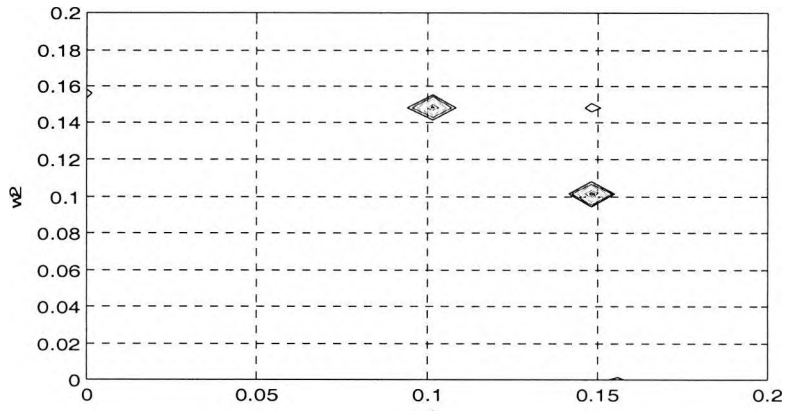


(b)

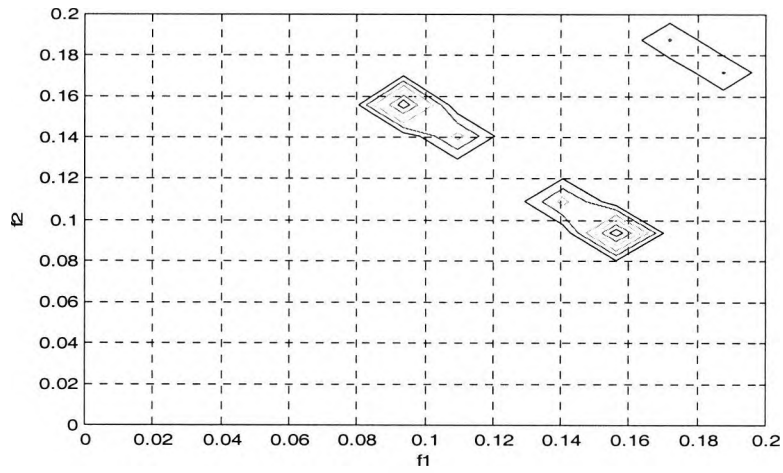


(c)

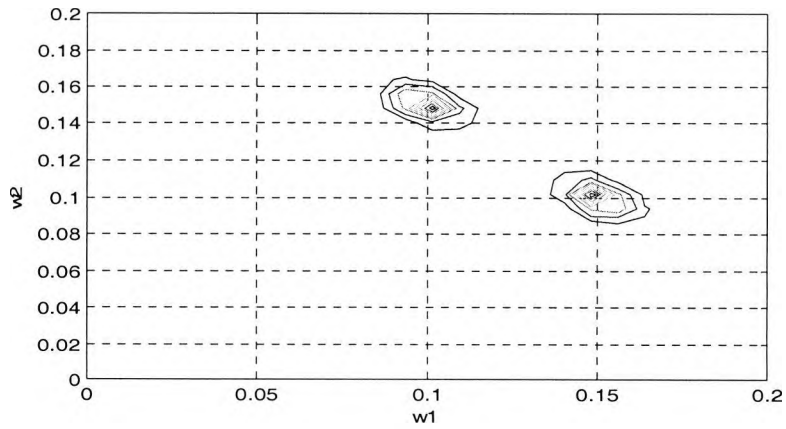
Figure 4.14 MUSIC-PB (a), direct method (b), and TOR (c) bispectrum contours for segment length of 128 samples and number of segments of 64.



(a)

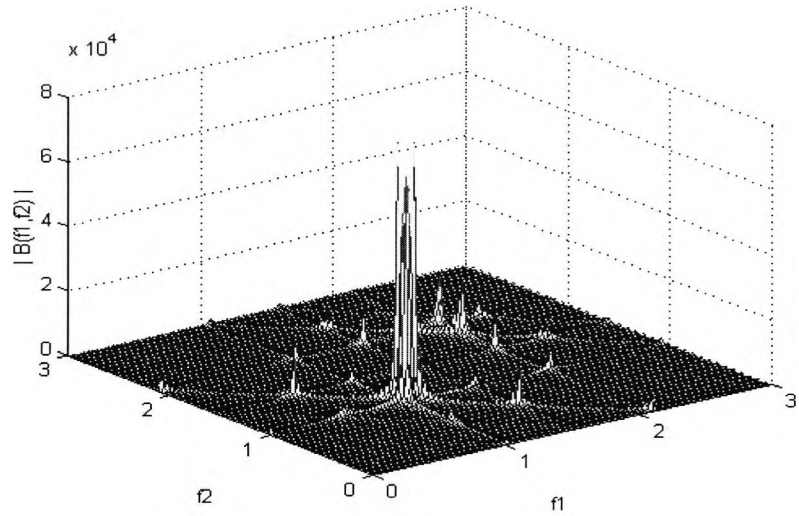


(b)

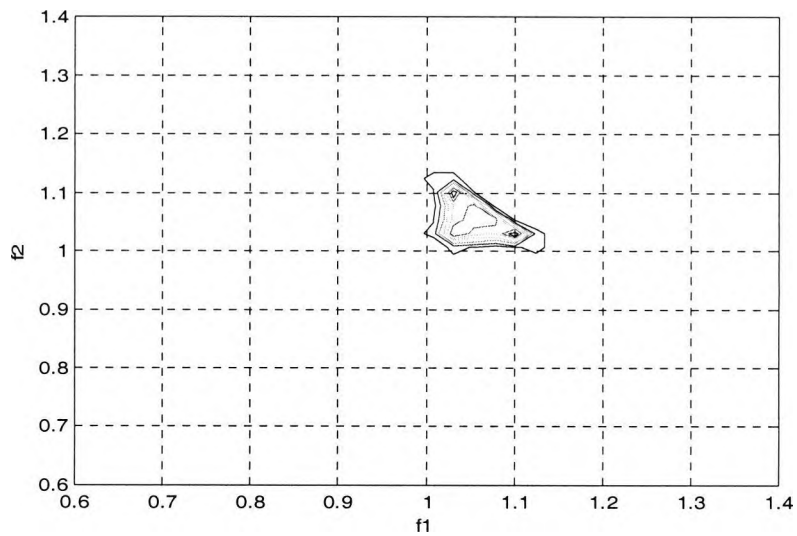


(c)

Figure 4.15 MUSIC-PB (a), direct method (b), and TOR (c) bispectrum contours for segment length of 64 samples and number of segments of 64.

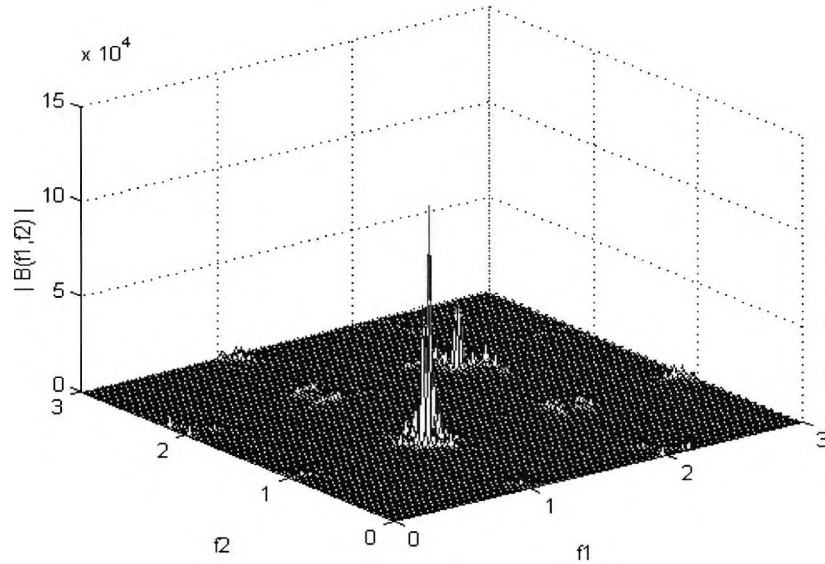


(a)

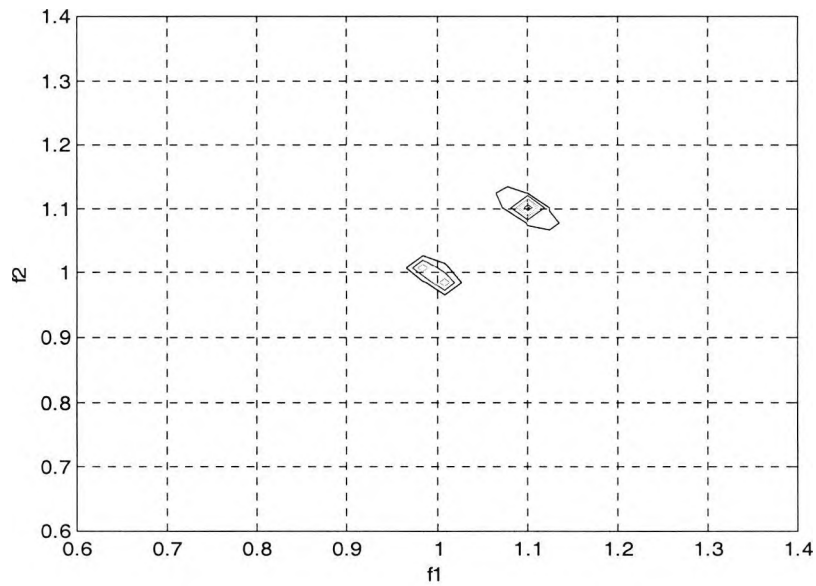


(b)

Figure 4.16 MUSIC-PB (a), and contour plot (b) for a sinusoid signal consists of two pairs of self coupled harmonics, with $f_1=1.0$, $f_3=1.1$ Hz, and $f_2=2*f_1$ and $f_4=2*f_3$. $p=5$.

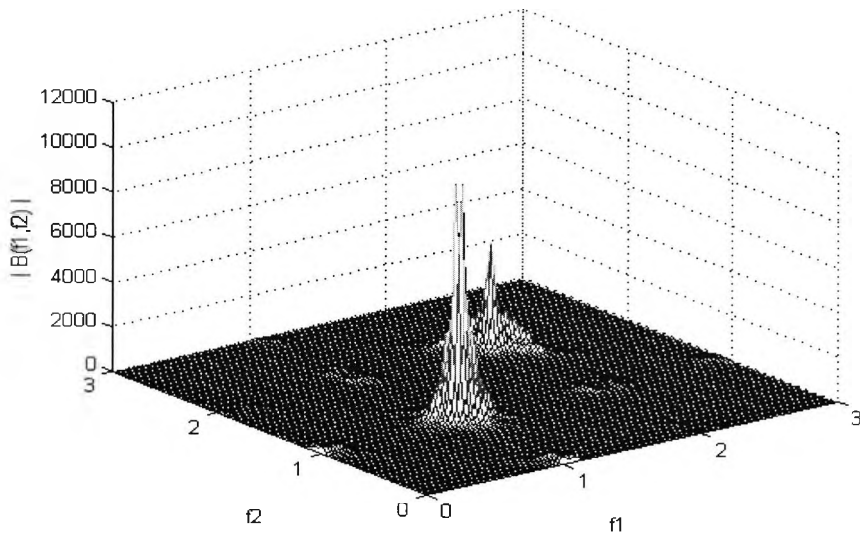


(a)

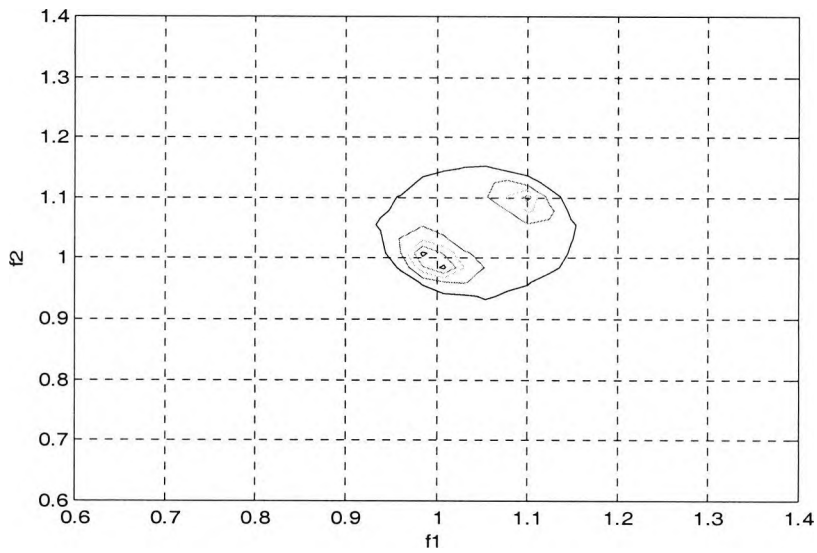


(b)

Figure 4.17 MUSIC-PB (a), and contour plot (b) for a sinusoid signal consists of two pairs of self coupled harmonics, with $f_1=1.0$, $f_3=1.1$ Hz and, $f_2=2*f_1$, $f_4=2*f_3$. $p=7$.



(a)



(b)

Figure 4.18 TOR bispectrum (a), and contour plot (b) for a sinusoid signal consists of two pairs of self coupled harmonics, with $f_1=1.0$, $f_3=1.1$ Hz and $f_2=2*f_1$, $f_4=2*f_3$. The AR model order=9.

Example 4

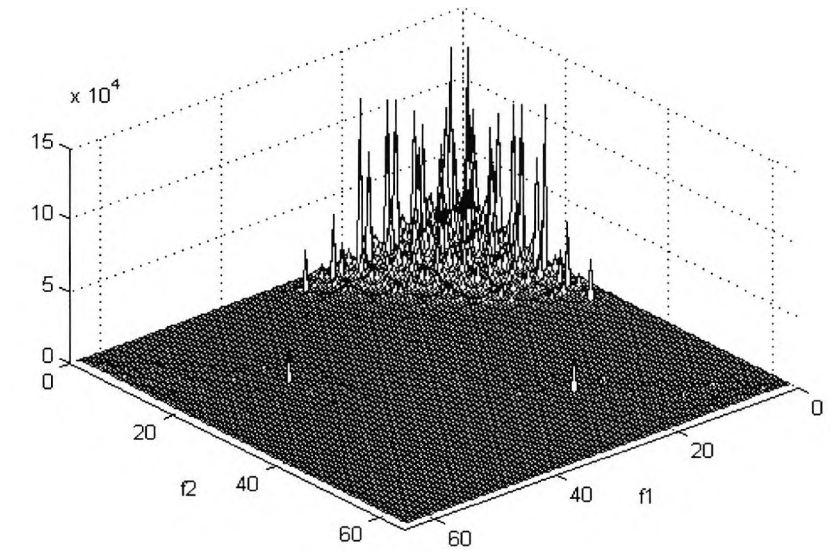
In this example the effect of added coloured noise with different SNR on frequency estimates is studied. Example 1 is repeated with $f_1=0.15$, $f_2=0.1$ Hz, $f_3=f_1+f_2$, $\varphi_3 = \varphi_1 + \varphi_2$ and $W(t)$ is coloured noise generated by passing white Gaussian noise on a MA filter with coefficients [1 -2.33 0.75 0.5 0.3 -1.4]. Table (4.3) presents the results obtained. Each entry in this table is calculated from averaging of the frequency estimates of three independent realisations of the signal $x(t)$. No significant change in the frequency estimates can be noticed with this decrement in the SNR, indicating the ability of this estimator to eliminate Gaussian noise.

SNR, dB	30	20	10	0
f_1	0.151	0.148	0.149	0.147
f_2	0.1	0.1	0.1	0.101

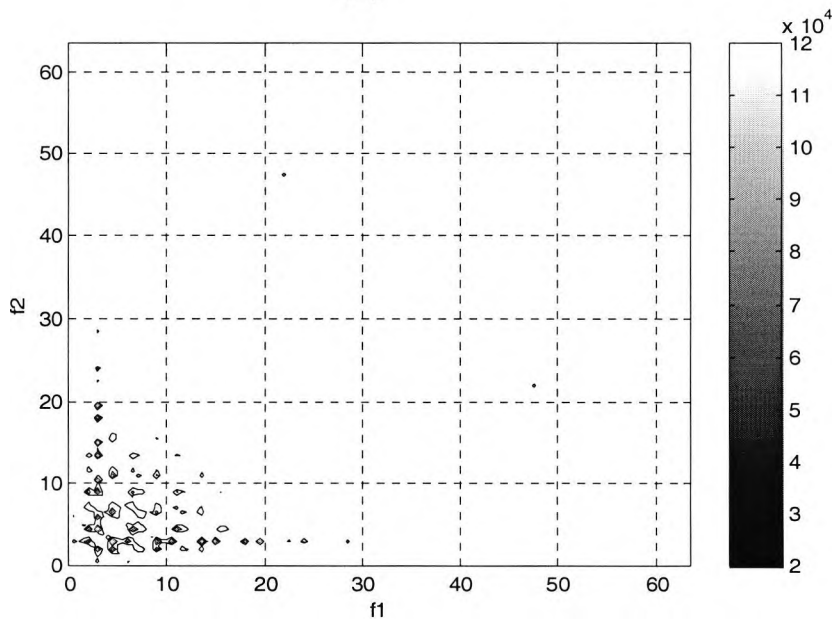
Table 4.3 Frequency estimates with changing the SNR.

4.4.4 Application to ECG Signal

The MUSIC pseudo-bispectrum is applied to some records from the NSR-DB. Figure 4.19 shows the bispectrum magnitude (a) mesh plot, and (b) its contour for record No. 18184. As oppose to the previously described bispectra, the MUSIC pseudo-bispectrum consists of many discrete impulses, which assure the high-resolution capability of the algorithm. The MUSIC-PB covers the same frequency region (0 - 20 Hz) as the direct method and the TOR bispectra. It also showed very similar frequency estimates for the quadratically coupled frequencies as that estimated by the parametric method. As explained earlier by example 3, the main problem for application of this algorithm to the ECG signal is the choice of the number of signals in the signal and the noise subspaces. Wrong choice of these numbers will lead to lots of spurious peaks in the bispectrum.



(a)



(b)

Figure 4.19 MUSIC-PB estimation for record No. 18184 (NSR-DB). (a) mesh plot, and (b) contour plot. Fifty segments are used in the third-order cumulant estimates, each segment is one ECG cycle. $p = 15$ and $L = 24$.

4.5 Discussion

In this chapter the ECG signal was characterised in the higher-order domain. First, the analysis of the third- and the fourth-order cumulants showed that the ECG signal is non-Gaussian. This finding is in agreement with the results obtained in chapter 3 (see section 3.2.1). Transforming the ECG signal to the higher-order domain automatically improves the SNR, as the Gaussian noise, such as the EMG, will be removed. Also the Gaussian part of the MA noise will be suppressed. Cumulant analysis of the normal and ischaemic ECG signals presents a novel feature, i.e., the NACs, to differentiate between the two classes. This feature was found to be more effective for the fourth-order cumulants since the two classes are completely separable using the chosen threshold.

Second, healthy ECG signals have been characterised in terms of their spectral content in the second- and third-order domains. The power spectrum was utilised to show the frequency content of the ECG signal. The bispectrum was used to detect quadratic non-linearity of the ECG signal, which cause bispectral combinations to emerge at harmonically related frequencies. The squared bicoherence index was used as a measure of the degree of phase coherence of the triple of wave harmonics. Three tests have been applied using the bispectrum. The direct method of bispectrum estimation was firstly used to obtain accurate estimation of the location of the coupled frequencies then the bicoherence index was used to show the degree of phase coupling in different frequency regions. The bispectrum indicates the existence of many harmonically related frequencies in the low frequency region (0 - 20 Hz) and the squared bicoherence reveals a strong phase coupling between these frequencies. Then the TOR method was utilised to show the differences between the conventional and parametric techniques and to confirm the results obtained by the direct method. Finally, the Hinich test statistically confirmed the nonzero bispectrum and the quadratic non-linearity of the ECG signals. The results indicated that the bispectral analysis of the ECG signal could reveal extra information not obtainable from the power spectrum.

Third, a new algorithm (MUSIC pseudo-bispectrum) for estimating the quadratic coupled frequency pairs in the bispectrum domain was proposed. The algorithm is based on SVD of a Toeplitz matrix derived from the third-order cumulant sequence of

the process. This matrix is decomposed into two orthogonal subspaces, the signal and the noise subspaces, then a frequency estimation function, matching to the one used in the MUSIC algorithm, was specifically developed to extract the phase-coupled frequencies imbedded in the third-order cumulants. Simulation results indicate the high-resolution capability of the proposed method in detecting and resolving quadratically phase-coupled frequencies. Comparable resolution to the direct and the TOR methods is obtained for the same data length and better resolution for short data segments.

In the MUSIC-like algorithm proposed by Parthasarathy, et al. (1994) the size of the matrix used for eigen-decomposition was $(N^2 \times N^2)$, while that size was $(N/3 \times N/3)$ for SVD in the MUSIC-PB. The MUSIC pseudo-bispectrum algorithm proposed here is computationally efficient than the MUSIC-like algorithm. Also the frequency estimation function used in the MUSIC pseudo-bispectrum was derived using the noise subspace, and that used in the MUSIC-like algorithm proposed by Parthasarathy, et al. (1994) used the signal subspace, which makes the performance of the MUSIC-PB analogous to the performance of the original MUSIC spectrum.

As a member of the parametric bispectrum estimation techniques, the main problem of the MUSIC pseudo-bispectrum is that the frequency estimates are sensitive to the choice of the number of the signals in the signal and noise subspaces this means that with wrong choice of these numbers the pseudo-bispectrum will show artificial frequency peaks or split the original peaks. It is also worth noting here that for applications of the parametric bispectrum techniques to real signals the problem of an optimal model order selection has not been yet solved. Considering this issue Parthasarathy, et al. (1994) suggested that an information theoretic criteria need to be developed for estimation of the signal eigen-values. For application of the parametric techniques to real time signals attention must be given to this choice otherwise, there will be serious consequences, namely, a significant frequency estimation error or loss of resolution.

The bispectral analysis of the normal ECG signals highlighted the fact that the bispectrum and bicoherence index are powerful tools in detecting and quantifying, respectively, the quadratic non-linearity in the signal. Chapter 5 will exploit these tools,

i.e., the polyspectrum and polycoherence indices, in detecting and quantifying higher-order non-linearities in normal and abnormal ECG signals. In this chapter the bispectrum domain of the normal ECG signals was investigated, chapter 5 is mainly concerned with comparison between normal and ischaemic ECGs first in the bispectrum domain then in the higher-order (>3) spectral domains.

Chapter 5

DETECTION OF HIGHER ORDER NON-LINEARITIES

5.1 Introduction

Recently evidence has accumulated that ECG signals are of non-linear nature. This motivated the investigation of the ECG signals with methods from non-linear dynamic system theory. This non-linearity has been studied from the points of view of chaotic system theory (Babloyantz and Destexhe 1988; Fell, et al. 2000a; Fell, et al. 2000b; Goldberger and West 1987; Signorini, et al. 1994), complexity measure (Zhang, et al. 1999), and wavelet transforms (Meste, et al. 1994; Zhang, et al. 1997). In this chapter the non-linearity character of the ECG signal will be studied from points of view of the HOS.

In spite of the powerful capabilities of the HOS in detecting and characterising non-linearities in time series, only a handful of papers have applied them in the analysis of the ECG signals. As previously explained in detail in chapter 1, HOS has been used for the detection of late potentials (Sabry-Rizk, et al. 1998; Spaargaren and English 1999; Speirs, et al. 1993), for fetal ECG detection (Sabry-Rizk, et al. 2000a; Sabry-Rizk, et al. 2000b; Sabry-Rizk, et al. 1997; Sabry-Rizk, et al. 1996), and for P-wave detection (Sabry-Rizk, et al. 2000c; Sabry-Rizk, et al. 2000d). On the other hand, HOS have been applied extensively in the field of EEG signal processing, examples of this work can be found in (Muthuswamy, et al. 1999; Ning and Bronzino 1989; Ning and Bronzino 1993; Sigl and Chamoun 1994; Zhang, et al. 2000).

The bispectral analysis in chapter four provides evidence for the quadratic non-linearity of the normal ECG signals. Since the quadratic non-linearity is of special importance in analysing such signals, it can be used to quantify the presence of higher-order non-

linearities. This quadratic non-linearity will be investigated for ischaemic ECG signals in this chapter. The differences between normal and ischaemic bispectral features will be established. The possibility of higher-order non-linearities in ECG signals will be investigated using an elegant algorithm proposed by Zhou and Giannakis (1995). In this algorithm an estimator of the diagonal slices of polyspectrum up to any order was proposed. These slices have the advantage of one-dimensionality, they are Gaussian noise free and informative with HOS features. Self-coupled harmonics are retrieved from the peaks on the diagonal slices of the polyspectrum. The peaks at the fundamental frequencies and the phase angles at these frequencies are then used to detect non-linearities. An extension of this algorithm to estimate the polycoherency index slices of any order, using the diagonal slice of the polyspectrum of the same order and the power spectrum, will be introduced. This will be used to quantify the degree of self-phase coupling between frequency components on the diagonal slices of the polyspectra. Normal and ischaemic ECG signals are analysed using the two methods, differences between the two physiological cases in the higher-order domain have been assessed, then the order ranges of non-linearity that can represent ECG signal dynamics for both them are identified.

5.2 Detection of K^{th} -order Non-linearity

The presence of coupled harmonics in the data is a symptom attributed to non-linear mechanisms generating the available time series. Self-coupling results in the presence of frequency pairs $(\omega_0, k\omega_0)$ and perhaps phase pairs $(\phi_0, k\phi_0)$ as well, with k an integer. It appears in periodic signals or when harmonics undergo non-linear transformations. The existence of self-frequency $(\omega_0, k\omega_0)$ and self-phase $(\phi_0, k\phi_0)$ coupling components strongly suggests the presence of k^{th} -order non-linearity. However, self-frequency coupling alone does not necessarily confirm the presence of k^{th} -order non-linearity. In such cases, self-frequency coupling information can be combined with other evidence to investigate system non-linearity (Huber, et al. 1971). To confirm the k^{th} -order non-linearity Zhou and Giannakis (1995) proposed a "self coupling detection algorithm" for retrieval of self-frequency coupling combined with the estimation of the phase angle at the self-coupled frequencies in the polyspectrum domain. However, in this study the self-

frequency coupling is accompanied by the estimation of the value of the polycherency indices at the self-coupled frequencies.

5.2.1 Self-Coupling Detection Algorithm

This algorithm (Zhou's algorithm) mainly uses one data segment for estimation of the diagonal slices of the polyspectrum. It consists of three steps; (i) it checks for self-frequency coupling along the diagonal of the polyspectrum, (ii) estimates the phase angle at the fundamental frequency, and (iii) statistically tests if this angle is zero via an estimated phase threshold. For this analysis Zhou and Giannakis (1995) assumed a harmonic process in an additive noise of the form:

$$x(t) = d(t) + v(t) = \sum_{l=1}^L A_l e^{j(\omega_l t + \phi_l)} + v(t) \quad (5.1)$$

where A_l 's are real, nonzero, and deterministic constants, ϕ_l 's are deterministic constants in $(-\pi, \pi]$ and ω_l 's are distinct and nonzero in $(-\pi, \pi)$. The noise $v(t)$ is zero-mean and stationary and the samples of $v(t)$ are assumed to be well separated and can be approximately independent.

5.2.1.1 Estimation of Polyspectrum Slices

The $(k+1)^{\text{st}}$ -order Fourier series polyspectrum is defined as the Fourier series coefficient of the $(k+1)^{\text{st}}$ -order moment and its estimator is given by Zhou and Giannakis (1995)

$$\hat{M}_{k+1}^x(\omega_1, \dots, \omega_k) = \frac{1}{N^{k+1}} X_N(\omega_1) \dots X_N(\omega_k) X_N^* \left(\sum_{l=1}^k \omega_l \right) \quad (5.2)$$

which is the scaled $(k+1)^{\text{st}}$ -order polyspectrum and it is asymptotically unbiased. The diagonal slice of this estimator is,

$$\hat{M}_{k+1}^x(\omega, \dots, \omega) = \hat{M}_{k+1}(\omega) = \left[\frac{X_N(\omega)}{N} \right]^k \left[\frac{X_N^*(k\omega)}{N} \right] \quad (5.3)$$

where $X_N(\omega) \equiv \sum_{t=0}^{N-1} x(t) e^{-j\omega t}$, N is the number of samples.

Assume the frequency coupling in Eq. (5.1) has the form $\omega_i = k\omega_j \bmod (2\pi)$, where i, j are integers and there is no other frequency coupling then the $(k+1)^{\text{st}}$ -slice will theoretically have the form

$$M_{(k+1)}^x(\omega) = A_1^k A_2 e^{j(k\phi_1 - \phi_2)} \delta(\omega - \omega_0), \quad (5.4)$$

where $\delta(\cdot)$ denotes the kronecker delta and ω_0 is the fundamental frequency.

A Self-Coupling Frequency Estimator

Zhou and Giannakis (1995) proposed the following estimator for self-coupled harmonics

$$\hat{\omega}_0 = \arg \max_{\omega} |\hat{M}_{k+1}^x(\omega)| \quad (5.5)$$

Phase Coupling Estimator

The phase estimate of the polyspectrum at $\hat{\omega}_0$ is given by

$$\hat{\phi} = \arg[\hat{M}_{k+1}^x(\omega_0)] \quad (5.6)$$

where "arg" denotes the principal value of the phase.

5.2.1.2 Summary of the Algorithm

The algorithm consists of the following steps:

Step 1: compute $\hat{M}_{k+1}^x(\omega)$ from Eq. (5.3)

Step 2: Peak in $|\hat{M}_{k+1}^x(\omega)| \Rightarrow k^{\text{th}}$ -order self-frequency coupling. Estimate ω_0 as in Eq. (5.5).

For the case of the ECG signal only peaks that satisfy the following conditions are picked.

(a) The standard separation criteria (Brillinger 1980), that is, for two peaks at $\hat{\omega}_i, \hat{\omega}_j$, the $\min|\hat{\omega}_j - \hat{\omega}_i| = N^{-1/2}, i \neq j$. (b) The peak amplitude $> k$ times the mean Fourier amplitude.

Step 3: Calculate $\hat{\phi}$ using Eq. (5.6).

Step 4: Statistical test

This to statistically check for the presence of the k^{th} -order self-phase coupling. If the phases ϕ_1 and ϕ_2 of two components whose frequencies are ω_1 and ω_2 , respectively, are self-coupled with $\phi_2 = k\phi_1$, then based on Eq. (5.4), the estimated phase of the polyspectrum is $\hat{\phi} = 0$ by Eq. (5.6). To check for the zeroness of $\hat{\phi}$ two hypotheses are set up:

$$H_0 : \phi = 0 \bmod 2\pi \text{ Versus } H_1 : \phi \neq 0 \bmod 2\pi \quad (5.7)$$

where $\bmod(2\pi)$ is included since in practice, ϕ can only be estimated in multiples of 2π . It has been shown by Zhou and Giannakis (1995) that $\sqrt{N}(\hat{\phi} - \phi)$ is asymptotically normal with zero mean and variance σ_ϕ^2 . Therefore $[\sqrt{N}(\hat{\phi} - \phi)]^2 / \sigma_\phi^2$ is central chi-squared distributed with one degree of freedom as denoted by $\chi^2(1)$. The probability of false alarm P_{FA} is defined as:

$$P_{FA} = \Pr \left\{ \frac{N\hat{\phi}^2}{\sigma_\phi^2} > \Gamma \mid H_0 \right\} \quad (5.8)$$

where Γ is determined from a central $\chi^2(1)$ table with tail probability P_{FA} . A threshold for the value of $\hat{\phi}$ can be calculated by:

$$\mathfrak{S} \equiv \Gamma \sigma_\phi^2 / N \quad (5.9)$$

The presence of phase coupling is statistically confirmed if $\hat{\phi}^2 < \mathfrak{S}$ and rejected otherwise. The variance of the phase estimate, $\sigma_{\hat{\phi}}^2$ in Eq. (5.8) is calculated using the following equation,

$$\sigma_{\hat{\phi}}^2 = \frac{k^2}{2SNR_1} + \frac{1}{2SNR_2}, \quad k \geq 2 \quad (5.10)$$

where $SNR_l, l=1,2$ is the peak signal-to-noise ratio at ω_l , and defined as follows

$$SNR_l \equiv \frac{A_l^2}{S_v(\omega_l)} \quad (5.11)$$

where $S_v(\omega_l)$ denotes the power spectral density of $v(t)$ and

$$\hat{A}_l^2 = \hat{M}_2^x(\hat{\omega}_l) \quad (5.12)$$

This algorithm is computationally efficient as it employs the diagonal polyspectrum slice to detect increasing orders of non-linearity without corresponding increase in the dimensionality and only a single segment is required for the phase-coupling detector and its frequency estimator requires a single harmonic to probe an unknown non-linearity. In addition to that performance evaluation by the authors reveals decreasing variance in slices of polyspectra of increasing order. For detection of phase coupling this algorithm relies on the estimation of phases at self-coupled harmonics and then estimation of the phase thresholds. This brings about a limitation of the use of this algorithm because of the following: (1) frequency bias is magnified in phase errors as described by the authors (Zhou and Giannakis 1995). (2) The estimation of the phase threshold is dependent on the estimation of the contaminated noise, in real signals this may lead to inaccurate and unreliable values for the phase threshold. In order to overcome the aforementioned limitations, the normalised polyspectrum slice (polycoherency index) is proposed in this study as a measure for the degree of phase coupling. I used the algorithm proposed by Zhou to estimate the diagonal slices of the polyspectrum, but with multiple independent segments, then to estimate the frequency-coupled harmonics. The value of the polycoherency index at the fundamental frequency is then estimated.

5.2.2 The Polyoherency Indices

The polycoherency indices are very useful in the detection and characterisation of non-linearities in time series and in discriminating linear processes from non-linear ones (Nikias 1993). For totally coupled harmonics $\omega_0, 2\omega_0, \dots, k\omega_0$, the k^{th} -order polycoherency index, P_{k+1}^x , at the fundamental frequency, ω_0 , is one and it is zero when these components are uncorrelated. The following estimator for k^{th} -order polycoherency index is proposed:

$$\hat{P}_{k+1}^x(\omega_1, \omega_2, \dots, \omega_k) = \frac{\hat{M}_{k+1}^x(\omega_1, \dots, \omega_k)}{\sqrt{\hat{M}_2^x(\omega_1) \hat{M}_2^x(\omega_2) \dots \hat{M}_2^x(\sum_{i=1}^k \omega_i)}} \quad (5.13)$$

Its diagonal slice can be calculated from:

$$\hat{P}_{k+1}^x(\omega, \omega, \dots, \omega) = \hat{P}_{k+1}^x(\omega) = \frac{\hat{M}_{k+1}^x(\omega)}{\sqrt{(\hat{M}_2^x(\omega))^k \hat{M}_2^x(k\omega)}} \quad (5.14)$$

where $\hat{M}_{k+1}^x(\omega)$ and $\hat{M}_2^x(\omega)$ can be calculated from Eq. (5.3). In contrast to Zhou's method, multiple independent segments are required for correct estimation of the polycoherency index, which in turn increases the computations required but still has the advantage of one dimensionally.

5.2.2.1 Summary of the Algorithm

Step 1: follow step 1 and 2 in the previous algorithm but with multiple independent segments to estimate $\hat{M}_{k+1}^x(\omega)$.

Step 2: compute $\hat{M}_2^x(\omega)$ from Eq. (5.3), using $k=1$.

Step 3: compute $\hat{P}_{k+1}^x(\omega)$ from Eq. (5.14).

Step 4: If $\hat{P}_{k+1}^x(\hat{\omega}_0) \geq 0.9 \Rightarrow k^{\text{th}}$ order self-phase coupling exists (for 90% confidence).

5.3 Results

5.3.1 Introduction

Normal ECG data from the NSR-DB (MIT-CD 1997) and ischaemic ECG data from the European ST-T database (Taddei, et al. 1992) are used in this analysis. The analysis consists of three steps; first the bispectrum and bicoherency index will be estimated (in section 5.3.2) for all normal and ischaemic cases used in this analysis then the differences between them in the bispectrum domain will be investigated. The second step is to apply Zhou's algorithm to detect higher-order non-linearities for all normal and ischaemic cases (section 5.3.3.1). The third step is to investigate the results obtained in the second step using the polyspectrum and polycoherency indices (section 5.3.3.2). Data from 18 normal cases and 21 ischaemic cases are analysed. Throughout this analysis, the segment length is taken equal to lp , calculated for individual ECG records. Sample ECG waveforms from normal ECG cycle taken from the NSR-DB (record No. 16272, left) and an ischaemic ECG cycle from E-DB (record No. e0105, right) are displayed in Figure 5.1.

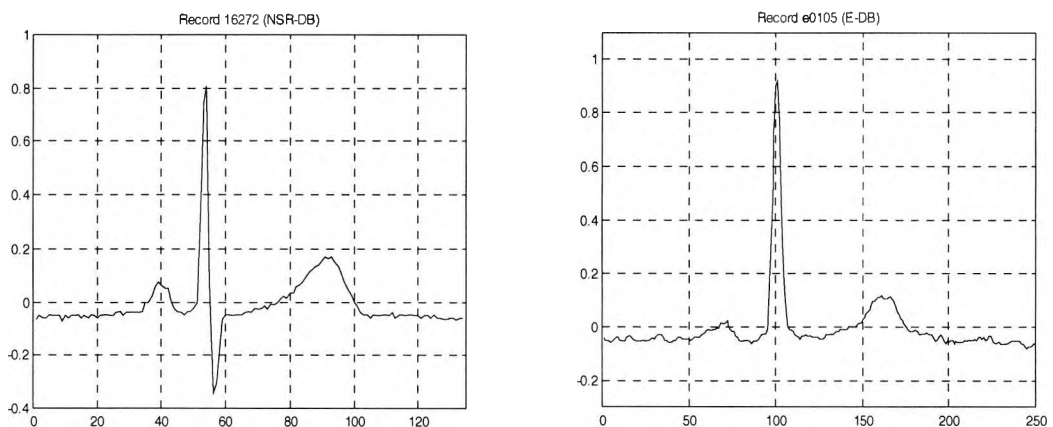


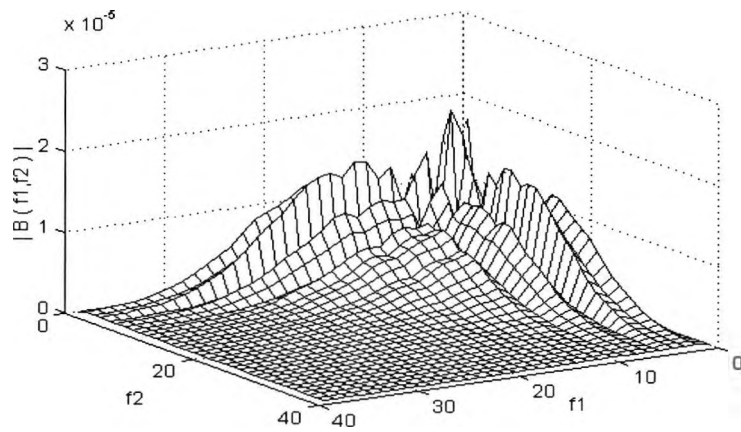
Figure 5.1 Time domain of an ECG cycle from record No. 16272, NSR-DB (left) and record No. e0105, E-DB (right).

5.3.2 Bispectral Analysis of Normal/Ischaemic ECG Signals

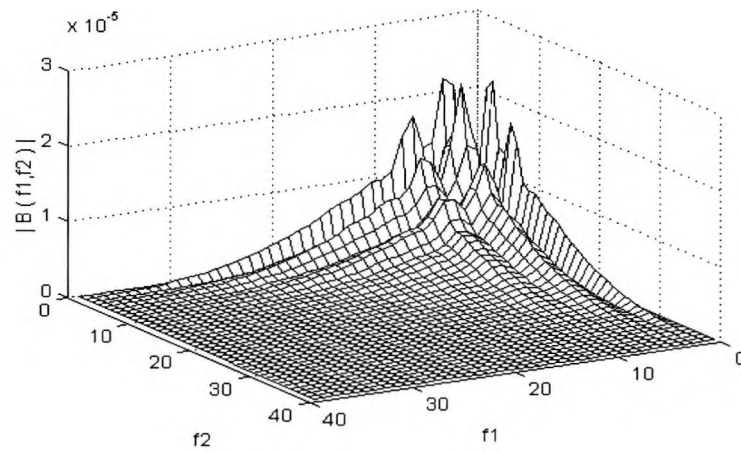
The bispectrum is calculated using the direct method of estimation Eq. (4.15) and the squared bicoherence index, " bic^2 ", is calculated using Eq. (4.16). The bispectrum is calculated as an average of 50 individual bispectra. Typical magnitude bispectra from a normal case (record No. 16539) and an ischaemic case (record No. e0103) are shown in Figure 5.2 (a), (b), respectively. Figure 5.2 (c) is the diagonal slices for the normal (left) and ischaemic (right) cases. Figure 5.3 is a contour plot of the squared bicoherence index and its diagonal slice for each of these cases. Observations from these figures include:

- 1- The bispectrum of a normal ECG signal has harmonics that cover a wide range of frequencies (0 - 30 Hz) while that of an ischaemic ECG signal covers a narrower range of frequencies (0 - 20 Hz). This finding comes in agreement with the results obtained by Clayton, et al. (1993) for the power spectral analysis of normal and abnormal ECGs.
- 2- The bispectra in Figure 5.2 reveal how closely the frequency components interact quadratically among themselves in both normal and ischaemic cases. This indicates the existence of phase-coupled frequencies. To quantify the degree of this phase coupling the bicoherence-squared contours and their slices in Figure 5.3 are used. The contour plots Figures 5.3 (a), (b) are drawn in gray scale levels with white and black areas correspond to maximum and minimum bicoherence indices, respectively. According to this scale the low frequency region (0 - 20 Hz) in the bicoherence contours indicates a high degree of phase coupling between frequency components in this region. A value of $bic^2 \geq 0.9$ means that it is 90% confident that these components are due to totally phase coupled frequencies.
- 3- The diagonal slices in Figure 5.3 (c) and 5.3 (d) confirm the previous finding as the self-coupled frequencies show a value near to one for the bicoherence indices in this region especially for normal ECG signal.
- 4- Using the bispectrum further processing is made to extract features that may characterise the normal and abnormal ECG signals, as follows;

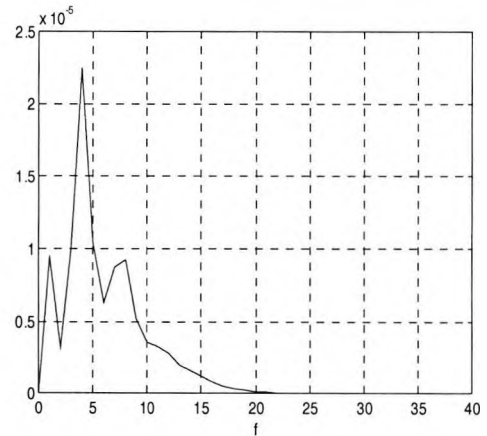
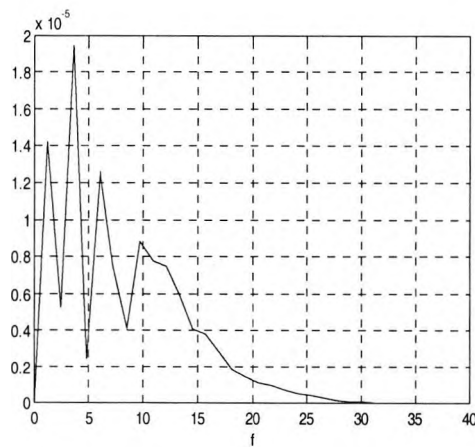
- First a pilot study has been made to extract features from the phase of bispectrum. The bispectrum is calculated for segments starts from the R peak to the end of T-wave (RST-T) of normal and abnormal ECG signals (Sabry-Rizk, et al. 1999). In this study the bispectrum phases are employed to develop discriminant contour patterns in the multi-dimensional phase of the polyspectra (polyphase) of 'normal' looking ECG signals in outpatients having weariness and general malaise or chest pain. Similar polyphase patterns have been found in the ECG signals from acute myocardial infarct patients with or without diagnostic ST segment and T-wave changes. Three cases from hospital recordings and some from the ST Change-DB showed discriminant biphasic contour patterns but no further success is obtained in this direction.
- Second the bispectrum magnitude and bicoherence-squared index are investigated. Two features have been extracted: (a) the Maximum Bicoherence Index (MBI), i.e., the value of the bicoherence index at the frequency of the maximal intensity, f_m (the fundamental frequency) on the bispectrum magnitude. (b) The Average Bicoherence Index (ABI), i.e., the mean value along the diagonal slice of the bicoherence indices in the frequency range (0 - 20 Hz). Similar features have been employed by (Muthuswamy, et al. 1999) to detect burst suppression patterns in EEG signals in the bispectrum domain.



(a)



(b)



(c)

Figure 5.2 Bispectrum magnitude of a normal case, No. 16539 (a), of an ischaemic case, No. e0103 (b), and their diagonal slices (c), for the normal (left) and for the ischaemic (right) bispectra. Each bispectrum is calculated from averaging of 50 individual bispectra.

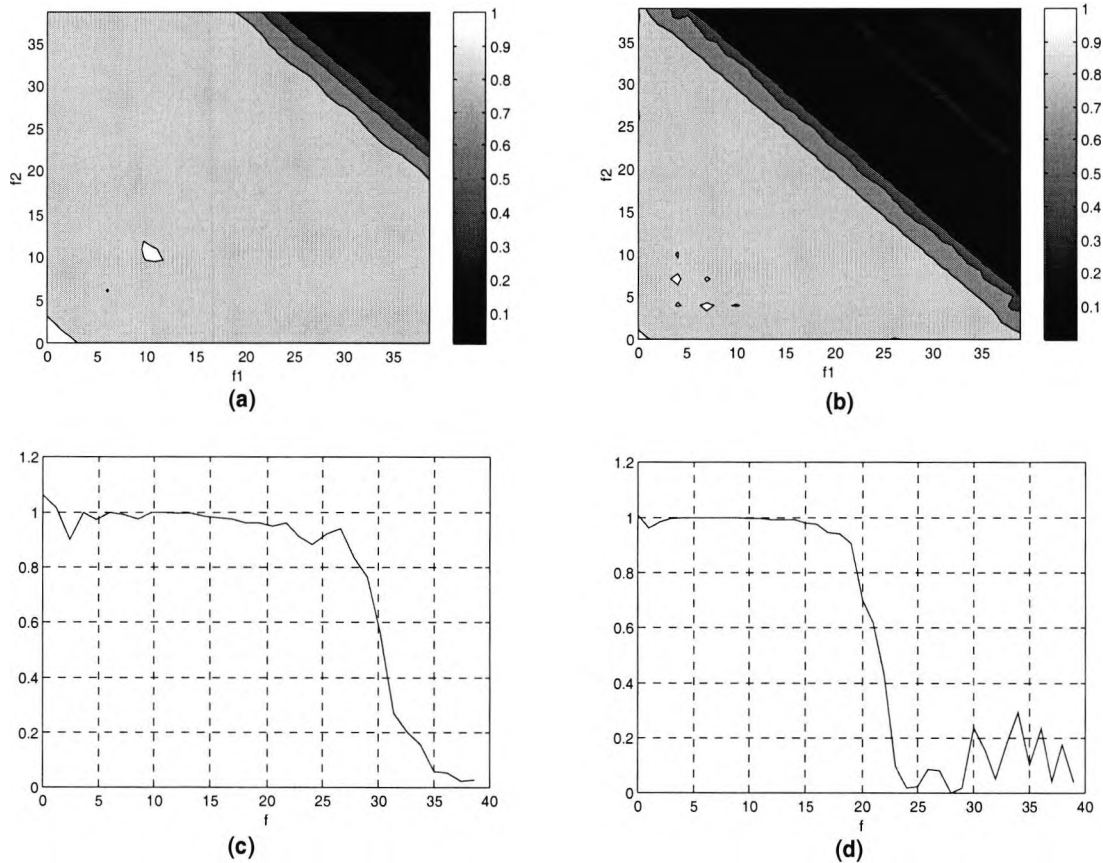
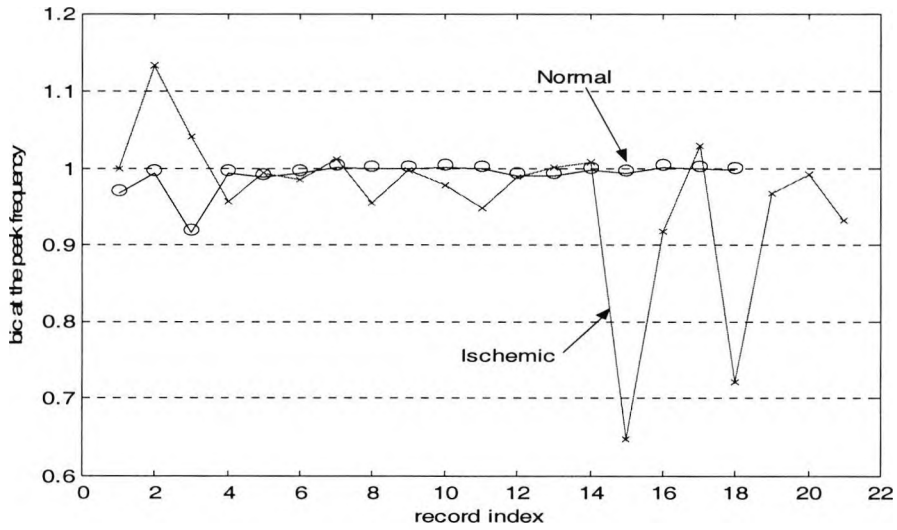
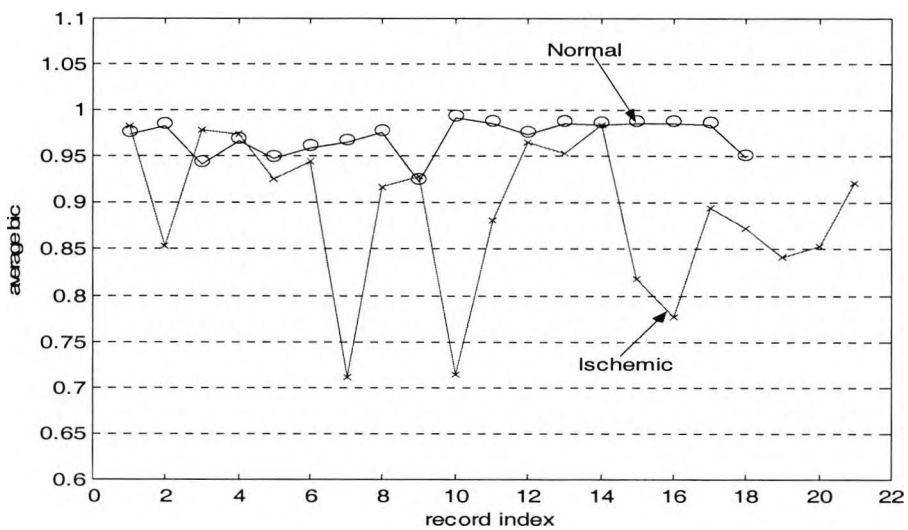


Figure 5.3 Contour plots (a, b) and diagonal slices (c, d) of the bicoherence indices of a normal case, No. 16539 (a, c) and an ischaemic case No. e0103 (b, d). Each bispectrum is calculated from averaging of 50 individual bispectra.

The MBI and ABI are estimated for all normal and ischaemic cases included in this study. Figure 5.4 shows the results obtained from this analysis. The x-axis represents the record index in both figures and the y-axis represents the MBI in (a) and the ABI in (b). Both of the bicoherence measures, MBI and ABI, in Figures 5.4 (a) and 5.4 (b) for normal ECG signals are almost larger than that of the ischaemic ECG signals. According to the MBI one can conclude that both the normal and the ischaemic ECG signals contain quadratic non-linearity. But according to the ABI, Figure 5.4 (b), it is likely to say that the normal ECG signals are more consistent with the quadratic non-linearity than the ischaemic ones and are more likely to have higher-order non-linearities. This will be studied in the following section.



(a)



(b)

Figure 5.4 Bicoherence analysis of 18 normal and 21 abnormal records. (a) The Maximum Bicoherence Index (MBI), and (b) the Average Bicoherence Index (ABI). The x-axis represents the record index for both normal and ischaemic cases and the y-axis represents the value of the MBI (a) and the ABI (b).

5.3.3 Higher-order Spectral Analysis

This analysis consists of the following steps: (1) Calculate the diagonal slices of the polyspectrum for orders $k=2$ to 10. (2) Detect the peaks on the polyspectrum slices that satisfy the previously mentioned conditions, and estimate their frequencies. (3) Apply

algorithms described in sections (5.2.1 and 5.2.2) to check the existence of the self-phase coupling phenomenon in normal and ischaemic ECG signals. (4) Evaluate the performance and the differences between the results obtained from the two algorithms. (5) Extract some features to differentiate between normal and ischaemic ECG signals and define the non-linearity order that can model the dynamics of the two physiological cases. The following two subsections (5.3.3.1 and 5.3.3.2) present the results for Zhou's algorithm and the polycoherency indices, respectively. First samples from the diagonal slices of the polyspectrum for orders $k=3,5,7$ for a normal case (No. 16272) and an ischaemic case (No. e0104) are shown in Figure 5.5. As observed before in the bispectrum analysis these polyspectrum slices show that generally the abnormal ECG signal spectra cover narrower band of frequencies than the normal ones.

5.3.3.1 *Detection of Non-linearities using Zhou's Algorithm*

In this part of the study the diagonal slices of the polyspectrum for fifty segments from each record are calculated for all normal and ischaemic cases. Each slice is estimated using one segment (i.e., no averaging). The power spectrum, $S_v(\omega_l)$, of the contaminated noise in Eq. (5.11) is estimated using record 'em' from NST-DB (MIT-CD 1997). This record contains electrode motion artefact (usually the result of intermittent mechanical forces acting on the electrodes), with significant amounts of baseline wander and muscle noise as well.

Tables 5.1 to 5.9 show the results obtained for all normal and ischaemic ECG signals. The first column is the record number, the second is the segment number which show the most reliable results for that order, the third is the frequencies at which the self-coupling is detected, the fourth is $\hat{\phi}^2$, the fifth is the threshold value, \mathfrak{S} , for 5% PFA, and the last column lists the NSC which is the number of segments, out of 50, that show self-phase coupling for that order.

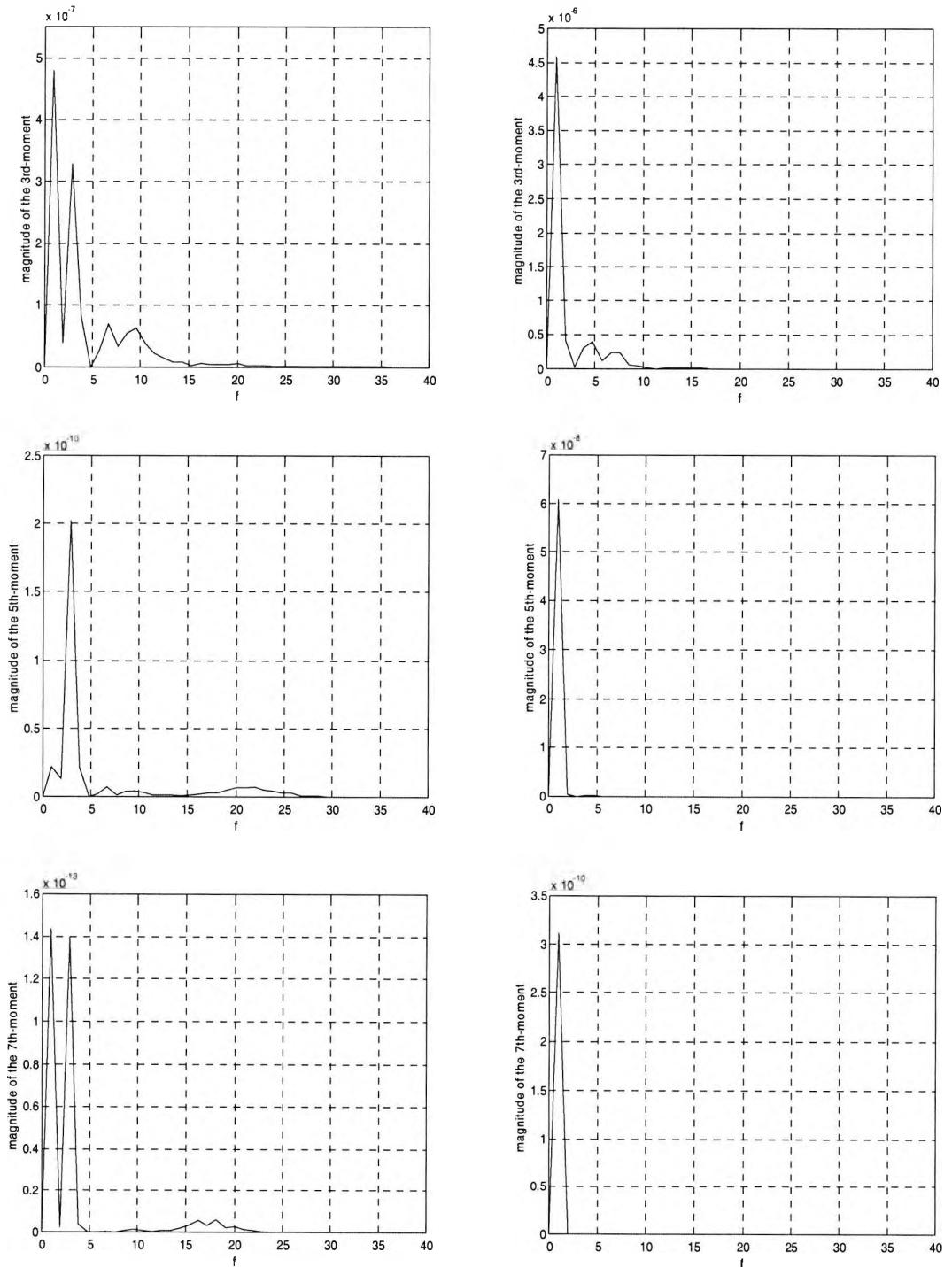


Figure 5.5 The magnitude of polyspectrum slices of a normal case (No. 16272, left) and an ischaemic case (No. e0104, right) for moment orders $k=3, 5$ and 7 from top to bottom, respectively. segment length= one ECG cycle, one segment is used to calculate the polyspectrum slices.

Record Number	Segment Number	Frequency (Hz)	Polyphase Squared (rad ²)	Threshold (PFA=5%)	NSC*
16273	8	6.957	2.31E-06	1.80E-03	43
16483	25	4.174	1.22E-04	5.54E-03	13
16539	29	10.868	4.92E-07	1.08E-04	12
16773	32	4.491	2.03E-05	4.69E-03	21
18177	39	7.046	2.92E-06	2.07E-03	19
19090	17	8.072	3.61E-07	5.29E-04	21
19093	19	4.000	2.36E-03	4.37E-03	4
19140	12	7.385	2.21E-05	2.59E-03	8
19830	48	8.727	1.55E-04	1.13E-03	1
e0103	43	7.968	4.27E-06	6.67E-05	4
e0104	19	7.576	2.41E-08	2.24E-04	4
e0105	24	2.768	3.17E-06	3.34E-04	7
e0107	40	7.246	5.80E-07	1.24E-04	6
e0111	23	11.307	3.93E-05	7.64E-04	7
e0115	40	5.515	5.52E-06	2.99E-03	12
e0116	24	5.800	9.64E-06	2.60E-04	5
e0121	21	3.906	3.07E-05	2.25E-03	12
e0162	18	3.769	1.08E-05	1.53E-03	8
e0166	8	9.328	3.54E-05	7.14E-05	1
e0202	41	3.968	1.28E-05	2.31E-03	11
e0203	26	2.825	8.24E-04	2.47E-03	1

Table 5.1 Results of the self-coupling detection algorithm for the order $k=2$. The above values of the frequency, phase angle, and threshold are obtained for the corresponding tabulated segment number that led to the smallest phase value. *The number of segments out of 50 that show self-phase coupling for $k=2$.

Record Number	Segment Number	Frequency (Hz)	Polyphase Squared (rad ²)	Threshold (PFA=5%)	NSC
16265	20	6.454	8.58E-07	2.34E-03	10
16272	47	6.687	1.01E-07	1.01E-03	8
16273	50	4.174	4.41E-04	7.88E-03	15
16539	33	3.623	2.20E-05	6.10E-03	6
16773	50	4.491	2.09E-03	1.08E-02	1
16795	40	0.977	1.05E-03	4.62E-03	1
18177	15	7.046	5.86E-05	4.69E-03	11
19093	19	4.000	7.54E-04	9.47E-03	1
19830	22	8.727	1.79E-05	2.38E-03	1
e0103	12	7.968	1.50E-07	1.21E-04	8
e0105	37	5.535	2.93E-07	1.58E-04	6
e0107	39	7.246	5.07E-05	2.68E-04	1
e0115	47	5.515	1.06E-04	5.20E-03	4
e0119	37	4.975	8.97E-05	3.20E-04	1
e0121	43	3.906	2.00E-04	7.53E-03	6
e0122	34	8.278	6.95E-06	5.32E-04	1
e0161	47	2.451	6.63E-03	1.53E-02	1
e0166	12	0.933	6.39E-04	1.57E-02	1
e0205	22	1.894	2.67E-04	5.31E-03	2

Table 5.2 Results of the self-coupling detection algorithm for the order $k=3$. The above values of the frequency, phase angle, and threshold are obtained for the corresponding tabulated segment number that led to the smallest phase value. *The number of segments out of 50 that show self-phase coupling for $k=3$.

Record Number	Segment Number	Frequency (Hz)	Polyphase Squared (rad^2)	Threshold (PFA=5%)	NSC*
16273	3	4.17E+00	2.72E-03	0.014323	1
16420	40	5.07E+00	7.55E-03	0.02892	2
16539	30	1.21E+00	1.97E-05	0.008403	7
16773	50	4.49E+00	6.03E-03	0.019211	1
16795	27	2.93E+00	7.31E-05	0.015957	8
17052	44	3.23E+00	2.39E-02	0.040318	1
19093	19	4.00E+00	5.86E-03	0.016753	1
19830	45	8.73E+00	1.60E-03	0.004319	1
e0103	42	7.97E+00	1.16E-04	0.000262	1
e0105	6	5.54E+00	1.78E-06	0.000172	8
e0106	6	2.20E+00	3.54E-09	0.010394	5
e0107	4	1.81E+00	7.28E-03	0.014561	1
e0115	18	5.51E+00	8.19E-03	0.011083	1
e0116	2	5.80E-01	1.18E-04	0.01671	1
e0121	39	3.91E+00	7.29E-05	0.011828	4
e0122	49	4.97E+00	4.91E-03	0.020324	1
e0161	5	1.23E+00	7.03E-05	0.053631	2
e0162	49	3.77E+00	1.01E-04	0.006313	8
e0166	30	1.87E+00	5.83E-04	0.008819	4
e0205	29	1.89E+00	1.97E-03	0.008191	2

Table 5.3 Results of the self-coupling detection algorithm for the order $k=4$. The above values of the frequency, phase angle, and threshold are obtained for the corresponding tabulated segment number that led to the smallest phase value. *The number of segments out of 50 that show self-phase coupling for $k=4$.

Record Number	Segment Number	Frequency (Hz)	Polyphase Squared (rad ²)	Threshold (PFA=5%)	NSC
16539	43	3.623	4.60E-03	1.62E-02	5
16773	50	4.491	1.01E-02	3.01E-02	1
19088	13	1.293	1.57E-03	1.31E-02	5
19830	14	1.455	5.94E-03	2.18E-02	4
e0103	45	3.984	9.21E-07	1.50E-05	1
e0105	26	2.768	2.17E-04	1.94E-03	1
e0106	48	2.203	5.81E-04	1.82E-02	3
e0111	10	1.256	7.78E-04	1.41E-02	2
e0113	49	1.214	2.30E-02	2.48E-02	1
e0115	25	1.838	2.99E-03	1.73E-02	4
e0119	6	4.975	4.17E-04	9.22E-04	1
e0121	39	3.906	2.34E-03	1.85E-02	2
e0122	38	8.278	4.16E-04	1.86E-03	6
e0147	17	2.183	6.62E-06	1.52E-02	3
e0161	30	3.676	7.34E-03	7.36E-03	2
e0162	29	3.769	2.28E-04	1.19E-02	7
e0166	47	1.866	6.85E-04	1.43E-02	3
e0203	26	2.825	9.37E-03	1.46E-02	1
e0205	9	5.682	2.61E-03	1.38E-02	1

Table 5.4 Results of the self-coupling detection algorithm for the order $k=5$. The above values of the frequency, phase angle, and threshold are obtained for the corresponding tabulated segment number that led to the smallest phase value. *The number of segments out of 50 that show self-phase coupling for $k=5$.

Record Number	Segment Number	Frequency (Hz)	Polyphase Squared (rad ²)	Threshold (PFA=5%)	NSC
16272	5	2.866	4.20E-06	3.93E-02	41
16539	43	3.623	2.67E-05	2.33E-02	8
19140	47	1.231	3.37E-06	6.33E-03	21
19830	30	1.455	4.25E-05	4.53E-02	7
e0105	39	2.768	8.41E-05	2.22E-03	10
e0111	50	1.256	9.37E-05	1.11E-02	12
e0119	1	2.488	2.77E-04	5.74E-02	7
e0121	40	3.906	1.18E-04	2.74E-02	4
e0122	9	3.311	5.80E-06	5.69E-02	13
e0123	21	2.488	3.76E-05	3.00E-02	10
e0147	39	1.092	1.21E-04	1.45E-02	4
e0161	6	1.225	1.11E-07	7.54E-02	4
e0162	18	3.769	1.18E-05	1.31E-02	6
e0205	40	1.894	5.63E-03	1.53E-02	1

Table 5.5 Results of the self-coupling detection algorithm for the order $k=6$. The above values of the frequency, phase angle, and threshold are obtained for the corresponding tabulated segment number that led to the smallest phase value. *The number of segments out of 50 that show self-phase coupling for $k=6$.

Record Number	Segment Number	Frequency (Hz)	Polyphase Squared (rad^2)	Threshold (PFA=5%)	NSC
16272	39	0.955	4.50E-04	4.27E-02	8
16539	33	3.623	4.89E-06	3.32E-02	12
16786	48	1.032	1.62E-07	1.80E-02	3
17052	31	1.076	1.58E-02	2.31E-02	1
18184	20	0.992	1.40E-06	3.81E-02	5
19093	48	1.000	2.41E-06	1.85E-02	18
19830	22	1.455	2.76E-05	5.63E-02	17
e0103	48	3.984	2.08E-05	3.81E-05	2
e0104	38	0.947	1.74E-04	1.91E-02	3
e0105	18	2.768	1.61E-04	5.26E-03	5
e0106	7	2.203	8.38E-06	3.20E-02	4
e0107	32	2.717	2.43E-04	6.07E-03	6
e0111	41	1.256	8.30E-04	2.32E-02	7
e0115	4	3.676	3.93E-05	3.72E-02	2
e0119	44	2.488	7.55E-04	5.95E-02	4
e0121	40	3.906	2.98E-02	3.73E-02	1
e0122	43	4.967	1.00E-02	4.49E-02	5
e0161	42	2.451	9.80E-04	6.46E-02	3
e0162	40	3.769	1.69E-02	1.93E-02	4
e0166	22	0.933	6.92E-02	7.06E-02	1
e0202	37	7.937	5.02E-03	3.52E-02	2
e0203	1	2.825	4.23E-03	2.58E-02	5
e0205	39	1.894	3.19E-05	2.56E-02	3

Table 5.6 Results of the self-coupling detection algorithm for the order $k=7$. The above values of the frequency, phase angle, and threshold are obtained for the corresponding tabulated segment number that led to the smallest phase value. The number of segments out of 50 that show self-phase coupling for $k=7$.

Record Number	Segment Number	Frequency (Hz)	Polyphase Squared (rad^2)	Threshold (PFA=5%)	NSC
16272	30	0.955	1.36E-03	4.89E-02	1
16483	33	1.391	7.40E-04	4.90E-02	2
16539	33	3.623	3.44E-04	4.34E-02	10
16786	15	1.032	3.65E-05	2.72E-02	19
16795	40	0.977	7.17E-04	2.64E-02	5
17052	2	1.076	3.93E-03	3.23E-02	3
18184	2	0.992	7.58E-07	5.52E-02	20
19088	26	1.293	8.54E-03	2.00E-02	1
19093	42	1.000	6.33E-04	2.37E-02	3
19830	32	2.909	3.40E-03	5.36E-02	4
e0103	20	3.984	5.60E-06	4.14E-05	1
e0104	13	0.947	1.51E-03	4.61E-02	7
e0105	7	2.768	6.18E-05	4.17E-03	2
e0106	32	2.203	1.34E-03	4.41E-02	5
e0107	30	2.717	6.51E-04	6.92E-03	6
e0111	36	1.256	4.55E-03	3.03E-02	1
e0115	2	1.838	2.63E-05	5.17E-02	5
e0119	2	1.244	2.53E-02	1.37E-01	2
e0121	40	3.906	1.46E-02	4.87E-02	2
e0122	44	4.967	2.86E-04	5.53E-02	2
e0147	43	1.092	4.94E-04	4.50E-02	3
e0161	28	3.676	5.24E-04	2.55E-02	5
e0162	18	3.769	9.10E-03	2.35E-02	3
e0166	13	0.933	1.34E-02	9.25E-02	2
e0203	3	2.825	3.15E-04	3.51E-02	7
e0205	11	1.894	8.70E-03	3.42E-02	5

Table 5.7 Results of the self-coupling detection algorithm for the order $k=8$. The above values of the frequency, phase angle, and threshold are obtained for the corresponding tabulated segment number that led to the smallest phase value. *The number of segments out of 50 that show self-phase coupling for $k=8$.

Record Number	Segment Number	Frequency (Hz)	Polyphase Squared (rad ²)	Threshold (PFA=5%)	NSC
16265	11	4.303	1.05E-02	8.04E-02	4
16483	20	1.391	4.31E-05	6.26E-02	17
16539	29	3.623	7.44E-04	5.09E-02	12
16795	22	0.977	6.86E-04	4.98E-02	5
17052	48	1.076	8.55E-04	3.45E-02	1
18184	4	0.992	5.06E-04	6.90E-02	5
19088	17	1.293	5.78E-03	2.51E-02	5
19090	14	3.459	1.88E-03	6.48E-02	1
e0103	42	3.984	1.71E-08	9.34E-05	1
e0104	27	0.947	2.28E-04	3.10E-02	8
e0108	6	1.078	2.58E-06	5.74E-02	9
e0113	13	1.214	7.58E-03	5.31E-02	8
e0115	29	3.676	2.45E-04	5.31E-02	10
e0116	12	2.320	3.31E-04	1.92E-03	1
e0119	14	2.488	9.85E-03	7.45E-02	5
e0121	47	1.302	3.22E-05	1.66E-01	2
e0122	50	3.311	6.82E-02	1.41E-01	1
e0147	38	1.092	1.13E-04	7.54E-02	4
e0161	17	3.676	9.09E-03	4.14E-02	9
e0162	46	2.513	7.10E-02	9.85E-02	1
e0166	36	1.866	2.60E-06	5.15E-02	10
e0202	46	3.968	4.67E-04	1.93E-02	2
e0203	6	2.825	4.56E-07	4.35E-02	19

Table 5.8 Results of the self-coupling detection algorithm for the order $k=9$. The above values of the frequency, phase angle, and threshold are obtained for the corresponding tabulated segment number that led to the smallest phase value. *The number of segments out of 50 that show self-phase coupling for $k=9$.

Record Number	Segment Number	Frequency (Hz)	Polyphase Squared (rad^2)	Threshold (PFA=5%)	NSC
16265	23	4.303	6.26E-03	1.02E-01	4
16539	21	3.623	5.78E-04	6.46E-02	9
16795	26	0.977	5.69E-04	6.09E-02	7
17052	42	1.076	2.96E-02	5.02E-02	1
18184	22	0.992	3.74E-03	8.53E-02	5
19088	8	1.293	4.06E-04	5.44E-02	6
19090	16	3.459	8.92E-06	7.95E-02	23
e0103	20	0.996	9.51E-03	1.73E-01	10
e0104	18	0.947	2.54E-03	5.22E-02	7
e0106	2	2.203	3.67E-04	5.88E-02	3
e0108	35	1.078	9.44E-05	5.14E-02	12
e0113	41	1.214	3.64E-04	5.81E-02	3
e0115	23	1.838	1.84E-02	8.08E-02	2
e0119	8	3.731	1.55E-03	7.02E-02	7
e0121	19	2.604	2.72E-03	1.47E-01	5
e0122	45	8.278	5.80E-03	1.25E-02	14
e0123	32	2.488	1.78E-03	1.13E-01	8
e0147	15	2.183	1.09E-05	5.70E-02	5
e0161	45	2.451	1.64E-04	1.60E-01	5
e0162	31	2.513	2.45E-02	1.82E-01	4
e0166	10	1.866	5.44E-03	5.02E-02	6
e0202	17	3.968	5.57E-04	3.26E-02	7
e0203	12	2.825	2.27E-05	5.60E-02	18

Table 5.9 Results of the self-coupling detection algorithm for the order $k=10$. The above values of the frequency, phase angle, and threshold are obtained for the corresponding tabulated segment number that led to the smallest phase value. *The number of segments out of 50 that show self-phase coupling for $k=10$.

The self-coupling detection algorithm (Zhou's algorithm) shows that both normal and ischaemic ECG signals contain up to 10^{th} -order non-linearity. A closer look at Tables 5.1 to 5.9 show that the NSCs are larger for the normal ECG signals for most of the polyspectrum orders. This number is estimated for all normal and all ischaemic cases and accumulated individually, for each order. The results are summarised in Figure 5.6, in this figure y-axis shows number of segments % (which is, total number of NSCs over all records for each order to total number of segments that has been tested for that order over all records percent) and x-axis represent the polyspectrum order, k .

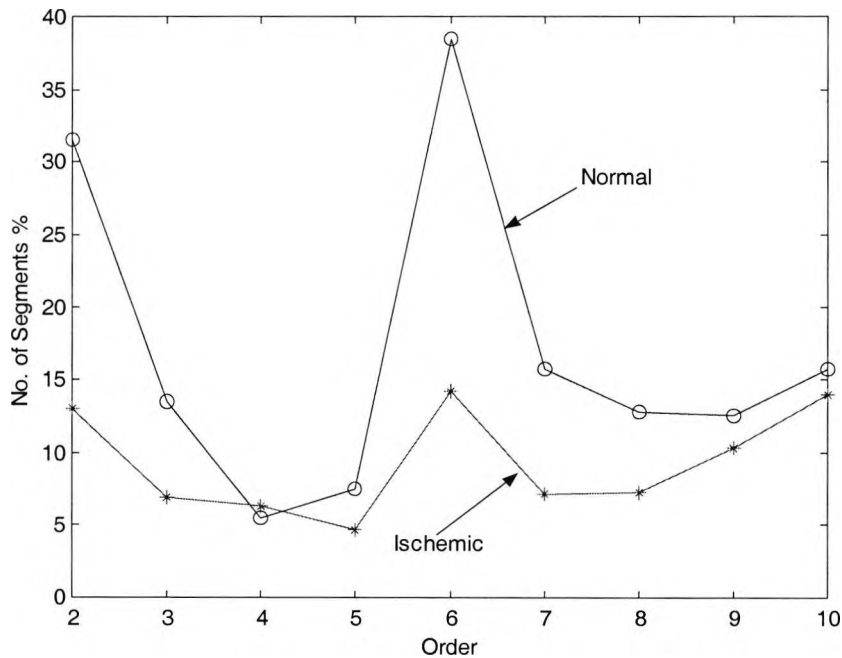


Figure 5.6 The total number of NSCs over all records for each order to total number of segments that has been tested for that order percent as a function of the polyspectrum order, k .

5.3.3.2 Detection of Non-linearities using the Polycoherency Indices

First the use of the polycoherency indices in quantifying self-phase coupling frequencies will be demonstrated in the following example.

Example

Consider the process used by Zhou and Giannakis (1995) which is generated by self-coupled harmonics Eq. (5.1) with $L=4$, $\omega_1 = \omega_0 = 1$, $\omega_2 = 2$, $\omega_3 = 3$, $\omega_4 = 4$, $A_1=2$, $A_2=1.5$ and $A_3=1.8$ and $A_4=1.0$. The angles are uniformly distributed random variables in $(-\pi, \pi]$. Two cases are considered here; (case-1) frequency and phase coupled harmonics, $\omega_l = k\omega_0$, and $\varphi_l = k\varphi_0$ and, (case-2) frequency coupled harmonics, $\omega_l = k\omega_0$ and $\varphi_l \neq k\varphi_0$, $l=1,2,\dots,4$ and k is the non-linearity order. Sixty-four statistically independent records with 128 samples each are used. The additive noise $v(t)$ is generated by passing

zero-mean, i.i.d., exponentially distributed deviates with unit variance through a first order FIR filter with parameters [1, 0.3].

Figure 5.7 shows the diagonal slices of the polyspectrum (LHS) and polycoherency index (RHS) for $k=3$ (a, b, c, d) and $k=4$ (e, f, g, h). Figures 5.7 (a) and 5.7 (e) are the polyspectrum slices and Figures 5.7 (b) and 5.7 (f) are their polycoherency slices for 'case-1', respectively. Figures 5.7 (c), (g), (d), and (h) are the corresponding slices for 'case-2'. The polyspectrum slices peak at $\omega_0=1$ for 'cases-1 and-2'. The amplitude of the peak is much smaller for 'case-2'. For 'case-1' the polycoherency slices show peaks of amplitude approximately one at ω_0 indicating the presence of totally phase coupled harmonics for $k=3$ and 4. For 'case-2' the polycoherency slices are approximately zero for $k=3$ and 4 indicating the absence of phase coupling. From this example one conclude that the polycoherency slices are very effective in checking if the peaks on the polyspectrum slices are due to phase coupled harmonics and hence confirms the non-linearity.

Now the ECG signals will be analysed. To obtain reliable estimates for the polycoherency indices the diagonal slices of the polyspectrum and polycoherency indices are calculated using averaging of more than 50 polyspectrum slices. Each plot in Figure 5.8 consists of two parts, the magnitude of the diagonal slice of the 6th moment is shown in the upper panel and the corresponding polycoherency slice is shown in the bottom panel for a normal case (record No. 18184, a) and an ischaemic case (record No. e0107, b). The polyspectrum slices in this figure indicate the presence of self-coupled frequency components at 4 and 3.6 Hz for normal and ischaemic cases, respectively. The polycoherency indices are 0.95 and 0.66 at these frequencies, respectively, indicating higher degree of phase coupling for the normal case.

The diagonal slices of the polyspectrum and polycoherency index are estimated for all normal and ischaemic records for orders $k=2$ to $k=10$. Similar features to the MBI and ABI are employed in this analysis: a) The Maximum Polycoherency Index (MPIS) i.e., the value of the polycoherency index at the frequency of the maximal intensity, f_m (peak frequency) on the polyspectrum slice. b) The Average Polycoherency Index (APIS), i.e., the mean value along the diagonal slice of the polycoherency indices in the frequency

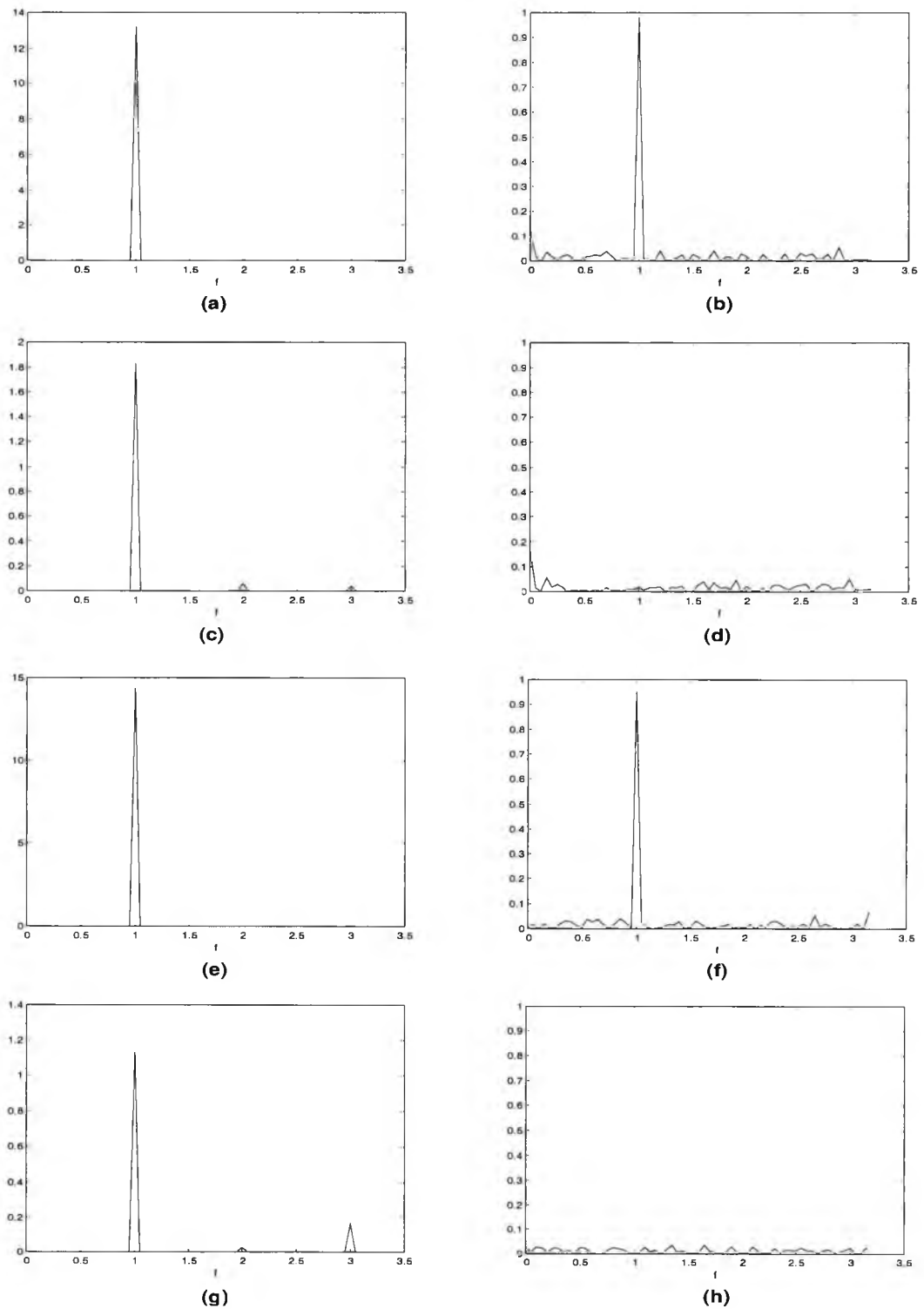


Figure 5.7 The diagonal slices of the polyspectrum (LHS) and polycoherency index (RHS) for $k=3$ (a,b,c,d) and $k=4$ (e,f,g,h). The polyspectrum slices in figures (a,e) and their polycoherency slices in figures (b,f), respectively, are the results obtained for case-1. Figures (c,g), and figures (d,h) are the corresponding slices for case-2.

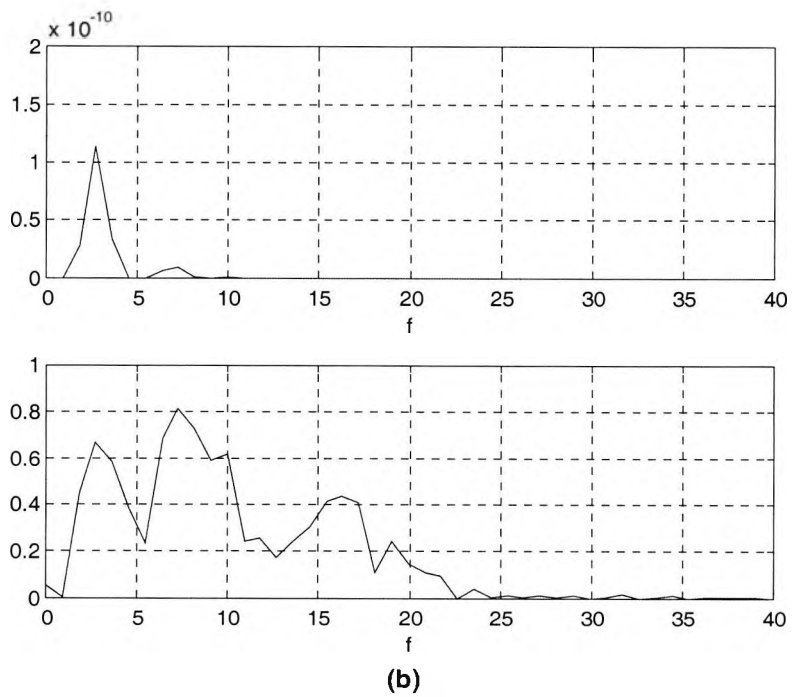
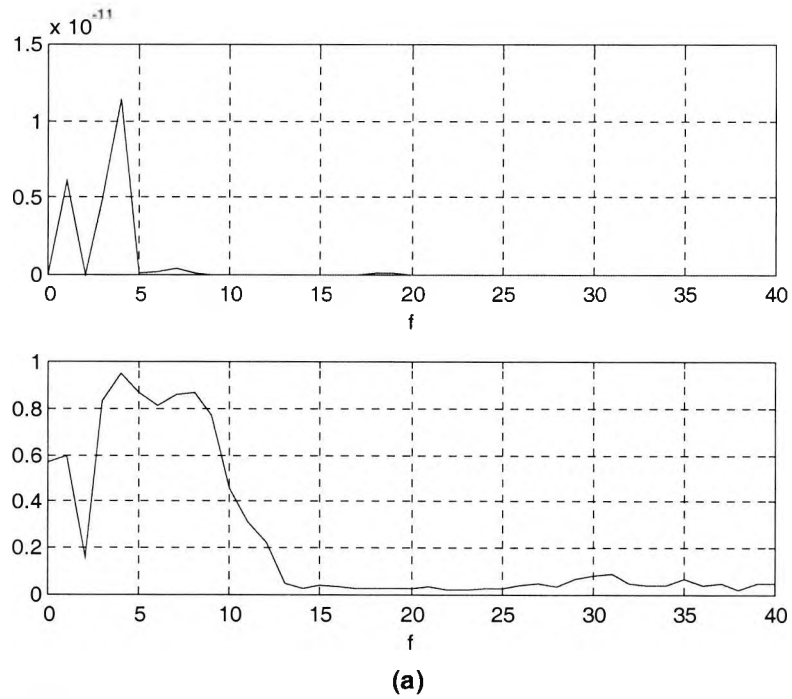


Figure 5.8 Persistent characteristics of the diagonal slices of the polyspectrum (upper panels) and polycoherency indices (bottom panels) for a normal person (a) and an ischaemic person (b) for $k=6$.

range (0 - 10 Hz). They are considered as measures to check if the self-coupled frequency components in this region are due to phase-coupled harmonics.

In Figures 5.9, 5.10, and 5.11 the x-axis represents the record index for both normal and ischaemic records and y-axis represents the value of the MPIS (left) or the APIS (right) for orders $k=2$ to $k=10$. The MPIS and APIS for normal ECG signals are higher than that for ischaemic ECG signals for all polyspectrum orders indicating that the self-coupled frequencies for normal ECG signals are more likely to be due to phase-coupled harmonics. An important note from Figure 5.10 is that the MPIS for one of the normal records ($k=7$ and record index=4) has a value of zero. Theoretically, this means that the harmonics at that frequency are completely uncorrelated. However, this represents an odd result as the data analysed here are real ECG signals.

The value of the MPIS and that of the APIS normalised over all normal and over all ischaemic records are calculated to spot the difference between the normal and abnormal ECGs and to estimate the appropriate non-linearity order for each of these ECGs, as shown in Figure 5.12. Figure 5.12 is a summary for all the results obtained in this analysis. The x-axis correspond to the polyspectrum order, k , and the y-axis correspond to the mean value of the MPIS (a) and the mean value of the APIS (b) calculated over all normal and all ischaemic records for orders $k=2$ to $k=10$. The normal ECG signals can be differentiated from ischaemic ECG signals by each of the polycoherency measures. The non-linearity order that represents the ECG signal dynamics for normal and ischaemic conditions can be predicted using these two polycoherency measures. For example, for 90%, 80% and 70% confidence levels the mean APIS and the mean MPIS indicate order ranges 3-5, 4-6, and 6-8, respectively, for normal ECG signals and 1-2, 2-4, and 3-4, respectively, for ischaemic ECG signals. On average the normal and ischaemic ECG signal dynamics can be modelled using a non-linearity order range of 5-7 and 2-4, respectively.

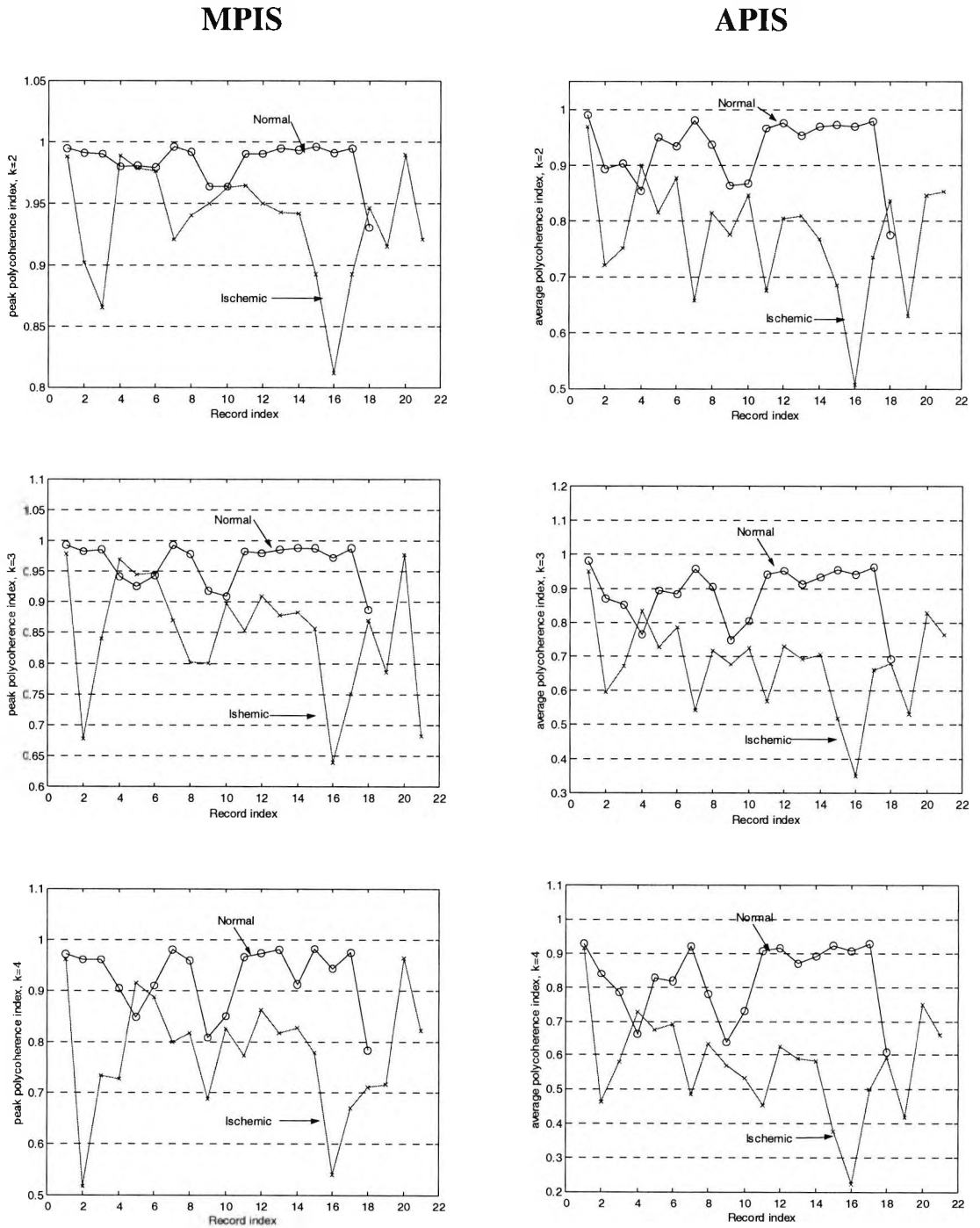


Figure 5.9 Polycoherency indices for 18 normal and 21 ischaemic records. The Maximum Polycoherency Index (MPIS), and the Average Polycoherency Index (APIS), are employed. The x-axis represents the record index for both normal and ischaemic cases and the y-axis represents the value of the MPIS (left) and the APIS (right) for $k=2$ (top), $k=3$ (middle) and $k=4$ (bottom).

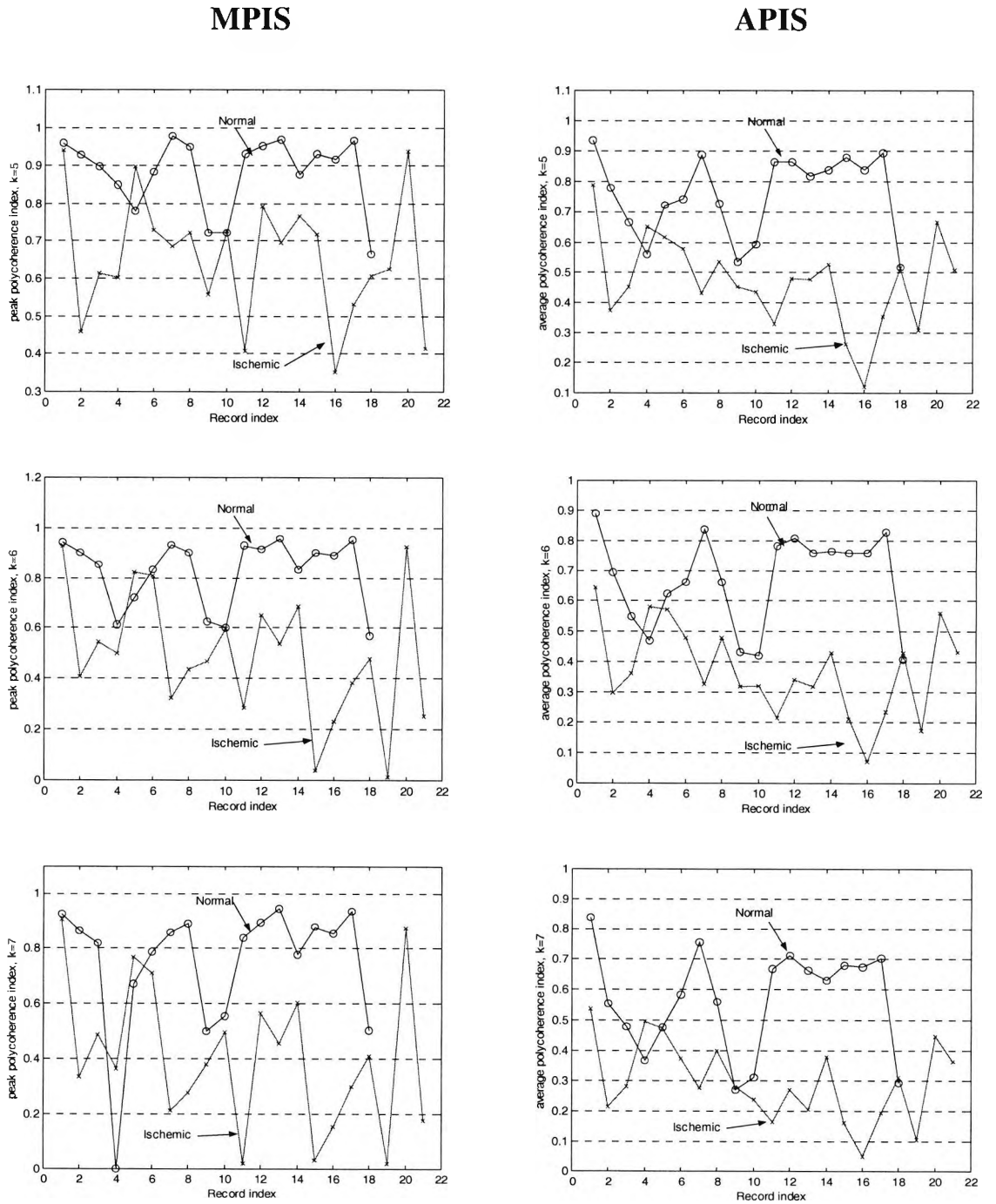


Figure 5.10 Polycherency indices for 18 normal and 21 ischaemic records. The Maximum Polycherency Index (MPIS), and the Average Polycherency Index (APIS), are employed. The x-axis represents the record index for both normal and ischaemic cases and the y-axis represents the value of the MPIS (left) and the APIS (right) for $k=5$ (top), $k=6$ (middle) and $k=7$ (bottom).

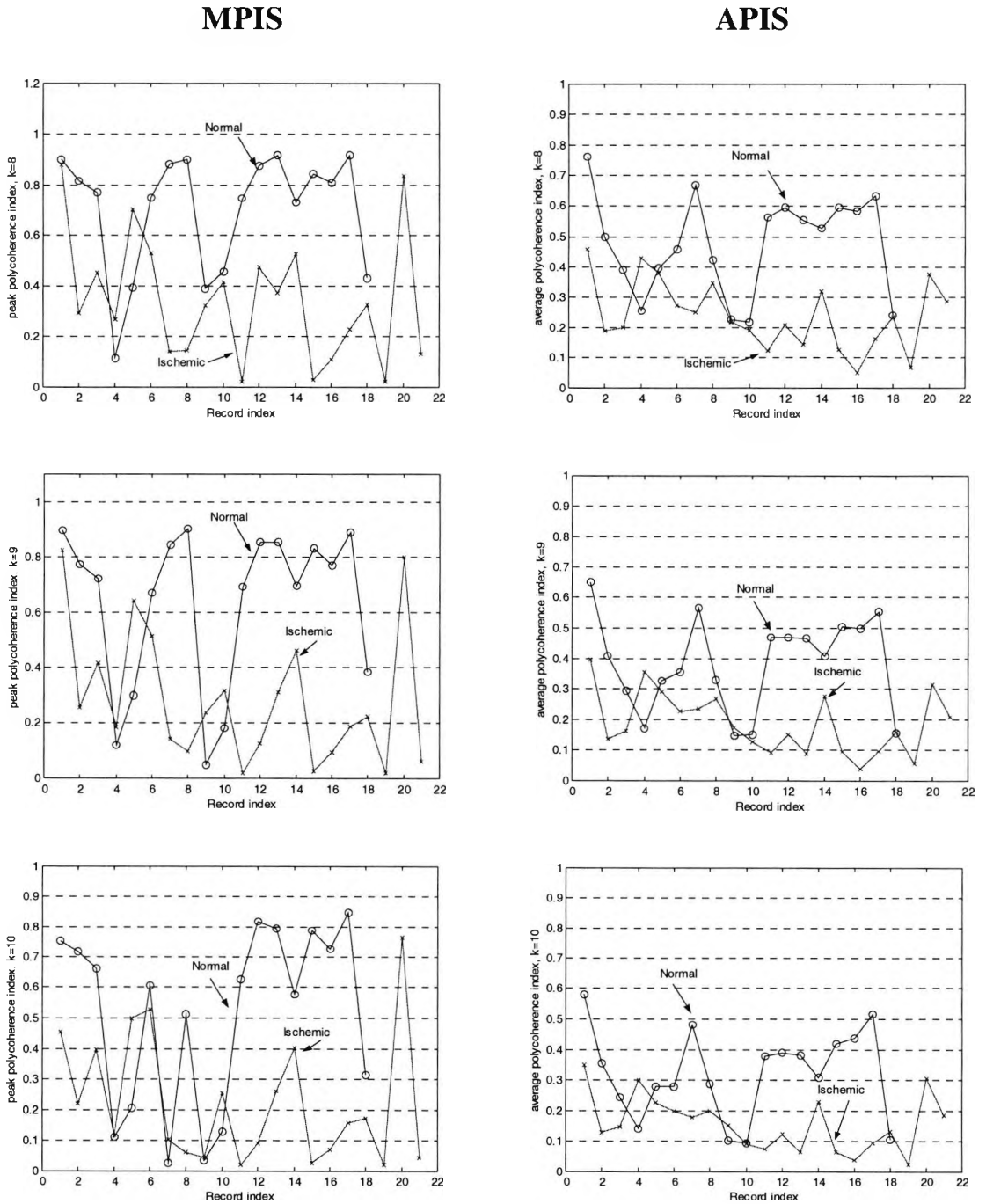
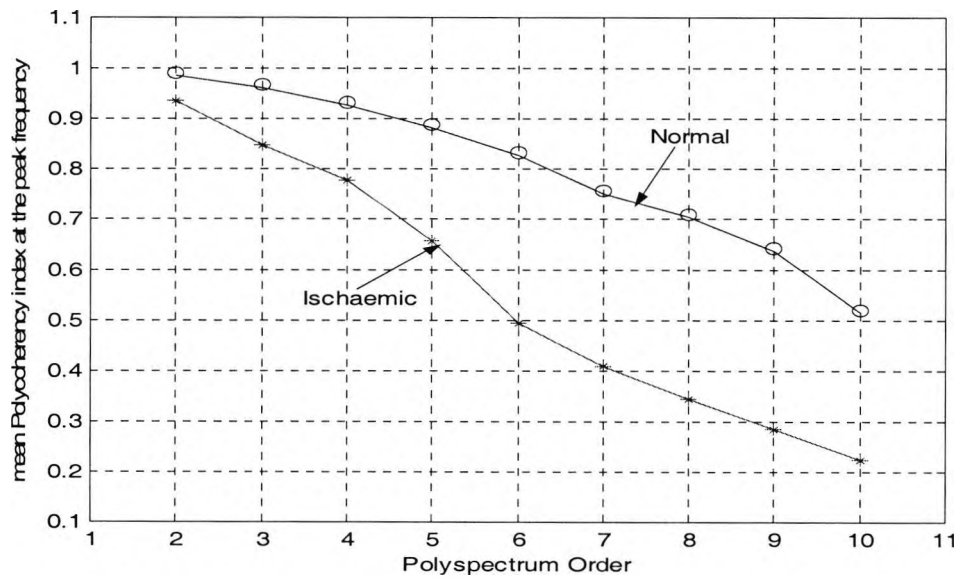
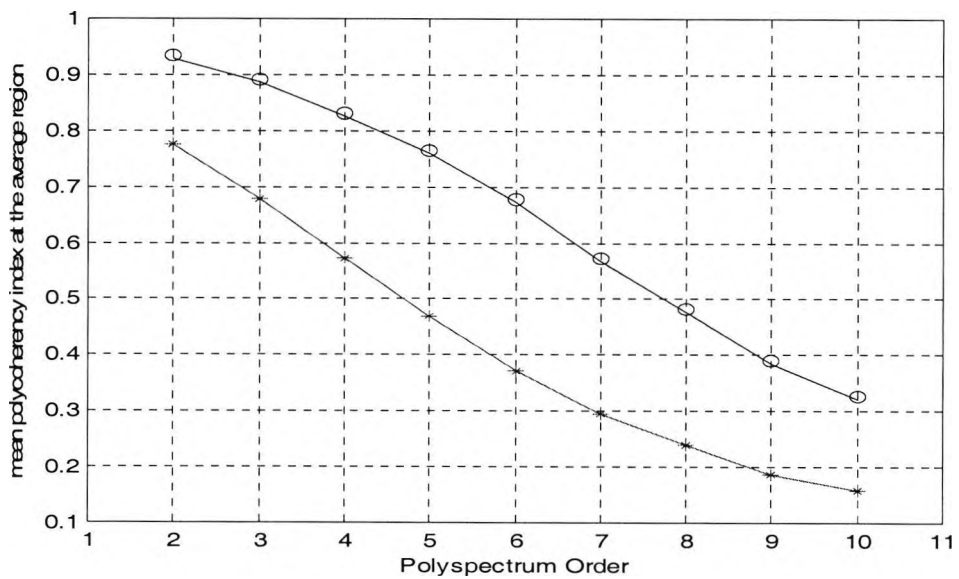


Figure 5.11 Polycherency indices for 18 normal and 21 ischaemic records. The Maximum Polycherency Index (MPIS), and the Average Polycherency Index (APIS), are employed. The x-axis represents the record index for both normal and ischaemic cases and the y-axis represents the value of the MPIS (left) and the APIS (right) for $k=8$ (top), $k=9$ (middle) and $k=10$ (bottom).



(a)



(b)

Figure 5.12 Average of the polycherency indices measures, i.e., the mean MPIS and the mean APIS, calculated over all the normal and all the ischaemic records for polyspectrum orders $k=2$ to $k=10$. The x-axis represents the polyspectrum order and the y-axis represents the value of the mean MPIS (a) and the mean APIS (b).

5.4 Discussion

Physiological and pathological cases from the MIT/BIH (MIT-CD 1997) and from the European ST-T (Taddei, et al. 1992) databases have been studied. All the available normal data were studied, while, the number of the abnormal data records was limited to patients with ischaemic heart disease. Records for patients with abnormalities that may affect other parts (for example, the QRS complex) of the ECG cycle and also records with small number (< 50 episode) or positional changes (for example, axis shift) ST-T episodes were excluded from the analysis.

The analysis of the bispectrum and bicoherence index revealed tight quadratical interactions among frequencies in the region (0 - 20 Hz). The bicoherence index indicated that these coupled frequencies are due to phase-coupled frequencies that strongly suggests the existence of quadratic non-linearities in both normal and ischaemic ECG signals. The diagonal slices of the polyspectrum and polycoherency index constitute important features to discriminate between physiological and pathological conditions of the heart. These slices are Gaussian noise free, preserve phase information and they are one-dimensional with all polyspectrum orders. In addition to that, it is theoretically proven (Pozidis and Petropulu 1998) that even short length segments (64 samples) are appropriate for HOS slices estimation and could result in lower variance and better estimation than using the whole HOS information.

Generally, the frequency domain of the normal ECG signals covers a wide range of frequencies while the frequency domain of the ischaemic ECG signals covers a narrower range of frequencies for all polyspectrum orders that have been tested in this study.

Normal and ischaemic ECG signals were analysed in the higher-order domain using the self-coupling detection algorithm (Zhou's algorithm) and the proposed extension to this algorithm (polycoherency indices). Zhou's algorithm revealed the existence of higher-order non-linearities, up to the tenth order for both normal and ischaemic ECG signals. Using the same segments of data to calculate the polycoherency indices it has been shown that the inherent non-linearity in the ECG signal dynamics decreases with ischaemic conditions and specified order ranges of 5-7 and 2-4 for normal and ischaemic ECG signals, respectively. However, the results of the polycoherence indices were found to be

consistent with some results in the literature. Previous studies using chaotic theory and which mainly applied to arrhythmia detection and heart rate variability showed the following observations about the dynamics of the normal and abnormal ECG signals: Pool (1989) found that strictly periodic cardiac dynamics are correlated with pathological states. According to the results obtained by Golgberger, et al. (1990) irregularity and unpredictability are important features of health; on the other hand, decreased variability and accentuated periodicities are associated with ageing and disease. Signorini, et al. (1994) studied the dynamics of the cardiovascular variability signals and found that in general a decrease in the system complexity is correlated to pathological conditions. Zhang, et al. (1997) declared that ECG signal dynamics is dominated by a 5-6-dimensional non-linear system, whose complexity is about 0.7. Fell, et al. (2000a) applied the false nearest neighbours method and the saturation of the correlation dimension on healthy persons and suggested that an embedding dimension from 6 to 8 may be regarded suitable for the topological proper reconstruction of ECG signals. Hence the loss of complexity in ECG signal dynamics may be an important marker of susceptibility to disease.

The results showed that higher-order spectral analysis of the ECG signals can reveal useful information and provide insights regarding the physiological state of the heart. The extracted features from the bispectrum/bicoherence, i.e., the MBI and ABI, and from the polyspectrum/polycoherency slices, i.e., the MPIS and APIS are found to be informative and effective in detecting abnormality. These findings are of interest from the physiological viewpoint as they motivate a new approach to help illuminate quantitatively and non-invasively, ECG signal dynamics. From a practical point of view, quantification of the MPIS and APIS may have potential applications for Holter tape monitoring.

These valuable features from the HOS will be utilised in the following chapter to extract informative input patterns for the neural network-based ECG signal classifier.

Chapter 6

NEURAL NETWORKS

6.1 Introduction

The aim of this chapter is to utilise adaptive Neural Networks (NNs) to classify normal and abnormal (the abnormality of interest being ischaemic heart disease) ECG signals in their higher-order statistical domain. This is an implementation of an automated ECG signal classifier. Automated ECG signal analysis is important during ambulatory electrocardiographic monitoring, in interpretation of noisy ECG episodes...etc. It is also of particular interest in long term ECG signal monitoring called Holter monitoring, here, the ECG signal of a patient is recorded on a magnetic tape for as long as 24 h. Beat by beat visual examination is almost impossible in this case. Artificial Neural Networks (ANNs) can be taught by experts for such tasks, and so may be particularly suitable. Also since the NN approach is essentially a pattern matching technique based on non-linear input output mapping, it is well suited for detecting morphological changes especially in non-linear signals such as the ECG signal. For NN applications, it is important to find informative and robust features that reflect any changes, which may occur between successive ECG episodes. These features should enable the network classifier to differentiate between normal and abnormal ECG signals. In this work slices from the higher-order spectra have been used as the input features to the NN classifier. As the HOS preserve phase information these slices will reflect the non-linear character of the signal. The previous work by Maglaveras, et al. (1998) and Stamkopoulos, et al. (1998) was based on the analysis of the time domain ST segments. The input features to the NN were the difference between an ischaemic ST segment template and the normal template in the former, and the principal components of the normal ST segments in the latter.

6.2 Artificial Neural Networks

Neural Networks have received much attention in the research community in recent years. They have been proven to powerfully achieve solutions to problems in pattern recognition, associative memory, target detection, classification, non-linear modelling, database retrieval and data compression. The topic of neural networks is given various names by different authors. Some of these names are 'Artificial Neural Networks', 'Connectionist Models', 'Parallel Distributed Processing Models', 'Self-Adapted or Self-Organised Systems', 'Cyberware' and 'Neurocomputers'.

6.2.1 Rational for using Neural Networks

Neural networks have a number of important properties that befit their use for signal processing applications, in particular (Haykin 1994; Haykin 1996):

- 1) The NN is a distributed non-linear device. This property is a direct result of the fact that each processing unit (i.e., neuron) of a neural network has a built-in activation function (for example, in the form of a logistic function) that is non-linear. Accordingly, the NN has inherent ability to model non-linearities contained in the physical mechanisms responsible for generating the input data.
- 2) The NN consists of massively parallel processors that have the potential to be fault tolerant. A multi-layer perceptron consists of a large number of neurons arranged in the form of layers, with each neuron in a particular layer connected to a large number of source nodes/neurons in the previous layer. This form of global interconnectivity has the potential to be fault tolerant.
- 3) The NN has a natural ability to adapt its free parameters to statistical changes in the environment in which they operate. As a rule of thumb, we may say that the more we make a non-linear system adaptive, the more robust the performance of that system is likely to be when it operates in a non-stationary environment, subject to the requirement that the system remains stable.
- 4) The NN provides a nonparametric approach for the non-linear estimation of data. The non-linear, feedforward class of NN (encompassing multi-layer perceptron and

radial basis-function networks) learns from examples by constructing an input-output mapping for the problem at hand. It can also approximate any continuous input-output mapping to any desired degree of approximation, given a sufficient number of hidden layers, and thus working as a universal approximator.

The scope of neural networks is too wide to be covered in one chapter, so a simple structural, functional and conceptual overview of the relevant neural network architectures will be provided in the following sections.

6.2.2 Basic Element

Figure 6.1 shows the structure of the basic element (called neuron) of an artificial neural network that models the behaviour of a biological neuron. The body of the j^{th} neuron is often represented by a weighted linear sum, z_j , of the input signals followed by a linear or non-linear function, $y_j=f(z_j)$. This function is called the activation function; it determines the output of a neuron in terms of the activity level at its input.

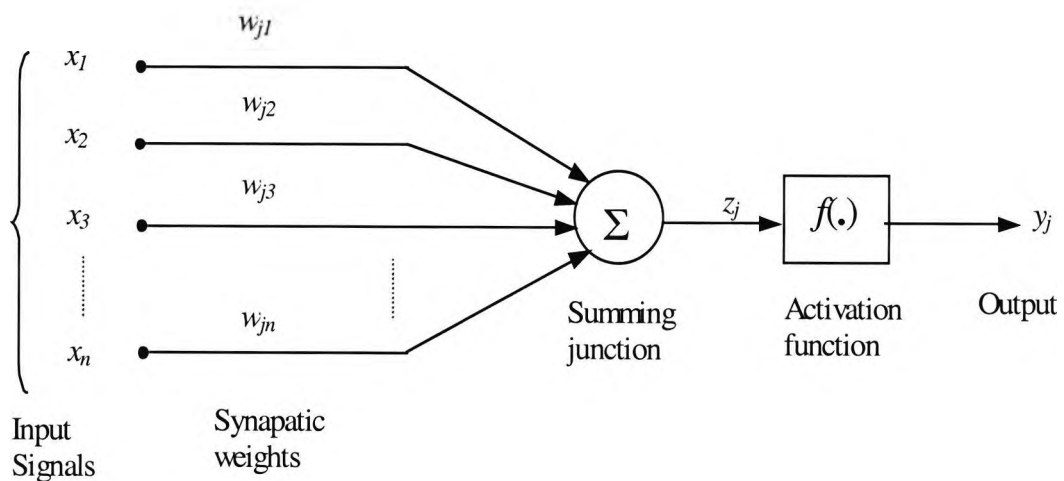


Figure 6.1 Neuron model.

The following notation will be used:

- 1) The indices i, j, k refer to different neurons in the network; neuron j lies in a layer to the right of neuron i , and neuron k lies in a layer to the right of neuron j when j is a hidden unit.
- 2) $d_j(t)$, $y_j(t)$, $e_j(t)$ are the desired response, the output and the error, respectively, for neuron j at discrete time t .
- 3) The symbol $w_{ji}(t)$ denotes the synaptic weight connecting the output of neuron i to the input of neuron j at iteration t .

The neuron output signal is given by the following relationship:

$$y_j = f(z_j) = f\left(\sum_{i=1}^n w_{ji}x_i\right) = f(\mathbf{w}_j^T \mathbf{x}) \quad (6.1)$$

where \mathbf{w}_j is the weight vector defined as $\mathbf{w}_j = [w_1, w_2, \dots, w_n]^T$, and \mathbf{x} is the input vector: $\mathbf{x} = [x_1, x_2, \dots, x_n]^T$. Different Neural Networks use different activation functions. The activation function, $f(\cdot)$, can be linear or non-linear such as sigmoidal, hyperbolic tangent and threshold functions. Two well known sigmoidal functions can be written as follows (Zurada 1992):

$$f(z) = \frac{2}{1 + \exp^{-\eta z}} - 1 \quad \text{Bipolar sigmoidal function} \quad (6.2)$$

$$f(z) = \frac{1}{1 + \exp^{-\eta z}} \quad \text{Unipolar sigmoidal function} \quad (6.3)$$

The parameter $\eta > 0$, in Eqs. (6.2 and 6.3), is proportional to the neuron gain determining the steepness of the function $f(z)$ near $z=0$. The activation functions of Eqs. (6.2 and 6.3) are shown in Figure 6.2 for various η . As $\eta \rightarrow \infty$ these two functions reaches the limit of $\text{sgn}(z)$:

$$f(z) = \text{sgn}(z) = \begin{cases} +1, \dots, z > 0 \\ -1, \dots, z < 0 \end{cases} \quad \text{Bipolar Binary function, or} \quad (6.4)$$

$$f(z) = \text{sgn}(z) = \begin{cases} 1, \dots, z > 0 \\ 0, \dots, z < 0 \end{cases} \quad \text{Unipolar Binary function.} \quad (6.5)$$

Setting η equal to 2 in Eq. (6.2) will be equivalent to the hyperbolic tangent function:

$$f(z) = \tanh\left(\frac{z}{2}\right) = \frac{1 - \exp^{-z}}{1 + \exp^{-z}} \quad \text{Hyperbolic Tangent Function} \quad (6.6)$$

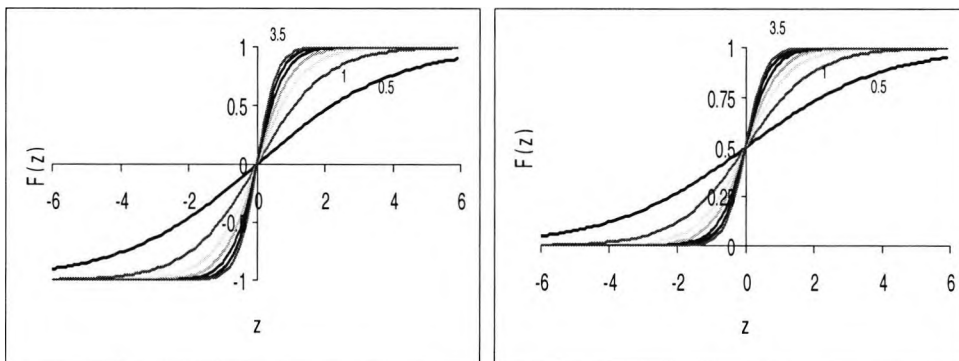


Figure 6.2 Activation functions of a neuron. Bipolar continuous (left) and unipolar continuous (right) with η varies from 0.5 to 3.5.

Neural networks may have fixed weights or adaptable weights. For networks with fixed weights, the strength of the interconnections has to be determined explicitly from the description of the problem. The latter type uses learning laws to adjust the values of the weights. Learning by itself may be supervised and unsupervised. In supervised learning we assume that at each instant of time when the input is applied, the desired output of the system is provided. The distance between the actual and the desired response of the network is used as error measure and serves to correct the network parameters externally. This mode of learning is used in many situations of natural learning. A set of input and output patterns called training set is required for this learning mode. On the other hand, in unsupervised learning the desired response is not known, thus, explicit error cannot be used to the correct network behaviour and learning can be accomplished using observations of responses to inputs that we have no knowledge about. Unsupervised learning can be used, for example, in finding the boundary between classes of input patterns (Haykin 1994; Zurada 1992). The scope of our application will be mainly adaptable weights and supervised learning neural networks.

6.2.3 Learning Rules

Learning rules determine how the network is going to adjust its weights using an error function or some other criteria. A general learning rule has been used by Amari (1990) the weight vector w_j increases in proportion to the product of the input vector x and learning signal r . The learning signal r is in general a function of w_{ji} , x_i and sometimes of the desired response d_j . This can be formulated mathematically as follows:

$$r(t) = r(w_{ji}(t), x_i(t), d_j(t)) \quad (6.7)$$

The increment of the weight vector w_{ji} resulting from the application of the general learning rule at time step t can be written as:

$$\Delta w_{ji}(t) = \beta \cdot r(w_{ji}(t), x_i(t), d_j(t)) \cdot x_i(t) \quad (6.8)$$

where β is a positive number known as the learning constant, which determines the rate of learning. Using this weight increment, the weight vector at time $(t+1)$ becomes:

$$w_{ji}(t+1) = w_{ji}(t) + \Delta w_{ji}(t) \quad (6.9)$$

where $w_{ji}(t)$ and $w_{ji}(t+1)$ are the old and new values of the synaptic weight w_{ji} . According to the form of the function r we can get different learning rules. Here are some examples of these learning rules (Zurada 1992).

$$\Delta w_{ji}(t) = \beta y_j(t) x_i(t) \quad \rightarrow \text{Hebbian Learning Rule}$$

$$\Delta w_{ji}(t) = \beta [d_j(t) - \text{sgn}(w_{ji}(t) x_i(t))] x_i(t) \quad \rightarrow \text{Perceptron learning Rule (6.10)}$$

$$\Delta w_{ji}(t) = \beta (d_j(t) - y_j(t)) x_i(t) \quad \rightarrow \text{Delta Learning Rule}$$

The delta learning rule, sometimes called normalised Least Mean Squares (LMS), represents one of the most popular learning algorithms. The basic idea of this algorithm depends on using the gradient, or steepest descent, procedure to minimise the mean squared error signal.

6.2.4 Multi-Layer Neural Networks

A single layer feedforward neural network can be thought of performing a linear combination of a set of input variables with weights being proportionality coefficients. This sort of network can be used, for example, to build a linear model or to achieve correct classification of linearly separable classes. For problems with complex mappings, a single layer neural network will not perform well. Because in this case, for a classification problem, the network will try to separate between patterns using a linear boundary while the actual boundary is a complex curved one. A multi-layer feedforward neural network is capable of implementing arbitrary complex input/output mappings. The multi-layer network consists mainly of a number of single layered networks with the output of the first layer is directly connected to the input of the second layer (feedforward) and so on. The layers other than the first (input) and the last (output) layers are called hidden layers. Figure 6.3 shows the structure of a typical multi-layer feed forward neural network.

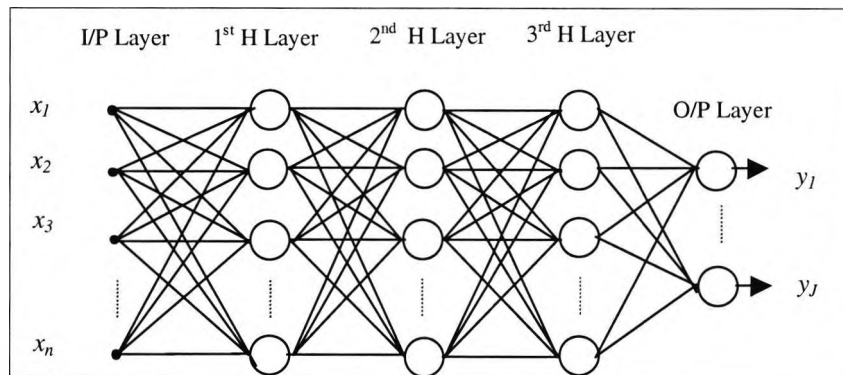


Figure 6.3 Multi-layer feedforward neural network.

6.2.5 Back-Propagation Algorithm

In the single layer network with the delta learning rule, the estimated error at the output of the network has been used to modify the weights from the input to the output nodes (Zurada 1992). Now for the multi-layer network this error can be used to update only the weights of connections between the output and the last hidden layer. For the other connections between the hidden layers and between the input layer and the first hidden

layer this error cannot be used. This is what the back-propagation technique (Lippmann 1987; Rumelhart, et al. 1986) is all about.

There are two phases involved in the back-propagation learning. During the first phase, the inputs are presented to the network, which propagate forward to produce the output for each neuron in the output layer. The activity of each neuron is determined by Eqs.(6.1) and (6.2) or (6.3). Then the error signal is generated. It is defined at the output of neuron j at iteration t by,

$$e_j(t) = d_j(t) - y_j(t) , \quad \text{neuron } j \text{ is an output node} \quad (6.11)$$

The instantaneous sum of squared errors of the network is written as

$$\zeta(t) = \frac{1}{2} \sum_{C \in j} e_j^2(t) \quad (6.12)$$

where the set C includes all neurons in the output layer of the network. In a similar way to the LMS algorithm, $\zeta(t)$ is minimised by the weight update rule. During the second phase, the error signals propagate backward through the network to allow the recursive computation of the weight updates. The back-propagation algorithm applies a correction $\Delta w_{ji}(t)$ to the synaptic weight $w_{ji}(t)$, which is proportional to the instantaneous gradient $\partial \zeta(t) / \partial w_{ji}(t)$. Applying the "chain rule" to differentiate (6.12) with respect to $w_{ji}(t)$, and using Eqs.(6.11) and (6.1) we get, (Haykin 1994):

$$\frac{\partial \zeta(t)}{\partial w_{ji}(t)} = -\varepsilon_j(t) y_i(t) \quad (6.13)$$

where $y_i(t)$ is the input signal of neuron j and the local gradient or the modulated error, $\varepsilon_j(t)$, is defined by

$$\varepsilon_j(t) = e_j(t) f_j'(z_j(t)) \quad , \quad \text{neuron } j \text{ is in the output layer} \quad (6.14)$$

$$\varepsilon_j(t) = f_j'(z_j(t)) \sum_k \varepsilon_k(t) w_{kj}(t) \quad , \quad \text{neuron } j \text{ is hidden} \quad (6.15)$$

where in Eq. (6.14) the error term can be calculated directly from Eq. (6.11) and the factor $f'_j(z_j(t))$ in both equations depends solely on the activation function associated with the neuron j . In Eq.(6.15) the term $\varepsilon_k(t)$ requires knowledge of the error signal $e_k(t)$, for all those neurons that lie in the layer to the right of the hidden neuron j and that are directly connected to neuron j , the term $w_{kj}(t)$ consists of the synaptic weights associated with these connections.

The correction $\Delta w_{ji}(t)$ applied to $w_{ji}(t)$ is defined by the delta rule

$$\Delta w_{ji}(t) = -\beta \frac{\partial \zeta(t)}{\partial w_{ji}(t)} \quad (6.16)$$

The use of minus sign in Eq. (6.16) accounts for gradient descent in weight space. Eqs.(6.13) and (6.16) yield

$$\Delta w_{ji}(t) = \beta \varepsilon_j(t) y_i(t) \quad (6.17)$$

For the network to learn, the generalised delta rule (Haykin 1994) is applied to update the synaptic weight $w_{ji}(t)$.

$$w_{ji}(t+1) = w_{ji}(t) + \beta \varepsilon_j(t) y_i(t) \quad (6.18)$$

The following flow chart shows a summary of error back-propagation algorithm.

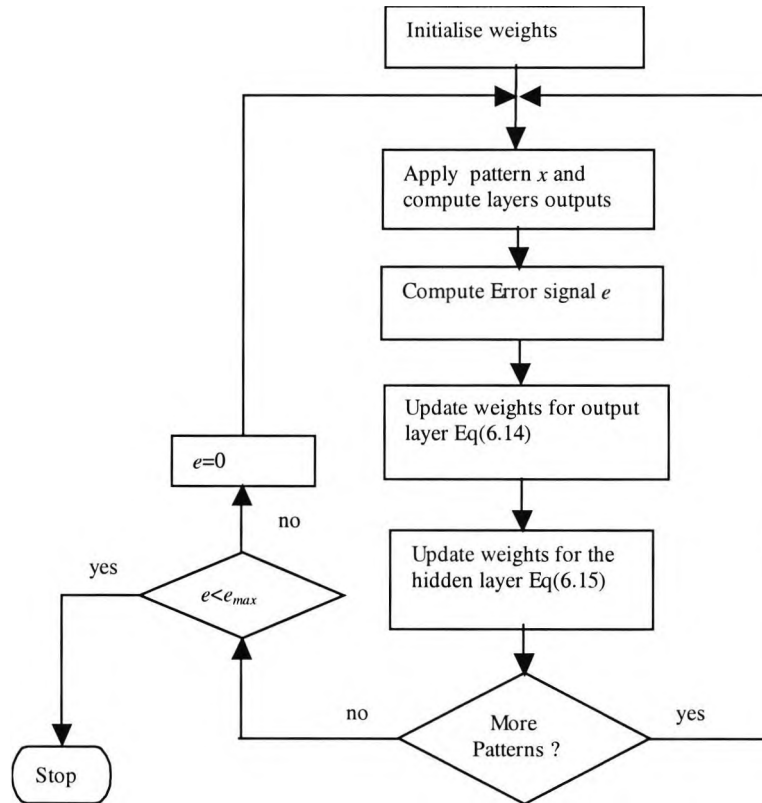


Figure 6.4 Error back-propagation learning algorithm flow chart.

6.2.5.1 *Faster Convergence of the Backpropagation Algorithm*

One of the critical parameters that has a significant effect on the rate of convergence of the back-propagation algorithm is the learning constant. In general, the optimum value for the learning constant depends on the problem being solved and should be chosen experimentally. Large learning constants will speed up the convergence but may cause overshoot in the solution for problems with steep and narrow minima. On the other hand, however, small learning constants will guarantee a solution; the price is the increased number of steps that need to be made to reach the satisfactory solution. Many suggestions have been made of how to adaptively change the learning constant (Kesten 1958; Saridis 1970) and for a complete survey of the learning algorithms, see (Anderson 1986). The following section describes two methods that have been used to increase the rate of convergence of the backpropagation algorithm, namely, the momentum and the delta-bar-delta learning rule.

6.2.5.1.1 Momentum

The momentum, α , represents one of the heuristics that have been used to overcome the convergence problem mentioned in the previous paragraph. The method involves feeding a portion of the previous delta weight through the current delta weight in Eq. (6.18) to have the following form:

$$\Delta w_{ji}(t) = \beta \varepsilon_j(t) y_i(t) + \alpha \Delta w_{ji}(t-1) \quad (6.19)$$

Typically, α is chosen between 0.1 and 0.9. This, in effect, acts as a low pass filter to reduce the overshooting behaviour and maintaining fast convergence.

6.2.5.1.2 Delta-Bar-Delta Learning Rule

An effective algorithm to adaptively update the learning constant was proposed by Jacobs (1988). He proposed four heuristics for achieving faster rate of convergence through learning constant adaptation. These heuristics suggest that: 1) every weight of a network should be given its own learning rate; 2) these rates should be allowed to vary over time. Additionally the heuristics suggest how the learning rates should be adjusted that is, 3) when the derivative of a parameter possesses the same sign for several consecutive time steps, the learning rate for that parameter should be increased, 4) when the sign of that derivative alternates for several consecutive time steps, the learning rate for that parameter should be decreased.

Jacobs introduced the delta-bar-delta (DBD) learning rule as an implementation for these heuristics. The DBD learning rule consists of a weight update rule and a learning constant update rule.

The weight update rule

$$w_{ji}(t+1) = w_{ji}(t) - \beta_{ji}(t+1) \frac{\partial \zeta(t)}{\partial w_{ji}(t)} \quad (6.20)$$

where $\beta_{ji}(t)$ is the learning rate value corresponding to $w_{ji}(t)$ at time t .

The learning rate update rule

The learning rate update rule is defined as follows (Jacobs 1988):

$$\Delta\beta_{ji}(t+1) = \begin{cases} \kappa & \text{if } \bar{\delta}_{ji}(t-1)\delta_{ji}(t) > 0 \\ -\vartheta\beta_{ji}(t) & \text{if } \bar{\delta}_{ji}(t-1)\delta_{ji}(t) < 0 \\ 0 & \text{Otherwise} \end{cases} \quad (6.21)$$

where κ is constant, $\delta_{ji}(t) = \partial\zeta(t)/\partial w_{ji}(t)$ and $\bar{\delta}_{ji}(t) = (1-\theta)\delta_{ji}(t) + \theta\bar{\delta}_{ji}(t-1)$ is a weighted average gradient of the current and past derivatives with θ , which is a positive constant, as the base. According to Eq. (6.21) if the current derivative of a weight and the weighted average of the weight's previous derivatives possess the same sign, then the learning rate for that weight is incremented by a constant, κ , and if they possess opposite signs, then the learning rate for that weight is decremented by a proportion, ϑ , of its current value.

6.3 ANN-Based ECG Signal Classifier

6.3.1 Introduction

The feedforward multi-layer neural network with error back-propagation learning algorithm has been used as normal/abnormal ECG signals classifier. During the training phase, the input patterns are presented to the classifier along with the category to which each particular pattern belongs. In the test phase, new patterns are presented to the network, which has not seen before. This classification as described above belongs to a supervised learning problem and has the advantage of constructing non-linear decision boundaries between the normal/abnormal ECGs in a nonparametric fashion, and thereby offer a practical method for solving highly complex pattern classification problems.

6.3.2 The NN Classifier Structure

Figure 6.5 shows the general configuration of the different stages employed in the classification process. Data from NSR-DB (MIT-CD 1997) and E-DB (Taddei, et al. 1992) have been used in this analysis. A total of 800,000 samples or about 6420 ECG beats from 18 normal subjects and 1650,000 samples or about 6600 ECG beats from 27 ischaemic subjects are analysed. This is in total equivalent to about 1.0833×10^7 ms.

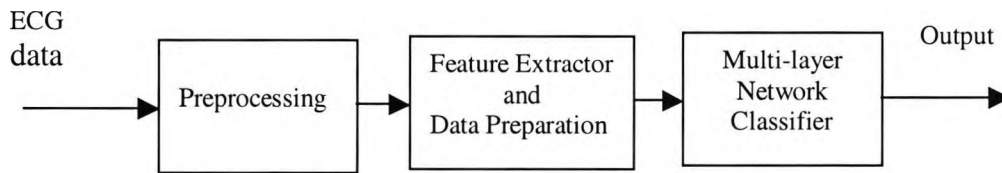


Figure 6.5 The ECG signal NN-based classifier.

The signal pre-processing stage applies the same procedure described in chapter four. The feature extractor stage consists of two main programs and three subroutines written in Matlab by the author to calculate the polyspectrum and polycoherency slices, these slices are used as input features to the neural classifier. Using a Pentium II, 333 MHz, 196 Mbytes RAM computer, the CPU time was about 0.15-sec/polyspectrum slice and 6-sec/polycoherency slice. The data preparation part is a Matlab program made to prepare the input data files and the desired patterns in the format required for the NN training and testing phases. The desired pattern is the binary sequence used to encode different cases for the output, i.e., [1 0] is used to represent normal ECG signals and [0 1] for ischaemic ECG signals. A feedforward multi-layer neural network with error back-propagation learning algorithm is built using a NN software package (NeuralWorks Pro II Plus with Predict[®]¹ program).

6.3.3 Classifier Training and Testing

It has been found in the previous chapter that the diagonal slices of the polyspectrum and polycoherency indices constitute very important features to discriminate between normal and ischaemic ECG signals. An experimental investigation is carried out targeted at the choice of the best input features and the best NN structure. Towards achieving this aim, information from the previous chapter combined with a trail and error procedure has been used to choose the order of the polyspectrum and the most informative training sets of slices, based on this investigation three different training

¹ NeuralWorks Pro II/plus, NeuralWare Inc. 1993. NeuralWorks Predict[®] program is an accompanying part of the NeuralWorks Pro II/Plus package with an interface to Excel work sheet for data input and output. Predict has the feature of automating much of the painstaking manipulation, selection, and pruning of data that takes up most of the time in building a neural network application.

sets are examined. First slices from the polyspectrum magnitude for orders 5 and 6 are used but no convergence is obtained in this case. Then two sets (S1 and S2) have been successfully used in training and testing the NNs, these are:

1. The polycoherency index slices in the frequency range from 0 to 20 Hz for polyspectrum order $k = 6$ (S1). The order is chosen based on the analysis and conclusions from the previous chapter. This set requires an input layer of 20 neurons. Figure 6.6 shows examples of this input feature for normal and ischaemic ECG signals. S1 consists of 120 patterns or examples for the training phase and 74 different patterns for the test phase.
2. Multiple features from the HOS domain (S2). These are the polyspectrum order k , the diagonal slices of the polyspectrum for orders 2 to 10 in the frequency range 0 - 20 Hz, the MPIS and the APIS for each order. S2 can be represented by an input layer of 23 neurons. S2 consists of 234 examples for the training phase and 117 different examples for the test phase.

Three NN structures (NN1, NN2 and NN3) are implemented and tested using these feature sets. An adaptive gradient learning method with back-propagation (Jacobs 1988; Minia and Williams 1990) has been used, with different initial learning constants for hidden and output layers during the learning phase. Initial selection of the number of neurons in the hidden layers is based on trial and error along with various heuristics from previous studies (Lippmann 1987; Sietsma and Dow 1991). The methodology adopted in training the network and included in the neural network package used is as follows:

- 1) Restricting the architecture of the network by restricting the number of allowable hidden nodes to a small number to start with.
- 2) Adding hidden nodes one or more at a time and retraining the network. The node giving best performance on the objective function (the pre-set minimum output error) is retained and established in the network.
- 3) During training the squared error $e^2(t)$, which is the error between the desired and the actual output, is minimised by using the back-propagation algorithm. Each network has

been trained using one training set of examples and tested using new examples, from the same group, that have not been seen during training phase.

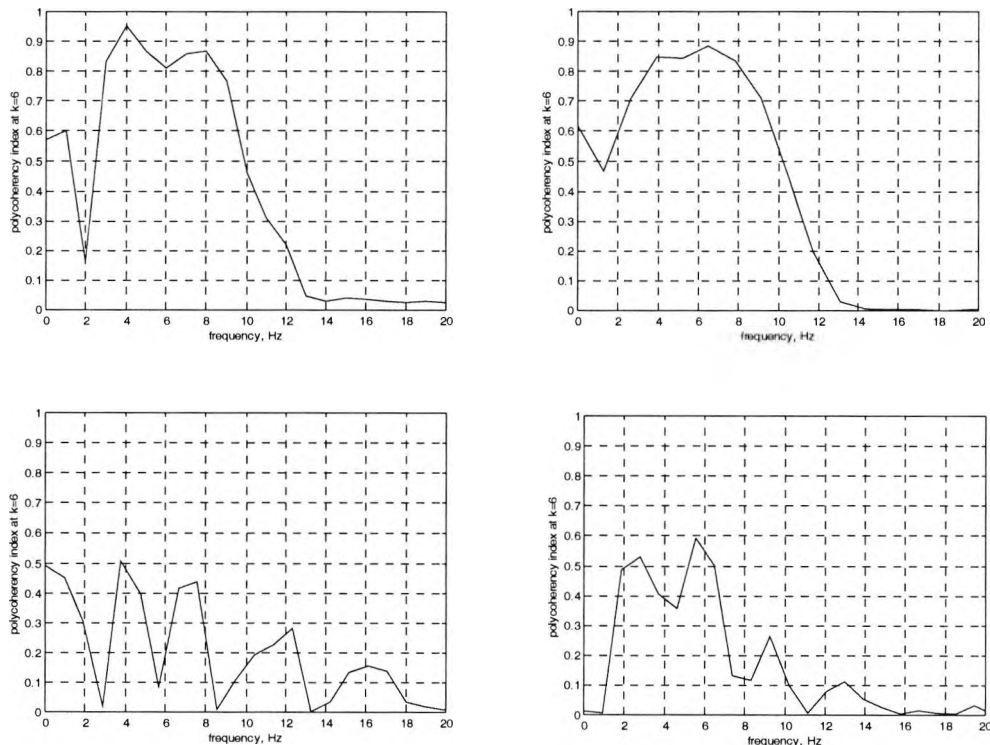


Figure 6.6 Polycoherency slices used in training the NN. The figure consists of two slices for normal cases (18184, 19088, up) and two for ischaemic cases (e0104, e0105, bottom), the slices are calculated for $k=6$ and from averaging of 50 individual polyspectra.

6.3.4 Implementation of the Three NN

NN1 is implemented using the NeuralWorks Pro II package. The first set of input features, S1, is used in training this network. An output layer of two neurons is used, the output of each of these neurons assumes a value between zero and one. To study the effect of the various learning rules mentioned in the previous sections on the performance of the network, NN1 is trained using Delta Rule (DR), Delta-Bar-Delta (DBD), and Extended Delta-Bar-Delta (EDBD)¹. Using one and two hidden layers, two

¹ The Extended Delta-Bar-Delta, developed by (Minai and Williams 1990), is an extension of DBD which also calculates a momentum term for each connection.

different structures are applied, 20-5-2 and 20-5-3-2. The activation functions within each neuron in the input, hidden and output layers are the hyperbolic tan.

Figure 6.7 shows the RMS error during the learning phase of NN1 as a function of epoch (during the training phase each time step is called an epoch, it is defined to be a single sweep through all the training patterns. At the end of each epoch, the weights of the network are updated). Using the DR no convergence is achieved while the DBD resulted in slow convergence. The EDBD rule gave a faster convergence and a smaller RMS error. Figure 6.8 are bar charts depict the sum squared error, between the NN output sequence during the training (LHS) and test (RHS) phases and the correct sequence at the output layer, versus the input/target pairs. Table 6.1 summarises the results obtained using DR, DBD, EDBD and EDBD with two hidden layers. The training parameters are $\alpha=0.8$ and $\beta=0.3, 0.2,$ and 0.15 for the first and second hidden and output layers, respectively, and the epoch=30 patterns.

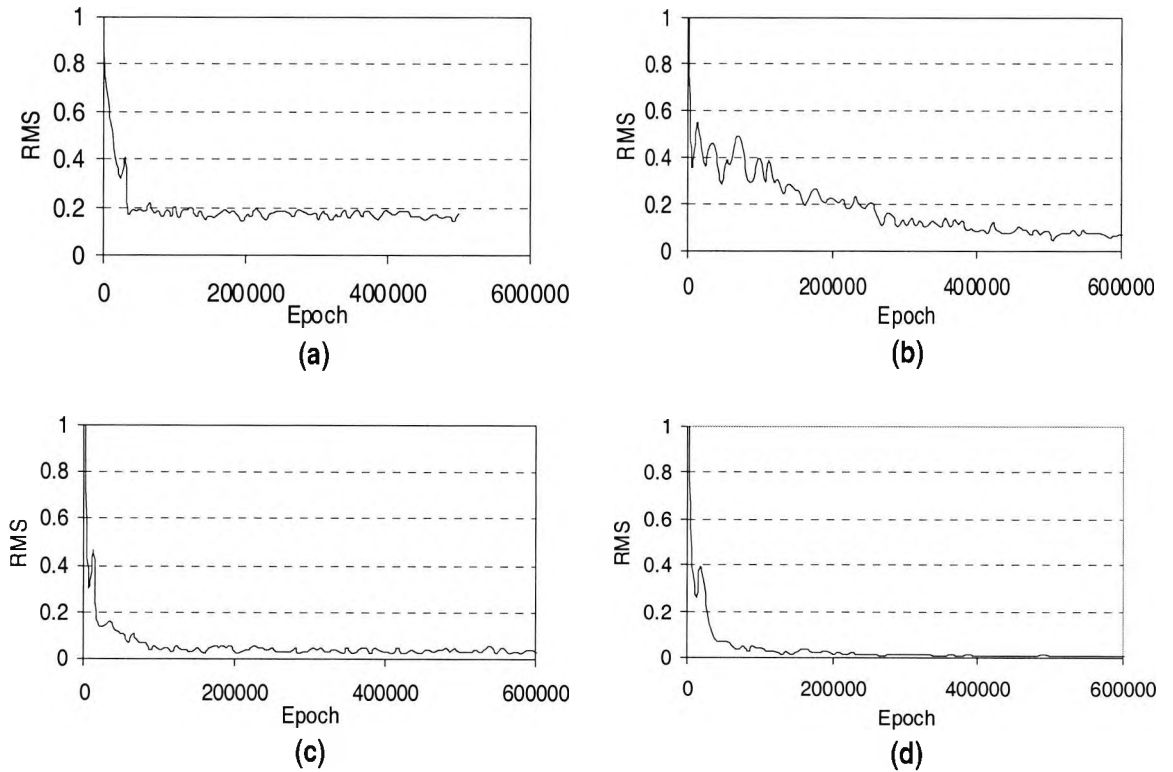


Figure 6.7 Training phase RMS error for NN1 trained with DR (a), DBD (b), EDBD (c), and EDBD using two hidden layers (d). The training parameters are $\alpha=0.8$ and $\beta=0.3, 0.2$, and 0.15 for the first and second hidden and the output layers, respectively.

Learning Rule	Final RMS	Classification Rate
Delta Rule	0.158	88%
Delta-Bar-Delta (DBD)	0.0551	90%
Extended DBD	0.018	89%
Extended DBD with two hidden layers	0.0056	93%

Table 6.1 The RMS and the classification rate obtained using DR, DBD, EDBD and EDBD with two hidden layers using NN1 structure.

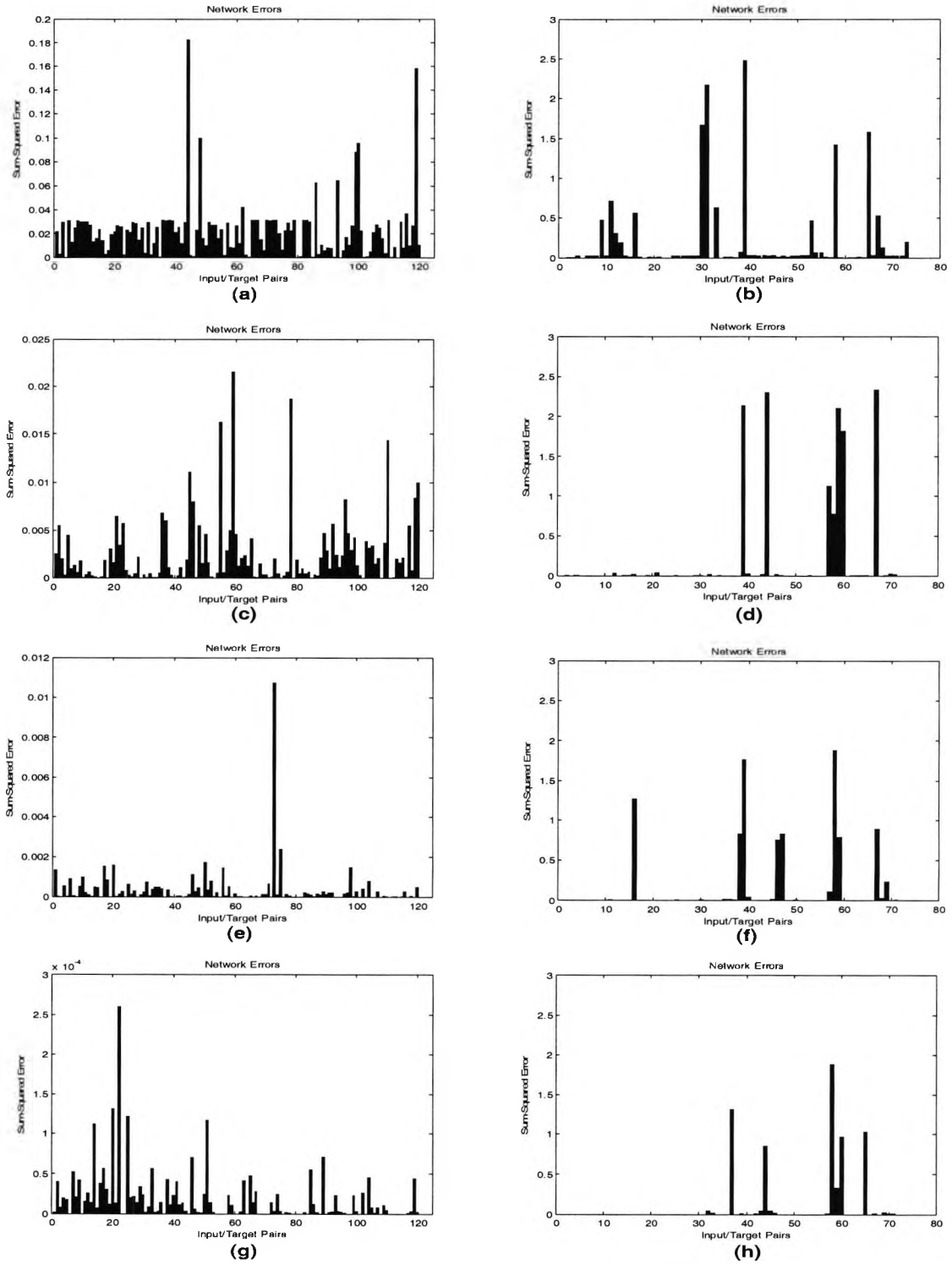


Figure 6.8 Bar chart for the sum squared error at the output layer during training (LHS) and test (RHS) phases for NN1 trained with DR (a,b), DBD (c,d), EDBD (e,f), EDBD using two hidden layers (g,h). The training parameters are $\alpha=0.8$ and $\beta=0.3, 0.2,$ and 0.15 for the first, second hidden and the output layers, respectively.

The NeuralWorks Predict® program has been used for the implementation of NN2 and NN3. NeuralWorks Predict® provides mechanisms to automatically transform user data into formats suitable for the neural network. A variety of analyses are performed to determine if an input field should be eliminated, or how it might be transformed to maximise the performance of the network, see appendix D.

The two previously explained sets of features, namely, S1 and S2 constitute 'the basic inputs' to the NN2 and NN3 classifiers, respectively. A single neuron, with two binary states, has been used as the output of the two classifiers. An output value of '0' corresponds to the ischaemic case while a value of '1' at the output corresponds to the normal case. Direct connections from the input layer to the output layer have also been included in the network architecture. Cascade connections are also employed which allows connections from previously established hidden processing elements to more recently established hidden processing elements. The activation functions within each neuron in the input and hidden layers are the hyperbolic tan while a softmax¹ function is used for the output neuron.

NN2 is trained using S1 with and without hidden layer. As without hidden layer the network assumes linear input-output mapping, much better results have been obtained in the structure with hidden layer. This comes in agreement with the nature of the ECG signal, which is highly non-linear as explained in the previous chapter and with the results obtained using NN1. The 'basic inputs' are used to train NN2 with a layer structure of 20-3-1 (or 20-1 without hidden layer).

Table 6.2 shows the performance of the NN2 classifier. A total of 74 patterns have been used in this test. Forty-three patterns are from normal ECG signals while the rest (31) corresponding to ischaemic ECG signals. The classifier managed to detect 68 patterns with a classification rate of 92.7%. Figure 6.9 shows the receiver operating characteristics of the classifier with the hit rate on the vertical axis and the false alarm rate on the horizontal axis.

¹ The SoftMax function can only be used for problems where the transformed output data is probabilistic. In other words, for each output record, the sum of values is equal to 1 and each individual output value is between 0 and 1.

Confusion Matrix	Ischaemic (Network O/P)	Normal (Network O/P)	Total	Classification Rate
Ischaemic (Actual)	28	3	31	90.3%
Normal (Actual)	3	40	43	95.2%
Total	31	43	74	92.7%

Table 6.2 Performance of the NN2 classifier. The table shows the classification rate results of the test data set.

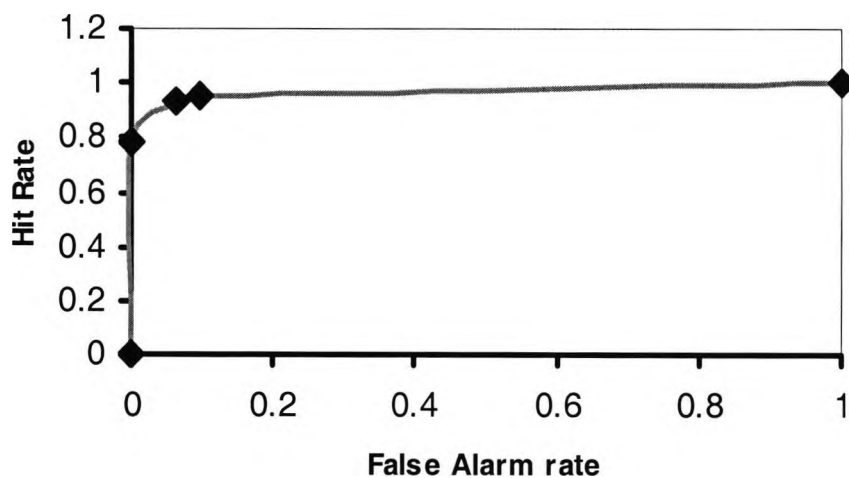


Figure 6.9 Receiver operating characteristic (ROC) curve of the NN2 classifier. As a Figure of merit of the classifier, the area under the ROC curve has been calculated to be 96.7%.

In training NN3 some transformation functions, for example, logarithmic function, inverse fourth power function and square function (see appendix D) are applied to the input features S2. These inputs are called 'the transformed inputs' to distinguish them from the basic inputs. A single hidden layer with two neurons has been used based on the best results for the classifier. Table 6.3 shows the performance of the NN3 classifier. A total of 117 patterns have been used in this test. Fifty-four patterns are from normal ECG signals while the rest (63) corresponding to ischaemic ECG signals.

The classifier managed to detect 88 patterns with a classification rate of 75.4%. Figure 6.10 shows the receiver operating characteristics of the classifier with the hit rate on the vertical axis and the false alarm rate on the horizontal axis.

Confusion Matrix	Ischaemic (Network O/P)	Normal (Network O/P)	Total	Classification Rate
Ischaemic (Actual)	46	17	63	73%
Normal (Actual)	12	42	54	77.7%
Total	58	59	117	75.4%

Table 6.3 Performance of the NN3 classifier (Network structure 7-2-1). The table shows the classification rate results of the test data set.

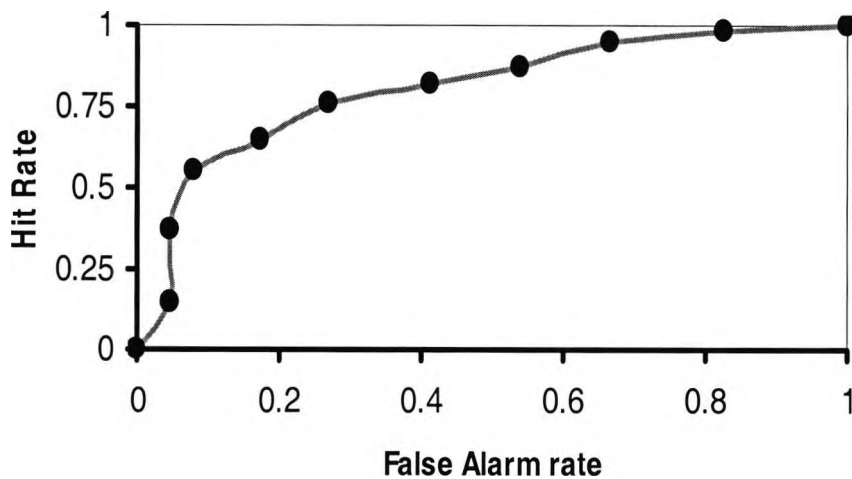


Figure 6.10 Receiver operating characteristic (ROC) curve of the NN3 classifier. As a Figure of merit of the classifier, the area under the ROC curve has been calculated to be 80.3%.

The following table summarises the results of the previously built neural networks.

Data set		
Package	Data Set S1	Data Set S2
NeuralWorks Pro II	NN1 → 93 %	No convergence
NeuralWorks Predict	NN2 → 92.7 %	NN3 → 75.4 %

Table 6.4 Summary of the neural networks structures and classification rates obtained.

6.4 Discussion

This chapter describes the implementation of an adaptive backpropagation NN-based classifier for detection of ischaemic heart abnormality using slices from the higher-order spectral domain of the ECG signals. The performance of this automated classifier was tested on the European ST-T database, which has been described as particularly appropriate for testing the performance of ischaemia detection algorithms (Taddei, et al. 1992). A high rate of successful classification in the discrimination problem between normal and ischaemic cases was achieved.

An effective approach has been adopted in this analysis. The previous chapter highlighted the fact that a decrease in the order of the non-linearity is associated with ischaemic conditions, this means that the normal and ischaemic ECG signals will be presented by different dynamics. This finding is the basis for the automatic ECG signal classifier. The polyspectrum and polycoherency indices slices are excellent features to represent these dynamics. These slices were calculated using the whole ECG cycle as one segment for polyspectrum estimation (as mentioned in the previous chapter) so in this approach information from the whole ECG cycle was used. This is considerably different from the previous ischaemia detection algorithms in that: 1) it avoids the use of the J-point and the ST-segment whose detection are often problematic and time consuming. 2) The training set is slices from the frequency domain. 3) The effective power of the HOS in detecting non-linearities was exploited by using features from the

higher-order domain. These features are one-dimensional slices and can be calculated within few seconds, which allows the use of this classifier in practical applications. Using these slices the NN was trained for ischaemic episode detection rather than ischaemic beat detection.

The steps of the procedure used in training and testing the three neural networks and using the three different training sets can be summarised as follows:

- 1) Applying slices from the polyspectrum magnitude for orders 5 and 6 as input features resulted in no convergence. This could be due to the fact that these slices contain only magnitude information.
- 2) The set S2 has been tried but no convergence was obtained using the NeuralWorks pro II. However, using the NeuralWorks Predict program-based NN (NN3) convergence was achieved with a total classification rate of 75.4%.
- 3) To improve this classification rate the feature set S1 was used with the original NeuralWorks pro II (NN1) then with the NeuralWorks Predict program (NN2). NN1 was trained using different learning rules and two different structures to achieve the best RMS, convergence time and classification rate. A significant increase has been achieved in the classification rate (93% for NN1 using EDBD learning rule with two hidden layers and 92.7% for NN2).
- 4) The receiver operating characteristic (ROC) curve was used to assess the performance of the NN classifiers.

It was expected that taking multiple features from the higher-order domain (S2) will result in the best classification rate but the polycoherency slices (S1) tend to be the optimal choice for this classification problem. One possibility may be due to the limited number of input patterns and their variabilities for different subjects and from one polyspectrum order to the other. This makes the use of multiple features in the input difficult for the NN to learn. So the NN in this case may need over one thousand input patterns. Another reason is the choice of these multiple features, which needs more investigation about which feature to use in the input pattern. This explains why the

NeuralWorks Predict program-based NN (NN3) has converged using the 'transformed inputs' from S2, while using the 'basic inputs' convergence could not be achieved.

In previous studies (Jager, et al. 1991; Maglaveras, et al. 1998; Taddei, et al. 1995), a sensitivity for ischaemic episode detection between 83% and 88% was obtained. A sensitivity of 73% for ischaemic episode detection using PCA neural network; was obtained by Silipo, et al. (1995). In a study by Stamkopoulos, et al. (1998) the total normal and abnormal classification indices of 79.32% and 75.19%, respectively, were obtained for ischaemic beat detection. An average beat classification performance of 80.4% was achieved by Papadimitriou, et al. (2001) using a self-organizing map model supplemented by supervised learning based on the radial basis function. In the current study HOS combined with an adaptive backpropagation NN yield superior performance in ischaemic episode detection.

The next and final chapter will summarise the main results obtained in this thesis, and give the some directions for future work.

Chapter 7

SUMMARY AND FUTURE WORK

7.1 Summary

Most work done on ECG analysis, over the last three decades, with the exception of Dr. Rizk's HOS-based research at City University, Spaargaren and English (1999) and more recently the work by Osowski and Linh (2001), relied heavily on using second-order statistical tools. However, because of the ECG signal's inherent non-linearity, describing it only in terms of the second-order statistics poses certain limitations. The motivation, therefore, behind this research work was primarily to analyse and characterise the ECG signals in the higher-order statistical domains, and ultimately, find new methodologies to classify them in those noise-free domains. From a signal processing point of view this research was aimed at sampling cumulants and polyspectral patterns in a selected number of domains and analysing their magnitudes, frequency and phase components. This allows the exploitation of the non-Gaussian and non-linear properties of the ECG signals. From a medical point of view this research sought to identify some discriminant features in HOS domains which in turn help to establish criteria in the decision making of certain ECG pathologies (e.g., ischaemic heart disease).

Towards achieving this aim several preliminary studies have been carried out on several ECG databases. These include noise cancellation using adaptive filtering techniques, testing for non-stationarity and quasi-periodicity in order to pave the way for appropriately dealing with the signal later using the HOS. The performance of adaptive filters to converge and track the non-stationary dynamics of the ECG signals, without prior information about the signal or the contaminating noise and with a pre-set MSE error value, has been analysed. Good results regarding the output MSE error and the fastest convergence rate were achieved especially for the Kalman filter. However, the basic limitation of Kalman filtering is the computational complexity, which is a direct

consequence of the matrix formulation of the solution to the Kalman filtering problem. The LMS-based algorithm is simple, and its tracking capability to the non-stationary ECG signals is better than the Kalman algorithm. Similar performance to the LMS-based filter was obtained, with smaller MSE, using LMS-based non-linear Volterra filter; this gives non-linear filtering an advantage over linear filtering for ECG application. Higher MSE, slower rate of convergence and lower output SNR are the main limitations of the LMF algorithm, which makes this filter unsuitable for ECG prediction or filtering purposes (see chapter 2 for more details).

The statistical and spectral analysis of the ECG signals resulted in clear views about the nature of the signal. From the statistical analysis it was demonstrated that the signal is pseudo-periodic, cyclostationary and predominantly non-Gaussian. This statistical characterisation was very beneficial when exploiting the cumulants and the polyspectrum. The spectral analysis showed that the spectrum of the ECG signal covers a limited band of frequencies, and its spectral content is harmonic in nature. Some frequency components are due to the P-wave, QRS complex and T-wave. Moreover, the very low frequency components are mainly due to some contaminating noise and the middle- to high-frequency components are due to interactions between some principal frequencies associated with the P-wave, QRS complex, and the T-wave, and their harmonics. An important outcome of this spectral analysis was the development of a technique to detect ischaemic heart disease. This detection was based on the MUSIC spectrum of the ST-T complexes taken from normal and ischaemic ECGs. In this study, normal ECGs were obtained from the NSR-DB (MIT-CD 1997) and ischaemic ones from the ST Change-DB (MIT-CD 1997). The ST-Change-DB mainly contains records from exercise-induced ischaemia. Episodes from both the initial resting and the peak effort phases of each of these exercise ECG recordings were interrogated and two independent and highly experienced physicians annotated these episodes. The MUSIC spectrum of the ST-T complexes taken from the above mentioned episodes revealed persistent high frequency components (HFC) in the range 60 – 180 Hz during these intervals. In normal subjects such high frequency components were not found in most of their ST-T complexes. This is due to the fact that the ST-T segments were taken from the edge of the QRS complex (e.g., starting at the point delineated R-wave + 50 msec), where most of the high-frequency energy can be found and is attributed to late

potentials or signals from areas in the myocardium of delayed conduction. These high-frequency components constitute an indicator to discriminate between normal and ischaemic ECGs. Furthermore, it should be emphasised here that normal-looking ST-T complexes gave the same MUSIC high frequency components. Hence, it may be possible to detect ischaemic heart disease using the initial phase of the exercise test or even in some cases without exercise. This is certainly the case for MI patients as explained in details in chapter 3.

Theoretical studies on higher-order statistics are found in chapter 4, where both conventional and new techniques for the estimation of cumulants and bispectra were discussed. Cumulant analysis of normal and ischaemic ECG signals revealed their discriminant features. Notably, a higher classification rate was obtained using the fourth-order cumulants as opposed to that due to the second- or the third-order cumulants for a pre-selected threshold. Three bispectral estimation methods were utilised to investigate the normal ECG signals in the third-order domain. As expected, the direct method of bispectrum estimation yielded much smaller variance than the indirect method. In terms of spectral resolution, parametric bispectrum estimation showed no advantage over the non-parametric estimation in the case of ECG analysis (chapter 4). Investigation of the frequency content of both the power spectrum and bispectrum of the normal ECG signals has revealed the existence of many harmonically related frequencies in the low frequency region (0 - 20 Hz). In this chapter, the bispectrum together with the squared bicoherence were used to investigate quadratic non-linearity in normal ECG signals over their low frequency end of the spectrum as opposed to detecting quadratic non-linearity in the high frequency region of abnormal ECG signals (Sabry-Rizk, et al. 1998). The squared bicoherence index was used as a measure for the degree of phase coherence of the triple-wave harmonics which causes the bispectrum to emerge at harmonically related frequencies. It revealed, for the first time, a strong phase coupling between these frequencies and confirms the quadratic non-linearity of the normal ECGs. Hinich independent tests statistically confirm the non-Gaussianity, and non-linearity of the ECG signals.

To benefit from the super-resolution capability of the eigendecomposition-based algorithms in the bispectrum domain, a novel subspace-based bispectrum estimator was

introduced and applied to simulated sinusoids and to the ECG signal (see chapter 4). It is termed the MUSIC pseudo-bispectrum and is aimed at extracting the quadratically coupled frequencies rather than estimating the true bispectrum. Its frequency estimation function was designed to enhance the spectral content of the third-order cumulant sequence responsible for the quadratically coupled harmonics. Furthermore, it was shown that the MUSIC pseudo-bispectrum gave higher resolution in comparison with the direct and TOR methods for short data lengths. However, the MUSIC pseudo-bispectrum estimator is sensitive to model order and hence it is strongly recommended to have a reliable model order criterion in the third-order domain, and not to rely on the commonly known Akaike Information criterion (AIC), Minimum Description Length (MDL) Criteria, and the Final Prediction Error (FPE) (Marple 1987).

To extract features from the polyspectrum domain to discriminate between normal and ischaemic (ambulatory) ECGs taken from the E-DB (Taddei, et al. 1992), three tests have been carried out in chapter 5. First, the magnitude and the phase of the bispectrum were investigated. In the study of the bispectrum magnitude and its bicoherence index two features are extracted, the maximum and the average bicoherence indices, these indices showed that both of these physiological states of the heart contain quadratic non-linearity. Also a pilot study on the bispectrum phases has been carried out but it failed to generate a general criterion or feature to differentiate between the two cases. Second, higher-order polyspectral slices were calculated for polyspectrum orders 2 to 10 and an algorithm by Zhou and Giannakis (1995) was applied to detect higher-order non-linearities in normal and ischaemic ECGs. This detection showed that both of these ECGs contain up to tenth-order non-linearity. Third, chapter 5 presented a proposed extension to this algorithm to calculate the polycoherency indices slices. Analysis of non-linearities in 1-D slices taken from both the polyspectral and the polycoherency in normal and ischaemic ECGs helped to establish two discriminant criteria. These are the maximum polycoherency index and the average polycoherency index. From these criteria non-linearity order ranges for normal and ischaemic ECGs were specified. The results obtained using the polycoherency indices tend to be more consistent with many of the previous work on ECG non-linear dynamics (see chapter 5 for more details).

Several neural network-based classifiers were deployed to automatically classify normal and ischaemic ECGs and assessed in chapter 6. These classifiers were trained using the polyspectrum patterns and the extracted features from the higher-order spectral analysis of chapter 5. These input patterns are Gaussian noise-free and contain both amplitude and phase information. To achieve the highest classification rate from these classifiers, three neural network structures employing either one or two hidden layers, and using two different input sets with three learning rules were examined. Based on this assessment, the highest classification rate was obtained from using the polycoherency index slices as input features, with the extended delta-bar-delta learning rule and two hidden layers.

7.2 Directions for Future work

A few proposals that could form a stimulating extension to this thesis include

1. It is worth studying the ECG signals non-stationarity properties in the higher-order domain. Since general approaches have rather limited applicability, this could be done by estimating the so-called cyclic moments/cumulants and the associated spectra. These cyclic higher-order statistics/spectra are defined for the k^{th} -order cyclostationary processes.
2. A more rigorous study towards the identification of ischaemic patients without exercise stress test is a primary extension to this work. This can be accomplished by applying more input data especially from the high resolution ECG recording to the MUSIC algorithm using the technique developed in chapter 3. The MUSIC spectra of the high resolution ECG data will provide a complete picture of the HFC, one that could not be obtained in this work because of the limited sampling rate of the available data. On-line application of this technique is also an interesting task; this means the interpretation of the exercise ECG data during the test using the software program made in this work. As some patients could not proceed in the exercise test, this interpretation may be useful in detecting ischaemic events before making an extensive effort on the patient's heart.

3. An interesting problem to look at would be to develop an information theoretic criterion for estimating the number of signals in the signal and noise subspaces for the MUSIC pseudo-bispectrum estimator. This could be done by extending the AIC criteria to handle the subspace separation problem in the third-order domain following the strategy adopted in its extension to the second-order domain. Subsequent to the development of this criterion an extensive application of the MUSIC pseudo-bispectrum to ECG signals and other real signals is a natural extension to this thesis. Studying the statistical behaviour of the MUSIC pseudo-bispectrum is also necessary.
4. Ischaemic conditions of the heart range from effort angina, mixed angina, resting angina and MI, then risk of VT. A study on the relation between the values of MPIS/APIS and the degree of the ischaemic conditions to assign threshold values for these polycoherency indices may help to separate each class.
5. Applying the higher-order spectral analysis developed in chapter 5 to other cardiac abnormalities or arrhythmias, and to other physiological signals is another possibility for future work.

APPENDIX A

CUBIC SPLINE INTERPOLATION

The cubic interpolation define an interpolated data point y on one particular interval, between x_j and x_{j+1} as

$$y = Ay_j + By_{j+1} + Cy_j'' + Dy_{j+1}'' \quad (\text{A.1})$$

Where

$$y_i = y(x_i), i = 1, \dots, N, \quad (\text{A.2})$$

$$A \equiv \frac{x_{j+1} - x}{x_{j+1} - x_j}, \dots, B \equiv 1 - A = \frac{x - x_j}{x_{j+1} - x_j}, \quad (\text{A.3})$$

$$C \equiv \frac{1}{6}(A^3 - A)(x_{j+1} - x_j)^2, \dots, D \equiv \frac{1}{6}(B^3 - B)(x_{j+1} - x_j)^2, \quad (\text{A.4})$$

$$\frac{dy}{dx} = \frac{y_{j+1} - y_j}{x_{j+1} - x_j} - \frac{3A^2 - 1}{6}(x_{j+1} - x_j)y_j'' + \frac{3B^2 - 1}{6}(x_{j+1} - x_j)y_{j+1}'' \quad (\text{A.5})$$

$$\frac{d^2y}{dx^2} = Ay_j'' + By_{j+1}'' \quad (\text{A.6})$$

Two boundary conditions at x_1 and x_n are needed to calculate Eq (A.1). There are two common ways of doing this (Press, et al. 1990):

- 1- Set one or both of them equal to zero, giving the so-called natural cubic spline, which has zero second derivative on one or both of its boundaries.
- 2- Set either of y_1'' or y_n'' to values calculated from Eq (A-6) so as to make the first derivative of the interpolating function has specified value on either or both boundaries.

APPENDIX B

KAISER WINDOW

The Kaiser-Bessel window is defined by Harris (1978):

$$w(t) = \frac{I_0 \left[\pi\alpha \sqrt{1.0 - \left(\frac{t}{N/2} \right)^2} \right]}{I_0[\pi\alpha]}, \quad 0 \leq |t| \leq \frac{N}{2} \quad (\text{B.1})$$

Where I_0 is the zero-order modified Bessel function of the first kind defined by

$$I_0(x) = \sum_{k=0}^{\infty} \left[\frac{\left(\frac{x}{2} \right)^k}{k!} \right] \quad (\text{B.2})$$

The parameter $\pi\alpha$ is half the time-bandwidth product. When $\alpha=0$, the Kaiser window corresponds to the rectangular window. When $\pi\alpha$ is 5.44, the resulting window is very similar to the Hamming window. The value of α is determined by the stop-band attenuation requirements and may be estimated, empirically, by the equation:
 $\pi\alpha=0.1102(A-8.7)$

If $A \geq 50$ dB, where $A=-20 \log_{10}(\delta)$ is the stop-band attenuation, δ is the minimum of the pass-band and the stop-band attenuations. The number of filter coefficients, N , is given by $N \geq \frac{A-7.95}{14.36\Delta f}$ where Δf is the normalised transition width. The values of α and N are used to compute the coefficients for the Kaiser window $w(t)$.

APPENDIX C

HINICH TEST

Hinich (1982) presented a sample estimator of the bispectrum, he used this sample bispectrum to construct a statistic to test whether the bispectrum of $[x(t)]$ is non-zero. A rejection of the null hypothesis implies a rejection of the hypothesis that $[x(t)]$ is Gaussian. He also constructed another test statistics for testing the hypothesis that $[x(t)]$ is linear. In the following part, Hinich's approach is summarised.

A sample bispectrum of an input signal $[x(0), x(1), \dots, x(N-1)]$ is defined by

$$F(i, j) = N^{-1} X(i)X(j)X^*(i + j) \tag{C.1}$$

To obtain a consistent estimate of the bispectrum, the sample bispectrum is smoothed over a square of M^2 points centred at $((2m-1)M/2, (2n-1)M/2)$ in the two dimensional frequency plane. The estimator is

$$\hat{B}_x(m, n) = M^{-2} \sum_{i=(m-1)M}^{mM-1} \sum_{j=(n-1)M}^{nM-1} F(i, j) \tag{C.2}$$

Since the asymptotic distribution of each estimator in (C.2) is complex normal, the distribution of

$$\zeta_{m,n} = \frac{\hat{B}_x(m, n)}{[N/M^2]^{1/2} [\hat{S}_x(m)\hat{S}_x(n)\hat{S}_x(m+n)]^{1/2}} \tag{C.3}$$

is complex normal with unit variance. Here \hat{S}_x is the estimator of the power spectrum of $x(t)$. Consequently, $|\zeta_{m,n}|^2$ is approximately chi-square with two degrees of freedom.

The statistics $\hat{S} = 2 \sum_m \sum_n |\zeta_{m,n}|^2$ (C.4)

is approximately $\chi_{2p}^2(\lambda)$ where p is the degree of freedom defined in the principle domain and λ is the centrality parameter of the chi-square distribution.

Testing for Gaussianity

Under the null hypothesis, $\hat{B}_x(m,n) \equiv 0$ and thus \hat{S} is approximately $\chi_{2p}^2(0)$ for large N . Gaussianity can be determined by comparing \hat{S} to the probability of exceeding their values under a Gaussian zero mean unit variance distribution. If the null hypothesis is rejected, then the Gaussian assumption must be rejected. If not, then the process may be non-Gaussian but the data is consistent with a zero bispectrum.

Testing for linearity

If the process is linear, its skewness is constant over the region of interest. Recall that under the null hypothesis $[2|\zeta_{m,n}|^2]$ is approximately chi-square with two degrees of freedom. Thus the expected value of these chi-square variates are the same for all m, n under the null hypothesis, otherwise the expected values are different. Rather than using an F test of constant means, Hinich used a nonparametric test based on a robust measure of dispersion, he uses the interquartile range of a subset of the $[2|\zeta_{m,n}|^2]$, which is robust to some bad values of the $\zeta_{m,n}$. Let R denote the sample interquartile range of the $[2|\zeta_{m,n}|^2]$ and \hat{R} is its estimated interquartile range. Reject the linearity if $R \gg \hat{R}$ or $R \ll \hat{R}$.

APPENDIX D

THE NEURALWORKS PREDICT PROGRAM

As mentioned in chapter 6, some transformation functions are applied to the basic features used in training NN3. The general form of, for example, a continuous transformation is:

$$y = \mathbf{s}_o F(\mathbf{s}_i x + \mathbf{o}_i) + \mathbf{o}_o$$

where F is a continuous function, \mathbf{s}_i , \mathbf{o}_i that implements an inner scaling of the raw data to map them to an optimal sub-domain of F and \mathbf{s}_o , \mathbf{o}_o implement an outer scaling so that y lies within a suitable range for the neural network

The purpose of these transformations is to manipulate the distribution of the data to enhance the possibility that knowledge can be extracted from it. For example, the distribution of a field may be skewed. There may be information in this skewness, in which case it would be advantageous to scale the data into an appropriate range, and pass the scaled data on for classification. But if there is no information in the skewness, it would be better to find a transform which makes the data more uniformly distributed to make optimum use of the dynamic range of the activation function of the neurons. Another example, which would need such transformations, is the existence of outliers (i.e., points remote from the bulk data).

There is wide range of continuous functions which can be applied. For example, the function F , in the above equation, can be a linear transform with the average of the data mapped to the mid point of the transformed range or a Fuzzy Left (right) function for outlier detection of small (large) values of x . The following table lists some of the functions available in Predict program.

Function	Description	Example
Linear	Identity function	$y = ax, a = \text{constant}$
Log	Natural logarithm function	$y = \log(x)$
Exp	Exponential function	$y = \exp(x)$
Pwr2	Square function	$y = x^2$
Pwr4	Fourth power function	$y = x^4$
Rt2	Square root function	$y = \sqrt{x}$
Rt4	Fourth root function	$y = \sqrt[4]{x}$
Inv	Inverse function	$y = 1/x$
IncPwr2	1/(square function)	$y = 1/x^2$
IncPwr4	1/(fourth square function)	$y = 1/x^4$
InvRt2	1/(square root function)	$y = 1/\sqrt{x}$
InvRt4	1/(fourth root function)	$y = 1/\sqrt[4]{x}$
Tanh	Hyperbolic tangent function	$y = \tanh(x)$
Fzleft	Fuzzy left function	See text for more details
Fzright	Fuzzy right function	

Table D.1 A sample of the transformation functions supported by Predict package

The data Analysis part of the Predict program analyses each data field and determines the type of field and the types of transformation that will convert the field for effective use by the Neural Network and may create more than one transformation per field. The variable selection component of Predict will determine which set of fields and transformations work well together to achieve high performance by comparing all the possible structures and scoring each result. If any field did not meet the criteria for any of the selected transformations, this field will be skipped.

APPENDIX E

GLOSSARY OF TERMS

ABI Average Bicoherence Index.

AIC Akaike Information Criteria.

APIS Average Polycoherency Index on the polycoherency diagonal Slice.

AR Autoregressive time-series model.

ARMA Autoregressive-moving average time-series model.

Atrial pacing a non-invasive method for inducing cardiac stress by an electrical pulse. This pulse is transferred by an electrode placed deeply into the oesophagus below the left atrium and connected to a transesophageal cardiac stimulator.

BW Baseline drift/Wander.

DBD Delta-Bar-Delta learning rule.

DR Delta Rule.

Dynamic exercise is a technique to assess the cardiac response to exercise. The ECG is recorded whilst the patient walks or runs on a motorised treadmill or cycles on a stationary cycle ergometer.

EDBD Extended Delta-Bar-Delta learning rule.

EMG Muscle contractions, represent an artefact on the ECG signal.

Excess MSE difference between steady state MSE and MSE of an optimum filter.

FFT Fast Fourier Transform.

FIR Finite Impulse response Filter. The current output is a combination of the present and a finite number of past inputs.

FPE Final Prediction Error criterion.

FT Fourier Transform.

Gradient error the weight error in the LMS algorithm.

HFC High Frequency Components observed on the MUSIC spectrum.

HOS Higher-Order Statistics.

ICE Ischaemic Confirmed Episodes.

i.i.d. independent identically distributed. If $[v(t)]$ is i.i.d. and non-Gaussian then

$$c_k^v(\tau_1, \dots, \tau_{k-1}) = \begin{cases} \gamma_k^v, \tau_1 = \tau_2 = \dots = \tau_{k-1} = 0 \\ 0, \text{otherwise} \end{cases}$$

where γ_k^v denotes the k th-order cumulants of $v(t)$.

IIF Infinite Impulse response Filter. The current output is a combination of the present and a finite number of past inputs and past outputs.

Ill-conditioning a problem is ill conditioned if its solution is very sensitive to small changes in the data.

ISE Ischaemic Suspected Episodes.

Isometric exercise is a muscular exercise in which muscle groups are pitted against each other so that strong contraction occurs without movement.

LMF Least mean fourth adaptive filtering algorithm.

LMS Least mean square adaptive filtering algorithm.

LPs Late potentials.

MA Motion artefacts.

MBI Maximum Bicoherence Index corresponding to the maximum peak on the bispectrum mesh plot.

MDL Minimum Description Length criteria.

MEM Maximum Entropy Method.

Misadjustment the ratio between the excess MSE and MSE of an optimum filter.

MI Myocardial Infarction.

MPIS Maximum Polycoherency Index corresponding to the maximum peak on the diagonal Slice of the polyspectrum.

MSE Mean Square Error. A quadratic function of the filter weights when the filter output is a linear function of its weights.

MUSIC Multiple Signal Classification.

NAC2 is the Normalised Area under the curve of 2nd-order cumulants (c_2).

NADC3 is the Normalised Area under the curve of the Diagonal slice of the 3rd-order cumulants (c_3).

NADC4 is the Normalised Area under the curve of the Diagonal slice of the 4th-order cumulants (c_4).

NCE Normal Confirmed Episodes.

NLE Normal Looking Episodes.

NSC Number of Segments out of 50 that show self-phase Coupling for a specific polyspectrum order.

PDF Probability Distribution Function. The distribution of signal values generated by a deterministic or random process.

Pharmacological stress is a technique to stress the heart by drugs such as dipyridamole or dobutamine.

Process deterministic or random mechanism responsible for the generation of the observed signal or data sequence.

SNR Signal-to-Noise Ratio.

Stability a system is stable if its output remains bounded in response to a bounded input. An algorithm is stable if round-off errors introduced at one stage of the computation do not propagate through later stages with increasing magnitude.

Stationary random process whose statistics are time-invariant.

Steady-state phase following convergence in a stationary or non-stationary environment.

Step-size parameter controlling the speed of adaptation in of the LMS and LMF filters weights during convergence and tracking.

SVD Singular Value Decomposition.

SVF Second-order Volterra Filters.

TOR Third-order Recursion.

Tracking steady-state phase during which the weights of an adaptive filter have to be readjusted in response to non-stationarities.

VT Ventricular Tachycardia.

White noise random process consisting of a sequence of uncorrelated random variables. Characterised by a flat power spectral density.

*APPENDIX F***LIST OF SOFTWARE**

All algorithms are derived from the relevant literature (where applicable), and written by the author using the following software (programming languages, libraries and toolboxes):

1. Fortran 77 accompanied by the NAG and GINO (a registered trademark of Bardly Associates Ltd) libraries, which is based on a Sun-Sparc (a trademark of Sun Microsystems, Inc.) workstation under the Unix operating system (a registered trademark of UNIX Systems Laboratory, Inc.) in a time-sharing environment.
2. PC-based MATLAB (the name stands for MATrix LABoratory) programming language (a trademark of the MathWorks, Inc.), which is a high-performance language for technical computing. Both versions 5.0 and 5.3 are used. Some toolboxes (a comprehensive collections of MATLAB functions to solve particular classes of problems) are used as extensive library subroutines, and others are updated and extended to handle certain aspects related to this research work.
3. A neural network package, NeuralWorks Professional II plus (NeuralWare, Inc.).
4. All figures are produced with MATLAB and Excel 97. The text was typed in Word 97.
5. The reference list was generated using Endnote version 3.0.1 software (Niles software Inc.). This program is an online search tool, reference database and bibliography maker.

APPENDIX G**LIST OF PUBLICATIONS**

- [1] M. Sabry-Rizk, W. Zgallai, S. El-Khafif, E. Carson, and K. Gratten, "Higher-order ambulatory electrocardiogram identification and motion artefact suppression with adaptive second- and third-order volterra filters," presented at SPIE98, San Diego, USA, 1998.
- [2] M. Sabry-Rizk, S. El-Khafif, W. Zgallai, E. Carson, K. Gratten, C. Morgan, and P. hardiman, "Suspicious polyphase patterns of normal looking ECG's provide early diagnosis of a coronary artery disease," BMES/EMBS, 1999.
- [3] M. Sabry-Rizk, W. Zgallai, S. El-Khafif, E. R. Carson, K. Grattan, and P. Thompson, "Highly accurate higher-order statistics based neural network classifier of specific abnormality in electrocardiogram signals," presented at ICASSP-99, Arizona, USA, 1999.
- [4] M. Sabry-Rizk, W. Zgallai, E. R. Carson, S. El-Khafif, C. Morgan, and K. T. V. Grattan "Novel decision strategy for P-wave detection utilising non-linearly synthesised ECG components and their enhanced pseudospectral resonances", IEE International conference, MEDSIP2000, Bristol, UK, September 2000.
- [5] M. Sabry-Rizk, W. Zgallai, C. Morgan, S. El-Khafif, E. R. Carson, and K. T. V. Grattan, "Novel decision strategy for P-wave detection utilising nonlinearly synthesised ECG components and their enhanced pseudospectral resonances," IEE Proceedings Science, Measurement and Technology, Special section on Medical Signal Processing, vol. 147, pp. 389-397, 2000.
- [6] S. El-Khafif, M. Sabry-Rizk, E. R. Carson and K. T. V. Grattan, "Bispectral analysis of normal electrocardiogram signals" 4th JIEEEC Conference, 16-18 April 2001.
- [7] S. El-Khafif and M. Sabry-Rizk, *Member IEEE*. "MUSIC pseudo-bispectrum," In final preparation.

- [8] S. El-Khafif, et al. "Detection of non-linearities in ECG signals using higher-order spectral analysis," In final preparation.
- [9] S. El-Khafif, et al, "Pseudo-spectral MUSIC unravels high frequency components associated with ischaemic/infraction ECGs in the first few cycles of stress test," In final preparation.

REFERENCES

- [1] Aase, S. O., Eftestol, T., Husoy, J. H., Sunde, K., and Steen, P. A., "CPR artifact removal from human ECG using optimal multichannel filtering," *IEEE Trans. Biomed. Eng.*, vol. BME-47, pp. 1440-1449, 2000.
- [2] Abboud, S., Cohen, R., Selwyn, A., Ganz, P., Sadeh, D., and Friedman, P., "Detection of transient myocardial ischaemia by computer analysis of standard and signal-averaged high-frequency electrocardiograms in patients undergoing percutaneous transluminal coronary angioplasty," *Circulation*, vol. 76, pp. 585-596, 1987.
- [3] Ahlstrom, M. L. and Tompkins, W. J., "Digital filters for real-time ECG signal processing using microprocessors," *IEEE Trans. Biomed. Eng.*, vol. BME-32, pp. 708-713, 1985.
- [4] Akaike, H., "Power spectrum estimation through autoregression model fitting," *Ann. Inst. Statist. Math.*, vol. 21, pp. 407-419, 1969.
- [5] Al-Nashash, H. A., "Noninvasive beat-to-beat detection of ventricular late potentials," *Med. Biol. Eng. Comput.*, vol. 27, pp. 64-68, 1989.
- [6] Amari, S., "Mathematical foundations of neurocomputing," *Proc. IEEE*, vol. 78, pp. 1443-1463, 1990.
- [7] Anderson, C. W., "Learning and Problem Solving with Multilayer Connectionist Systems," Ph.D Thesis, University of Massachusetts, 1986.
- [8] Armstrong, W. F., "Treadmill exercise echocardiography: Methodology and clinical role," *Eur. Heart J.*, vol. 18, pp. D2-D8, 1997.
- [9] Arnold, M., Miltner, W. H. R., Witte, H., Bauer, R., and Braun, C., "Adaptive AR modelling of nonstationary time series by means of Kalman filtering," *IEEE Trans. Biomed. Eng.*, vol. BME-45, pp. 553-562, 1998.

- [10] Babloyantz, A. and Destexhe, A., "Is the normal heart a periodic oscillator," *Biol. Cybern.*, vol. 58, pp. 203-211, 1988.
- [11] Bennett, W. R., "Statistics of regenerative digital transmission," *Bell Syst. Tech. J.*, vol. 37, pp. 1501-1542, 1958.
- [12] Breithardt, G., Borggrefe, M., and Haerten, K., "Ventricular late potentials and inducible ventricular tachyarrhythmias a marker for ventricular-tachycardia after myocardial-infarction," *Eur. Heart J.*, vol. 7, pp. 127-134, 1986.
- [13] Breithardt, G., Cain, M. E., El-Sherif, N., Flowers, N., Hombach, V., Janse, M., Simson, M. B., and Steinbeck, G., "Standards for analysis of ventricular late potentials using high resolution or signal-averaged electrocardiography," *Eur. Heart J.*, vol. 12, pp. 473-480, 1991.
- [14] Brillinger, D. R., "An introduction to polyspectra," *Ann. Math. Statist.*, vol. 36, pp. 1351-1374, 1965.
- [15] Brillinger, D. R., "The comparison of least squares and third-order periodogram procedures in the estimation of bifrequency," *J. Time Series Anal.*, vol. 1, pp. 95-102, 1980.
- [16] Bruce, R., Gey, G., Cooper, M., Fisher, L., and Peterson, D., "Seattle heart watch clinical circulatory and electrocardiographic responses to maximal exercise," *Amer. J. Cardiol.*, vol. 33, pp. 459-469, 1974.
- [17] Burg, J. P., "Maximum entropy spectral analysis," presented at 37th Meet. Soc. Exploration Geophysicists, Oklahoma, 1967.
- [18] Burke, S. R., "The Cardiovascular System," in *Human Anatomy and Physiology for Health Sciences*, S. R. Burke, Eds. New York: Wiley, pp. 153-187, 1985.
- [19] Camm, A. J., "Cardiovascular Disease," in *Clinical Medicine*, P. Kumar and M. Clark, Eds. W. B. Saunders, pp. 625-743, 1998.
- [20] Chialvo, D. R., Gilmour, R. F., and Jalife, J., "Low dimensional chaos in cardiac tissue," *Nature*, vol. 343, pp. 653-657, 1990.

- [21] Chialvo, D. R. and Jalife, J., "Nonlinear dynamics of cardiac excitation and impulse propagation," *Nature*, vol. 330, pp. 749-752, 1987.
- [22] Clayton, R., Murray, A., and Campbell, R., "Comparison of four techniques for recognition of ventricular fibrillation from surface ECG," *Med. Biol. Eng. Comput.*, vol. 31, pp. 111-117, 1993.
- [23] Coker, M. J. and Simkins, D. M., "A nonlinear adaptive noise canceller," in *Proc. IEEE Int. Conf. Acoust., Speech, Signal Process., ASSP-80*, vol. 2, pp. 470-473, 1980.
- [24] Cox, J. R., Nolle, F. M., and Arthur, R. M., "Digital analysis of the electroencephalogram, the blood pressure wave, and the electrocardiogram," *Proc. IEEE*, vol. 60, pp. 1137-1164, 1972.
- [25] Dandawate, A. V. and Giannakis, G. B., "Nonparametric polyspectral estimators for kth-order (almost) cyclostationary processes," *IEEE Trans. Inform. Theory*, vol. 40, pp. 67-84, 1994.
- [26] Davila, C. E., Welch, A. J., and Rylander, H. G., "A 2nd-order adaptive Volterra filter with rapid convergence," *IEEE Trans. Acoust., Speech, Signal Process.*, vol. ASSP-35, pp. 1259-1263, 1987.
- [27] El-Khafif, S. H., Sabry-Rizk, M., Carson, E. R., and Grattan, K. T. V., "Bispectral analysis of normal electrocardiogram signals," presented at *the 4th JIEEEEC*, Amman-Jordan, 2001.
- [28] Fell, J., Mann, K., Roschke, J., and Gopinathan, M. S., "Nonlinear analysis of continuous ECG during sleep I. Reconstruction," *Biol. Cybern.*, vol. 82, pp. 477-483, 2000a.
- [29] Fell, J., Mann, K., Roschke, J., and Gopinathan, M. S., "Nonlinear analysis of continuous ECG during sleep II. Dynamical measures," *Biol. Cybern.*, vol. 82, pp. 485-491, 2000b.

- [30] Forster, P. and Nikias, C. L., "Bearing estimation in the bispectrum domain," *IEEE Trans. Signal Process.*, vol. 39, pp. 1994-2006, 1991.
- [31] Friesen, G. M., Jannett, T. C., Jadallah, M. A., Yates, S. L., and Quint, S. R., "A comparison of the noise sensitivity of nine QRS detection algorithms," *IEEE Trans. Biomed. Eng.*, vol. BME-37, pp. 85-105, 1990.
- [32] Gardner, W. A. and Franks, L. E., "Characterisation of cyclostationary random signal processes," *IEEE Trans. Inform. Theory*, vol. 21, pp. 4-14, 1975.
- [33] Geddes, L. S. and Cascio, W. E., "Effects of Acute Ischemia on Cardiac Electrophysiology," in *The Heart and Cardiovascular System.*, vol. 2, H. A. Fozzard, Eds. New York: Raven, pp. 2021-2054, 1991.
- [34] Godard, D. N., "Channel equalisation using a Kalman filter for fast data transmission," *IBM J. Res. Develop.*, vol. 18, pp. 267-273, 1974.
- [35] Goldberger, A. L. and West, B. J., "Applications of nonlinear dynamics to clinical cardiology," *Ann. N. Y. Acad. Sci.*, vol. 504, pp. 195-213, 1987.
- [36] Goldschlager, N. and Goldman, M. J., *Principles of Clinical Electrocardiography*. East Norwalk: Prentice-Hall, 1989.
- [37] Goldberger, A. L., Rigney, D. R., and West, B. J., "Chaos and fractals in human physiology," *Sci. Amer.*, pp. 43-49, 1990.
- [38] Golub, G. H. and Van Loan, C. F., *Matrix Computations*. Baltimore: John Hopkins University Press, 1989.
- [39] Gomis, P., Jones, D. L., Caminal, P., Berbari, E. J., and Lander, P., "Analysis of abnormal signals within the QRS complex of the high-resolution electrocardiogram," *IEEE Trans. Biomed. Eng.*, vol. BME-44, pp. 681-693, 1997.
- [40] Green, D. M. and Swets, J. A., *Signal Detection Theory and Psychophysics*. New York: Wiley, 1966.

- [41] Hamilton, P. S. and Tompkins, W. J., "Adaptive matched filtering for ECG detection," presented at *IEEE Int. Conf. Eng. Med. Biol. Soc., EMBS-88*, 1988.
- [42] Hamilton, P. S. and Tompkins, W. J., "Quantitative investigation of QRS detection rules using the MIT/BHI arrhythmia database," *IEEE Trans. Biomed. Eng.*, vol. BME-33, pp. 1157-1165, 1986.
- [43] Hampton, J. R., *The ECG Made Easy*, Edinburgh: Churchill Livingstone, 1992.
- [44] Harris, F. J., "On the Use of windows for harmonic analysis with the discrete Fourier transform," *Proc. IEEE*, vol. 66, pp. 51-83, 1978.
- [45] Hasselman, K., Munk, W., and MacDonald, G., "Bispectrum of ocean waves," in *Time Series Analysis*, M. Rosenblatt, Eds. New York: Wiley, 1963.
- [46] Hayes, M. H., *Statistical Digital Signal Processing and Modelling*. New York: John Wiley & Sons, Inc, 1996.
- [47] Haykin, S., *Communication Systems*. New York: Wiley, 1983.
- [48] Haykin, S., *Adaptive Filter Theory*. New Jersey: Prentice-Hall, 1991.
- [49] Haykin, S., *Neural Networks: Comprehensive Foundation*. New York: Macmillan College Publishing Company, 1994.
- [50] Haykin, S., "Neural networks expand SP's horizons," *IEEE signal process. magazine*, vol. 13, pp. 24-49, 1996.
- [51] Hinich, M. J., "Testing for Gaussianity and linearity of a stationary time series," *J. Time Series Anal.*, vol. 3, pp. 169-176, 1982.
- [52] Hinich, M. J. and Gary, R. W., "Detection of non-Gaussian signals in non-Gaussian noise using the bispectrum," *IEEE Trans. Acoust., Speech, Signal Process.*, vol. ASSP-38, pp. 1126-1131, 1990.

- [53] Hsia, P. e. a., "An automated system for ST segment and arrhythmia analysis in exercise radionuclide ventriculography," *IEEE Trans. Biomed. Eng.*, vol. BME-33, pp. 585-593, 1986.
- [54] Huber, P., Kleiner, B., Gasser, T., and Dumermuth, G., "Statistical methods for investigating phase relations in stationary stochastic processes," *IEEE Trans. Audio Electroacoust.*, vol. AU-19, pp. 78-86, 1971.
- [55] Huhta, J. C. and Webster, J. G., "60-Hz interference in electrocardiography," *IEEE Trans. Biomed. Eng.*, vol. BME-20, pp. 91-101, 1973.
- [56] Ivaturi, S. N., Mandayam, R., Rangaraj, R., Jayaram, K., and Goyal, A. K., "Homomorphic analysis and modelling of ECG signals," *IEEE Trans. Biomed. Eng.*, vol. BME-26, pp. 330-344, 1979.
- [57] Jacobs, R. A., "Increased rates of convergence through learning rate adaptation," *Neural Networks*, vol. 1, pp. 295-307, 1988.
- [58] Jadvar, H., Jenkins, J. M., Stewart, R. E., Schwaiger, M., and Arzbaecher, R. C., "Computer-analysis of the electrocardiogram during esophageal pacing cardiac stress," *IEEE Trans. Biomed. Eng.*, vol. BME-38, pp. 1089-1099, 1991.
- [59] Jager, F., Mark, R., and Moody, G., "Analysis of transient ST segment changes during ambulatory monitoring," *Comput. Cardiol.*, vol. 18, pp. 453-456, 1992.
- [60] Jager, F., Moody, G. B., Taddei, A., and Mark, R. G., "Performance measures for algorithms to detect transient ischemic ST segment changes," *Comput. Cardiol.*, pp. 369-372, 1991.
- [61] Kalman, R. E., "A new approach to linear filtering and prediction problems," *Trans. ASMA J. Basic Eng., SER D*, vol. 82, pp. 35-45, 1960.
- [62] Kalman, R. E. and Bucy, R. S., "New results in linear filtering and prediction theory," *Trans. ASMA J. Basic Eng., SER D*, vol. 83, pp. 95-108, 1961.
- [63] Kesten, H., "Accelerated stochastic approximation," *Ann. Math. Statist.*, vol. 29, pp. 41-59, 1958.

- [64] Kim, Y. C. and Powers, E. J., "Digital bispectrum analysis of self-excited fluctuation spectra," *Phys. Fluids*, vol. 21, pp. 1452-1453, 1978.
- [65] Kim, Y. C. and Powers, E. J., "Digital bispectrum analysis and its applications to nonlinear wave interactions," *IEEE Trans. Plasma Sci.*, vol. PS-7, pp. 120-131, 1979.
- [66] Koh, T. and Powers, E. J., "2nd-order Volterra filtering and its application to nonlinear-system identification," *IEEE Trans. Acoust., Speech, Signal Process.*, vol. ASSP-33, pp. 1445-1455, 1985.
- [67] Leyman, A. R. and Durrani, T. S., "Signal-subspace processing using higher-order statistics," *Electron. Lett.*, vol. 30, pp. 1282-1284, 1994.
- [68] Li, C., Zheng, C., and Tai, C., "Detection of ECG characteristic points using wavelet transforms," *IEEE Trans. Biomed. Eng.*, vol. BME-42, pp. 21-28, 1995.
- [69] Lippmann, R. P., "An introduction to computing with neural network," *IEEE ASSP Magazine*, pp. 4-22, 1987.
- [70] Maglaveras, N., Stamkopoulos, T., Pappas, C., and Strintzis, M. G., "An adaptive backpropagation neural network for real-time ischemia episodes detection: Development and performance analysis using the European ST-T database," *IEEE Trans. Biomed. Eng.*, vol. BME-45, pp. 805-813, 1998.
- [71] Makhoul, J., "Linear prediction: A tutorial review," *Proc. IEEE*, vol. 63, pp. 561-580, 1975.
- [72] Marple, L., "A new autoregressive spectrum analysis algorithm," *IEEE Trans. Acoust., Speech, Signal Process.*, vol. ASSP-28, pp. 441-454, 1980.
- [73] Marple, S. L., *Digital Spectral Analysis with Applications*. New Jersey: Prentice Hall, 1987.
- [74] Marques, J. P., "Digital FIR filtering for removal of ECG baseline wander," *J. Clin. Eng.*, vol. 8, pp. 235-240, 1982.

- [75] Mazeika, P. K., Nadazdin, A., and Oakley, C. M., "Dobutamine stress echocardiography for detection and assessment of coronary-artery disease," *J. Amer. Coll. Cardiol.*, vol. 19, pp. 1203-1211, 1992.
- [76] Mendel, J. M., "Use of higher-order statistics in signal processing and system theory," *SPIE*, vol. 975, pp. 126-144, 1988.
- [77] Mendel, J. M., "Tutorial on higher-order statistics (spectra) in signal processing and system theory: Theoretical results and some applications," *Proc. IEEE*, vol. 79, pp. 277-305, 1991.
- [78] Meste, O., Rix, H., Caminal, P., and Thakor, N. V., "Ventricular late potentials characterization in time-frequency domain by means of a wavelet transform," *IEEE Trans. Biomed. Eng.*, vol. BME-41, pp. 625-634, 1994.
- [79] Michael, B. and Simson, M. D., "Use of signals in the terminal QRS complex to identify patients with ventricular tachycardia after myocardial infarction," *Circulation*, vol. 64, pp. 235-242, 1981.
- [80] Minia, A. A. and Williams, R. D., "Acceleration of back-propagation through learning rate and momentum adaptation," *Int. Joint Conf. neural networks*, vol. I. January, pp. 676-679, 1990.
- [81] MIT-CD, "MIT-BIH Arrhythmia Database CD-ROM," 3rd ed: Harvard-MIT Division of Health Sciences and Technology, 1997.
- [82] Mood, A. M., Graybil, F. A., and Boes, D. C., *Introduction to the Theory of Statistics*, Eds. New York: McGraw-Hill, 1974.
- [83] Mukhopadhyay, S. and Sircar, P., "Parametric modelling of ECG signal," *Med. Biol. Eng. Comput.*, vol. 34, pp. 171-174, 1996.
- [84] Mulgrew, B. and Mclaughlin, S., "A Reduced complexity sub-optimal nonlinear predictor," presented at *IEE Colloquium*, Savoy Place, London, Digest no. 6/1-6/13, 1994.

- [85] Muthuswamy, J., Sherman, D. L., and Thakor, N. V., "Higher-order spectral analysis of burst patterns in EEG," *IEEE Trans. Biomed. Eng.*, vol. BME-46, pp. 92-99, 1999.
- [86] Nikias, C. L., *Higher-Order Spectra Analysis: A Nonlinear Signal Processing Framework*. New Jersey: Printice Hall, 1993.
- [87] Nikias, C. L. and Mendel, J. M., "Signal processing with higher-order spectra," *IEEE Signal Process. Magazine*, pp. 10-37, 1993.
- [88] Nikias, C. L. and Raghuveer, M. R., "Bispectrum estimation: A digital signal processing framework," *Proc. IEEE*, vol. 75, pp. 869-891, 1987.
- [89] Ning, T. and Bronzino, J. D., "Bispectral analysis of the rat EEG during various vigilance states," *IEEE Trans. Biomed. Eng.*, vol. BME-36, pp. 497-499, 1989.
- [90] Ning, T. and Bronzino, J. D., "Nonlinear analysis of the hippocampal subfields of CA1 and the dentate gyrus," *IEEE Trans. Biomed. Eng.*, vol. BME-40, pp. 870-876, 1993.
- [91] Niranjana, U. C. and Murthy, I. S. N., "ECG component delineation by Prony's method," *Signal Process. J.*, vol. 31, pp. 191-202, 1993.
- [92] Osowski, S. and Linh, T. H., "ECG beat recognition using fuzzy hybrid neural network," *IEEE Trans. Biomed. Eng.*, vol. BME-48, pp. 1265-1271, 2001.
- [93] Owen, S. G., Stretton, T. B., and Vallance-owen, J., *Essentials of Cardiology*. London: LLOYD-LUKE (medical books) LTD, 1968.
- [94] Palit, S. and Kanjilal, P. P., "On the singular value decomposition, applied in the analysis and prediction of almost periodic signals," *Signal Process.*, vol. 40, pp. 269-285, 1994.
- [95] Pan, J. and Tompkins, W. J., "A real-time QRS detection algorithm," *IEEE Trans. Biomed. Eng.*, vol. BME-32, pp. 230-236, 1985.

- [96] Papadimitriou, S., Mavroudi, S., Vladutu, L., and Bezerianos, A., "Ischemia detection with a self-organizing map supplemented by supervised learning," *IEEE Trans. Neural Networks*, vol. 12, pp. 503-515, 2001.
- [97] Parthasarathy, H., Prasad, S., and Joshi, S. D., "A Music-like method for estimating quadratic phase coupling," *Signal Process.*, vol. 37, pp. 171-188, 1994.
- [98] Patel, J. K. and Read, C. B., *Handbook of the Normal Distribution*. New York: M. Dekker, 1982.
- [99] Pool, R., "Is it healthy to be chaotic," *Science*, vol. 243, pp. 604-607, 1989.
- [100] Porat, B. and Friedlander, B., "Direction finding algorithms based on higher order statistics," *IEEE Trans. Signal Process.*, vol. 39, pp. 2016-2024, 1991.
- [101] Pozidis, H. and Petropulu, A., "Use of selected HOS information for low variance estimate of band limited systems with short data records," presented at *IEEE Int. Conf. Acoust., Speech, Signal Process., ASSP-98*, Seattle, Washington, USA, 1998.
- [102] Press, W., Flannery, B., Teukolsky, S., and Vetterling, W., *Numerical Recipe in C*. Cambridge: Cambridge University Press, 1990.
- [103] Priestley, M. B., *Spectral Analysis and Time Series*, vol. 1. London: Academic Press, 1981.
- [104] Raghuveer, M. R. and Nikias, C. L., "Bispectrum estimation: A parametric approach," *IEEE Trans. Trans. Acoust., Speech, Signal Process.*, vol. ASSP-33, pp. 1213-1230, 1985.
- [105] Raghuveer, M. R. and Nikias, C. L., "Bispectrum estimation via AR modelling," *Signal Process.*, vol. 10, pp. 35-48, 1986.
- [106] Rissanen, J. A., "A universal prior for the integers and estimation by minimum description length," *Ann. Statist.*, vol. 11, pp. 417-431, 1983.

- [107] Romare, D., "The Application of Adaptive Linear and Non-linear Filters to Fringe Order Identification in White-Light Interferometry Systems," Ph.D. Thesis, *Department of Electrical Engineering*, City University, London, 1998.
- [108] Rosenblatt, M., "Linear processes and bispectra," *J. Appl. Probab*, vol. 17, pp. 265-270, 1980.
- [109] Rosenblatt, M. and Van Ness, J. W., "Estimation of the bispectrum," *Ann. Math. Statist.*, vol. 36, pp. 1120-1136, 1965.
- [110] Rumelhart, D. E., Hinton, G. E., and Williams, R. I., "Learning Internal Representations by Error Propagation," in *Parallel Distributed Processing*, vol. 1, D. E. Rumelhart and J. L. McClelland, Eds. Cambridge, MA: MIT Press, 1986.
- [111] Sabry-Rizk, M., El-Khafif, S., Zgallai, W., Carson, E., Grattan, K., Morgan, C., and Hardiman, P., "Suspicious polyphase patterns of normal looking ECG's provide early diagnosis of a coronary artery disease," presented at *IEEE Int. joint Conf. EMBS/BMES*, 1999a.
- [112] Sabry-Rizk, M., Romare, D., Zgallai, W., Grattan, K. T. V., Hardiman, P., and O'Riordan, J., "Higher order statistics (HOS) in signal processing: Are they of any use?," presented at *IEE Colloquium*, Savoy Place, London, Digest no.111, 1995a.
- [113] Sabry-Rizk, M. and Zgallai, W., "Higher order statistics are indispensable tools in the analysis of electrocardiogram signals," presented at *IEE Colloquium Statist. Signal Process.*, Savoy Place, London, UK., 1999.
- [114] Sabry-Rizk, M. and Zgallai, W., "subject to patent," 2001.
- [115] Sabry-Rizk, M., Zgallai, W., Carson, E. R., Grattan, K. T. V., Hardiman, P., Thompson, P., and Maclean, A., "Modified MUSIC pseudospectral analysis reveals common uterus and fetal heart resonances during labour contractions," presented at *the 22nd IEEE Int. Conf. Eng. Med. Biol. Soc., EMBS-00*, USA, 2000a.

- [116] Sabry-Rizk, M., Zgallai, W., Carson, E. R., Grattan, K. T. V., MacLean, A., and Hardiman, P., "Non-linear dynamic tools for characterising abdominal electromyographic signals before and during labour," *Trans. Inst. Meas., Contr.*, vol. 22, pp. 243-270, 2000b.
- [117] Sabry-Rizk, M., Zgallai, W., Carson, E. R., S. El-Khafif, Morgan, C., and Grattan, K. T. V., "Novel decision strategy for P-wave detection utilising non-linearly synthesised ECG components and their enhanced pseudospectral resonances," presented at *IEE Int. Conf., MEDSIP-00*, Bristol, UK, 2000c.
- [118] Sabry-Rizk, M., Zgallai, W., El-Khafif, S., Carson, E., and Grattan, K., "Higher-order ambulatory electrocardiogram identification and motion artifact suppression with adaptive second- and third-order Volterra filters," presented at *SPIE-98, Advanced Signal Processing Algorithms, Architectures and Implementations VIII*, San Diego, USA, 1998.
- [119] Sabry-Rizk, M., Zgallai, W., El-Khafif, S., Carson, E. R., Grattan, K., and Thompson, P., "Highly accurate higher-order statistics based neural network classifier of specific abnormality in electrocardiogram signals," presented at *IEEE Int. Conf. Acoust., Speech, Signal Process., ASSP-99*, Arizona, USA, 1999b.
- [120] Sabry-Rizk, M., Zgallai, W., Hardiman, P., and Oriordan, J., "Third-order cumulant signature matching technique for non-invasive fetal heart beat identification," presented at *IEEE Int. Conf. Acoust., Speech, Signal Process., ASSP-97*, Germany, 1997a.
- [121] Sabry-Rizk, M., Zgallai, W., Hardiman, P., and O'Riordan, J., "Applications of adaptive polycepstral based filtering to ECG analysis," presented at *Int. workshop Med., Biol., Signal Process.*, Plymouth, UK, 1995b.
- [122] Sabry-Rizk, M., Zgallai, W., Hardiman, P., and O'Riordan, J., "Blind deconvolution-homomorphic analysis of abnormalities in ECG signals," presented at *IEE Colloquium*, Savoy Place, London, Digest no. 144, 1995c.

- [123] Sabry-Rizk, M., Zgallai, W., Hardiman, P., and O'Riordan, J., "Applications of higher order cepstral techniques in problems of fetal heart signal extraction," presented at *SPIE-96 Int. Symp. Opt. Sci., Meas.*, Colorado, USA, 1996.
- [124] Sabry-Rizk, M., Zgallai, W., Hardiman, P., and O'Riordan, J., "MUSIC-based bispectrum detector: A novel non-invasive detection method for overlapping fetal and mother ECG signals," presented at *the 19th IEEE Int. Conf. Eng. Med. Biol. Soc., EMBS-97*, USA, 1997b.
- [125] Sabry-Rizk, M., Zgallai, W., McLean, A., Carson, E. R., and Grattan, K. T. V., "Virtues and vices of source separation using linear independent component analysis for blind source separation of non-linearly coupled and synchronised fetal and mother ECGs," presented at *IEEE EMBS*, Istanbul, Turkey, 2001a.
- [126] Sabry-Rizk, M., Zgallai, W., Morgan, C., Carson, E. R., and Grattan, K. T. V., "A modified pseudo-bispectral MUSIC technique for on-line identification of abnormal atrial activations in noisy ECG signals," presented at *the 3rd Int. Conf. Signal, Image Process., IASTED-SIP-01*, Hawaii, 2001b.
- [127] Sabry-Rizk, M., Zgallai, W., Morgan, C., El-Khafif, S., Carson, E. R., and Grattan, K. T. V., "Novel decision strategy for P-wave detection utilising nonlinearly synthesised ECG components and their enhanced pseudospectral resonances," *IEE Proc. Sci., Meas., Tech., Special section on Medical Signal Processing*, vol. 147, pp. 389-397, 2000d.
- [128] Sahakian, A. V. and Furno, G. F., "An adaptive filter for distorted line-frequency noise," *Biomed. Sci. Instrum.*, vol. 19, pp. 47-52, 1983.
- [129] Saridis, G. N., "Learning applied to successive approximation algorithms," *IEEE Trans. Sys., Sci., Cybern.*, vol. SSC-6, pp. 97-103, 1970.
- [130] Schels, H. F., Haberl, R., Jilge, G., Steinbigler, P., and Steinbeck, G., "Frequency-analysis of the electrocardiogram with maximum entropy method for identification of patients with sustained ventricular tachycardia," *IEEE Trans. Biomed. Eng.*, vol. BME-38, pp. 821-826, 1991.

- [131] Schetzen, M., *The Volterra and Wiener Theories of Nonlinear Systems*. New York: Wiley, 1980.
- [132] Schmidt, R. O., "Multiple emitter location and signal parameter estimation," presented at *RADC Spectrum Estimation Workshop*, 1979.
- [133] Schmidt, R. O., "A Signal Subspace Approach to Multiple Emitter Location and Spectral Estimation," Ph.D Thesis, *Department of Electrical Engineering*. Stanford University: Stanford, 1981.
- [134] Sebert, G. and Elgar, S., "Statistics of bicoherence and biphasic," presented at *Workshop of Higher-Order Spectral Analysis*, Vail, CO, 1989.
- [135] Sicuranza, G. L., "Quadratic filters for signal-processing," *Proc. IEEE*, vol. 80, pp. 1263-1285, 1992.
- [136] Sietsma, J. and Dow, R. J., "Creating artificial neural networks that generalize," *Neural Networks*, vol. 4, pp. 67-79, 1991.
- [137] Sievanen, H., Karhumaki, L., Vuori, I., and Malmivuo, J., "Compartmental multivariate-analysis of exercise ECGs for accurate detection of myocardial-ischemia," *Med., Biol., Eng., Comput.*, vol. 32, pp. S3-S8, 1994.
- [138] Sigl, J. C. and Chamoun, N., "An introduction to bispectral analysis for the electroencephalogram," *J. Clin. Monit.*, vol. 10, pp. 392-404, 1994.
- [139] Signorini, M. G., Cerutti, S., Guzzetti, S., and Parola, R., "Nonlinear dynamics of cardiovascular variability signals," *Methods Inf. Med.*, vol. 33, pp. 81-84, 1994.
- [140] Silipo, R., Laguna, P., Marchesi, C., and Mark, R. G., "ST-T segment change recognition using artificial neural networks and principal component analysis," *Comput. Cardiol.*, pp. 213-216, 1995.
- [141] Simson, M. B., "Use of signals in the terminal QRS complex to identify patients with ventricular tachycardia after myocardial infarction," *Circulation*, vol. 64, pp. 234-242, 1981.

- [142] Simson, M. B., Horowitz, L., Josephson, M., and Moove, E. N., "A marker for ventricular tachycardia after myocardial infarction," *Circulation*, vol. 62, pp. 262, 1980.
- [143] Skordalakis, E., "Recognition of the ST segment in ECG waveforms," *IEEE Trans. Biomed. Eng.*, vol. BME-33, pp. 972-974, 1986.
- [144] Spaargaren, A. and English, M. J., "Bispectral analysis of high resolution ECG," *Electron. Lett.*, vol. 35, pp. 1216-1217, 1999.
- [145] Speirs, C. A., Soraghan, J. J., Stewart, R. W., and Polson, M. J. R., "Bispectral analysis for the detection of ventricular late potentials," *Proc. IEEE Int. Conf. Acoust., Speech, Signal Process., ASSP-93*, pp. 427-430, 1993.
- [146] Stamkopoulos, T., Diamantaras, K., Maglaveras, N., and Strintzis, M., "ECG analysis using nonlinear PCA neural networks for ischemia detection," *IEEE Trans. Signal Process.*, vol. 46, pp. 3058-3067, 1998.
- [147] Stokes, V. P., Lanshammar, H., and Thorstensson, A., "Dominant pattern extraction from 3-D kinematic data," *IEEE Trans. Biomed. Eng.*, vol. BME-46, pp. 100-106, 1999.
- [148] Suzuki, Y. and Ono, K., "Personal Computer System for ECG ST-Segment Recognition Based on Neural Networks," *Med., Biol., Eng., Comput.*, pp. 2-8, 1992.
- [149] Svensson, O., Sornmo, L., and Pahlm, O., "Effects of digital resolution on characterisation of cardiac late potentials," *Med., Biol., Eng., Comput.*, vol. 32, pp. S9-S15, 1994.
- [150] Swami, A. and Mendel, J. M., "Cumulant-based approach to the harmonic retrieval and related problems," *IEEE Trans. Acoust. Speech, Signal Process.*, vol. ASSP-39, pp. 1099-1109, 1991.

- [151] Taddei, A., Costantino, G., silipo, R., Emdin, M., and Marchesi, C., "A system for the detection of ischemic episodes in ambulatory ECG," *Comput. Cardiol.*, pp. 705-708, 1995.
- [152] Taddei, A., Distante, G., Emdin, M., Pisani, P., Moody, G., Zeelenberg, C., and Marchesi, C., "The European ST-T database: Standard for evaluating systems for the analysis of ST-T changes in ambulatory electrocardiography," *Eur. Heart J.*, vol. 13, pp. 1164-1172, 1992.
- [153] Thakor, N. V., Webster, J. G., and Tompkins, W. J., "Optimal QRS detector," *Med., Biol., Eng., Comput.*, vol. 21, pp. 343-350, 1983.
- [154] Thakor, N. V., Webster, J. G., and Tompkins, W. J., "Estimation of QRS complex power spectra for design of a QRS filter," *IEEE Trans. Biomed. Eng.*, vol. BME-31, pp. 702-706, 1984.
- [155] Thakor, N. V. and Zhu, Y. S., "Applications of adaptive filtering to ECG analysis noise cancellation and arrhythmia detection," *IEEE Trans. Biomed. Eng.*, vol. BME-38, pp. 785-794, 1991.
- [156] Tompkins, W. J., *Biomedical Digital Signal Processing*. New Jersey: Prentice Hall, 1993.
- [157] Walach, E. and Widrow, B., "The least mean 4th (Lmf) adaptive algorithm and its family," *IEEE Trans. Inform. Theory*, vol. 30, pp. 275-283, 1984.
- [158] Waldo, D. and Chitrapa, P. R., "On Wigner Ville distribution of finite duration signals," *Signal Process. J.*, vol. 24, pp. 231-238, 1991.
- [159] Weisner, S. J., Tompkins, W. J., and Tompkins, B. M., "A compact, microprocessor-based ECG ST-segment analyser for the operating-room," *IEEE Trans. Biomed. Eng.*, vol. BME-29, pp. 642-649, 1982.
- [160] Widrow, B., Glover, J. R., McCool, J. M., Kaunitz, J., Williams, C. S., Hearn, R. H., Zeidler, J. R., Dong, E., and Goodlin, R. C., "Adaptive noise cancelling: principles and applications," *Proc. IEEE*, vol. 63, pp. 1692-1716, 1975.

- [161] Widrow, B., McCool, J. M., Larimore, M. G., and Johnson, C. R., "Stationary and nonstationary learning characteristics of the LMS adaptive filter," *Proc. IEEE*, vol. 64, pp. 1151-1162, 1976.
- [162] Xue, Q. Z., Hu, Y. H., and Tompkins, W. J., "Neural-network-based adaptive matched filtering for QRS detection," *IEEE Trans. Biomed. Eng.*, vol. BME-39, pp. 317-329, 1992.
- [163] Xue, Q. Z. and Reddy, B. R. S., "Late potential recognition by artificial neural networks," *IEEE Trans. Biomed. Eng.*, vol. BME-44, pp. 132-143, 1997.
- [164] Yamada, K. E. A., "Observer variation in electrocardiographic interpretation," *Ann. Rep. Inst. Environ. Med.*, vol. 16, pp. 27-41, 1968.
- [165] Yelderman, M., Widrow, B., Ciloffi, J. M., Hesler, E., and Leddy, J. A., "ECG enhancement by adaptive cancellation of electrosurgical interference," *IEEE Trans. Biomed. Eng.*, vol. BME-30, pp. 392-398, 1983.
- [166] Youngson, R. M., "Collins Dictionary of Medicine," Great Britain: HarperCollins Manufacturing, Glasgow, 1992.
- [167] Zgallai, W., "The Application of high-order Statistics and Non-linear Filtering to Non-invasive Fetal Heartbeat Detection," Ph.D Thesis, *School of Engineering, City University*. London, UK, 2002.
- [168] Zhang, J. W., Zheng, C. X., and Xie, A., "Bispectrum analysis of focal ischemic cerebral EEG signal using third-order recursion method," *IEEE Trans. Biomed. Eng.*, vol. BME-47, pp. 352-359, 2000.
- [169] Zhang, Q. and Haykin, S., "Tracking characteristics of the Kalman filter in a nonstationary environment for adaptive filter applications," *Proc. IEEE Int. Conf. Acoust., Speech, Signal Process., ASSP-83*, Boston, pp. 671-674, 1983.
- [170] Zhang, X. S., Zhu, Y. S., Thakor, N. V., and Wang, Z. Z., "Detecting ventricular tachycardia and fibrillation by complexity measure," *IEEE Trans. Biomed. Eng.*, vol. BME-46, pp. 548-555, 1999.

- [171] Zhang, X. S., Zhu, Y. S., and Zhang, X. J., "New approach to studies on ECG dynamics: extraction and analyses of QRS complex irregularity time series," *Med., Biol., Eng., Comput.*, vol. 35, pp. 467-473, 1997.
- [172] Zhou, G. and Giannakis, G., "Retrieval of self-coupled harmonics," *IEEE Trans. Signal Process.*, vol. 43, pp. 1173-1186, 1995.
- [173] Zurada, J. M., "Fundamental Concepts and Models of Artificial Neural Networks," in *Introduction to Artificial Neural Systems*. New York: West Publishing Company, 1992, pp. 25-92.